



The Journal of Gemmology

Volume 37 / No. 6 / 2021

The Book of Hours of
King Francis I of France
.....

Precious Coral
Identification Using
LA-ICP-MS Analysis

Iridescent Ammonite
Fossil Shell Material
from Russia
.....

Blue Dravite from
Sri Lanka

.....
Grinding Hardness of
Ornamental Stones

SSEF

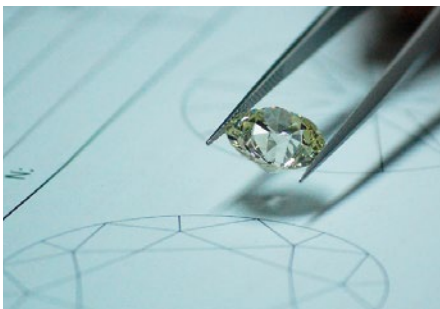
SCHWEIZERISCHES GEMMOLOGISCHES INSTITUT
SWISS GEMMOLOGICAL INSTITUTE
INSTITUT SUISSE DE GEMMOLOGIE



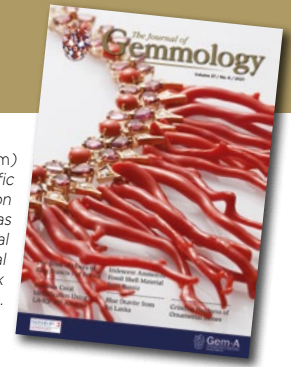
ORIGIN DETERMINATION · TREATMENT DETECTION

DIAMOND GRADING · PEARL TESTING

EDUCATION · RESEARCH



THE SCIENCE OF GEMSTONE TESTING™



Cover photo: Coral from the Mediterranean Sea (*Corallium rubrum*) can be separated from *C. japonicum* coral from the western Pacific Ocean by its trace-element composition, as described in an article on pp. 596–607 of this issue. This necklace by Chantecler was constructed in 2017 and features Mediterranean *C. rubrum* coral branches (54 in total, measuring 3–7 cm long) and 18 coral cabochons accompanied by 307 diamonds and 57 pink tourmalines. Photo courtesy of Chantecler (Naples, Italy).

COLUMNS

What's New

555

IndiGo and IndiGo Fluor
UVA-C Spectrometers |
Sheffield Red Compensator |
Sherlock Holmes 3.0 |
SmartPro Optimum 1 |
*Catalog of the Museum of
Faceting Technology* |
Consumer Research on
Synthetic Diamonds | De
Beers 2020 Diamond Market
Reports | Gem Testing
Laboratory (Jaipur, India)
Newsletter | *Journal of Gems
& Precious Metals* | A 'Ruby'
Necklace Set with Flux-grown
Synthetic Rubies | *Sparkling
Jewels, Opaque Supply Chains*
| Tortoiseshell Global Trade
Report | CIBJO's Responsible
Sourcing Toolkit | Webinars
and Other Online Content for
Gemmological Education |
American Museum of Natural
History Halls Open

Gem Notes

562

Unusual Inclusion Feature
in Amethyst from Brazil |
Colour-Change Andradite |
Chrome Diopside from
Ethiopia | Grandidierite from
Madagascar Showing Sheen
and Chatoyancy | 'Herkimer
Diamond' Quartz from
North-western Iran |
Hematite Inclusions in Red
Trapiche Quartz from Inner
Mongolia | Blue Persistent
Luminescence (Phosphores-
cence) of Sodalite | A Roman
Ring Set with a Turquoise |
Near-Colourless HPHT-grown
Synthetic Diamonds that Test
as Synthetic Moissanite |
Production and Cutting of
Synthetic Moissanite in China
| Trapiche Sapphire Imitation

ARTICLES

The Book of Hours of King Francis I of France: History and Gemmological Analysis **580**

By Gérard Panczer, Elodie Romeo and Geoffroy Riondet

Identification of Precious Corals (*Corallium rubrum* vs *C. japonicum*) Using LA-ICP-MS Analysis **596**

By Daniel Vielzeuf, Bruna Giordano, Jean-Luc Devidal, Angèle Ricolleau, Jonathan Perrin, Catherine Balme-Heuze and Nicole Floquet

Iridescent Ammonite Fossil Shell Material from Norilsk, Krasnoyarsk Krai, Russia **608**

By Viktor A. Radko, Sergey A. Ananyev, Dmitry A. Petrochenkov and Svetlana S. Bondina

Blue Dravite ('Indicolite') from the Elahera Gem Field, Sri Lanka **618**

By Lutz Nasdala, Manfred Wildner, Gerald Giester, Chutimun Chanmuang N., Maria Rosa Scicchitano and Christoph Hauzenberger

An Investigation of Grinding Hardness of Some Ornamental Stones **632**

By Henry A. Hänni, Richard Brunk and Leander Franz



Gem-A Notices **644** New Media **651**

Learning Opportunities **648** Literature of Interest **656**

The Journal is published by Gem-A in collaboration with SSEF and with the support of AGL.



The Journal of Gemmology

EDITORIAL STAFF

Editor-in-Chief
Brendan M. Laurs
brendan.laurs@gem-a.com

Executive Editor
Alan D. Hart

Editorial Assistant
Carol M. Stockton

Editor Emeritus
Roger R. Harding

ASSOCIATE EDITORS

Ahmadjan Abduriyim
Tokyo Gem Science LLC,
Tokyo, Japan

Raquel Alonso-Perez
Harvard University,
Cambridge, Massachusetts,
USA

Edward Boehm
RareSource, Chattanooga,
Tennessee, USA

Maggie Campbell Pedersen
Organic Gems, London

Alan T. Collins
King's College London

Alessandra Costanzo
National University of
Ireland Galway

John L. Emmett
Crystal Chemistry, Brush
Prairie, Washington, USA

Emmanuel Fritsch
University of Nantes,
France

Rui Galopim de Carvalho
PortugalGemas Academy,
Lisbon, Portugal

Al Gilbertson
Gemological Institute
of America, Carlsbad,
California

Lee A. Groat
University of British
Columbia, Vancouver,
Canada

Thomas Hainschwang
GTL Laboratories,
Balzers, Liechtenstein

Henry A. Hänni
GemExpert, Basel,
Switzerland

Jeff W. Harris
University of Glasgow

Alan D. Hart
Gem-A, London

Ulrich Henn
German Gemmological
Association, Idar-Oberstein

Jaroslav Hyršl
Prague, Czech Republic

Brian Jackson
National Museums
Scotland, Edinburgh

Mary L. Johnson
Mary Johnson Consulting,
San Diego, California, USA

Stefanos Karamelas
Laboratoire Français de
Gemmologie, Paris, France

Lore Kiefert
Dr. Lore Kiefert Gemmology
Consulting, Heidelberg,
Germany

Hiroshi Kitawaki
Central Gem Laboratory,
Tokyo, Japan

Michael S. Krzemnicki
Swiss Gemmological
Institute SSEF, Basel

Shane F. McClure
Gemological Institute
of America, Carlsbad,
California

Jack M. Ogden
London

Federico Pezzotta
Natural History Museum
of Milan, Italy

Jeffrey E. Post
Smithsonian Institution,
Washington DC, USA

Andrew H. Rankin
Kingston University, Surrey

Benjamin Rondeau
University of Nantes,
France

George R. Rossman
California Institute of
Technology, Pasadena,
USA

Karl Schmetzer
Petershausen, Germany

Dietmar Schwarz
Bellerophon Gemlab,
Bangkok, Thailand

Menahem Sevdemish
Gemewizard Ltd, Ramat
Gan, Israel

Andy H. Shen
China University of
Geosciences, Wuhan

Guanghai Shi
China University of
Geosciences, Beijing

James E. Shigley
Gemological Institute
of America, Carlsbad,
California

Christopher P. Smith
American Gemological
Laboratories Inc.,
New York, New York

Elisabeth Strack
Gemlogisches Institut
Hamburg, Germany

Tay Thye Sun
Far East Gemological
Laboratory, Singapore

Frederick 'Lin' Sutherland
Port Macquarie, New
South Wales, Australia

Pornsawat Wathanakul
Kasetsart University,
Bangkok

Chris M. Welbourn
Reading, Berkshire

Bear Williams
Stone Group Laboratories
LLC, Jefferson City,
Missouri, USA

J. C. (Hanco) Zwaan
National Museum of
Natural History 'Naturalis',
Leiden, The Netherlands



Gem-A
THE GEMMOLOGICAL ASSOCIATION
OF GREAT BRITAIN

21 Ely Place
London EC1N 6TD
UK

t: +44 (0)20 7404 3334
f: +44 (0)20 7404 8843
e: information@gem-a.com
w: <https://gem-a.com>

Registered Charity No. 1109555
A company limited by guarantee and
registered in England No. 1945780
Registered office: Palladium House,
1-4 Argyll Street, London W1F 7LD

PRESIDENT

Maggie Campbell Pedersen

VICE PRESIDENTS

David J. Callaghan
Alan T. Collins
Noel W. Deeks
Andrew H. Rankin

HONORARY FELLOWS

Gaetano Cavaliere
Andrew Cody
Terrence S. Coldham
Emmanuel Fritsch

HONORARY DIAMOND MEMBER

Martin Rapaport

CHIEF EXECUTIVE OFFICER

Alan D. Hart

COUNCIL

Justine L. Carmody – Chair
Nevin Bayoumi-Stefanovic
Kathryn L. Bonanno
Louise Goldring
Joanna Hardy
Philip Sadler
Christopher P. Smith

BRANCH CHAIRMEN

Midlands – Louise Ludlam-Snook
North East – Mark W. Houghton
North West – Liz Bailey

COVERED BY THE FOLLOWING ABSTRACTING AND INDEXING SERVICES:

Clarivate Analytics' (formerly Thomson Reuters/ISI) Science Citation Index Expanded (in the Web of Science), *Journal Citation Reports (Science Edition)* and *Current Contents (Physical, Chemical and Earth Sciences)*; Elsevier's Scopus; Australian Research Council's Excellence in Research for Australia (ERA) Journal List; China National Knowledge Infrastructure (CNKI Scholar); EBSCO's Academic Search Ultimate; ProQuest (Cambridge Scientific Abstracts); GeoRef; CrossRef; Chemical Abstracts (CA Plus); Mineralogical Abstracts; Index Copernicus ICI Journals Master List; Gale Academic OneFile; British Library Document Supply Service; and Copyright Clearance Center's RightFind application.



CONTENT SUBMISSION

The Editor-in-Chief is glad to consider original articles, news items, conference reports, announcements and calendar entries on subjects of gemmological interest for publication in *The Journal of Gemmology*. A guide to the various sections and the preparation of manuscripts is given at <https://gem-a.com/membership/journal-of-gemmology/submissions>, or contact the Editor-in-Chief.

SUBSCRIPTIONS

Gem-A members receive *The Journal* as part of their membership package, full details of which are given at <https://gem-a.com/membership>. Laboratories, libraries, museums and similar institutions may become direct subscribers to *The Journal*; download the form from *The Journal's* home page.

ADVERTISING

Enquiries about advertising in *The Journal* should be directed to advertising@gem-a.com.

COPYRIGHT AND REPRINT PERMISSION

For full details of copyright and reprint permission contact the Editor-in-Chief. *The Journal of Gemmology* is published quarterly by Gem-A, The Gemmological Association of Great Britain. Any opinions expressed in *The Journal* are understood to be the views of the contributors and not necessarily of the publisher.

DESIGN & PRODUCTION

Zest Design, London. www.zest-uk.com

PRINTER

DG3 Group (Holdings) Ltd, London. www.dg3.com



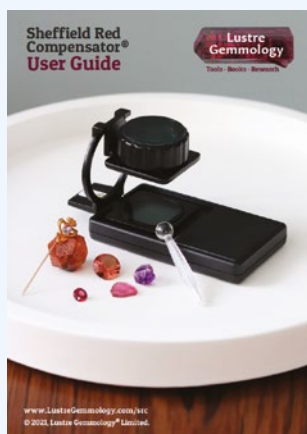
© 2021 Gem-A (The Gemmological Association of Great Britain)
ISSN 1355-4565 (Print), ISSN 2632-1718 (Online)

What's New

INSTRUMENTATION

IndiGo and IndiGo Fluo UVA-C Spectrometers

In addition to its GoSpectro device (see *The Journal*, Vol. 35, No. 8, 2017, p. 464), Goyalab (Talence, France) introduced two new instruments in May 2021: the IndiGo modular visible-range spectrometer and the IndiGo Fluo UVA-C fluorescence spectrometer. The two instruments are remarkably small and work via Bluetooth 5.0 with a smartphone or tablet, with a free app available for iOS, Android and Windows operating systems. The visible-range unit allows measurement of emission, absorption or transmission spectra in the 380–720 nm range. The fluorescence spectrometer includes the basic visible-range unit plus an excitation module with four long-wave (365 nm) and two short-wave (254 nm) LEDs, enabling the device to obtain fluorescence spectra in the 370–810 nm range. Visit www.goyalab.com/product/indigo-visible-spectrometer and www.goyalab.com/product/indigo-fluo-uva-c-a-fluorescence-spectrometer-with-uvauvc-excitation.



Sheffield Red Compensator

Lustré Gemmology Ltd (Sheffield, South Yorkshire) released its Sheffield Red Compensator in April 2021. The instrument is a combination polariscope, first-order red compensator

and loupe. When used with a conoscope and suitable flat-light source (not included), a stone's optic character can be determined without employing a refractometer (particularly useful for rough or cabochon-cut gems). It is also valuable for locating inclusions and their associated stress-induced birefringence. A free user guide is available for download. Visit <https://lustregemmology.com/shop/ols/products/sheffield-red-compensator>.

Sherlock Holmes 3.0 Detector

In January 2021, Yehuda announced the release of its latest-generation diamond detector. The Sherlock Holmes 3.0 builds on the capabilities of version 2.0 (see *The Journal*, Vol. 36, No. 5, 2019, p. 393), also still available. The 3.0 reportedly can distinguish natural diamonds from CVD and HPHT synthetic diamonds (loose and mounted) as well as unmounted simulants (such as synthetic moissanite and CZ-coated diamonds). The unit offers long-wave and short-wave UV and photoluminescence imaging, with zoom magnification (up to 8×) and focusing, and can test multiple stones or jewellery items simultaneously.

Test images can be saved for later reference. In addition, the instrument can be operated remotely via mobile phone, tablet or computer with an Internet connection. For additional information, including video tutorials, visit <https://yehuda.com>.

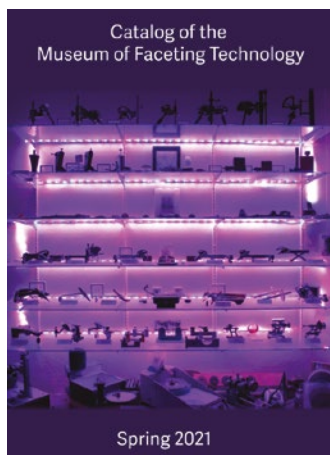


SmartPro Optimum 1 Diamond Tester

In the first quarter of 2021, SmartPro released its Optimum 1 portable diamond tester. The handheld unit reportedly can separate colourless to near-colourless (D–M) diamonds from synthetic diamonds (CVD and HPHT) and synthetic moissanite, but does not screen for CZ, glass or other simulants. It can test polished stones weighing 0.015–10 ct (both loose and mounted, including closed-back settings). The unit operates using UV LED fibre-optic technology and includes a torch mode to test for fluorescence. An integrated 6.1 cm LCD touch screen provides the user interface and delivers test results. The unit is available from various third-party retail websites; search for 'SmartPro Optimum 1'. For additional information about SmartPro, visit www.smartproinstrument.com.



NEWS AND PUBLICATIONS

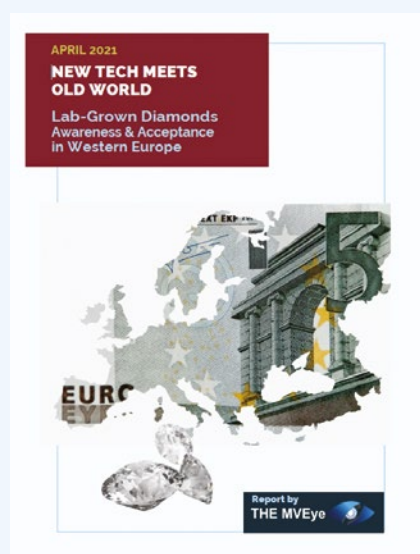


Catalog of the Museum of Faceting Technology

This spring 2021 catalogue documents the collection of gemstone-fashioning equipment assembled by Justin K Prim (Bangkok, Thailand) since February 2018. As of April 2021, the collection consisted of 52 machines, faceting heads and handpieces from 21 countries. The goal of the ongoing project is to acquire at least one style of machine from each country that has a history of faceting. The catalogue provides illustrations, descriptions and historical notes for 45 pieces of equipment from 22 countries, dating from the 19th century to the present, plus a few associated items. Download the 54-page catalogue at www.justinusprimitive.com/Catalog-MuseumofFacetingTechnology-Spring2021.

Consumer Research on Synthetic Diamonds

USA-based The MVEye performed a survey of 1,530 consumers in five European countries—France, Italy, Germany, Spain and the UK—regarding attitudes towards synthetic diamonds. The April 2021 report—*New Tech Meets Old World: Lab-Grown Diamonds Awareness & Acceptance in Western Europe*—reveals an unexpectedly high awareness of the product. Overall, more than 77% knew of lab-grown diamonds before taking the survey, and 41% reported purchasing or receiving synthetic diamond jewellery. Reasons for the high level of consumer acceptance included respondents considering lab-grown diamonds to be more environmentally friendly and sustainable—and also that they are visually identical to, and 30% less costly, than natural diamonds. To purchase a copy of the detailed report, which also compares European to previous USA survey results, visit www.themveye.com/download-premium-report.php?report=8.



De Beers 2020 Diamond Market Reports

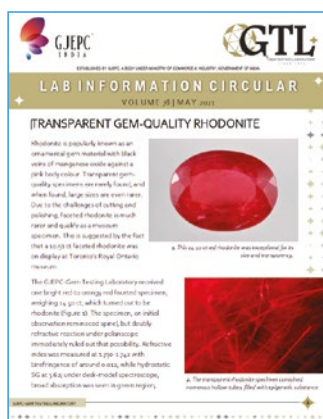
In November 2020, De Beers Group released two reports on the diamond market: *The Diamond Insight Report 2020* and the *De Beers Group 2020 Diamond Value Chain Dashboard*. The first is a 25-page report that examines diamond demand during the COVID-19 pandemic and focuses on how retailers can adapt 'to our new normality'. It discusses how to connect with customers online, how to re-open retail stores safely and how to merge the two to optimise the retail experience. The second report is a market summary that covers 2019 jewellery and polished diamond demand and the impact of COVID-19 on the outlook for the diamond market, as well as global rough diamond production (which decreased 6% by volume in 2019, with the return to pre-COVID-19 levels

depending on the global economic recovery). Meanwhile, 2019 sales to cutting centres rose by value. To access these reports, go to www.debeersgroup.com/~media/Files/D/De-Beers-Group-V2/documents/reports/insights/2020/the-diamond-insight-report-2020.pdf and www.debeersgroup.com/~media/Files/D/De-Beers-Group-V2/documents/reports/insights/2020/the-diamond-value-chain.pdf.



Gem Testing Laboratory (Jaipur, India) Newsletter

GTL Jaipur published volume 78 of its *Lab Information Circular* in May 2021, with reports on rhodonite, heterosite-purpurite (resembling charoite or sugilite), green kyanite (imitating emerald), zoisite dyed to imitate ruby and emerald, a type IIa diamond with unusual laser drill holes and beads of resin-filled corundum. To download this and previous issues, go to www.gtljaipur.info/lab-information-circular1.aspx.



Journal of Gems & Precious Metals

This new journal from the Gemology Center of Shahid Beheshti University, Tehran, Iran, began publication in the spring of 2021. This first issue contains six articles, all in English, covering the Olivenput diamond-bearing pipe in South Africa, a newly proposed name for Persian turquoise-bearing gem material, gold mineralisation in Iran, Brunauer-Emmett-Teller testing of low-grade Iranian turquoise, the gem potential of apatite from Hormuz Island (Iran) and the effect of gamma rays on rock crystal quartz from Iran. The articles are available to download at https://gem.sbu.ac.ir/issue_14861_14862.html.



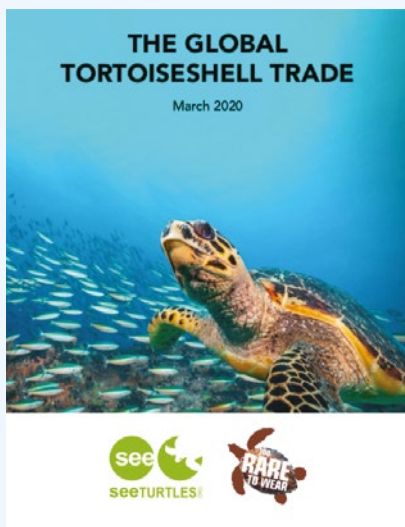
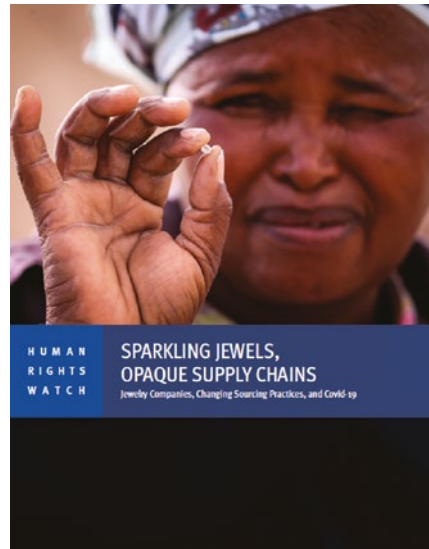
A 'Ruby' Necklace Set with Flux-grown Synthetic Rubies

In May 2021, GGTL Laboratories in Liechtenstein posted a report online about a necklace with approximately 50 'rubies' submitted for determination of treatment and country of origin. Microscopy revealed atypical inclusions suggestive of a flux-grown synthetic origin. Infrared spectroscopy, chemical analysis and DFI fluorescence testing confirmed the identity of the gems as flux-grown synthetic rubies. To read the report and view its detailed, informative illustrations (especially photomicrographs of inclusions), visit www.ggtl-lab.org/en/news/unusual-case-jewel-large-number-flux-grown-synthetic-rubies-sold-natural-rubies.



Sparkling Jewels, Opaque Supply Chains

Human Rights Watch released this report, subtitled 'Jewelry Companies, Changing Sourcing Practices, and Covid-19', in November 2020. It describes how 15 major jewellery companies worldwide addressed human rights issues in the gold and diamond supply chains between 2018 and 2020. The study found some progress in individual company practices, but most still failed to meet international standards, leaving much work still 'to be done to assure consumers that the jewellery they buy is sourced responsibly'. The report also acknowledges industry initiatives such as the Responsible Jewellery Council and the Initiative for Responsible Mining Assurance. A synopsis of the report is available at www.hrw.org/report/2020/11/24/sparkling-jewels-opaque-supply-chains/jewelry-companies-changing-sourcing, which includes a link to a video and the full 90-page report as a PDF download.



Tortoiseshell Global Trade Report

In April 2020, U.S.-based non-profit organisation SEE Turtles issued *The Global Tortoiseshell Trade*, which summarises new research about the ongoing trade in endangered hawksbill sea turtle shell ('tortoiseshell') in 40+ countries around the world. According to the report, almost 30,000 turtle products were sold online since 2017—mostly from Indonesia—but recent research has shown that the trade seems to be declining in at least five countries as a result of advocacy and enforcement. However, trade in tortoiseshell is still legal in three countries and is strong in at least 10. Visit www.seeturtles.org/turtlesell-research.

OTHER RESOURCES

CIBJO's Responsible Sourcing Toolkit

In April 2021, CIBJO launched a free online 'toolkit' to accompany the guidelines in its *Responsible Sourcing Book* released in 2019 (see *The Journal*, Vol. 36, No. 5, 2019, p. 397). The toolkit consists of a sequence of nine modules designed for use by participants at all levels of the jewellery supply chain. Each module includes a detailed introduction and downloadable files (such as



templates, forms and sample declarations) which can be used to assist with following the recommended due diligence. Visit www.cibjo.org/rs-toolkit.

Webinars and Other Online Content for Gemmological Education

During the COVID-19 pandemic, various educational and gem industry organisations continue to provide webinars and other archived video and audio content of interest to gemmologists (see also those listed in several previous What's New sections).

- **Chasing Color: A Gem Trader's Journey** is a 2020 short documentary film from Rob Himebaugh. The cinema-quality, award-winning film opens with a visit to a mine in Mogok, Myanmar, showing how the alluvial deposit is worked by hand methods. New York-based Australian gem trader Yvonne Jiew guides the viewer through various local gem markets and mining localities, as well as the GRS lab in Bangkok, and on to Jaipur cutting and sales facilities. The film focuses more on the people, culture and context of the gem trade than on gem production and sales. It concludes with Jiew's successful outreach to the gem community for donations to provide food for the poor in India. View the 24-minute video at <https://vimeo.com/358384549>.
- Two **GGTL Laboratories'** webinars were made available on the GGTL Liechtenstein YouTube channel in April 2021, in which Dr Thomas Hainschwang discusses brown diamonds and green diamonds, respectively. These webinars include the results of an extensive, ongoing GGTL research project to characterise brown and green diamonds, including treated-colour and synthetic products. Each video is roughly 1 hour 15 minutes in length. Visit www.youtube.com/channel/UChW6UMBs4pl_DTG445IbDuQ.



- The **Geological Society of South Africa's** YouTube channel offers an extensive array of videos, many added during the first half of 2021. Presentations related to diamond mining and exploration in Africa can be found in the 'Lunchtime Talks' and 'Overberg Geoscientists Group Talks' playlists. Visit www.youtube.com/channel/UC-KUo21b9xfN4pMlbKXoiPw/playlists.



- **Inside the Jewel Vault** podcasts began in March 2021 and currently include six episodes. The sessions feature fine-jewellery blogger Katerina Perez, jewellery expert Vivienne Becker, designer Hannah Martin, diamond mounter and 'digital maestro' Darren Sherwood, jewellery historian Dr Jack Ogden and fiction writer Josie Goodbody. Each individual discusses six pieces of jewellery from their life and career. Visit <https://vipjewelvault.com/inside-the-jewel-vault-podcast>.



- The **Kimberley Process Civil Society Coalition** acts as an observer of the Kimberley Process on behalf of civil society (the counterpart to the World Diamond Council's observer status on behalf of the industry). Members are primarily from African countries that are trading hubs for rough diamonds. The organisation's YouTube channel currently offers three videos, including two short introductory videos and KPCSC's first webinar (March 2021), focusing on communities in diamond mining areas. Visit www.youtube.com/channel/UCFrjXBvIZBwPkWDiXjJHhZg.



- The **Vancouver Kimberlite Cluster** is an educational collaboration of the University of British Columbia (Canada) and SRK Consulting (international mining and exploration consultants). Since November 2020, they have posted five video presentations on their YouTube channel at <https://tinyurl.com/h4ch62ks>:



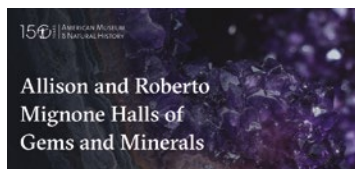
‘Primary Diamond Asset Development’, ‘Braúna 3 Mine – South America’s First Diamond Mine Developed on a Kimberlite Deposit’, ‘Diamonds and Their Inclusions from the Koffiefontein Pipe’, ‘Diamond Exploration in COVID Times’ and ‘Distinct Diamond-forming Mechanisms in the Lithosphere, Asthenosphere and Lower Mantle’. For information about the Cluster, and to access older videos, visit <https://diamonds.eoas.ubc.ca/vancouverkimberlitecluster>.

- **L'École School of Jewelry Arts** has archived its ‘L'École-Talks’ series as a playlist on its YouTube channel. The presentations currently include 26 videos (13 each in English and French) that cover such diverse topics as the French Blue diamond, ‘dancing jewels’, ‘sentimental jewels’, history of the pearl trade between the Gulf and France, floral jewellery design, Art Deco jewellery and much more. Each video is at least an hour in length. Visit www.youtube.com/channel/UCSURUbe7km7Rn0NXkuhXsZw/playlists.



MISCELLANEOUS

American Museum of Natural History Halls Open



On 12 June 2021, the American Museum of Natural History in New York, New York, USA, opened its new Allison and Roberto Mignone Halls of Gems and Minerals. On view in the Gems Hall are famous pieces such as the 563 ct Star of India sapphire, the 632 ct Patricia emerald and the Organdie necklace

featuring 110 carats of diamonds. The Minerals Hall includes the approximately 1-m-tall Tarugo purplish red tourmaline. A temporary exhibition space called the Melissa and Keith Meister Gallery also opened with an exhibition titled ‘Beautiful Creatures’, featuring jewellery pieces inspired by animal forms (curated by Marion Fasel). The Mignone Halls of Gems and Minerals are just some of many projects undertaken to celebrate the Museum's 150th anniversary. For more information about the exhibition, including a preview video, and to arrange a visit, go to www.amnh.org/exhibitions/permanent/gems-minerals.

What's New provides announcements of new instruments/technology, publications, online resources and more. Inclusion in What's New does not imply recommendation or endorsement by Gem-A. Entries were prepared by Carol M. Stockton unless otherwise noted.

An innovator in gemstone reporting

- Identification of colored gemstones • Country of origin determination • Full quality and color grading analysis



AMERICAN GEMOLOGICAL LABORATORIES



580 5th Ave • Suite 706 • New York, NY 10036, USA
www.agilgemlab.com • +1 (212) 704 - 0727

Gem Notes

COLOURED STONES

Unusual Inclusion Feature in Amethyst from Brazil

Amethyst is a very popular gem material, and synthetic amethyst has been common on the market for several decades. A good indication of the natural origin of amethyst is the presence of so-called tiger stripes—characteristic parallel lines caused by Brazil-law twinning (an alternation of left and right quartz)—which are always concentrated under the positive rhombohedron (Crowningshield *et al.* 1986). They can usually be detected with a polariscope, but sometimes they can be seen easily with just a loupe.

A large faceted amethyst bought by the author in Brazil in 2019 shows a very unusual inclusion feature, visible even without a loupe (Figure 1), which resembles the appearance of Brazil-law twinning. The feature actually consists of a ‘phantom’ in the quartz composed of three almost perpendicular planes, forming a rhombohedron. The surface of the phantom is decorated with

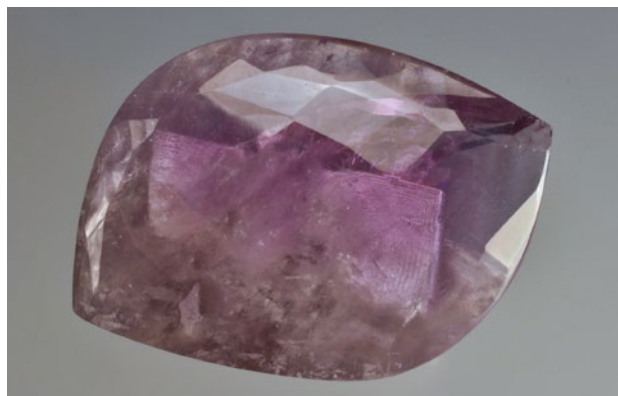


Figure 1: This Brazilian amethyst (159.15 ct) contains a prominent phantom that gives the appearance of the ‘tiger stripes’ associated with Brazil-law twinning. The maximum dimension of the phantom is 27 mm, thus occupying much of the interior of the 41-mm-long gem. Photo by J. Hyršl.

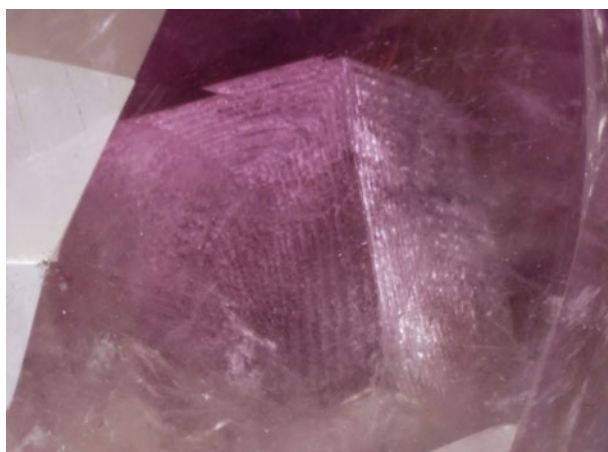


Figure 2: A closer examination of the amethyst reveals that the appearance of the phantom is distinct from that of typical Brazil-law twinning. The surface of an earlier-formed amethyst crystal was apparently etched and then enclosed by subsequent crystal growth, forming the textured phantom. Photomicrograph by J. Hyršl; image width 20 mm.

parallel lines (Figure 2) that probably formed when the original amethyst crystal was etched, which was then followed by another generation of amethyst that grew over the etched surface.

Inclusions such as this are always a very pleasant surprise for the gemmologist or quartz collector.

*Dr Jaroslav Hyršl (hyrsl@hotmail.com)
Prague, Czech Republic*

Reference

Crowningshield, R., Hurlbut, C. & Fryer, C.W. 1986. A simple procedure to separate natural from synthetic amethyst on the basis of twinning. *Gems & Gemology*, **22**(3), 130–139, <https://doi.org/10.5741/gems.22.3.130>.

Colour-Change Andradite

Recently submitted to Stone Group Laboratories was a ring featuring what had been represented to the client as an alexandrite. The stone was set in a mid-century-

design diamond ring, and it displayed a weak colour change from yellowish green to orange yellow. The weak colour change and ‘mossy’ green appearance in

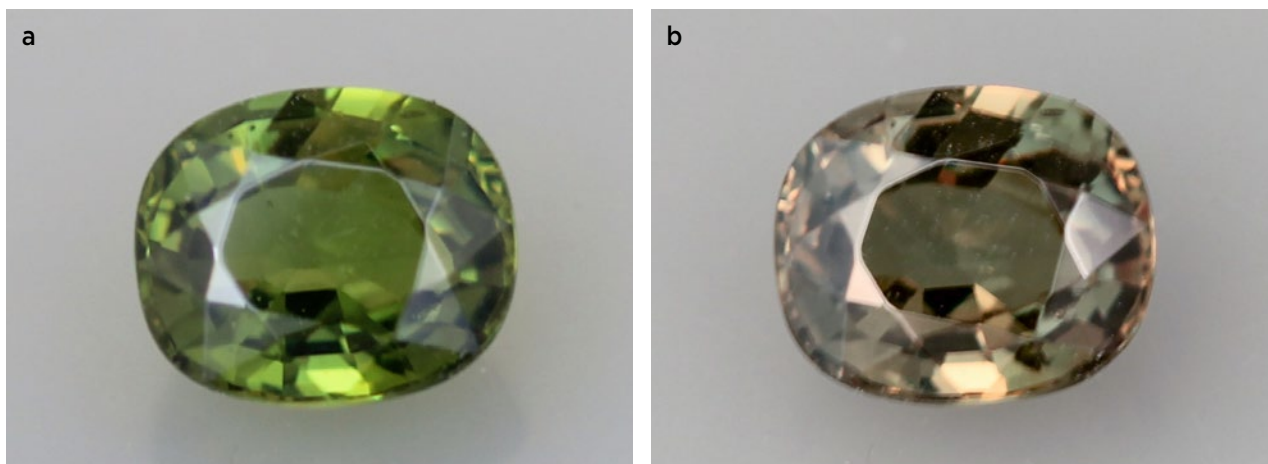


Figure 3: (a) The 3.06 ct andradite displays a yellowish green colour under daylight-equivalent illumination from a TrueColour Ott-Lite. (b) Under a standard incandescent light the stone displays a pale orangey yellow colour. Photos by B. Williams.

daylight-equivalent illumination were typical of some alexandrite, but the RI was over the limit of a standard refractometer, and the sample did not fluoresce to either long- or short-wave UV excitation, as would be expected for alexandrite. Permission was given to remove the 3.06 ct stone from the mounting in order to further analyse this unusual gem, which presumably had passed through several hands under the assumption it was alexandrite.

Under daylight-equivalent illumination the stone appeared slightly yellowish green, and it changed to a slightly brownish orangey yellow under incandescent lighting (Figure 3). Examination with a gemmological microscope showed that it was relatively clean, with only some scattered colourless crystals and small clusters of other tiny, colourless inclusions. The SG, measured hydrostatically, was 3.78.

Raman spectroscopy with a Magilabs GemmoRaman-532SG unit readily identified the stone as andradite (Figure 4), consistent with its over-the-limit RI measurement and its SG value. Although its colour appearance was suggestive of grossular-andradite from Mali, the Raman spectrum did not show the presence of a grossular component. Moderate dispersion was observed, but it was comparatively weak for andradite, possibly due to the stone's body colour, cut style, windowing or a poor finish on the cut.

Chemical analysis with an Amptek X123-SDD energy-dispersive X-ray fluorescence (EDXRF) spectrometer showed major Fe and minor Mn as possible chromophores. In addition, we detected the presence of the rare-earth element La, which is not a chromophore but has been previously reported in andradite (Pezzotta *et al.* 2011).

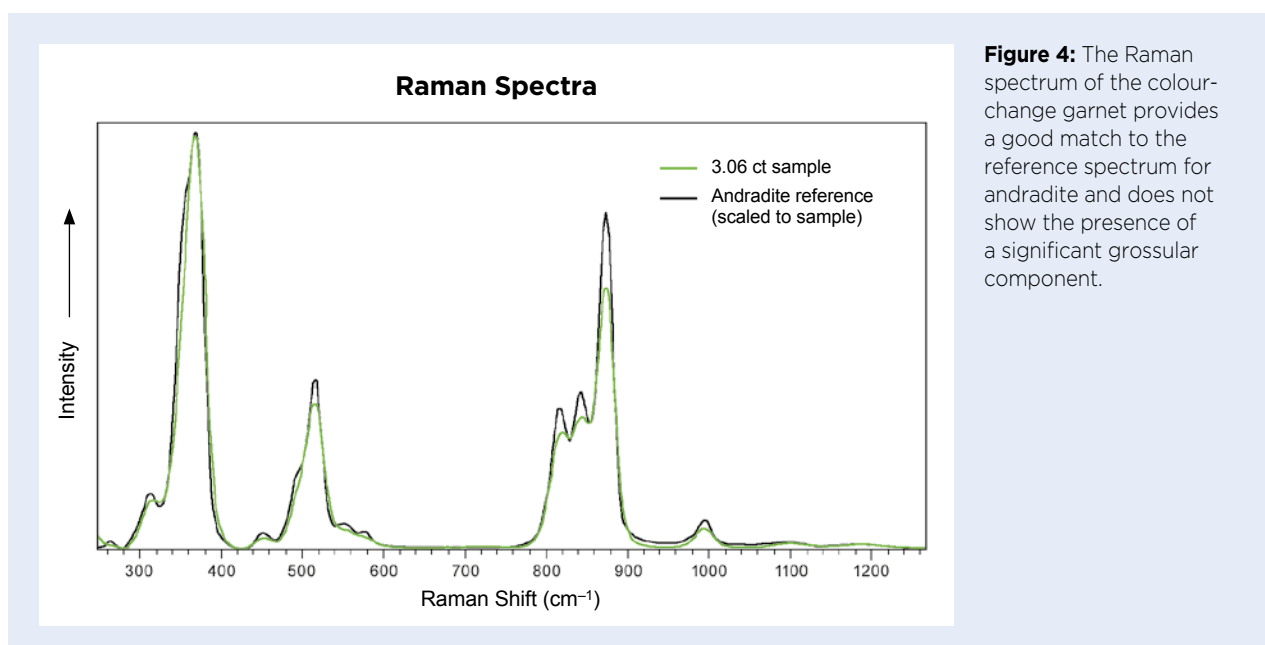


Figure 4: The Raman spectrum of the colour-change garnet provides a good match to the reference spectrum for andradite and does not show the presence of a significant grossular component.

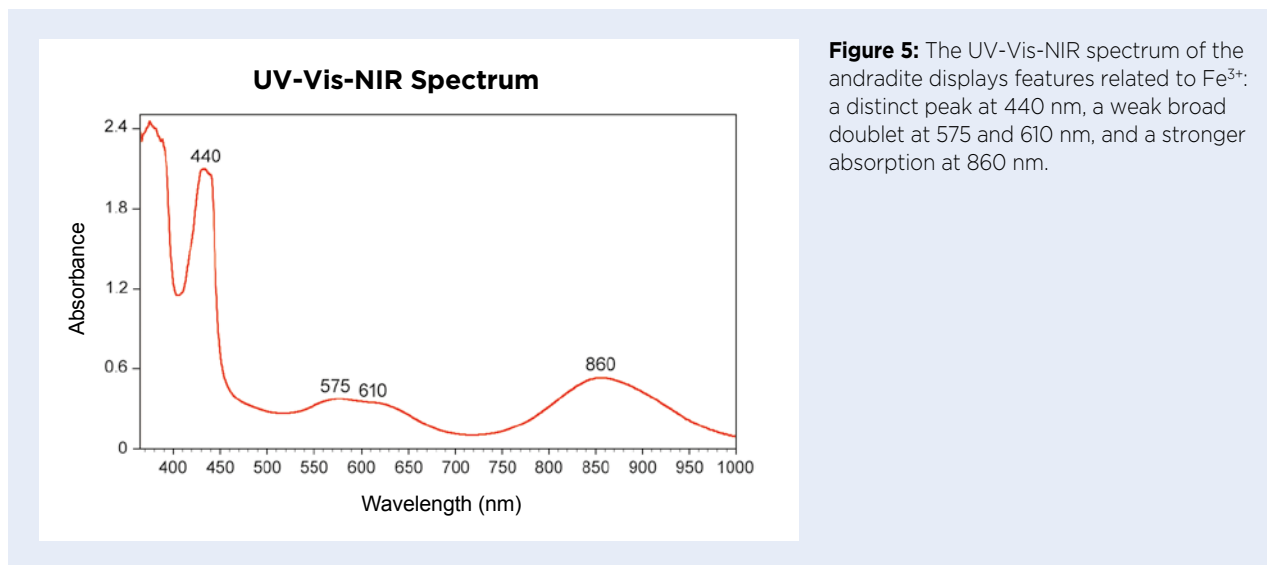


Figure 5: The UV-Vis-NIR spectrum of the andradite displays features related to Fe^{3+} : a distinct peak at 440 nm, a weak broad doublet at 575 and 610 nm, and a stronger absorption at 860 nm.

The ultraviolet-visible-near infrared (UV-Vis-NIR) spectrum of the andradite (Figure 5) obtained with a Magilabs GemmoSphere spectrometer yielded absorptions at ~440 and 860 nm due to Fe^{3+} ; in addition, a weak broad doublet at 575 and 610 nm corresponds to Fe^{3+} absorption in andradite in the 550–650 nm region (Dr George R. Rossman, pers. comm. 2021). Overall, the UV-Vis-NIR spectrum is quite similar to that of Namibian demantoid (see <http://minerals.gps.caltech.edu/FILES/Visible/Garnet/Index.html>).

Demantoid showing a significant colour shift—typically displaying a more saturated bluish green appearance in daylight—is known from Madagascar and elsewhere, and Pezzotta *et al.* (2011) proposed that trace amounts of the rare-earth elements Ce and Nd could be involved in this phenomenon. Moreover, colour-change effects are dependent on the spectral features of the particular light sources used, and with the current proliferation of LEDs, the waning popularity of fluorescent bulbs and the increased rarity of incandescent lighting,

this is a field that begs for attention and updating by the gemmological community (Williams 2007).

Although green andradite is called demantoid in the trade, the present stone was only green under certain (daylight) illumination conditions, so we refer to it as simply andradite.

Cara Williams FGA and
Bear Williams FGA
(info@stonegrouplabs.com)
Stone Group Laboratories
Jefferson City, Missouri, USA

References

- Pezzotta, F., Adamo, I. & Diella, V. 2011. Demantoid and topazolite from Antetetzambato, northern Madagascar: Review and new data. *Gems & Gemology*, **47**(1), 2–14, <https://doi.org/10.5741/gems.47.1.2>.
- Williams, B. 2007. Technology update—Ultraviolet light. *The Guide, Gem Market News*, January–February, 8–11.

Chrome Diopside from Ethiopia

In March 2021, Stone Group Laboratories received an unidentified 5.74 ct green gemstone reportedly from a new deposit in Ethiopia. It was submitted by Bennie Ulibarri, a gem cutter living in Ethiopia. He reported that this material was first seen in 2018 and he subsequently purchased a rough parcel in 2019 from local Borana miners in the Oromia Region of southern Ethiopia. Due to export limitations, only one sample was available for our examination, but Ulibarri also shared images of

rough material (Figure 6a), and of some cabochons that exhibited chatoyancy (Figure 6b).

The 5.74 ct faceted stone (Figure 7) displayed a peridot-like green colour with eye-visible inclusions and prominent pleochroism. It was readily identified as diopside by its photoluminescence spectrum recorded with a Magilabs GemmoRaman-532SG spectrometer. Gemmological characterisation showed RIs of 1.676–1.705 (birefringence 0.029) and the SG was measured



Figure 6: Chrome diopside has reportedly been found in recent years at a new deposit in Ethiopia. The diopside samples shown here include (a) a piece of rough (26 × 11 × 4 mm) and (b) a selection of cabochons (up to 10 mm long) showing chatoyancy. Photos by Bennie Ulibarri.



Figure 7: This faceted 5.74 ct chrome diopside (12.92 × 8.86 × 5.80 mm) from Ethiopia was examined for this report, and displays the potential for attractive transparent gems from this locality. Photo by C. Williams.

hydrostatically as 3.32. The stone was inert to long- and short-wave UV radiation. Pleochroism was distinct, in yellowish green and bluish green. This behaviour matches the pleochroism observed in Russian chrome diopside, suggesting that the face-up colour of the Ethiopian diopside could be improved by aligning the table perpendicular to an optic axis direction. However, this would be expected to reduce the cutting yield, and cabochons cut in this way would not exhibit chatoyancy due to the orientation of the elongated inclusions.

The most prominent inclusions consisted of rectangular negative crystals or growth tubes, all in parallel alignment (Figure 8). They showed low relief and appeared slightly whitish, giving the stone a turbid appearance. Also observed were fluid-filled ‘fingerprints’, twin planes and swirl-like liquid inclusions.

Fourier-transform infrared (FTIR) spectroscopy with a Magilabs GemmoFtir unit revealed a distinct hydroxyl (OH) band when compared to in-house samples of Russian diopside, which might be due to the more numerous fluid-filled inclusions in this sample. EDXRF spectroscopy with an Amptek X123-SDD instrument revealed prominent Fe, as well as Cr and Mn, along with traces of Sr and La. Compared to the authors’ Russian samples, the Fe in the Ethiopian sample was nearly three times higher, while the Cr concentration in the Russian material was approximately three times greater. UV-Vis-NIR spectra recorded with a Magilabs GemmoSphere unit showed similar Cr³⁺ absorptions as in Russian chrome diopside, along with a much stronger absorption in the near-infrared region due to Fe²⁺ (Figure 9).

Eastern Russia has been known for many years as the

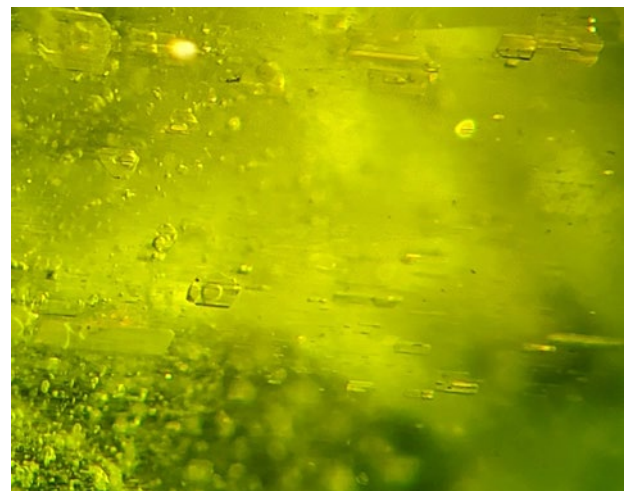


Figure 8: Prominent internal features in the stone in Figure 7 include fluid inclusions (blocky negative crystals or growth tubes in parallel alignment). Photomicrograph by B. Williams; image width 3 mm.

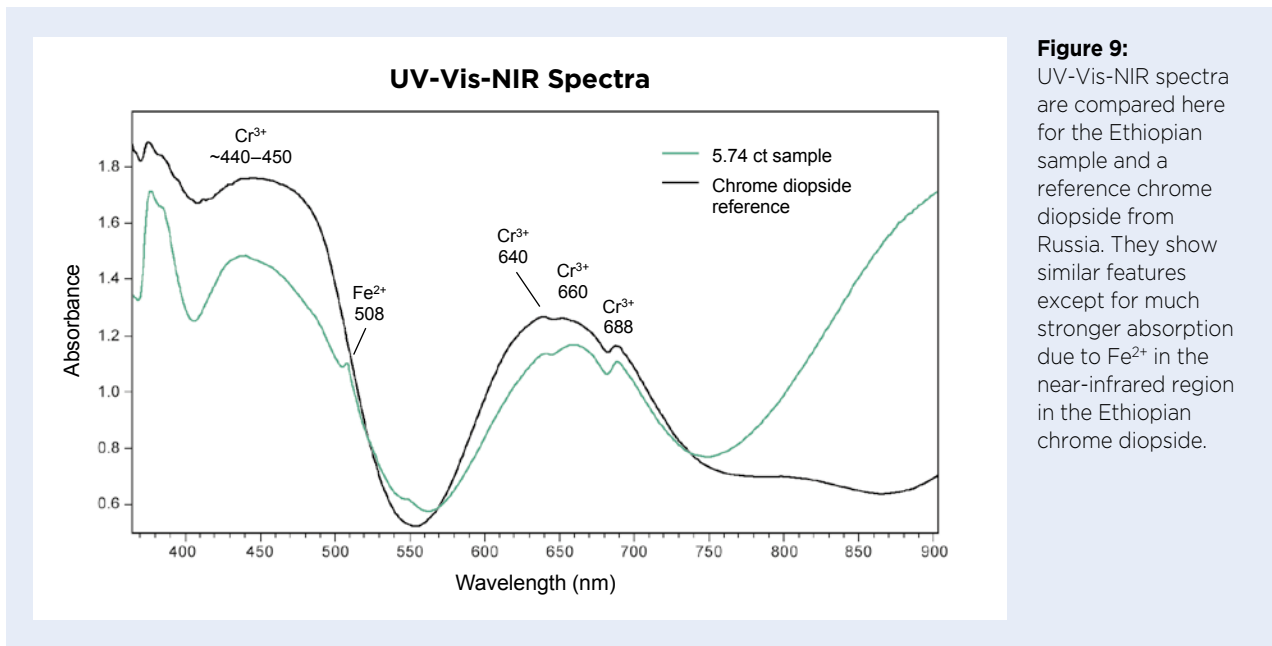


Figure 9: UV-Vis-NIR spectra are compared here for the Ethiopian sample and a reference chrome diopside from Russia. They show similar features except for much stronger absorption due to Fe^{2+} in the near-infrared region in the Ethiopian chrome diopside.

main source for gem-quality chrome diopside. We hope to see more of this attractive Ethiopian material as both faceted stones and cat's-eye gems. Based on the range of colours seen in Figure 6b, more research should be

done to confirm the presence of Cr in the various green hues of the Ethiopian diopside.

Cara Williams FGA and Bear Williams FGA

Grandidierite from Madagascar Showing Sheen and Chatoyancy

Grandidierite was first described from southern Madagascar in the early 1900s (Lacroix 1902; before it was recognised as a new mineral). Very small quantities were occasionally produced from this region until more significant finds took place starting in late 2014, from the Androy area in Tuléar Province (Laurs 2016). Although some attractive stones were faceted in recent years, gem-quality grandidierite remains exceedingly rare.

In January 2021, master faceter and gemstone artist Meg Berry (Megagem, Fallbrook, California, USA)

acquired about 1 kg of rough material from the relatively recent production of grandidierite. It appeared rather dark and displayed cross-hatched growth patterns with only small transparent areas. Berry suspected that the material might show optical effects such as chatoyancy after being polished, and in order to recognise suitable areas for cutting she carefully examined the rough using strong illumination while it was immersed in water. Initial cutting and polishing showed that properly oriented stones displayed interesting sheen and/or chatoyancy effects (e.g. Figure 10).



Figure 10: These grandidierite gems show different optical phenomena, including (a) sheen (as well as dark veining, similar in appearance to Gold Sheen sapphire), (b) chatoyancy and (c) both effects (with chatoyancy seen here). The cabochons weigh 13.96 ct (a) and 8.24 ct (b), and the carving weighs 36.85 ct (c). Courtesy of Bryan Lichtenstein (3090 Gems, San Francisco, California, USA); photos by Orasa Weldon.

So far Berry has cut approximately 40 cabochons ranging from 8.24 to 155.2 ct, as well as a few free-form carvings (up to 41.3 ct). Most of them exhibit a broad ‘flash’ of sheen when viewed in a particular orientation, and a few of the stones display a cat’s-eye effect. Rarely, both phenomena are visible in the same piece, with the chatoyancy seen at an angle of approximately 60° to the sheen.

Berry kindly donated some fragments of this grandidierite to Gem-A, and microscopic examination by the author showed that the optical phenomena are likely caused by arrays of minute reflective cleavage fractures, which is consistent with grandidierite’s good cleavage in two directions. No elongate inclusions (tubes or needles) were seen in the samples examined.

The presence of optical phenomena in this grandidierite adds interest to this rare and otherwise semi-transparent material.

Brendan M. Laurs FGA

References

- Lacroix, A. 1902. Note préliminaire sur une nouvelle espèce minérale. *Bulletin de la Société française de Minéralogie*, **25**(4–5), 85–86, <https://doi.org/10.3406/bulmi.1902.2632>.
- Laurs, B.M. 2016. Gem Notes: New production of grandidierite from Madagascar. *Journal of Gemmology*, **35**(1), 12–13.

‘Herkimer Diamond’ Quartz from North-western Iran

The term *Herkimer diamond* refers to rock crystal quartz that forms attractive, lustrous hexagonal-bipyramidal crystals hosted by sedimentary rocks that are sometimes associated with petroleum or coal deposits (and therefore may contain hydrocarbon inclusions; Walter 2014). The most famous source is Herkimer County, New York, where the crystals are found in vugs and fractures within the Little Falls Dolostone, which was deposited during the Late Cambrian. Other names for this quartz include *Middleville diamonds* (named after the town of Middleville, New York, USA), *Mohawk Valley crystals* (after the valley in Herkimer County, New York) and *Little Falls diamonds* (after the rock formation that hosts the mineralisation). Herkimer-type quartz is also known

from Tyrol, Austria; Tuscany, Italy; Northern Cape, South Africa; and other locations worldwide (Strasser 2007).

The present authors are also aware of some localities for Herkimer-type quartz in the north-western Zagros Mountains: Kermanshah and Kurdistan provinces of north-western Iran, and the Kurdistan Region of northern Iraq. Although Herkimer-type quartz from the Zagros Mountains has occasionally been used in traditional jewellery for hundreds or perhaps thousands of years, it was not ‘rediscovered’ in modern times until around 2014. The crystals are hosted by cavities and fractures within carbonate rocks (e.g. Figure 11), and for this report the authors studied about 0.5 kg of the quartz from the Jurassic-age Surmeh Formation (hosted by dolomitic limestone) and from two formations of the Cretaceous-age Bangestan Group (the Sarvak chert-bearing limestone and the Ilam limestone; Aghanabati 2004).

The crystals ranged from 0.1 to 50 mm in maximum dimension and could be divided into two groups: those that were mostly gem-quality (one third of them) and non-gem samples (the other two thirds; e.g. Figure 12). Overall, only 10% of the crystals were



Figure 11: This dolomitic limestone in north-western Iran hosts Herkimer-type quartz crystals. Photo by Mokhtar Sobhani.

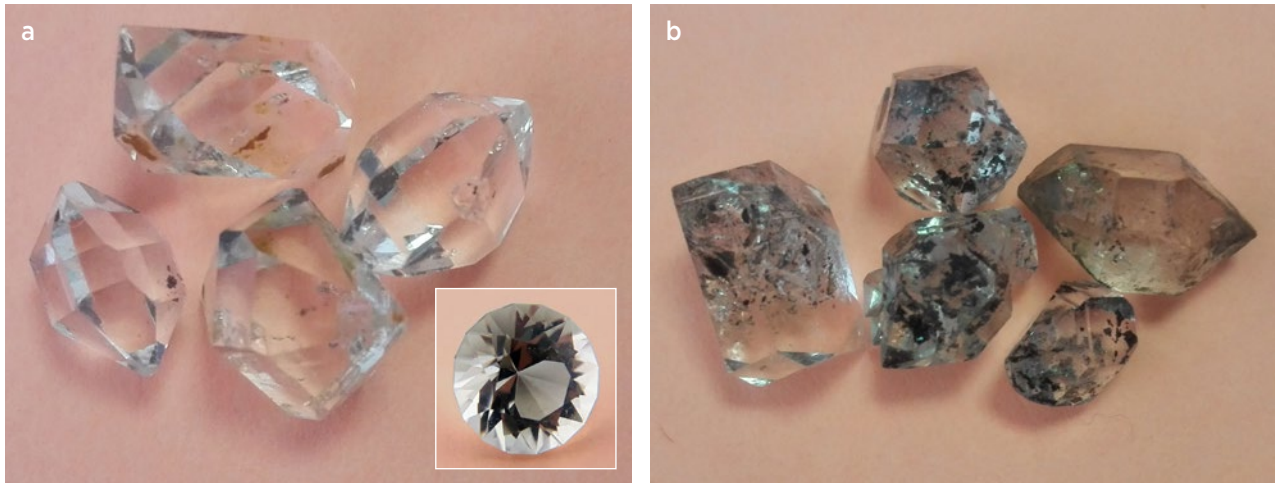


Figure 12: Herkimer-type quartz from north-western Iran occurs as (a) gem-quality crystals that are suitable for faceting and (b) non-gem samples containing abundant inclusions. The samples in (a) are 8–12 mm long (and the faceted stone in the inset weighs 3 ct), while the crystals in (b) are 6–12 mm in maximum dimension. Crystal photos by B. Rahimzadeh; inset photo by Arash Badamegan.

cuttable due to the common presence of numerous dark inclusions (probably kerogen, a solid insoluble organic substance from sedimentary rocks), as well as colourless primary fluid inclusions and fractures (Figures 12 and 13). Microscopic and fluid inclusion studies showed the presence of two phases in the fluid inclusions—a vapour and an aqueous liquid—without a liquid petroleum phase such as commonly seen in Herkimer-type quartz from Pakistan (Koivula & Tannous 2004; Laurs 2016). In addition, the fluid inclusions contained small dark particles that were probably kerogen. Our fluid inclusion study showed that the crystals formed at pressures of 1–2 atmospheres and temperatures of 80–120°C.

Compared to Herkimer-type quartz from Pakistan

(Koivula & Tannous 2004; Laurs 2016), the Zagros Mountain crystals are slightly smaller. Also, the organic material in the present quartz consists of black solids (inferred as kerogen), whereas in the Pakistan crystals it is formed mainly of liquid petroleum (with minor solid asphaltite). These inclusion variations may relate to differences in the formation temperatures of the quartz from these two deposits.

*Dr Bahman Rahimzadeh
(b_rahimzadeh@sbu.ac.ir)
and Parisa Hadipanah*

*School of Earth Sciences and Gemology Center
Shahid Beheshti University, Tehran, Iran*

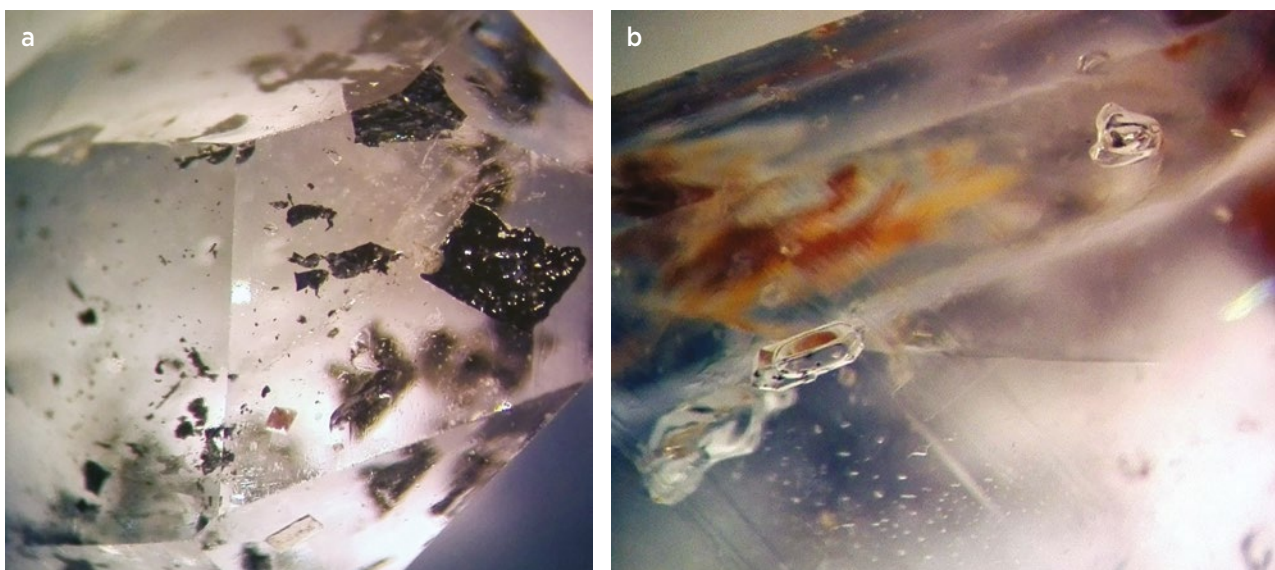


Figure 13: Common inclusions in the Herkimer-type quartz consist of (a) dark hydrocarbon masses (probably kerogen) and (b) primary two-phase (liquid and vapour) fluid inclusions. Photomicrographs by B. Rahimzadeh; magnified 10×.

References

- Aghanabati, A. 2004. *The Geology of Iran*. Geological Survey of Iran, Tehran, Iran, 586 pp.
- Koivula, J.I. & Tannous, M. 2004. Gem News International: Petroleum inclusions in quartz from Pakistan: A photoessay. *Gems & Gemology*, **40**(1), 79–81.
- Lauris, B. 2016. Gem Notes: Faceted quartz with petroleum inclusions from Baluchistan, Pakistan. *Journal of Gemmology*, **35**(1), 15.
- Strasser, M. 2007. Herkimer Quarze aus der Ehnbchklamm in Zirl, Tirol. *Lapis*, **32**(5), 23–24.
- Walter, M.R. 2014. *The Collector's Guide to Herkimer Diamonds*. Schiffer Publishing Ltd, Atglen, Pennsylvania, USA, 96 pp.

Hematite Inclusions in Red Trapiche Quartz from Inner Mongolia

Trapiche quartz and various gems with trapiche-type growth patterns have attracted a lot of attention from gemmologists since the 1990s. Trapiche structure was first defined for emerald, but the appellation has been extended in recent years to minerals such as corundum, tourmaline, pezzottaite and, more recently, quartz.

During the February 2017 gem shows in Tucson, Arizona, USA, Denis Gravier (Gravier & Gemmes, Poncin, France) displayed rough and cut specimens of trapiche quartz from Inner Mongolia, some of which contained conspicuous red inclusions (e.g. Figure 14). Similar slabs of trapiche quartz associated with black hematite inclusions were previously reported as coming from the Huanggang Fe-Sn deposit near Chifeng city in Inner Mongolia, China (Lauris 2016).

In the samples examined for this report, the red inclusions were concentrated towards the termination of the quartz crystal, and the trapiche pattern evolved from a typical whitish to greyish quartz pattern to one highlighted with red (as seen in the two polished slabs in Figure 14). The very tip of the crystal was simply red

without any zoning, and was fashioned as the cabochon on the far right in Figure 14. Examination of this sample with the microscope showed many bright red, mostly curved fibres that were distributed relatively homogeneously throughout the quartz. They sometimes formed brush-like bunches originating from a common, thicker base (Figure 15a). On rare occasions, they formed a loop (see centre of Figure 15b). These characteristics do not resemble those seen in any inclusions previously described in quartz (see, e.g., Hyršl & Niedermayr 2003). The extent and distribution of these inclusions indicated they were the cause of the red colour in the quartz.

To identify the fibrous mineral, and therefore elucidate the cause of the red colour in this quartz, we used a Jobin Yvon T64000 dispersive Raman spectrometer coupled to an Olympus microscope, together with a 514 nm argon-ion laser and a 100× objective, resulting in a power of about 15 mW on the sample. As the fibres were very thin, the confocal mode was implemented on the thickest inclusions to limit the Raman signal from the surrounding quartz. The resulting spectrum showed peaks associated



Figure 14: Three samples were cut from a trapiche quartz crystal from Inner Mongolia to illustrate the variation of the internal pattern and increasingly red colour towards the termination of the crystal. The base of the crystal is shown on the left, with two polished slabs and a red cabochon (1.8 cm long) on the right. Photo by Denis Gravier.

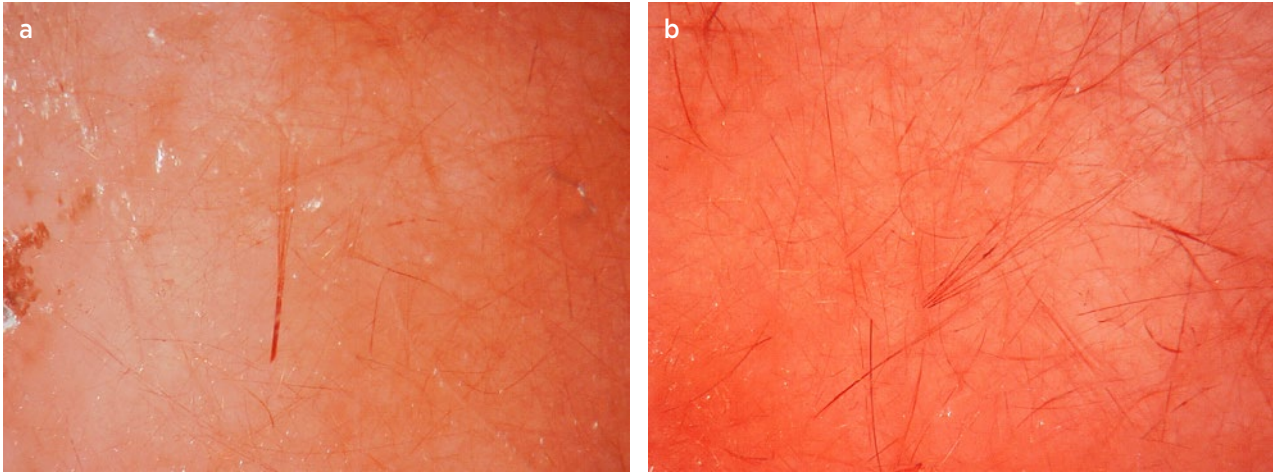


Figure 15: (a) The red colour of the quartz is due to abundant thin, hair-like hematite inclusions, sometimes grouped in bunches. (b) The hematite inclusions locally form loop-shaped (centre) and curved fibres in the quartz. Photomicrographs by E. Fritsch; image widths 2 mm.

with the fibres in addition to those of the quartz matrix (Figure 16). The additional peaks fit nicely with the five major vibration modes of hematite at about 220, 246, 292, 412 and 613 cm^{-1} . Thus, these unusual inclusions are a rare morphology of hematite (Fe_2O_3), which is otherwise a very common inclusion in quartz (Hyršl & Niedermayr 2003) and in many other gems.

Fibrous crystals or ‘whiskers’ (Sunagawa 2005) are the result of unusual growth conditions, not entirely elucidated, sometimes even resulting in coiled crystals (Sunagawa *et al.* 2004). In quartz, such morphologies have been identified for inclusions of rutile (Sunagawa 2005) and tremolite (Gübelin & Koivula 2005). Fibrous

hematite is rare, and to this author’s knowledge natural whisker-like crystals of hematite have not been observed previously in quartz. Those produced artificially by a chemical process were comparatively very short (about 1 μm) and straight, and were observable only with a scanning electron microscope (Gaballah *et al.* 1978; Song & Pistorius 2019). Thus, the red trapiche quartz from Inner Mongolia contains a new morphology of hematite inclusions, whether in quartz or in other gems.

Dr Emmanuel Fritsch FGA
(emmanuel.fritsch@cnr-immn.fr)

IMN-CNRS and University of Nantes, France

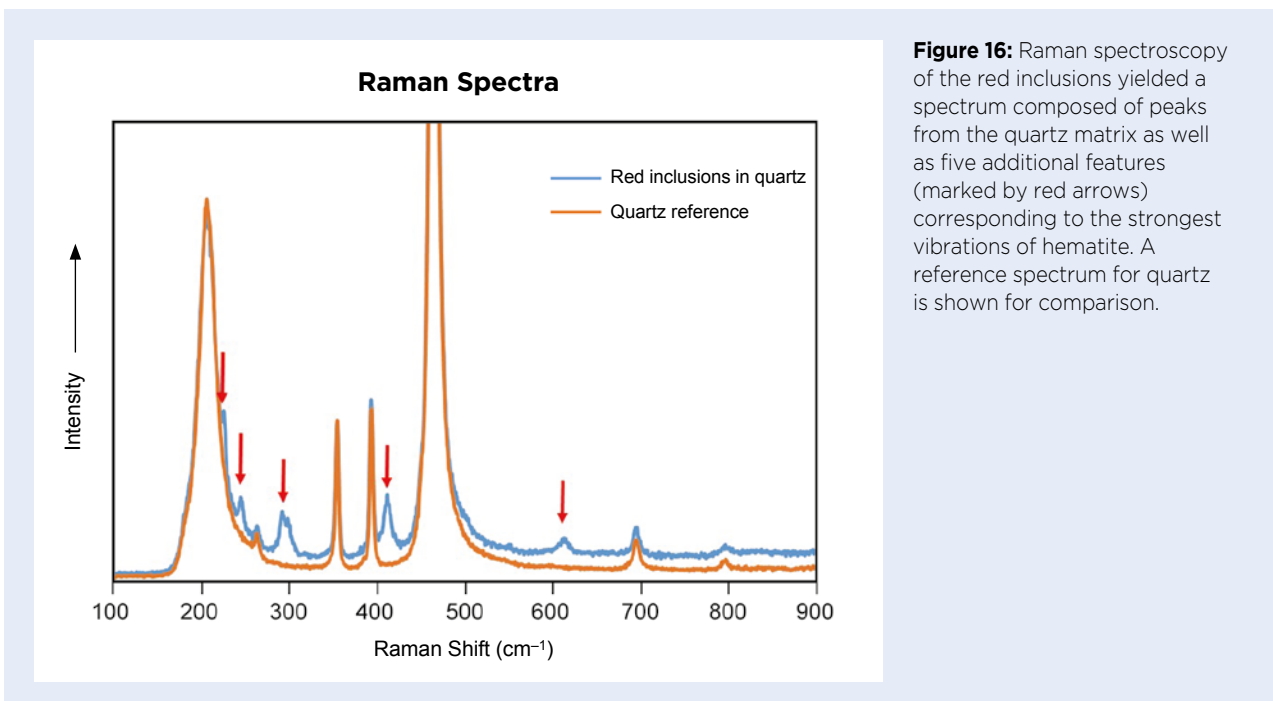


Figure 16: Raman spectroscopy of the red inclusions yielded a spectrum composed of peaks from the quartz matrix as well as five additional features (marked by red arrows) corresponding to the strongest vibrations of hematite. A reference spectrum for quartz is shown for comparison.

References

- Gaballah, I., Raghy, S.E. & Gleitzer, C. 1978. Oxidation kinetics of fayalite and growth of hematite whiskers. *Journal of Materials Science*, **13**(9), 1971–1976, <https://doi.org/10.1007/bf00552904>.
- Gübelin, E.J. & Koivula, J.I. 2005. *Photoatlas of Inclusions in Gemstones*, Vol. 2. Opinio Publishers, Basel, Switzerland, 829 pp.
- Hyršl, J. & Niedermayr, G. 2003. *Magic World: Inclusions in Quartz*. Bode Verlag, Haltern, Germany, 240 pp.
- Laurs, B. 2016. Gem Notes: Quartz slabs from Inner Mongolia. *Journal of Gemmology*, **35**(1), 15–16.
- Song, S. & Pistorius, P.C. 2019. Formation of hematite whiskers during magnetite concentrate oxidation. *ISIJ International*, **59**(10), 1765–1769, <https://doi.org/10.2355/isijinternational.ISIJINT-2018-755>.
- Sunagawa, I. 2005. *Crystals: Growth, Morphology and Perfection*. Cambridge University Press, Cambridge, 308 pp.
- Sunagawa, I., Jobbins, E.A. & Tinnyunt, E. 2004. Coiled ‘rutile’ whiskers in a quartz single crystal. *Journal of Gemmology*, **29**(1), 1–7, <https://doi.org/10.15506/JoG.2004.29.1.1>.

Blue Persistent Luminescence (Phosphorescence) of Sodalite

Sodalite is an aluminosilicate with various luminescence properties often caused by the substitution of a small amount of chlorine by other ions. For example, the well-known orange luminescence of sodalite is caused by S_2^- replacing Cl^- (Colinet *et al.* 2020). Red and green luminescence in sodalite have been ascribed, respectively, to Fe^{3+} and Mn^{2+} (Van Doorn & Schipper 1971; Kaiheriman *et al.* 2013). Recently, blue ‘phosphorescence’ (persistent luminescence) was described in synthetic hackmanite (Norrbo *et al.* 2015). We prefer the term *persistent luminescence* (PeL), rather than *phosphorescence*, because it corresponds better to the electronic processes found in gems and in many other inorganic materials (Holsa 2009).

In the course of our study of the photochromic effect in sodalite (hackmanite variety), we recently came across two samples that showed persistent blue luminescence (with a duration of about 4 s, as seen by the human eye). These consisted of a colourless faceted 0.84 ct sodalite and a 0.17 g rough specimen of hackmanite, both of which displayed distinct blue PeL (Figure 17) after exposure to short-wave UV (254 nm) radiation. They also fluoresced orange to long-wave UV (365 nm) due to S_2^- .

The corresponding emission and excitation spectra collected with a Horiba Jobin Yvon Fluorolog-3 spectrometer are presented in Figure 18. The PeL was best seen in the samples with 308 nm excitation (see below), and the resulting emission spectrum displayed a large band with two apparent maxima at about 440 and 456 nm (marked as 450 nm in Figure 18). In the colourless sodalite, an additional band at 520 nm broadens the range of its emission, making it closer to ‘white light’. Nevertheless, the overall luminescence colour of this

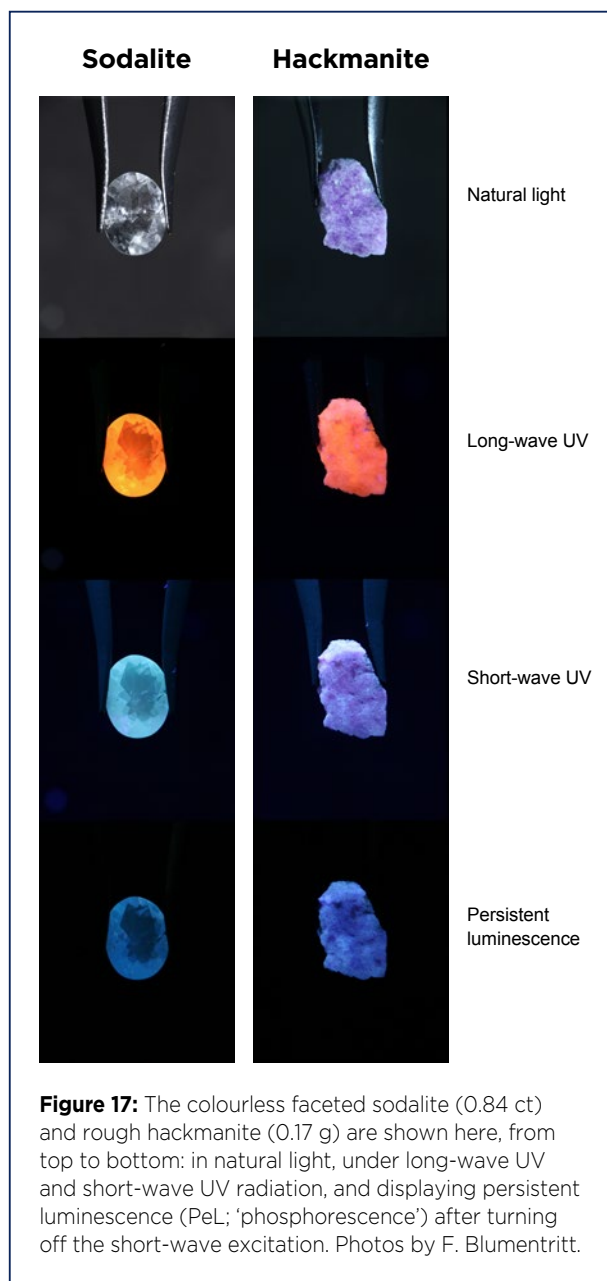


Figure 17: The colourless faceted sodalite (0.84 ct) and rough hackmanite (0.17 g) are shown here, from top to bottom: in natural light, under long-wave UV and short-wave UV radiation, and displaying persistent luminescence (PeL; ‘phosphorescence’) after turning off the short-wave excitation. Photos by F. Blumentritt.

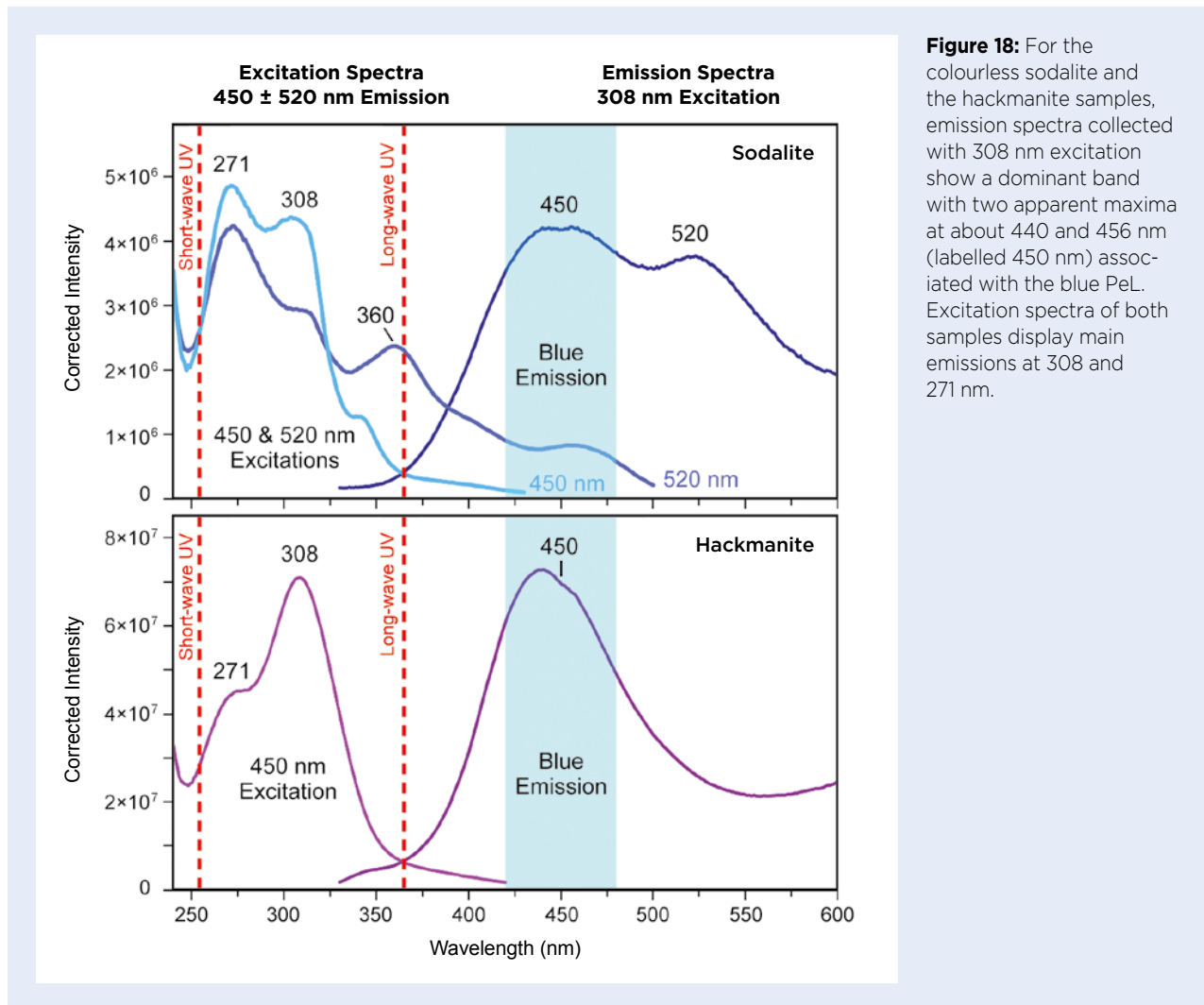


Figure 18: For the colourless sodalite and the hackmanite samples, emission spectra collected with 308 nm excitation show a dominant band with two apparent maxima at about 440 and 456 nm (labelled 450 nm) associated with the blue PeL. Excitation spectra of both samples display main emissions at 308 and 271 nm.

sodalite remains a greenish blue when exposed to short-wave UV radiation. Excitation spectra were measured for the 450 nm emission for both samples, and additionally for the 520 nm emission for the colourless sodalite in accordance with its two emission bands. The spectra of both samples showed dominant excitation features at about 271 and 308 nm.

Charge and decay curves for the blue luminescence in the two samples were recorded by measuring the 450 nm emission during continuous 310 nm excitation (Figure 19). As is typical for PeL in general, the intensity of the blue luminescence increased progressively during excitation, reaching a maximum after about 10 s. Once the excitation was turned off, the measured decay time could be adequately fitted only with two exponential functions corresponding to about 1 and 6 s. Decay times on the order of a second can be easily perceived by the human eye, and thus this emission would be described by gemmologists as phosphorescence. The advantage of the measurement is to quantify (in a non-trivial fashion)

the overall decay so it becomes observer independent.

Blue persistent luminescence in synthetic sodalite was compared to some natural, rough samples by Agamah *et al.* (2020). These authors proposed titanium (Ti^{3+}) in a very unusual tetrahedral coordination as the emitting centre. However, they did not find any clear correlation between Ti concentration and the intensity of blue PeL in the natural samples.

In our study, laser ablation inductively coupled plasma mass spectrometry revealed trace amounts of Ti in both samples. We measured about 5 ppm Ti in the colourless sodalite and 120 ppm Ti in the hackmanite, which is qualitatively consistent with the PeL intensity of each stone. However, we propose that their PeL could have multiple origins, given our data and other studies. Titanium could be involved as a titanate group (a classical origin of blue short-wave UV luminescence). However, europium (Gaft *et al.* 2015; not detected in our samples), oxygen (O^{2-} ; Van Doorn & Schipper 1971) and sulphur (Chang & Onton 1973) are also likely

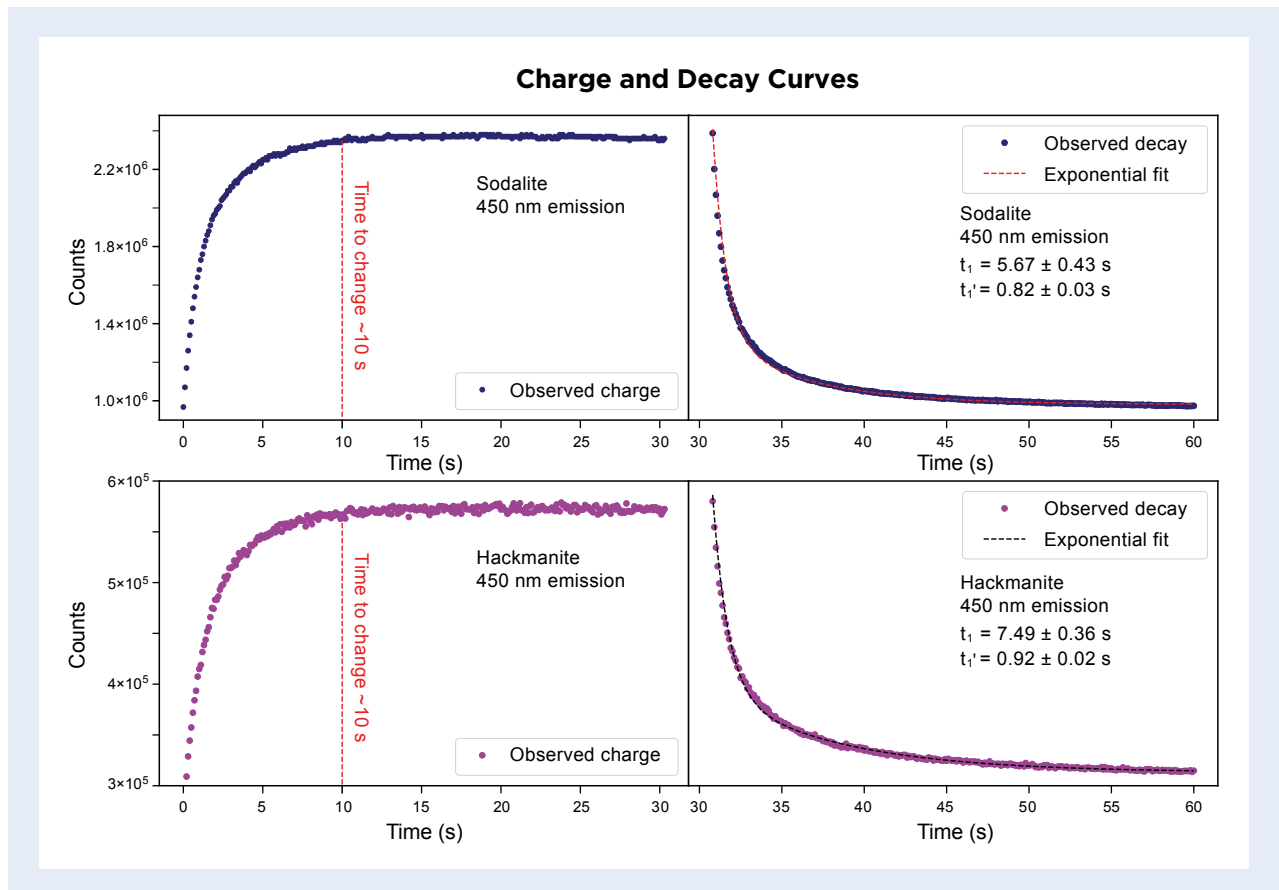


Figure 19: Charge (left) and decay (right) curves are shown for the colourless sodalite and the hackmanite. The charge curve indicates that the intensity of the blue luminescence reaches a maximum after about 10 s. The fit of the decay curve includes a combination of two exponential functions, corresponding to decay times of about 1 and 6 s.

candidates, especially because oxygen and sulphur were also present in both our samples (1500 and 1200 ppm S in the colourless sodalite and hackmanite, respectively). An electron trap must be involved to produce persistent phenomena. Oxygen vacancies have been proposed previously (Agamah *et al.* 2020), but their relation to PeL remains to be demonstrated.

Thus, we confirm the possibility that the blue PeL could be linked to titanium, as previously published in the literature, but based on our data we also propose

that other elements such as sulphur and oxygen could lead to the same PeL behaviour in sodalite. Further analyses and comparisons are currently underway with synthetic sodalites of controlled chemical composition that present the same blue PeL.

*Féodor Blumentritt, Maxence Vigier and
Dr Emmanuel Fritsch FGA
(emmanuel.fritsch@cnrs-imn.fr)
IMN-CNRS and University of Nantes, France*

References

- Agamah, C., Vuori, S., Colinet, P., Norrbo, I., de Carvalho, J.M., Okada Nakamura, L.K., Lindblom, J., van Goethem, L. *et al.* 2020. Hackmanite—The natural glow-in-the-dark material. *Chemistry of Materials*, **32**(20), 8895–8905, <https://doi.org/10.1021/acs.chemmater.0c02554>.
- Chang, I.F. & Onton, A. 1973. Optical properties of photochromatic sulfur-doped chlorosodalite. *Journal of Electronic Materials*, **2**(1), 17–46, <https://doi.org/10.1007/bf02658102>.
- Colinet, P., Gheeraert, A., Curutchet, A. & Le Bahers, T. 2020. On the spectroscopic modeling of localized defects in sodalites by TD-DFT. *Journal of Physical Chemistry C*, **124**(16), 8949–8957, <https://doi.org/10.1021/acs.jpcc.0c00615>.
- Gaft, M., Reisfeld, R. & Panczer, G. 2015. Luminescent minerals. In: *Modern Luminescence Spectroscopy of Minerals and Materials*, 2nd edn. Springer, Cham, Switzerland, 45–219, https://doi.org/10.1007/978-3-319-24765-6_4.

Holsa, J. 2009. Persistent luminescence beats the afterglow: 400 years of persistent luminescence. *Electrochemical Society Interface*, **18**(4), 42–45, <https://doi.org/10.1149/2.F06094IF>.

Kaiheriman, M., Maimaitinaisier, A., Rehiman, A. & Aierken, S. 2013. Photoluminescence properties of green and red luminescence from natural and heat-treated sodalite. *Physics and Chemistry of Minerals*, **41**(3), 227–235, <https://doi.org/10.1007/s00269-013-0634-0>.

Norrbo, I., Gluchowski, P., Paturi, P., Sinkkonen, J. & Lastusaari, M. 2015. Persistent luminescence of tenebrescent $\text{Na}_8\text{Al}_6\text{Si}_6\text{O}_{24}(\text{Cl},\text{S})_2$: Multifunctional optical marker. *Inorganic Chemistry*, **54**(16), 7717–7724, <https://doi.org/10.1021/acs.inorgchem.5b00568>.

Van Doorn, C.Z. & Schipper, D.J. 1971. Luminescence of O_2^- , Mn^{2+} and Fe^{3+} in sodalite. *Physics Letters A*, **34**(3), 139–140, [https://doi.org/10.1016/0375-9601\(71\)90792-4](https://doi.org/10.1016/0375-9601(71)90792-4).

A Roman Ring Set With a Turquoise

One puzzle from the ancient Mediterranean world is why there are not more examples of jewellery set with turquoise. The mines of the Sinai Peninsula and Iran are well known today, and we are aware that the Sinai mines were worked in antiquity by the Egyptians because there are texts telling us so (Aston *et al.* 2000, pp. 62–63; Mansour 2014). There is some surviving ancient Egyptian jewellery set with turquoise, but perhaps not as much as we might expect. When it comes to Greek and Roman jewellery, however, turquoise is noticeably absent. The present author knows of very few examples of turquoise set in ancient jewellery (for a discussion of this, see Ogden 1982, pp. 112–113).

This justifies documenting the ring shown in Figure 20. It has been in a private collection for some 40 years since the author first saw and illustrated it (in black and white; Ogden 1982, figure 5.13). Recently, the author had an opportunity to re-examine this ring and take better photos. It dates to around the first century AD, and is probably from the Eastern Roman Empire, quite possibly Asia Minor, in what is now Turkey. It is small—20.5 mm

across—and quite delicate. The low-cabochon turquoise is oval shaped and measures 7.9×4.9 mm. The ring itself is hollow, the gold being a thin sheet. This elegant, hollow form was popular in the early Roman world, but it is still unclear how such metalwork was formed. It is almost certainly filled, as was usual for Roman jewellery, with sulphur, which acted as both a support for the thin gold and a bedding for the gem (Ogden 1982, p. 40).

The gem was previously identified as turquoise based only on its visual appearance. This has now been confirmed by portable EDXRF analysis using an Oxford Instruments X-MET8000 unit, which revealed that the primary elements present were Cu, Al and P. Turquoise is a hydrated phosphate of copper and aluminium, with the theoretical chemical formula $\text{CuAl}_6(\text{PO}_4)_4(\text{OH})_8 \cdot 4\text{H}_2\text{O}$. In practice, Zn often replaces some of the Cu, and in this case traces of Zn were detected, as well as significant Fe and a small amount of As.

Recent research has shown the potential for determining turquoise sources on the basis of relative Fe, As and Zn contents (Carò *et al.* 2017; Mousavipak 2020).



Figure 20: Two views are shown of an early Roman ring (20.5 mm across) in thin sheet gold set with an oval turquoise cabochon. Private collection; photos by J. Ogden.

In this case, measuring the chemical composition of the turquoise with EDXRF was complicated by the relatively large beam diameter (about 3 mm), and precise analysis of small cabochons is difficult because of their surface topology and the inevitable analytical overlap with the metal setting. Nevertheless, even allowing for a reasonable margin of error, the proportions of Fe, Zn and As suggested that the gem's composition is consistent with an Iranian origin.

This certainly shows the potential for portable EDXRF technology for gem research, as long as its limitations are understood. It is hardly surprising that such instrumentation is increasingly being used in archaeogemmology, alongside the typically slightly less-portable Raman spectroscopy. Portable EDXRF analysis is non-invasive and can quickly identify the elements present (i.e. Na and heavier), which is usually sufficient to confirm the identity of a gem and in some cases make further deductions.

*Dr Jack M. Ogden FGA (jack@striptwist.com)
London*

References

- Aston, B.G., Harrell, J.A. & Shaw, I. 2000. Stone. In: Nicholson, P.T. & Shaw, I. (eds) *Ancient Egyptian Materials and Technology*. Cambridge University Press, Cambridge, 5–77.
- Carò, F., Schorsch, D. & Santarelli, B. 2017. Proveniencing turquoise artifacts from ancient Egyptian contexts: A non-invasive XRF approach. *Science of Ancient Egyptian Materials and Technologies (SAEMT) Conference*, Cairo, Egypt, 4–6 November, poster presentation.
- Mansour, A.M.A. 2014. *Turquoise in Ancient Egypt: Concept and Role*. British Archaeological Reports International Series 2602, BAR Publishing, Oxford, 124 pp., <https://doi.org/10.30861/9781407312347>.
- Mousavipak, N. 2020. *Physico-chemical characterization of Iranian turquoises: A tentative [sic] to trace Middle-Eastern turquoise-bearing artifacts*. PhD thesis, University of Lyon, France, 128 pp.
- Ogden, J. 1982. *Jewellery of the Ancient World*. Trefoil, London, 185 pp.

SYNTHETICS AND SIMULANTS

Near-Colourless HPHT-grown Synthetic Diamonds that Test as Synthetic Moissanite

Colourless diamond is an electrical insulator, whereas synthetic moissanite is a semiconductor of electricity. This difference is used by diamond testers that separate these similar-looking materials based on electrical conductivity. This conductivity occurs in diamonds that contain boron as a minor impurity within their crystal structure. Boron is also responsible for causing blue colour in diamond. In synthetic diamonds grown by the high-pressure, high-temperature (HPHT) technique, the boron impurities are due to the addition of boron oxide to the growth chamber during synthesis, possibly to reduce the pressures required. Approximately 70% of all colourless HPHT-grown synthetic diamonds contain traces of boron (see figure 15 of Eaton-Magaña *et al.* 2017). The concentration of boron in those samples is so low that it has little to no effect on colour. About 25% of HPHT synthetic diamonds exhibit a subtle blue hue, equivalent to G colour and below. This blue hue is termed a 'blue nuance' by some laboratory-grown-diamond retailers and grading laboratories. Nearly 80% of HPHT synthetic diamonds with this subtle blue hue

exhibit electrical conductivity (see table 1 of D'Haenens-Johansson *et al.* 2014). This behaviour seems to be limited to those that contain enough boron to subtly impact colour. There have been no reports of colourless HPHT synthetic diamonds equivalent to D–F colour grades exhibiting electrical conductivity.

Author JG recently highlighted the fact that some HPHT-grown synthetic diamonds may be identified as synthetic moissanite on diamond testers due to their electrical conductivity (Faulkner 2021). To investigate this further, author HD organised a preliminary study in which four HPHT synthetic diamonds (see Figure 21 and Table I) were tested with various diamond multi-testers. Each sample was accompanied by a laboratory-grown-diamond report from the International Gemological Institute (IGI). The samples weighed 1.01–1.31 ct and had clarity grades of VS₂ and above. One exhibited a yellow tint (equivalent to K colour, according to author HD's observations), while the other three appeared near-colourless (equivalent to a G–H colour grade) when viewed from the face-up position but showed extremely

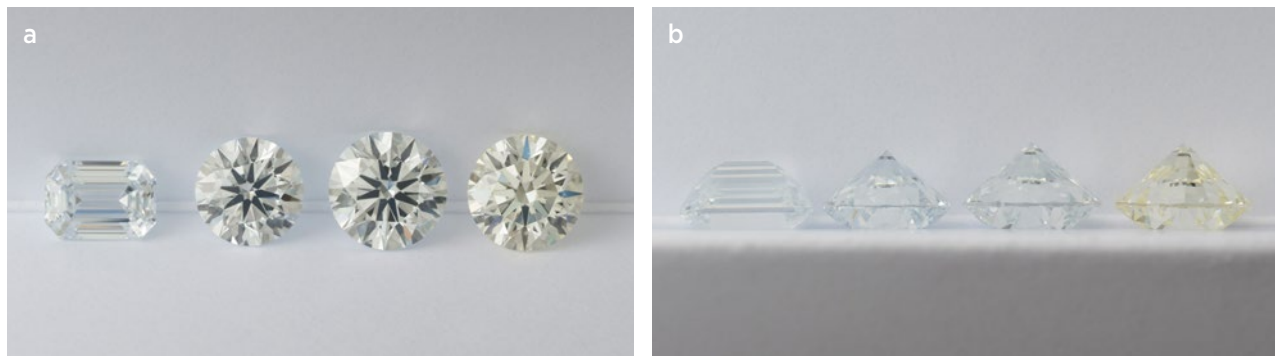


Figure 21: The four HPHT-grown synthetic diamonds tested in this preliminary study are shown here (a) face-up and (b) from the side. From left to right, they are 1.01 ct (faint blue), 1.01 ct (faint blue), 1.31 ct (equivalent to G colour with a 'blue nuance') and 1.26 ct (pale yellow, equivalent to K colour). See Table I for additional details. Photos courtesy of Stuller.

pale blue colour when observed from the side (again, see Figure 21). Such low colour saturation was difficult to discern without the use of master stones in a proper colour-grading environment. The blue tints were noted on the accompanying diamond reports as either a 'Faint blue' colour grade or as a 'blue nuance' as a comment on the report (see Table I footnote).

Room-temperature FTIR absorption spectra were collected using a Magilabs GemmoFtir unit to detect uncompensated boron, which is identified by a characteristic absorption band centred at 2800 cm^{-1} , as well as a weaker band at 4092 cm^{-1} . Electrical conductivity was tested using five different models of diamond multi-testers, which all test for both thermal and electrical conductivity: three from Presidium (Adamas, SAM and Multi TesterIII) and two from Gemoro (Testerossa and UltraTester 3+). Each sample was tested three times with each device.

The infrared spectrum of the yellow-tinted sample indicated no detectable boron, and this sample was correctly identified as 'diamond' on all five diamond testers. Boron was detected in the IR spectra of the other three samples, including the G-colour stone with no obvious faint blue tint when viewed face-up. All of these samples were incorrectly identified as 'moissanite' by each of the diamond testers.

These results further document that near-colourless HPHT synthetic diamonds behave as semiconductors when they contain traces of boron and exhibit a subtle blue hue. Further study is required to test the behaviour on diamond testers of HPHT synthetic diamonds equivalent to D–F grades that contain minute traces of boron.

This information is particularly key for those who buy second-hand jewellery directly from the consumer and use diamond testers to help identify colourless gems. To avoid misidentification, it is advisable to perform further

Table I: HPHT-grown synthetic diamond samples tested for this study.

Blue tint	Yes	Yes	Yes	No
Colour-grade equivalent*	Faint Blue	Faint Blue	G (with 'blue nuance')	K (slightly yellow)
Weight (ct)	1.01	1.01	1.31	1.26
Clarity	VS ₁	VVS ₂	VS ₁	VS ₂
Shape/cut	Emerald cut	Round brilliant	Round brilliant	Round brilliant
Boron detected by IR?	Yes	Yes	Yes	No
Test results	'Moissanite'	'Moissanite'	'Moissanite'	'Diamond'

* The equivalent colour grades are shown as listed on IGI reports (dated December and October 2020 for the 1.26 and 1.31 ct samples and September 2015 for both 1.01 ct samples). Initially, IGI's standard practice was to grade such pale-coloured samples in a similar fashion as fancy-colour diamonds by assigning them descriptive colour grades. More recently, this practice was superseded by assigning an individual letter grade from D to Z and adding the phrase 'blue nuance' to the comment section.

tests and observations (such as checking for single vs double refraction and observing UV fluorescence and phosphorescence) on all samples that give a ‘moissanite’ result with such testers.

Acknowledgements: We thank the members of the Diamonds and Tools departments at Stuller, who participated in assembling the sample set and performed the testing.

*Julia Griffith FGA DGA (julia@thegemac.com)
The Gem Academy, Online Education, UK*

*Harold Dupuy FGA
Stuller, Lafayette, Louisiana, USA*

References

- D’Haenens-Johansson, U.F.S., Moe, K.S., Johnson, P., Wong, S.Y., Lu, R. & Wang, W. 2014. Near-colorless HPHT synthetic diamonds from AOTC Group. *Gems & Gemology*, **50**(1), 30–45, <https://doi.org/10.5741/gems.50.1.30>.
- Eaton-Magaña, S., Shigley, J.E. & Breeding, C.M. 2017. Observations on HPHT-grown synthetic diamonds: A review. *Gems & Gemology*, **53**(3), 262–284, <https://doi.org/10.5741/gems.53.3.262>.
- Faulkner, R. 2021. Industry Opinion: HPHT laboratory-grown diamonds that test as “synthetic moissanite”. *Retail Jeweller*, 15 March, <https://tinyurl.com/h9pcsu7c>.

Production and Cutting of Synthetic Moissanite in China

The diamond simulant synthetic moissanite appeared on the jewellery market in the 1990s and it is now relatively common. In China, it is one of the most important jewellery products sold on the Internet.

China’s silicon carbide products fall into two types. One is industrial abrasive-grade powder consisting of polycrystals (often opaque black), mainly used to make grinding wheels and other grinding tools. Large quantities are produced in Henan Province (also the world’s main source of HPHT-grown synthetic diamond), Guizhou Province, the Ningxia Hui Autonomous Region and elsewhere in China. The annual national output is nearly 1 million tonnes (Jiao 2013). Only small amounts of polycrystalline synthetic silicon carbide are cut as gems, which are sold as black synthetic moissanite.

The other type of silicon carbide product is more commonly encountered in the jewellery market: synthetic moissanite single-crystal materials, which are grown mainly in the cities of Jinan (Shandong Province) and Taiyuan (Shanxi Province), and elsewhere. These products can be divided into two categories: substrate films and bulk crystals, of which the latter are transparent and show mostly brown or green hues. The brown crystals can be annealed to produce nearly colourless material. Synthetic single-crystal silicon carbide is mainly used for optoelectronic and semiconductor applications as well as other fields, while the substrate film products have a variety of industrial uses (e.g. in the field of LED luminescence, as a material substrate, etc.). According to product specifications given by Chinese silicon carbide manufacturers, the films may cover areas of 5–15 cm in diameter or even larger, and are about 0.3–0.4 mm thick. Current annual production of this

type of material in China is more than 150,000 pieces. The bulk-crystal material can have a diameter of 5–10 cm or even larger, and can exceed 1 cm thick (e.g. Figure 22); the annual production of this type of silicon carbide has not been disclosed. Bulk crystals with obvious flaws or breakages are cut for gem use.

Wuzhou in the Guangxi Zhuang Autonomous Region is important for cutting all kinds of synthetic gem materials, especially cubic zirconia (CZ). More than one-third of the global demand for CZ is cut in Wuzhou, and almost all synthetic moissanite in China is also cut there. In recent years, large-scale gem-cutting factories in Wuzhou have upgraded their production-line mechanisation and much of the work is done by automated machines, resulting in lower processing costs, higher product standardisation and greater production efficiency. Most synthetic



Figure 22: These two bulk-crystal plates of silicon carbide were photographed at SICC Materials Co. Ltd in Jinan, China. They are representative of some of the damaged silicon carbide material used to facet synthetic moissanite gems. The plate on the left weighs 422.2 g and the one on the right is 405.9 g. Photo by Jianjun Li.



Figure 23: Round brilliants cut from synthetic moissanite such as these with a diameter of about 6.5 mm are roughly the size of a 1 ct diamond. The black and green colours are as grown, while near-colourless gems are produced by annealing brown material, and pink and brownish orange colours are due to surface coatings. Photo by Jianjun Li.

moissanite is cut as round brilliants, but also common are square, oval and other fancy cuts. Finished gems range from 2 to 10 mm, although most round brilliants are about 6.5 mm in diameter, around the size of a 1 ct diamond (e.g. Figure 23).

Because the raw material used to cut the synthetic moissanite gems consists of defective plates from the crystal-growing factories, and since cutting costs are low and efficiency is high, the factory prices of the finished products are very low. For example, near-colourless round brilliants of about 6.5 mm in diameter are

priced at less than USD5.00 wholesale. Green material is slightly cheaper because it is easier to produce (the colour is as grown) and in less demand. Black gems are slightly more expensive due to the lower cutting yield resulting from the polycrystalline nature of this material. Yellow to brownish orange and pink colours (again, see Figure 23) are produced by a surface-coating process after polishing; their price can be up to USD15.00–20.00 per ct. Even after the synthetic moissanite is mounted into a ring in silver or other non-precious metal, the price is commonly less than USD30.00.

Some Chinese dealers sell synthetic moissanite with a grading report similar to those used for diamonds. Such reports follow almost no regulations, but they make synthetic moissanite jewellery seem more like diamond jewellery to consumers. This, combined with the convenience of Internet sales, has contributed to the explosion in popularity of synthetic moissanite jewellery in China.

Jianjun Li (geoli@vip.sina.com)

*National Gold & Diamond Testing Center
Shandong Provincial Key Laboratory of
Metrology and Measurement
Shandong Institute of Metrology, Jinan, China*

Reference

Jiao, M. 2013. *The study on international competitiveness status of Chinese silicon carbide industry*. Master's thesis, Henan University of Science and Technology, Luoyang, Henan, China (in Chinese with English abstract).

Trapiche Sapphire Imitation

Trapiche is the Spanish word for the cogwheel used to grind sugarcane. This structure was first described in an unusual Colombian emerald (McKague 1964), and was known exclusively for emeralds until the 1990s, when trapiche rubies appeared in gem markets in Vietnam and Myanmar (Schmetzer *et al.* 1999).

This report supplements the recent description of trapiche emerald and ruby imitations by Zwaan (2020). In December 2020, we analysed a similar sample in our laboratory, submitted as a 'natural trapiche sapphire' (Figure 24). It consisted of an oval slab measuring 22.96 × 19.92 × 2.95 mm and weighing 15.90 ct. It contained seven pieces of semi-transparent blue sapphire in a grey matrix, and showed the same general pattern as the



Figure 24: The 15.90 ct sample described here was submitted as a 'natural trapiche sapphire', but was revealed to consist of seven pieces of sapphire cemented in an artificial matrix composed of a mixture of materials. Photo by J. Štubňa.

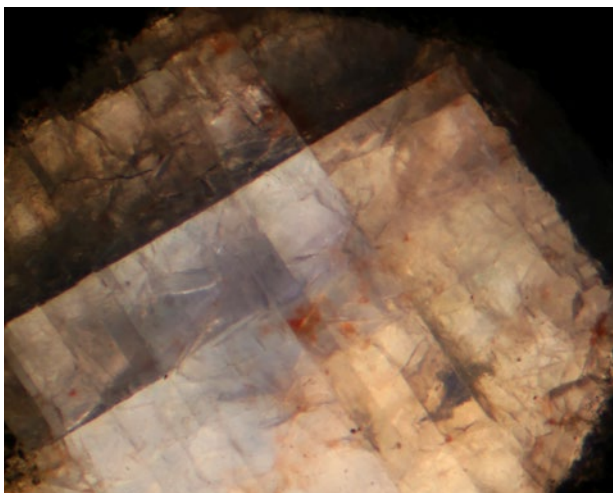


Figure 25: Twin lamellae are present in the pieces of sapphire that are embedded in the trapiche imitation. Photomicrograph by J. Štubňa; magnified 7.5x.

samples described by Zwaan (2020). Under magnification, the sapphire portions displayed twin lamellae (Figure 25). The sapphire areas were inert to long- and short-wave UV radiation, but they yielded photoluminescence spectra typical for traces of Cr.

We focused our examination on the grey matrix, which had a granular texture and fluoresced whitish blue to long-wave UV radiation, as was also documented in the samples examined by Zwaan (2020). EDXRF spectroscopy with an Olympus Delta Classic Plus handheld spectrometer (configured for analysing metal alloys) detected Zr, Fe, Pb and Co. This suggested the matrix was composed of a mixture of materials, and this was confirmed by microscopy and Raman spectroscopy,

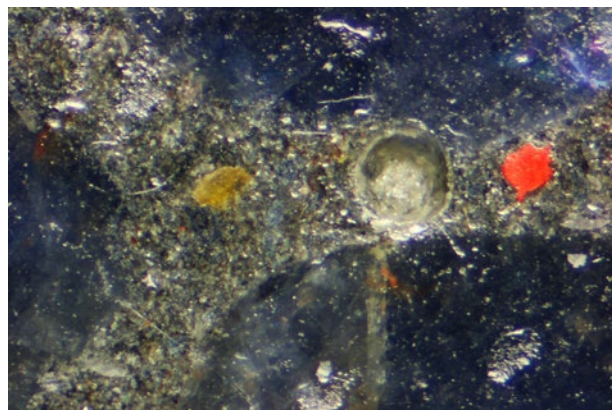


Figure 26: The grey matrix of the trapiche sapphire imitation consists of a granular mixture of cubic zirconia, lead glass, resin and other unidentified materials. A large gas bubble is also obvious in this portion of the matrix, as well as a red spot that appears to be some type of surface contamination. Photomicrograph by J. Štubňa; magnified 7.5x.

which showed the presence of cubic zirconia, lead glass, some unidentified transparent blue fragments and gas bubbles (Figure 26). In addition, Raman analysis clearly detected resin in the matrix material. Given their similarities, it seems likely that this sample came from the same source as the trapiche imitations described by Zwaan (2020).

*Dr Ján Štubňa (janstubna@gmail.com)
Gemmological Laboratory, Constantine the
Philosopher University, Nitra, Slovakia*

*Dr Peter Bačík and Dr Jana Fridrichová
Comenius University, Bratislava, Slovakia*

References

McKague, H.L. 1964. Trapiche emeralds from Colombia, part I. *Gems & Gemology*, **11**(7), 210–213.

Schmetzer, K., Beili, Z., Yan, G., Bernhardt, H.-J. & Hänni, H.A. 1999. Element mapping of trapiche rubies.

Journal of Gemmology, **26**(5), 289–301, <https://doi.org/10.15506/JoG.1999.26.5.289>.

Zwaan, J.C. 2020. Gem Notes: Imitations of trapiche ruby and emerald. *Journal of Gemmology*, **37**(1), 21–22, <https://doi.org/10.15506/JoG.2020.37.1.21>.

ERRATA

1. In the article by M. S. Krzemnicki *et al.* titled ‘A new type of emerald from Afghanistan’s Panjshir Valley’ (Vol. 37, No. 5, pp. 474–495), the title of Figure 17 should have been ‘Trace-Element Contents’.
2. In the Literature of Interest section of *The Journal*, Vol. 37, No. 5, 2020, p. 550, the hyalite article from *Rivista Italiana di Gemmologia/Italian Gemmological Review* should have been indicated as being published in issue No. 10.



Figure 1: This book of hours (8.5 × 8.0 × 2.6 cm), with its exceptional cover in enameled gold and gemstones, was acquired by King Francis I of France in 1538 as a probable gift to his niece, Jeanne d'Albret. Photo by E. Romeo.

The Book of Hours of King Francis I of France: History and Gemmological Analysis

Gérard Panczer, Elodie Romeo and Geoffray Riondet

ABSTRACT: The book of hours examined for this study is an illuminated Renaissance masterpiece: a small prayer book bound in enameled gold and gemstones that was bought in 1538 by King Francis I of France as a probable gift for his niece. In 2018, it was acquired by the Louvre Museum (Paris, France) from S. J. Phillips Ltd in London, and its nearly complete history is documented here. A first gemmological analysis of the stones adorning the book was conducted on site at the Louvre in 2020. The gems consist of carnelian (two intaglios and eight cameos), rubies (27 polished pieces), turquoise (24 cabochons) and rhodolite (one faceted stone in the book's clasp that has been described as tourmaline since 1942). We suggest that most of the rubies were mined from the Mogok area of Burma (now Myanmar). Based on historical considerations, the turquoise could have originated from Persia or possibly Uzbekistan, and the carnelian from either India or Saxony. The faceted rhodolite could have originated from India or Sri Lanka, and was most likely added to the clasp in more recent times, possibly between 1842 and 1884.

The Journal of Gemmology, 37(6), 2021, pp. 580–595, <https://doi.org/10.15506/JoG.2021.37.6.580>
© 2021 Gem-A (The Gemmological Association of Great Britain)

A book of hours is a type of Christian devotional book for the layperson, typically small so that it could be carried at all times, which was particularly popular during the Middle Ages. It is a type of missal with prayers, psalms and other texts, often illustrated (illuminated) and sometimes richly adorned with gemstones. Examples of some rare and precious medieval books of prayer embellished with gems include the Codex Aureus of St Emmeram (France, ca. 870), the Lindau Gospels (St Gall, Switzerland, ca. 880), the Gospels of Judith of Flanders (Canterbury, England, ca. 1060) and the Berthold Sacramentary codex (Weingarten, Germany, ca. 1215–1217).

The book of hours of King Francis I of France (reigned 1515–1547) is described in this article (Figure 1), and is hereafter referred to as simply ‘the Book of Hours’. It was acquired by the Louvre Museum, Paris, in 2018 from S. J. Phillips Ltd in London, specialists in European antique and estate jewellery. The small book (8.5 × 8.0 × 2.6 cm) fits in the palm of the hand and is embellished with enamelled gold that is set with numerous gemstones (polished pieces, cabochons, cameos and intaglios, and one faceted stone). The illuminated manuscript consists of 140 folios (pages) and includes 16 miniatures (illustrations). It is kept in a (possibly original) wooden storage box lined with quilted green silk, and is accompanied by a pendant (or ‘bookmark’) that is 6.2 cm long and set with rubies, turquoises and diamonds, in the same style as the Book of Hours.

Books of hours are written according to the division of the day into eight canonical hours—prayer times at certain hours of the day and night, fixed by the ecclesiastical canons since the 8th century, for a specific location. The book discussed in this article was to be used in Paris. It is a particularly remarkable example of such Renaissance illuminated manuscripts on parchment, and its provenance can be followed from century to century, so that almost its complete history is known (Malgouyres 2018; Figure 2).

Most scientific studies of books of hours have focused on analysing their ink and pigments (e.g. Melo *et al.* 2014; Mayer *et al.* 2018). However, over the past decade the development of portable and compact spectroscopic equipment has made on-site analysis possible for historical jewels, avoiding the need to transport these delicate

objects to laboratories (e.g. Reiche *et al.* 2004; Farges *et al.* 2015; Panczer *et al.* 2019). The resulting analyses are not as complete as those that could be obtained in a laboratory or on unset stones, but by combining the instrument data with historical information it is sometimes possible to propose geographical origins for the gems.

This article presents the results of this first scientific gemmological analysis conducted on the gems in the Book of Hours, carried out at the Louvre Museum. The associated bookmark-pendant has also been analysed and will be described in a separate publication.

HISTORICAL BACKGROUND

Most of the history of the Book of Hours described below is based on the research of Philippe Malgouyres (2018). It was bought in 1538 by King Francis I of France from Allard Plommyer, a trader and jeweller in Paris, as attested by the king’s accounting reports dating from 1539 (Cimber & Danjou 1835, pp. 99–100; Capefigue 1845, p. 170; de Laborde 1880, p. 241). These reports, written in Old French, describe it as ‘...a book of hours written on parchment, enriched with rubies and turquoises, covered with two large carnelians and adorned with a ruby, used to close it...’¹. A separate book of hours listed in the accounting reports of the king was acquired at the same time, but its provenance has been lost over time: ‘...another small book of hours also in parchment enriched with diamonds, rubies and emeralds...’².

The book of hours acquired by Francis I that is described here was most probably a gift to his niece, Jeanne d’Albret, who was at that time 10 years old. The book was listed in the inventory of d’Albret’s treasure at the Château de Pau in 1561 (Molinier & Mazerolle 1892; Plantey 2016), along with the associated bookmark-pendant, which was described as item no. 380, ‘A pillar of gold in which there is a beaten God who has been raised’³ (Malgouyres 2018). Later, the Book of Hours belonged, in sequence, to d’Albret’s son, King Henry IV of France (1553–1610); his second wife, Marie de Medici, Queen of France (1575–1642); and Cardinal Mazarin, first minister of France (1602–1661). After Mazarin’s death, it was listed in the inventory of his collection as

¹ ...ung livre d’heures escript en parchemin, enrichi de rubis et turquoises, couvert de deux grandes cornalynes et garni d’un rubis, servant à la fermeture d’icelluy...

² ...ung autre petit livre d’heures, aussi en parchemin enrichi de diamans, rubis et esmeraudes...

³ ...ung pillier d’or auquel il y a dedans ung Dieu battu eslevé...

Historic Provenance of the Book of Hours of King Francis I of France

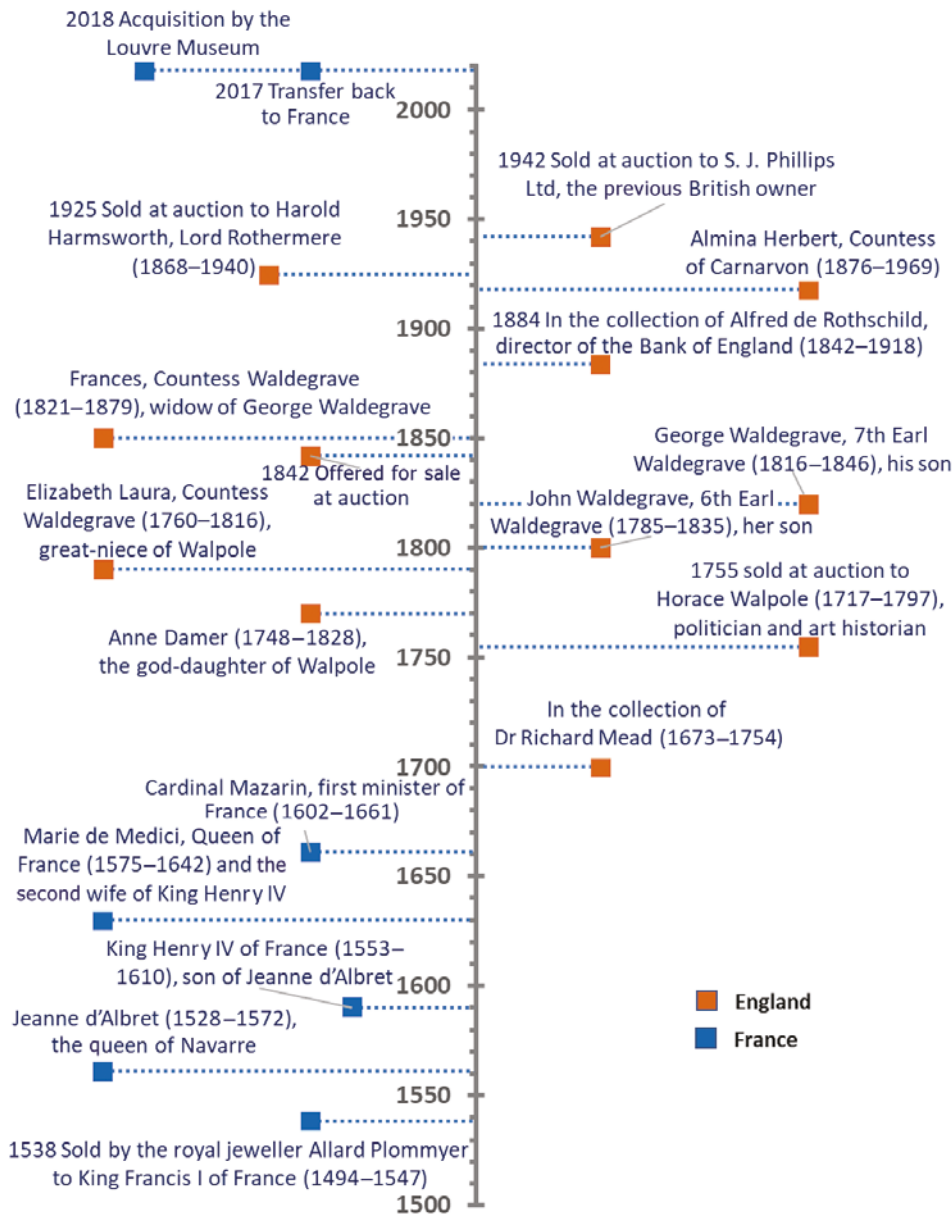


Figure 2: As summarised in this timeline, the Book of Hours of Francis I was owned by French royalty and powerful advisor Cardinal Mazarin from 1538 at least until the late 17th century. Then it was possessed by various British dignitaries until being transferred back to France in 2018, when it was acquired by the Louvre Museum.

‘another small volume book of hours written on vellum [thin white parchment] with a figure of miniature covered in gold, enriched with two carnelians engraved on the two covers and with rubies and turquoises estimated at 200 l [livres]’⁴ (Yoshida-Takeda *et al.* 2004).

Subsequently, the Book of Hours appeared in England

in the collection of Dr Richard Mead (1673–1754), a well-known English patron of literature, arts and sciences, and a member of the Royal Society (introduced to the Society in 1717 by Sir Isaac Newton), as well as personal physician to King George II. Mead’s collection was auctioned one year after his death, on

⁴ ...Un autre livre d’heures en petit volume escript sur velin avec figure de mignature couvert d’or, enrichy de deux carnalines gravées sur les deux couvercles et de rubis et tourquoises estimé 200 l.

the instructions of his executors, by London auctioneer Abraham Langford. The auction catalogue (Langford & Mead 1755, p. 12; fourth day of sale, lot 42) described the Book of Hours in (Old) English for the first time:

A Missale [missal] adorned with sixteen [sixteen] miniature paintings by *Raphael, Petro Perugino* and their scholars [scholars]. The cover is made of two large engraved cornelians fet [set] in *enamel'd gold frames*, the back and sides [sides] *richly ornamented* with *rubies* and *turquoises* [turquoises], the clasp [clasp] a large *garnite* [garnet].

This first reference to Raphael (1483–1520) and his master Petro Perugino (1452–1523) incorrectly attributes the work to these artists, perhaps to increase the potential value of the artwork. The miniatures are most probably the work of Noël Bellemare, a French painter and illuminator of Flemish origin who was active in Paris between 1515 and 1546, and his students (Malgouyres 2018).

An extant copy of the auction catalogue in the Getty Research Institute Library is annotated by hand, indicating that the Book of Hours was purchased by ‘Walpole’ for the sum of £48 6s. Thus the book entered the collection of Horace Walpole (1717–1797), a politician and art historian who resided at Strawberry Hill, a magnificent house he designed in West London. Another annotation by hand at the end of the catalogue adds, ‘belongd to Mary Q of Scots’ (Langford & Mead 1755, p. 12). This cannot be substantiated and seems unlikely. Mary Queen of Scots reigned 1542–1567 and was married to Francis II, grandson of Francis I, but her

possession of the Book of Hours would be inconsistent with the early chain of owners noted above, and she died before Mazarin did.

In 1749, an engraving by George Vertue depicted the acquisition by Margaret Harlet, Duchess of Portland, of eight jewels (British Museum, registration no. 1850,0223.697; see www.britishmuseum.org/collection/object/P_1850-0223-697). Among them is the first known drawing of the bookmark-pendant accompanying the Book of Hours.

Between 1781 and 1788, John Carter (1748–1817), architect and antiquarian, and Edward Edwards (1738–1806), painter and engraver, produced for Horace Walpole many famous prints and watercolours showing the interior of Strawberry Hill (ca. 1788). One of these watercolours (inventory no. sh-000202, The Lewis Walpole Library, Yale University, New Haven, Connecticut, USA) depicts three jewels displayed in the Tribune room at Strawberry Hill: the dagger of Henry VIII, the rock crystal sceptre of Henry V and a book of hours (Figure 3), this last being the first-known illustration of the book formerly owned by Francis I.

Walpole bequeathed Strawberry Hill and its contents to his god-daughter, English sculptor Anne Damer, who relinquished ownership to Walpole’s great-niece Elizabeth Laura, Countess Waldegrave (1760–1816). It then passed to her son, John Waldegrave, 6th Earl Waldegrave (1785–1835), followed by his son, George Edward Waldegrave, 7th Earl Waldegrave (1816–1846), who married Frances Braham, Countess Waldegrave (1821–1879). In his book, *Hawthorne and His Circle*, Julian Hawthorne recounts how Frances Waldegrave presented the Book of Hours to her visitors (Hawthorne 1903, p. 220):

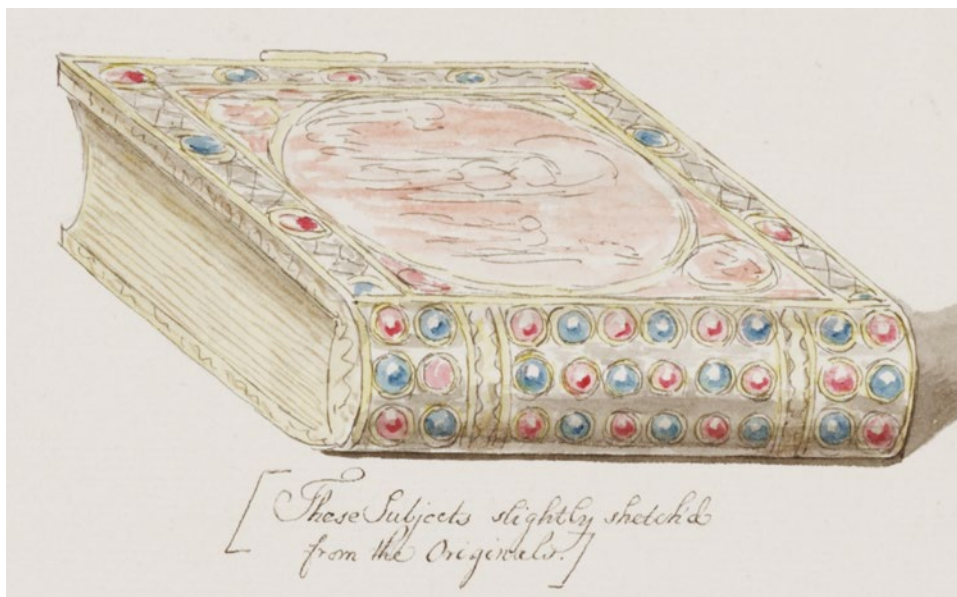


Figure 3: This detail from a watercolour painted in 1788 by Edward Edwards for Horace Walpole documented the Book of Hours when it was displayed in the Tribune room at Walpole’s Strawberry Hill residence. The painting also included Henry VIII’s dagger and Henry V’s crystal sceptre (not shown here). Below the Book of Hours is the note ‘These subjects slightly sketched from the originals’. Courtesy of The Lewis Walpole Library, Yale University (<https://libsvcs-1.its.yale.edu/strawberryhill/oneitem.asp?id=29>).

...she showed us some curious things which had formerly made part of Horace Walpole's collection at Twickenham — a missal, for instance, splendidly bound and beset with jewels, but of such value as no setting could increase, for it was exquisitely illuminated by the own hand of Raphael himself! I held the precious volume in my grasp, though I fancy (and so does my wife) that the countess scarcely thought it safe out of her own hands.

Horace Walpole's grandson, George Edward Waldegrave, was irresponsible with money and had to sell the contents of the house in 1842. The catalogue of this huge auction, which took place over 23 days, describes the Book of Hours as follows (Robins 1842, p. xix):

...gleaming with gold and jewels, is the missal painted by Raffaele and his scholars for Claude de France, the Queen of François Premier. It is covered with turquoises and rubies, and on each cover is an enormous cornelian, with an intaglio of the Crucifixion on one side, and a relievo on the other ; it is very small, and might be worn as an ornament.

The reference to Queen Claude of France (1499–1524), the first wife of Francis I, which appeared for the first time in Walpole's 1774 description (p. 88) of the Book of Hours, cannot be correct, since she died before it was acquired in 1538 (Malgouyres 2018).

The Book of Hours was reportedly sold on 11 May 1842, the 15th day of the auction. The catalogue further describes it as 'adorned with rubies and turquoises,

the sides are formed of 2 matchless cornelians, with an intaglio of the Crucifixion on one side and a Scripture History on the other, the clasp a large garnet' (Robins 1842, p. 156, lot 77). It also noted that Walpole purchased it from the Mead Collection, and that it was supposed to have been owned by Christophe de Thou (1508–1582), the first president of the Parliament of Paris and father of Jacques Auguste de Thou (known as Thuanus, 1553–1617), a French historian and book collector, who served Maria de Medici.

The Book of Hours was purchased at this auction for £115 10s (£115.5), reportedly by 'Earl Waldegrave' (per handwritten notes in Robins 1842, p. 156). A rather confusing note indicates that the Book of Hours was not sold by the end of the auction. Instead, it was 'revalued', either because the bids did not reach its reserve price or because there were no bidders at all. Thus, it remained the property of the seller. George Waldegrave died in 1846 and the Book of Hours became the property of his widow, Frances, Countess Waldegrave. She loaned it to the London International Exhibition of 1862, where it was displayed among other historical relics, including the book's associated bookmark-pendant (Malgouyres 2018). It was probably put on sale after her death in 1879, since she had no descendants.

No more than five years later the Book of Hours was in the possession of Alfred de Rothschild (1842–1918), the director of the Bank of England, as reported by Charles Davis in 1884. Davis (1884, item 150) further indicated that it was in Rothschild's collection at Halton House, and he included the first known photographs of the Book of Hours (Figure 4), along with the following description:



Figure 4: The first-known photographs of the Book of Hours, described as 'An Illuminated Missal', show the front (right) and back (left) covers. The stone on the clasp appears to be the same as the current one. Photos by J. Thompson (in Davis 1884).



Figure 5: The Book of Hours is an exceptional example of Renaissance art due to its back cover (left), spine (centre) and front cover (right) richly embellished with gold, rubies, turquoise and carnelian, with a large garnet in the clasp. Photos courtesy of S. J. Phillips Ltd.

This missal was painted in the early part of the sixteenth century. It is on vellum, and has illuminated capitals, and whole-page illustrations of subjects taken from the Bible. The cover is of gold, decorated with enamelled scrolls on the borders and back, and set with rubies and turquoises alternately; on the sides are two large oval red cornelian intaglios. [...]

On the front of the altar is the inscription—“O mater Dei, memento mei.” [Oh Mother of God, remember me.]...

Size, 3¼ in. by 2⅝ in.

Alfred de Rothschild bequeathed it, with much of his fortune, to Almina Herbert, Countess of Carnarvon (1876–1969), widely believed to be his illegitimate daughter. In May 1925 it sold at auction as lot 141 (Carnarvon 1925) to S. J. Phillips Ltd acting on behalf of Harold Harmsworth, Lord Rothermere (1868–1940). A leading British newspaper proprietor—whose political sympathies were controversial, to say the least—Harmsworth also acquired the bookmark-pendant. The auction catalogue, compiled by Christie’s, gave a very complete description of the Book of Hours (Carnarvon 1925, p. 29), including a brief biography of Dr Richard Mead and two photographs similar to those in Figure 4.

In March 1942, following Lord Rothermere’s death in 1940, the Book of Hours was sold at a London auction, where it was acquired again by S. J. Phillips Ltd, the previous British owner (Harmsworth 1942).

In 2017, S. J. Phillips Ltd offered the Book of Hours for sale, and a UK export licence was issued for it the same year (RCEWA 2017, 2018). In 2018, the Louvre Museum acquired the book for £8,890,000, thus bringing this French Renaissance masterpiece back to France. The acquisition was crowdfunded in the *Tous Mécènes!* (Become a patron!) campaign spearheaded by the French luxury retail group LVMH (Louvre 2018).

MATERIALS AND METHODS

The Book of Hours measures 8.5 × 8.0 × 2.6 cm. It is adorned with a black-enamelled gold cover, set with 52 gemstones and two large oval reddish orange intaglios that are each surrounded by four cameos of the same texture and colour (Figure 5). The intaglio on the front cover represents Christ on the cross, between St Jerome (on the right) and St Francis of Assisi (on the left, receiving the stigmata as symbolised by thin strings). The intaglio on the back cover shows the Virgin and Child between St Barbara and St Catherine of Alexandria (Malgouyres 2018). Each of the surrounding cameos displays the head and wings of a cherub. The work on the intaglios and cameos is attributed to the famous Italian Renaissance lapidary engraver Matteo dal Nassaro Veronese (1485 to ca. 1548), known as ‘engraver of the king’ in 1529 in Paris (de La Tour 1893). No document proves a direct link between Nassaro and these engravings, but it is recorded that in 1534 he was paid ‘to buy 4,000 pounds [approximately 1,814 kg] of esmery [corundum powder] which

he should have for engraving and carving stones...'⁵ (de Laborde 1880, p. 369; de La Tour 1893, pp. 12–13).

Our comprehensive gemmological analysis conducted on the gemstones of the Book of Hours was carried out at the Louvre Museum over two days in September 2020. The gems were examined on site with standard gemmological instruments, including a refractometer (Figure 6a), and long-wave (365 nm) and short-wave (254 nm) UV lamps. Due to handling restrictions at the museum, it was not possible to carry out a detailed microscopic investigation of the gems, so we performed rapid photographic documentation using a Euromex Q-scope USB microscope with internal polarisable ring illumination, which makes it possible to quickly obtain close-up photos of gems and their settings, sometimes showing larger inclusions.

Two portable Raman spectrometers were used to identify most of the gemstones (i.e. those that allowed unobstructed measurements). Both consisted of Ocean Optics R-3000-HR units equipped with fibre-optic probes, with one of them using a 785 nm (near-infrared) diode laser (250 mW; Figure 6b) and the other utilising a 532 nm (green) Nd-YAG solid-state laser (50 mW). The obtained Raman spectra were compared with the RRUFF database (Lafuente *et al.* 2015).

The chemical composition of each stone that allowed unobstructed measurements was analysed by energy-dispersive X-ray fluorescence (EDXRF) spectroscopy using a Thermo Niton XL3t 980 GOLDD+ XRF Analyser (2 W power, Ag anode). The handheld unit was mounted on a stand and could analyse elements with atomic number greater than 11 (i.e. Mg and heavier). The spatial resolution was 3 mm (giving an average composition of the area analysed) and the analysis time was 120 s. The pre-installed 'ores' mode was modified and calibrated using NIST SRM 610 and SRM 612 glass standards. The precision varied according to the element and material analysed. The detection limit was approximately 1500+ ppm for elements from Mg to Si, 100–400 ppm for P-Co and 5–90 ppm for Ni-U. The results were also strongly dependent on the nature of the sample; the most reliable data were obtained from a flat surface (such as the table of a faceted stone) and away from the gold setting. Results were less reliable for the smallest stones with curved surfaces (cabochons).

⁵ ...à achepter 4,000 livres d'esmerly qu'il luy convient avoir pour graver et tailler des pierres, ainsi que icelluy seigneur luy a commandé et ordonné...



Figure 6: Portable instruments used for the gemmological examination of the Book of Hours included (a) a refractometer and (b) a Raman spectrometer with a 785 nm red laser. Photos by G. Panczer.

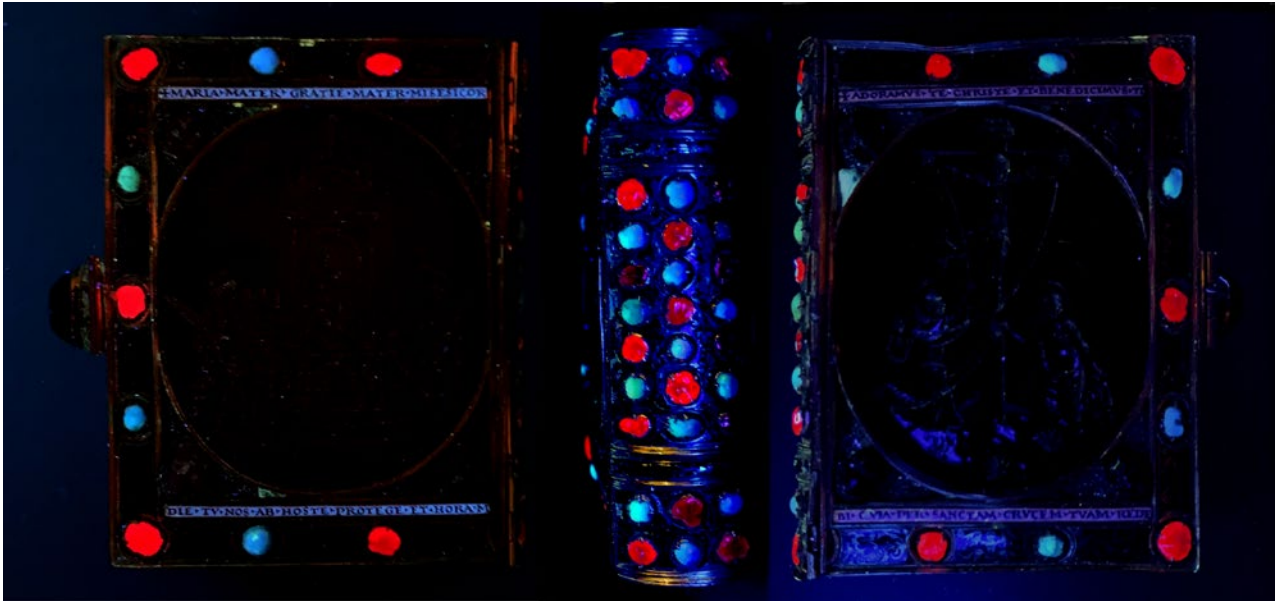


Figure 7: Long-wave UV radiation of the back cover (left), spine (centre) and front cover (right) of the Book of Hours reveals fluorescence typical of ruby and turquoise. In addition, whitish blue fluorescence from a portion of the upper left cameo on the front cover corresponds to where a broken section of carnelian has been replaced by pink resin. Composite photo by G. Panczer.

RESULTS

The gem materials decorating the Book of Hours were identified as carnelian (intaglios and cameos), ruby (polished pieces of rough), turquoise (cabochons) and garnet (faceted stone on the clasp), and each of these is described in more detail below. Evidence of restoration was seen using UV radiation as blue fluorescence emitting from one of the cherub cameos on the book's front cover (Figure 7, right), in which one of the wings had broken and was replaced by pink resin (Figure 8).

The engraving work and polish of the intaglios and

cameos are of fine, delicate quality (again, see Figure 8). The cabochons are each set in a gold bezel with added prongs, forming a hybrid setting that combines mounting of the stones with decoration (Figure 9). The stone in the book's clasp is set in a high gold collar, which is somewhat different from the other settings, and is the only one that is faceted (Figure 10). The fact that this stone was faceted (rather than cut as a cabochon) indicates that it was cut and set much later than when the book was originally created.



Figure 8: This detail of the upper left part of the front cover of the Book of Hours shows a carnelian cameo depicting a cherub (with one wing broken and repaired by pink resin) and a portion of the carnelian intaglio portraying Christ on the cross (with the stigmata symbolised by thin strings). The quality of the carving and polish is evident within the fine engraving of the intaglio. At the top are a ruby and a turquoise set in enameled gold. Each of the straight sides of the cameo measure 2.5 cm long. Photo by E. Romeo.



Figure 9: Details of the Book of Hours show (a) a ruby in a gold bezel setting with three prongs and (b) a turquoise in a similar gold bezel setting with four prongs. The width of the black-enamelled gold border is approximately 1 cm. Photos by E. Romeo.



Figure 10: The faceted stone (approximately 18 × 16 × 11 mm) in the clasp of the Book of Hours was identified as a rhodolite (pyrope-almandine) garnet. Its high-collar bezel setting differs in appearance from the settings of the other gems, such as those shown in Figure 9. Photo by E. Romeo.

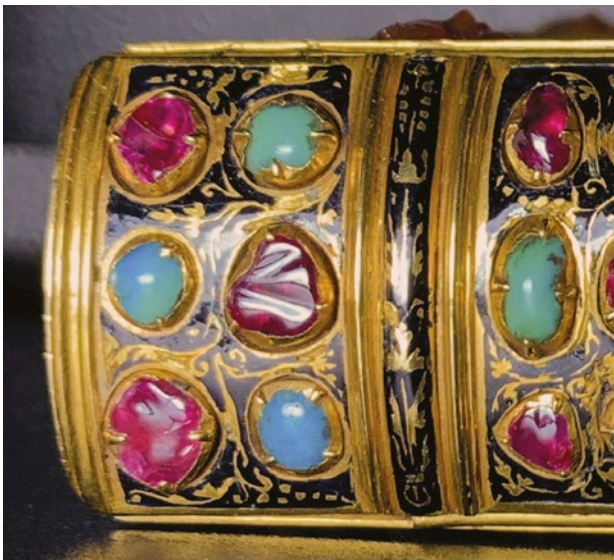


Figure 11: Many of the rubies have grooves that were likely made to grind away imperfections in the stones, as shown here on the spine of the Book of Hours. This practice has been documented for other historical gemstones. The spine of the book is 2.6 cm wide. Photo by G. Panczer.

Ruby

The Book of Hours is set with 27 rubies, five each on the front and back covers and 17 on the spine. They ranged from 4.8 to 5.2 mm in maximum dimension. The rubies mostly appeared to be in their rough shapes (i.e. polished crystal fragments; see, e.g., Figure 9a). Most of the rubies displayed groove-like features (Figure 11), consistent with the historical practice of grinding away imperfections from gemstones (Ogden 2013).

Examination with long-wave UV radiation (Figure 7) revealed the red fluorescence typical of Cr³⁺ in the ruby structure. Their fluorescence varied from moderate to strong, probably due to variations in the relative amounts of Cr and Fe.

The Raman spectra (Figure 12) confirmed that all of the reddish stones (except the one in the clasp) were rubies, despite the presence of a strong Cr³⁺ luminescence background. The Raman lines corresponded to the modes of vibration of AlO₆ groups in octahedral coordination in the corundum structure (Porto & Krishnan 1967).

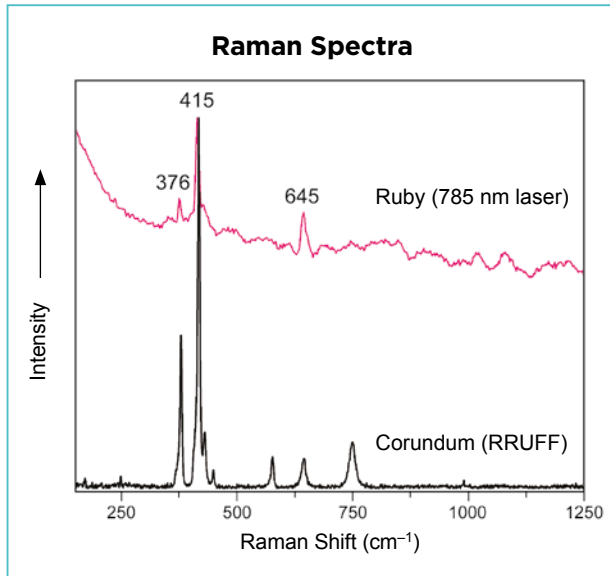


Figure 12: A representative Raman spectrum of one of the rubies is compared to a corundum reference spectrum and shows sufficient similarity to confirm its identity.

EDXRF chemical analysis of 15 of the rubies revealed the presence of the trace elements Fe, Cr, V, Ti and Ga (Table I). The relatively high Fe values might reflect the presence of microscopic inclusions since the Cr³⁺ fluorescence of the rubies was not extensively quenched by iron in the corundum structure.

Table I: Trace-element composition of the 15 analysed rubies in the Book of Hours.

Element (ppm)	Range	Mean	Error (±2σ)
Fe	120–5500	1600	400
Cr	300–5600	1500	50
V	20–1000	200	25
Ti	70–300	120	50
Ga	20–50	30	10

Turquoise

The Book of Hours is set with 24 turquoise cabochons, four each on the front and back covers and 16 on the spine. They measured from 4.7 to 5.3 mm in maximum dimension. The stones ranged from blue to green and exhibited weak to moderate whitish blue fluorescence under long-wave UV radiation (Figure 7). Viewed with a microscope, some of them presented a dark matrix pattern.

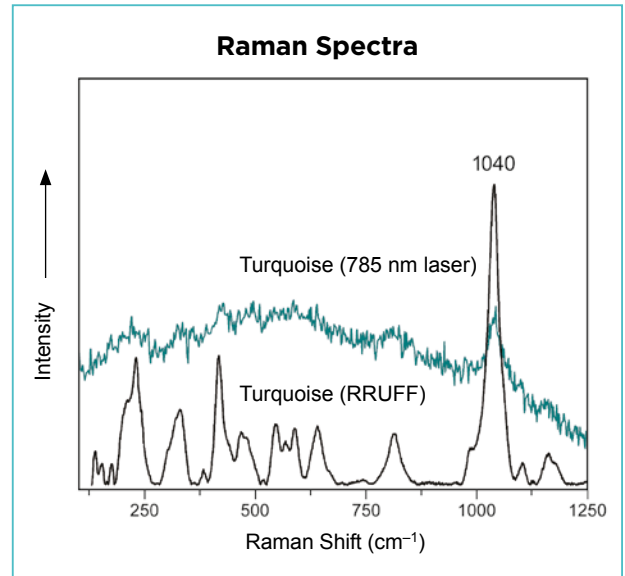


Figure 13: A representative Raman spectrum of one of the greener turquoise gems displays the characteristic main peak at 1040 cm⁻¹ that is exhibited by the turquoise reference spectrum.

Raman spectroscopy confirmed the blue-to-green stones as turquoise (Figure 13), although the signal was weak and noisy because turquoise has a microcrystalline structure, and it therefore provides a weaker Raman spectrum than single crystals such as quartz or corundum.

EDXRF analyses of the turquoise showed the main elements Cu, Al and P. The 15 blue turquoise cabochons analysed had a mean value of 2300 ppm Fe (0.3 wt. % Fe₂O₃), while the nine more greenish ones averaged 9200 ppm Fe (1.3 wt. % Fe₂O₃). Iron is expressed as Fe₂O₃ since Fe³⁺ substitutes for Al³⁺ in the turquoise structure and has a strong effect on turquoise colour (Mousavipak 2020). Therefore, the green hue might correlate with the amount of Fe³⁺ and, thus, to natural geological oxidising conditions. The jeweller who set the stones might have intentionally used green and blue ones, or all of them might have been blue originally—with some of them experiencing different degrees of ‘ageing’ due to wear (e.g. exposure to skin oil), according to slight differences in their microcrystalline structure and porosity. Although substitution of Cu by Zn in turquoise has been reported in the literature (Carò *et al.* 2017; Mousavipak 2020), no Zn was detected in our analyses (the detection limit was 20 ppm).

Carnelian

The two large oval intaglios (approximately 6.5 × 6.0 cm) and eight surrounding cameos (approximately 2.5 cm) in the Book of Hours all consist of carnelian (the orange to red variety of chalcedony).

Raman spectra (Figure 14) obtained from the two intaglios and one of the cameos confirmed their

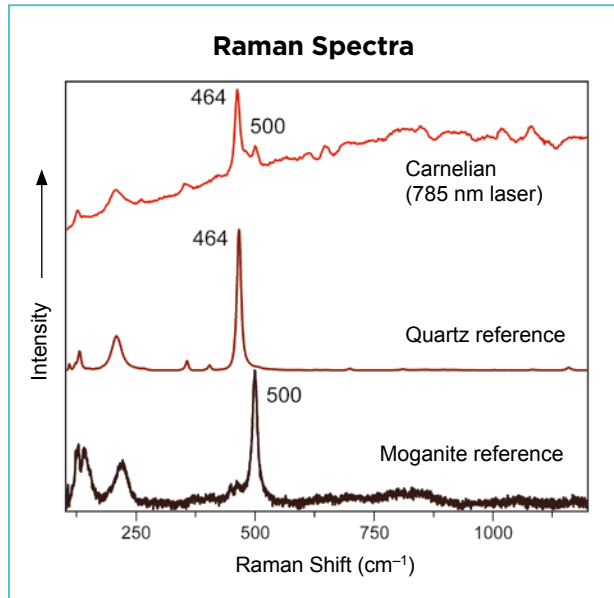


Figure 14: The Raman spectrum of a carnelian displays peaks corresponding to quartz (464 cm⁻¹) and moganite (500 cm⁻¹), as compared here to reference spectra from the RRUFF database and Schmidt *et al.* (2013), respectively.

composition as microcrystalline quartz (rhombohedral SiO₂) with subordinate moganite, a metastable monoclinic polymorph of quartz (Heaney & Post 2001; Schmidt *et al.* 2013). The proportions of quartz and moganite in chalcedony can be estimated by measuring the relative intensities of their main Raman peaks (at 464 and 500 cm⁻¹, respectively), as reported by Götze *et al.* (1998) and Gliozzo *et al.* (2014). Our Raman analyses revealed varying ratios of microcrystalline quartz and moganite, but all were distinctly dominated by quartz.

EDXRF analyses of the carnelian intaglios revealed traces of chemical impurities, such as 260 ppm Fe, either substituted in the structure of the quartz or associated with micro-inclusions of other mineral phases.

Rhodolite Garnet in the Clasp

The clasp is set with an oval faceted purplish pink transparent stone (approximately 18 × 16 × 11 mm, Figure 10), which was first described as ruby, then as garnet and, since 1942, as tourmaline (Harmsworth 1942). It contained elongated, colourless, oriented inclusions, too small to be identified by portable Raman spectroscopy.

Despite the table facet being slightly domed, we were able to determine the stone's RI as 1.762. This singly refractive RI value corresponds to that of an isotropic stone in the cubic crystal system and is consistent with that of rhodolite (RI range = 1.750–1.770). This intermediate member of the pyrope-almandine solid-solution series has the formula (Mg,Fe)₃Al₂³⁺(SiO₄)₃. The RI is not

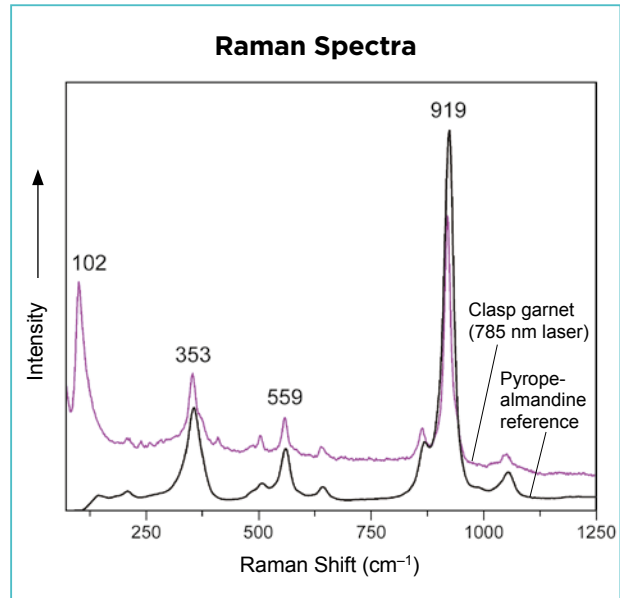


Figure 15: The Raman spectrum of the clasp stone provides a good match to that of a pyrope-almandine reference spectrum.

consistent with that of pink tourmaline (i.e. elbaite), which is, moreover, doubly refractive (RIs = 1.624–1.644).

The Raman spectrum of the garnet fit well with the rhodolite reference (Figure 15), which confirmed its identity and excluded, with high confidence, tourmaline, ruby or even a glass imitation.

The EDXRF chemical analysis of the rhodolite is given in Table II, and the calculated molar percentages of the pure garnet end members are as follows: pyrope (Mg) 56.6%, almandine (Fe) 37.2%, grossular (Ca) 4.9% and spessartine (Mn) 1.3%.

Table II: EDXRF chemical composition of the garnet in the clasp of the Book of Hours.

Oxide (wt.%)	Mean	Error (±2σ)
SiO ₂	44.5	0.6
Al ₂ O ₃	32.6	1.1
FeO	20.0	0.3
MgO	17.1	1.8
CaO	2.1	0.3
MnO	0.7	0.1
Cr ₂ O ₃	0.03	0.01
TiO ₂	nd*	nd

* nd = not detected

DISCUSSION

The presence of specific types of inclusions and measurement of trace elements, as well as observations of UV fluorescence, make it possible to propose hypotheses concerning the geographical or deposit origins for the gems in the Book of Hours. However, it is also necessary to consider historical data regarding trade routes.

Possible Ruby Origins

Historical reviews report that rubies from the Mogok Valley in Upper Burma have been mined since antiquity (Content 2016), and the stones were transported to Europe via the Silk Road (Caplan 2018) since the late 1400s (Hughes *et al.* 2017). In 1550, Georgius Agricola wrote in *De Natura Fossilium* (Mottana 2006) that the best rubies came from *Zaylon* (Ceylon or Sri Lanka). Other deposits, such as those in Afghanistan and Tajikistan, seem to have been active around the same time (Content 2016; Hughes *et al.* 2017).

Ten of the rubies on the Book of Hours had mean values of 0.27 wt.% Cr₂O₃ (i.e. 1500 ppm Cr) and 0.03 wt.% FeO (i.e. 270 ppm Fe). The Cr₂O₃/FeO ratio and relatively high content of vanadium (170 ppm V) suggest that they are from a marble-hosted deposit, consistent with rubies from Mogok (Peretti 2015; Giuliani *et al.* 2020). The other five rubies analysed presented lower mean chromium (0.15 wt.% Cr₂O₃ or 1200 ppm Cr) and higher average iron (0.3 wt.% FeO or 2300 ppm Fe) values, but the latter element is probably linked to contamination (e.g. inclusions, Fe-oxides and hydroxides in fissures, and/or analytical artefacts) since the Fe content does not strongly affect the Cr³⁺ fluorescence of the rubies. The Cr and Fe values of these five rubies correspond to what could be expected (when these elements are present in the corundum structure) for weakly fluorescent rubies from amphibolites and alkali basalts (e.g. Thailand; Giuliani *et al.* 2020). However, these five rubies in the Book of Hours also showed relatively high V concentrations (mean 250 ppm V), which is greater than that reported for Thai rubies (Palke *et al.* 2019) and more similar to that of Burmese rubies (Zaw *et al.* 2014; Palke *et al.* 2019; Sutherland *et al.* 2019). Interpreting these data with caution, we propose that most of the rubies adorning the Book of Hours are likely to be from a marble-type deposit and, taking into account the records of historic mining sources, they probably originated from Mogok.

Possible Turquoise Origins

Turquoise was mined in Egypt even earlier than in Persia (Iran), possibly around 6000 BC, and evidence shows

that since 3000 BC two Egyptian mines were known: Serabit el-Khadim ('mountain of the servant') and Wadi Maghareh ('the valley of the cave'; Tallet 2003). Little gemmological literature is available on identifying the provenance of turquoise from these localities on the basis of trace elements, but a fair amount has been done on archaeological material (Carò *et al.* 2017; Mousavipak 2020). Several historical turquoise mines in Iran have been reported, including Neyshapour (or Neyshabour) in Khorasan Province, Baghu in Semnan Province and Meyduk (or Meydook) in Kerman Province (Mousavipak 2020). In Uzbekistan, the Kyzylkum Desert (Muruntau region) was another source of turquoise during the Silk Road period and was exploited as early as the 4th millennium BC (Carò *et al.* 2017). However, the origin of the turquoise gemstones of the Book of Hours remains unknown.

Possible Carnelian Origins

The largest ancient deposits of carnelian seem to be in India (Gujarat, Madhya Pradesh and Maharashtra states) and Indonesia (Sumatra; Gliozzo 2019).

Most carved carnelian objects from antiquity are beads (prehistoric), Egyptian scarabs (of material probably from Egypt or the Arabian Peninsula), centimetre-sized intaglios worn in rings or medallions (Greek, Roman and Byzantine periods), and medieval rings, which often contained recycled ancient intaglios. Several carved carnelians of the size, quality and homogeneity as those decorating the Book of Hours are known from the Renaissance. Among them are a 4.2-cm-long orange-red cameo with a portrait of Savonarola dated before 1502 (Galleria Palatina, Palazzo Pitti, Florence, Italy), a 3.4-cm-long reddish orange intaglio attributed to Valerio Belli (1520) with an erotic scene (lot 551 sold by Bertolami in 2019), and a 3.8-cm-long orange intaglio representing Apollo and Marsyas dated to the second half of the 15th century (National Library of France, inv. 58.2299). The origins of these carnelians, however, are unknown.

Attempts have been made to determine the origins of carnelians based on the proportions of quartz and moganite, as determined by Raman spectrometry (Götze *et al.* 1998; Gliozzo *et al.* 2014). The carnelians in the Book of Hours contain approximately 80% quartz and 20% moganite. However, many carnelians have similar ratios, including those of Fezzan (southwest Libya; Gliozzo *et al.* 2014). According to Gliozzo (2019), India has provided the most beautiful carnelians since antiquity (and material is still being mined from Bharuch in Gujarat State), but there is no mention of any large pieces. Saxony (Hohenstein-Ernstthal, Zwickau,

Germany) has also been reported (Vollstädt & Baumgärtel 1977), but again without mention of large pieces. Thus, the origin of the carnelians in the Book of Hours remains uncertain, although we suggest, with reserve, that they might have come from either India or Saxony.

The Clasp Rhodolite: History and Possible Origins

Descriptions of the purplish pink stone in the clasp of the Book of Hours changed over time (Table III). Documents from 1539 (extracts from Francis I’s accounting reports; Cimber & Danjou 1835) and 1561 (inventory of the Château de Pau treasure; Molinier & Mazerolle 1892) describe it as a ruby. Later documents from 1755 to 1925 describe it as a large garnet (Langford & Mead 1755; Walpole 1774; Robins 1842; Davis 1884; Carnarvon 1925). The description of the book in the 1942 auction catalogue (Harmsworth 1942) for the first time described the clasp stone as a tourmaline. This identification has been repeated until recently. However, we have shown that this stone is, indeed, a rhodolite garnet.

It should be reiterated that early identifications of gemstones were often wrong, being based almost entirely on colour. The 16th century records of the Book of Hours describing the clasp stone as a ‘ruby’, and its replacement at some later point in time (during the 19th century) by

one identified as a ‘garnet’, are both consistent with the gem’s reddish colour.

The first visual representation of the Book of Hours is the 1788 watercolour by E. Edwards (Figure 3), but the clasp is not visible. The two black-and-white photographs of the book in Carnarvon (1925) clearly show the clasp and that the stone was faceted. The stone in those photos appears identical (i.e. depth, faceting and setting style) to the one that is currently mounted in the clasp.

To summarise: (1) the stone of the clasp was originally referred to as a ruby and starting in 1755 it was called a garnet; (2) this stone has been unchanged since at least 1884 (as per the ‘cut garnet’ description given by Davis); (3) its faceting and setting style indicate that it is a later addition to the clasp of the book; (4) this stone could be the garnet mentioned in 1755 (which possibly replaced an earlier ‘ruby’ mentioned in the 16th century) since early ‘brilliant cuts’ for coloured stones appeared in the 18th century, but more probably—according to its sophisticated cut (Figure 10)—could have been set between 1842 (the last time in the literature when it was mentioned as simply ‘a large garnet’) and 1884, when it was first described as ‘a large *cut* garnet’ (italics added; see Table III for a chronology of the clasp stone); and (5) the clasp stone was not replaced by a tourmaline sometime before 1942, when it was first described as

Table III: Chronology of the descriptions of the clasp stone in the Book of Hours.

Year	Description of the clasp	Image showing the Book of Hours	References
1539	<i>et garny d'un rubis, servant à la fermeture d'icelluy</i>	—	Cimber & Danjou (1835); Capefigue (1845); de Laborde (1880)
1561	<i>le fermet d'ung grand ruby</i>	—	Molinier & Mazerolle (1892); Plantey (2016)
1755	<i>the clasp a large garnite</i>	—	Langford & Mead (1755)
1774	<i>the clasp, a large garnet</i>	—	Walpole (1774)
1788	—	Watercolour (see Figure 3)	Edwards (1788)
1842	<i>the clasp a large garnet</i>	—	Robins (1842)
1884	<i>the clasp is ornamented with a large cut garnet</i>	Photograph (see Figure 4)	Davis (1884)
1925	<i>the clasp similarly enameled and set with a large garnet</i>	Photograph	Carnarvon (1925)
1942	<i>set with cornelian intaglios and cameos, rubies, and turquoises and a tourmaline</i>	Photograph	Harmsworth (1942)
2016	<i>framed with rubies, turquoises and a tourmaline</i>	Photograph	RCEWA (2017)
2017	<i>Le fermoir, quant à lui, s'orne d'une grosse tourmaline facettée</i>	Photograph	Louvre (2018)
2021	rhodolite (pyrope-almandine) garnet	See photo of clasp stone in Figure 10	This work

such (Harmsworth 1942). It could have been mistaken for a tourmaline due to its purplish pink colour and the appearance of its inclusions, especially since RI measurement by refractometer would have been complicated by the stone's slightly domed table.

The origin of the rhodolite in the clasp is difficult to assess. Historical deposits of rhodolite exist in south-eastern India (Titilagarh, Balangir, Odisha State) and the Central Province of Sri Lanka (Shigley *et al.* 2010; Dirlam *et al.* 2019), and both of these areas are still in production, but several additional localities for this relatively common gem material might have also existed at the time. However, the Bohemian garnets produced in early 16th century Europe consist instead of Mg-rich pyrope (Seifert & Vrána 2005).

Value of Portable Instrumentation for the Study of Historical Jewels

This study shows the value of portable Raman spectroscopy for identifying set gemstones and previously misidentified (or imitation) gems in historical jewels, as also demonstrated for the 11th-century Heinrich's Cross reliquary from the treasury of Basel cathedral (Reiche *et al.* 2004), the 13th-century head reliquary of St Eustace from the same treasury (Joyner *et al.* 2006), the 13th-century Chiaravalle Cross (Di Martino *et al.* 2019) and an 18th-century Slovenian baroque chalice (Jeršek & Kramar 2014). The on-site collection of Raman data in combination with portable EDXRF spectroscopy further enabled confident determination of the provenance of certain gemstones in the 9th-century Talisman of Charlemagne reliquary (Panczer *et al.* 2019) and the 17th-century Grand Sapphire of Louis XIV (Farges *et al.* 2015).

REFERENCES

- Capefigue, J.-B.H.R. 1845. *François I^{er} et la Renaissance: 1515–1547*. Amyot, Paris, France, 352 pp.
- Caplan, C. 2018. La vallée mythique de Mogok. In: Ho, K. & Fritsch, E. (eds) *Mogok. La Vallée des Pierres Précieuses*. Editions Glénat, Grenoble, France, 27–51 (see pp. 32–33).
- Carnarvon, A. 1925. *Catalogue of Fine French Furniture, Sèvres Porcelain and Objects of Art and Vertu, the Property of the Right Hon. Almina, Countess of Carnarvon*. Christie, Manson & Woods, London, 74 pp.
- Carò, F., Schorsch, D. & Santarelli, B. 2017. Proveniencing turquoise artifacts from ancient Egyptian contexts: A non-invasive XRF approach. *Science of Ancient Egyptian Materials and Technologies (SAEMT) Conference*, Cairo, Egypt, 4–6 November, poster presentation.
- Cimber, L. & Danjou, F. 1835. Extraits des comptes de dépense de François Premier. In: Cimber, L. (ed) *Archives Curieuses de l'Histoire de France depuis Louis XI jusqu'à Louis XVIII*, 1st Series, Vol. 3. Bourgogne et Mariné, Paris, France.
- Content, D.J. 2016. *Ruby, Sapphire & Spinel: An Archaeological, Textual and Cultural Study*. Brepols, Turnhout, Belgium, viii + 452 pp.
- Davis, C. 1884. *A Description of the Works of Art Forming the Collection of Alfred de Rothschild*, Vol. 2. Chiswick Press, London, 277 pp.
- de La Tour, H. 1893. *Matteo dal Nassaro* (Extrait de la *Revue Numismatique*, 1893). C. Rollin et Feuwardent, Paris, France, 45 pp. + 2 plates.

CONCLUSIONS

The history of the Book of Hours is followed here nearly continuously from 1538, when it was purchased by King Francis I of France, to the present time (see Figure 2), through descriptions in collection inventories and auction catalogues associated with its various French and English owners. In 2017 it was transferred back to France, and in 2018 it was acquired by the Louvre Museum.

We analysed the gemstones adorning the Book of Hours on site at the Louvre, with limited time and equipment, which nevertheless enabled us to better understand its history and to propose some hypotheses about the origins of its gems. The vanadium contents of the rubies are compatible with those of marble-hosted origins, and they most likely originate from the Mogok area of Myanmar. The various turquoise cabochons appear not to be organised in any pattern according to various hues from blue to green, which suggests that some of them could have experienced differential 'ageing' due to exposure to oil or finger grease. We identified the purplish pink faceted stone in the clasp as a rhodolite, which could have originated from south-eastern India or Sri Lanka, both established as historical sources of this garnet variety. Furthermore, we propose that this stone—with its sophisticated faceting—represents a late addition or replacement that was probably set between 1842 and 1884.

Although the Book of Hours still retains some secrets, this masterpiece jewel of the French Renaissance has found its way back to France after 350 years in England and can presently be admired at the Louvre Museum in Paris.

- de Laborde, M.L. 1880. *Les Comptes des Bâtiments du Roi 1528–1571, Suivis de Documents Inédits sur les Châteaux Royaux et les Beaux-Arts au XVI^e Siècle*, Vol. 2. J. Baur, Paris, France, 512 pp.
- Di Martino, D., Benati, G., Alberti, R., Baroni, S., Bertelli, C., Blumer, F., Caselli, L., Cattaneo, R. *et al.* 2019. The Chiaravalle Cross: Results of a multidisciplinary study. *Heritage*, **2**(3), 2555–2572, <https://doi.org/10.3390/heritage2030157>.
- Dirlam, D.M., Rogers, C.L. & Weldon, R. 2019. Gemstones in the era of the Taj Mahal and the Mughals. *Gems & Gemology*, **55**(3), 294–319, <https://doi.org/10.5741/gems.55.3.294>.
- Farges, F., Panczer, G., Benbalagh, N. & Riondet, G. 2015. The Grand Sapphire of Louis XIV and the Ruspoli sapphire: Historical and gemological discoveries. *Gems & Gemology*, **51**(4), 392–409, <https://doi.org/10.5741/gems.51.4.392>.
- Giuliani, G., Groat, L., Fallick, A., Pignatelli, I. & Pardieu, V. 2020. Ruby deposits: A review and geological classification. *Minerals*, **10**(7), article 597 (583 pp.), <https://doi.org/10.3390/min10070597>.
- Gliozzo, E. 2019. Variations on the silica theme: Classification and provenance from Pliny to current supplies. In: G. Artioli & R. Oberti (eds) *The Contribution of Mineralogy to Cultural Heritage*, EMU Notes in Mineralogy, **20**, 13–86, <https://doi.org/10.1180/EMU-notes.20.2>.
- Gliozzo, E., Mattingly, D.J., Cole, F. & Artioli, G. 2014. In the footsteps of Pliny: Tracing the sources of Garamantian carnelian from Fazzan, south-west Libya. *Journal of Archaeological Science*, **52**, 218–241, <https://doi.org/10.1016/j.jas.2014.07.029>.
- Götze, J., Nasdala, L., Kleeberg, R. & Wenzel, M. 1998. Occurrence and distribution of “moganite” in agate/chalcedony: A combined micro-Raman, Rietveld, and cathodoluminescence study. *Contributions to Mineralogy and Petrology*, **133**(1–2), 96–105, <https://doi.org/10.1007/s004100050440>.
- Harmsworth, H.S. 1942. *Description of an Illuminated Manuscript in a Gold and Jewelled Renaissance Binding*. Sotheby & Co., London, 7 pp.
- Hawthorne, J. 1903. *Hawthorne and His Circle*. Harper & Brothers, New York, New York, USA, and London, 372 pp.
- Heaney, P.J. & Post, J.E. 2001. Evidence for an *I2/a* to *Imab* phase transition in the silica polymorph moganite at ~570 K. *American Mineralogist*, **86**(11–12), 1358–1366, <https://doi.org/10.2138/am-2001-11-1204>.
- Hughes, R.W., Manorotkul, W. & Hughes, E.B. 2017. *Ruby & Sapphire: A Gemologist's Guide*. RWH Publishing/Lotus Publishing, Bangkok, Thailand, 816 pp.
- Jeršek, M. & Kramar, S. 2014. Raman microspectroscopy of gemstones from a chalice made in 1732. *Journal of Raman Spectroscopy*, **45**(11–12), 1000–1005, <https://doi.org/10.1002/jrs.4560>.
- Joyner, L., Freestone, I. & Robinson, J. 2006. Crowning glory: The identification of gems on the head reliquary of St Eustace from the Basle [sic] Cathedral Treasury. *Journal of Gemmology*, **30**(3–4), 169–182, <https://doi.org/10.15506/JoG.2006.30.3.169>.
- Lafuente, B., Downs, R.T., Yang, H. & Stone, N. 2015. The power of databases: The RRUFF project. In: Armbruster, T. & Danisi, R.M. (eds) *Highlights in Mineralogical Crystallography*. Walter de Gruyter GmbH, Berlin, Germany, 1–29, <https://doi.org/10.1515/9783110417104-003>.
- Langford, A. & Mead, R. 1755. *A Catalogue of the Genuine and Entire Collection of Valuable Gems, Bronzes, Marble and Other Busts and Antiquities, of the Late Doctor Mead*. Mr. Langford, London, 15 pp., <https://doi.org/10.5962/bhl.title.60533>.
- Louvre 2018. Tous mécènes ! du Livre d'heures de François I^{er} [Become a Patron! Of King François I's Book of Hours]. Musée du Louvre, Paris, France, https://r.lvmh-static.com/uploads/2017/10/dp_louvre_tous-mecenes_livre-dheures-de-francois-ier.pdf, accessed 21 March 2021.
- Malgouyres, P. 2018. *Le Livre d'Heures de François 1^{er}*. Somogy Éditions and Musée du Louvre, Paris, France, 56 pp.
- Mayer, D.D., Mayo, H., Mysak, E., Smith, T.J. & Eremin, K. 2018. Technical examination of the Emerson-White Book of Hours: Observations on pigment preferences and media application in a Flemish manuscript. *Heritage Science*, **6**(1), article 48 (29 pp.), <https://doi.org/10.1186/s40494-018-0211-4>.
- Melo, M.J., Otero, V., Vitorino, T., Araújo, R., Muralha, V.S.F., Lemos, A. & Picollo, M. 2014. A spectroscopic study of brazilwood paints in medieval books of hours. *Applied Spectroscopy*, **68**(4), 434–444, <https://doi.org/10.1366/13-07253>.
- Molinier, E. & Mazerolle, F. 1892. *Inventaire des Meubles du Château de Pau*, 1561–1562. Morgand, Paris, France, 235 pp.
- Mottana, A. 2006. Italian gemology during the Renaissance: A step toward modern mineralogy. In: Vai, G.B., Glen, W. & Caldwell, E. (eds) *The Origins of Geology in Italy*. Geological Society of America Special Paper 411, 1–21, [https://doi.org/10.1130/2006.2411\(01\)](https://doi.org/10.1130/2006.2411(01)).
- Mousavipak, N. 2020. *Physico-chemical characterization of Iranian turquoises: A tentative [sic] to trace Middle-Eastern turquoise-bearing artifacts*. PhD thesis, University of Lyon, France, 128 pp.
- Ogden, J. 2013. Gems and the gem trade in India. In: Jaffer, A. (ed) *Beyond Extravagance: A Royal Collection of Gems and Jewels*. Assouline, New York, New York, USA, 542–593.
- Palke, A.C., Saeseaw, S., Renfro, N.D., Sun, Z. & McClure, S.F. 2019. Geographic origin determination of ruby. *Gems & Gemology*, **55**(4), 580–612, <https://doi.org/10.5741/gems.55.4.580>.

- Panczer, G., Riondet, G., Forest, L., Krzemnicki, M.S., Carole, D. & Faure, F. 2019. The Talisman of Charlemagne: New historical and gemological discoveries. *Gems & Gemology*, **55**(1), 30–46, <https://doi.org/10.5741/gems.55.1.30>.
- Peretti, A. 2015. The making of an international color standard by GRS: “Pigeon’s Blood” and “Royal Blue”. GRS GemResearch Swisslab AG, www.gemresearch.ch/news/2015/04/30/the-making-of-an-international-color-standard-by-grs-pigeons-blood-and-royal-blue, accessed 20 March 2021.
- Plantey, D. 2016. Généalogie féminine et livresque des Albret Navarre aux xv^e et xvi^e siècles. Les livres. In: Plantey, D. (ed) *Les Bibliothèques des Princesses de Navarre au XVI^e Siècle*. Presses de l’Esssib, Villeurbanne, France, 219–242, <https://doi.org/10.4000/books.pressesenssib.4900>.
- Porto, S.P.S. & Krishnan, R.S. 1967. Raman effect of corundum. *Journal of Chemical Physics*, **47**(3), 1009–1012, <https://doi.org/10.1063/1.1711980>.
- Reiche, I., Pages-Camagna, S. & Lambacher, L. 2004. *In situ* Raman spectroscopic investigations of the adorning gemstones on the reliquary *Heinrich’s Cross* from the treasury of Basel Cathedral. *Journal of Raman Spectroscopy*, **35**(8–9), article 719725 (9 pp.), <https://doi.org/10.1002/jrs.1197>.
- Reviewing Committee on the Export of Works of Art and Objects of Cultural Interest (RCEWA) 2017. *Annex A: Statement of [...] Expert Adviser to the Secretary of State that Case 3 (2016-17): Book of Hours in Enamelled Gold Binding Meets Waverley Criteria Two and Three*. Arts Council England, London, 4 pp., www.artscouncil.org.uk/sites/default/files/download-file/BookofHours_easubmission.pdf.
- Reviewing Committee on the Export of Works of Art and Objects of Cultural Interest (RCEWA) 2018. Case 2 Book of Hours in enamelled gold binding. In: *Export of Objects of Cultural Interest, 2016–17*. Arts Council England, London, 20–21, https://assets.publishing.service.gov.uk/government/uploads/system/uploads/attachment_data/file/702504/Export_Objects_Cultural_Interest17_web.pdf.
- Robins, G.H. 1842. *Strawberry Hill, the Renowned Seat of Horace Walpole*. Hazen’s, London, xxiv + 250 pp.
- Schmidt, P., Bellot-Gurlet, L., Leá, V. & Sciau, P. 2013. Moganite detection in silica rocks using Raman and infrared spectroscopy. *European Journal of Mineralogy*, **25**(5), 797–805, <https://doi.org/10.1127/0935-1221/2013/0025-2274>.
- Seifert, A.V. & Vrána, S. 2005. Bohemian garnet. *Bulletin of Geosciences*, **80**(2), 113–124.
- Shigley, J.E., Laurs, B.M., Janse, A.J.A., Elen, S. & Dirlam, D.M. 2010. Gem localities of the 2000s. *Gems & Gemology*, **46**(3), 188–216, <https://doi.org/10.5741/gems.46.3.188>.
- Sutherland, F., Zaw, K., Meffre, S., Thompson, J., Goemann, K., Thu, K., Nu, T., Zin, M. *et al.* 2019. Diversity in ruby geochemistry and its inclusions: Intra- and inter-continental comparisons from Myanmar and eastern Australia. *Minerals*, **9**(1), article 28 (28 pp.), <https://doi.org/10.3390/min9010028>.
- Tallet, P. 2003. Notes sur la zone minière du Sud-Sinai au Nouvel Empire. *Bulletin de l’Institut Français d’Archéologie Orientale*, **103**, 459–486.
- Vollstädt, H. & Baumgärtel, R. 1977. *Einheimische Edelsteine*, 2nd edn. Steinkopff, Dresden, Germany, 230 pp.
- Walpole, H. 1774. *A Description of the Villa of Horace Walpole: Youngest Son of Sir Robert Walpole Earl of Orford, at Strawberry-Hill, Near Twickenham. With an Inventory of the Furniture, Pictures, Curiosities, &c.* Thomas Kirgate, London, 158 pp.
- Yoshida-Takeda, T., Jouve, C.L. & Delumeau, J. 2004. *Inventaire Dressé Après le Décès en 1661 du Cardinal Mazarin*. Peeters Publishers, Leuven, Belgium, xviii + 454 pp.
- Zaw, K., Sutherland, L., Yui, T.-F., Meffre, S. & Thu, K. 2014. Vanadium-rich ruby and sapphire within Mogok gemfield, Myanmar: Implications for gem color and genesis. *Mineralium Deposita*, **50**(1), 25–39, <https://doi.org/10.1007/s00126-014-0545-0>.

The Authors

Prof. Dr Gérard Panczer and Elodie Romeo

Institut Lumière Matière, UMR5306 CNRS Université Claude Bernard – Lyon 1, 12 rue Ada Byron, 69622 Villeurbanne Cedex, France
Email: gerard.panczer@univ-lyon1.fr

Geoffroy Riondet

Maison Riondet, 2 place Gailleton, 69002 Lyon, France

Acknowledgements

The authors warmly thank Philippe Malgouyres, curator at the Decorative Arts and Sculpture departments at the Louvre Museum, Paris, for having allowed us to analyse this major Renaissance masterpiece, and for his contribution to reconstructing the history of the Book of Hours. We thank Dr Jack M. Ogden, London, for providing information and illustrations on the ancient grooving technique. Thanks also to PRISM Lyon (the on-site spectroscopic characterisation centre of cultural heritage materials), ILMTech (the scientific and technological platform of the Light & Matter Institute, Lyon) and CECOMO (Joint Centre for Optical Microspectrometry, Lyon) for their technical support of this study.

Identification of Precious Corals (*Corallium rubrum* vs *C. japonicum*) Using LA-ICP-MS Analysis

Daniel Vielzeuf, Bruna Giordano, Jean-Luc Devidal, Angèle Ricolleau, Jonathan Perrin, Catherine Balme-Heuze and Nicole Floquet

ABSTRACT: Concentrations of Ba and Pb measured by LA-ICP-MS make it possible to distinguish the precious corals *Corallium rubrum* from the Mediterranean Sea and *C. japonicum* from the Pacific Ocean with a high degree of confidence. Compared to *C. japonicum*, *C. rubrum* coral contains higher Ba and Pb (>6 and >0.2 ppm, respectively). This chemical fingerprinting technique was developed by the authors' group during prior research and is successfully tested here on three polished red coral cabochons of known origin. This minimally destructive, relatively inexpensive and easy-to-implement method can help enforce trade regulations by distinguishing CITES-listed *C. japonicum* from non-CITES-listed *C. rubrum* precious corals.

The Journal of Gemmology, 37(6), 2021, pp. 596–607, <https://doi.org/10.15506/JoG.2021.37.6.596>
© 2021 Gem-A (The Gemmological Association of Great Britain)

Precious red coral, *Corallium rubrum* (originally *Madrepora rubra*, Linnaeus 1758; Figure 1), comes from the Mediterranean Sea and adjacent Atlantic Ocean (Zibrowius *et al.* 1984). It has been appreciated for its beauty and used in jewellery and *objets d'art* since antiquity (Hickson 1924; Iwasaki 2010; Tsounis *et al.* 2010; Cooper *et al.* 2011; Santangelo *et al.* 2012; Fürst *et al.* 2016). Mediterranean red coral has been supplied to the jewellery industry through two sources: primarily by fishing present-day colonies, and secondarily from stockpiles of long-dead coral branches collected from sea-floor sediments (mostly during 1875–1914; Bavestrello *et al.* 2021). Indeed, large amounts of *C. rubrum* red coral harvested in Italy in the last 150 years came from the sediments of the Sciacca banks of Sicily, Italy (Rajola 2012; Cattaneo-Vietti *et al.* 2016; e.g. Figure 2). For example, 16,330 t of Sciacca coral were collected over 34 years in the Sicily Channel from the late 19th to early 20th centuries (Cattaneo-Vietti *et al.* 2016). Jewels and beads of Sciacca coral

are still commercialised, particularly from dealers in Torre del Greco, Italy, and in antiques markets. Other *Corallium* species, such as *C. japonicum* (Kishinouye 1903) and *Pleurocorallium elatius* (formerly *C. elatius*, Ridley 1882), both of which come from the western Pacific Ocean, have been traded since the second half of the 19th century (Cooper *et al.* 2011; Nonaka *et al.* 2014). Interestingly, long-dead coral branches (some exceeding 5,000 years old) have also been collected and traded in the Pacific since the 1900s (Okumura *et al.* 2021).

Various studies of precious corals concerning their history, economy, fishing techniques, biology, ecology, mineralogy, chemistry and crystallography are referenced in two proceedings of international workshops (Bussoletti *et al.* 2010; Precious Coral Protection and Development Association 2012). As noted by Cooper *et al.* (2011), precious corals are vulnerable to over-exploitation, and various trade regulations are enforced by different countries. International agreements concerning these species are promulgated by the Convention on International Trade



Figure 1: Precious coral is represented here by (a) a colony of Mediterranean red coral (*C. rubrum*) after removal of the organic tissues (80 g; basal diameter 21 mm), and (b) necklaces and a brooch of *C. rubrum* (beads 12 mm in maximum diameter and brooch 5 cm across). (a) Specimen provided by J. G. Harmelin and photo by D. Vielzeuf; (b) jewellery courtesy of C. Balme-Heuze, and photo by D. Vielzeuf and C. Balme-Heuze.

in Endangered Species of Wild Fauna and Flora (CITES). In 2011, four Coralliidae species (*C. japonicum*, *Pleurocorallium elatius*, *P. konojoi* and *P. secundum*¹, all from the Pacific Ocean) were listed in CITES Appendix III² (Table I). However, *C. rubrum* is not listed in CITES appendices and may be freely traded. Parties to the Convention are required to enforce CITES regulations for listed species, including control of documentation that accompanies exports and imports from registered companies. This enforcement may require the identification of the products on site. From the trade perspective, this problem is covered in *The Coral Book* (CIBJO 2020). However, unambiguous identification criteria for polished coral products are scarce, debatable or difficult to implement.



Figure 2: Sciacca coral comes from sediments in the Sicily Channel, where catastrophic events in this tectonically and volcanically active area deposited broken branches of *C. rubrum*. This specimen (15.7 × 10.0 cm) consists of a mixture of Sciacca coral (orange), sediments (light brown) and calcareous worm tubes (white). Photo by G. Rajola.

Previous Work and Aims of the Present Study

In two previous studies by the authors' group, more than 1,000 analyses were performed by laser ablation inductively coupled plasma mass spectrometry (LA-ICP-MS) on 36 different samples of *C. rubrum*, *C. japonicum*, *P. elatius* and *P. konojoi* (Vielzeuf *et al.* 2018; Ricolleau *et al.* 2019). The 2019 article focused on the variation of Pb contents in *C. rubrum* over several decades. The 2018 article examined variations in the concentrations of Ca, Mg, Na, Sr, S, Li, Ba, Pb and U—within a species and among different species—together with correlations between elements. We observed that some element concentrations (Ca, Mg, Na, Sr, Li and U) depend on growth rate, while others (Ba and Pb) do not. An important conclusion of this work was that the presence of growth rings (marked

¹ The taxonomy used in this article follows the updated classification from the World Register of Marine Species (www.marinespecies.org/aphia.php?p=taxdetails&id=125325). However, renaming of taxa occurred in 2016, after the last CITES listings of precious corals, so CITES uses different biological names (e.g. *C. elatius* instead of *P. elatius*; see Table I). Note also that in jewellery industry terminology, 'precious coral' refers only to corals in the Coralliidae family, whereas in biological lexicon, 'precious coral' encompasses all corals that might be used for decorations.

² CITES Appendix III is meant for species that are not endangered, but have been included at the request of a specific country that already has internal trade regulations in place and is seeking cooperation from other countries to help prevent what it considers to be unsustainable or illegal exploitation. For Coralliidae species currently listed in CITES Appendices, see <https://tinyurl.com/h9seerz6>.

Table I: Descriptions and definitions of the precious corals in this study.^a

Region	Current Scientific Name	CITES classification name	Commercial names	Colours	Fishing areas and depths	Morphology, size and weight	CITES Appendix	Notes and comments
Mediterranean Sea	<i>Corallium rubrum</i> ^b	<i>Corallium rubrum</i>	Mediterranean, Sardinian, Sardegna	Dark red, uniform red to dark orange	Primary: Western Mediterranean Sea Secondary: Eastern Atlantic coast (south Portugal and north-west Africa) Depth: 50-1000 m	Fan or bush shaped Avg. height: 10-20 cm Avg. trunk diam.: 8 mm Avg. weight: 50-300 g	Not included in any appendix	Can be exported and imported in every country
	<i>Corallium rubrum</i>	<i>Corallium rubrum</i>	Sciacca	Orange, pink and darkened 'smoked' orange	Long-dead <i>C. rubrum</i> recovered in Mediterranean Sea sediments, southern Sicily Depth: 30-60 m	Small broken branches Avg. height: 7-10 cm Avg. trunk diam.: 5 mm Avg. weight: 8-30 g	Not included in any appendix	Can be exported and imported in every country
Pacific Ocean	<i>Corallium japonicum</i>	<i>Corallium japonicum</i>	Aka, Moro, Oxblood	Dark red and very dark red with lengthwise white 'soul'	Japan Depth: 80-300 m	Fan shaped Avg. height: 5-30 cm Avg. trunk diam.: 5-25 mm Avg. weight: 100-500 g	Appendix III	CITES listing requested by China
	<i>Pleurocorallium elatius</i>	<i>Corallium elatius</i> (red to dark pink)	Cerasuolo, Momo, Satsuma	Bright red, 'salmon', orange, dark pink and 'flesh' colour with lengthwise white 'soul'	Taiwan and Japan Depth: 150-350 m	Fan shaped Avg. height: 15-40 cm Avg. trunk diam.: 10-50 mm Avg. weight: 100-5000 g	Appendix III	CITES listing requested by China
	<i>Pleurocorallium elatius</i>	<i>Corallium elatius</i> ('flesh' pink)	Angel Skin, Boké, Magai, Peau d'Ange, Pelle d'Angelo	'Flesh' pink with different colour intensities	Japan and Taiwan Depth: 150-350 m	Fan shaped Avg. height: 15-40 cm Avg. trunk diam.: 10-50 mm Avg. weight: 100-5000 g	Appendix III	CITES listing requested by China
	<i>Pleurocorallium konojoi</i>	<i>Corallium konojoi</i>	Pure White, Shiro, Bianco	Milky white and red or pink, speckled white	South China Sea and Vietnam Depth: 80-300 m	Fan shaped Avg. height: 10-40 cm Avg. trunk diam.: 10-30 mm Avg. weight: 100-700 g	Appendix III	CITES listing requested by China

^a Modified after CIBJO (2020).

^b The name 'corallium rubrum' (*corallo rosso*, *corail rouge*, *coral rojo*, etc.) has been used in Mediterranean cultures at least since the Renaissance (e.g. Mesue 1544), long before the attribution of a scientific name to this species. Thus, in Mediterranean cultures the name 'red coral' refers primarily to *C. rubrum*.

by variations in composition) in coral skeletons is due to the alternation of fast and slow growth stages during the year. Although differences in the concentrations of Ba and Pb between precious corals from the Mediterranean Sea and the Pacific Ocean were briefly mentioned in that work, we had not developed this point previously.

The main goal of the present study was to determine whether precious corals have different chemical signatures that can be applied to their separation in a gemmological context. We performed a statistical analysis of our previous LA-ICP-MS data to determine whether differences in the chemical composition of precious corals are statistically significant, with an emphasis on Mediterranean *C. rubrum* and Pacific *C. japonicum*. We focused on these two species because of (1) their historical interest, (2) their distinct geographic origins, (3) the fact that they both can show highly saturated red colour (keeping in mind that other species such *P. elatius* can have a similar colour) and (4) their economic significance (considering that *C. japonicum* fetches the highest prices in today's markets). We also focused on *C. rubrum* and *C. japonicum* corals because they represent the largest number of specimens that we had studied, providing greater reliability of the statistical analysis. In addition, preliminary results for other precious coral species from the Pacific Ocean (*P. elatius* and *P. konojoi*) are briefly discussed.

MATERIALS AND METHODS

The present-day or recent (less than about 100 years old) skeletons of *C. rubrum* used for this study came from the rocky coasts of the Mediterranean Sea in Algeria, Italy, France and Spain. The long-dead *C. rubrum* samples came from the Sciacca banks of Sicily, Italy (this material is hereafter referred to in this article as 'Sciacca coral'). Concerning Pacific samples, colonies of *P. elatius* and *C. japonicum* came from various locations in Tosa Bay (off Shikoku Island, Kochi Prefecture, Japan). Additional specimens of *P. elatius* and *C. japonicum* of unknown origin and harvested before 2016 were obtained from a jeweller's private collection. Descriptions of these samples and their localities are provided in Vielzeuf *et al.* (2018) and Ricolleau *et al.* (2019). In addition, three cabochons—one each of *C. rubrum*, *C. japonicum* and Sciacca coral (Figure 3)—of certified origin, were provided by the Antonino de Simone SRL coral factory in Torre del Greco, Italy. These three samples were analysed for this study to test the applicability of the proposed technique on polished, jewellery-quality samples. LA-ICP-MS analyses were performed on these three cabochons and compared with our previously published data, as a test

of the discriminating method and as a demonstration of the feasibility and the minimally destructive character of the technique.

The trace-element analyses were obtained at Laboratoire Magmas et Volcans (Université Clermont Auvergne, Clermont-Ferrand, France) on an Agilent 7500cs inductively coupled plasma mass spectrometer (ICP-MS) coupled to a Resonetics M-50-E 193 nm excimer laser ablation system with maximum laser fluence of 2.8 J/cm². Analyses were made with a laser pulse frequency of 2 Hz and a beam diameter of 40 µm. The ablated material was carried by helium (0.7 l/min) and then mixed with nitrogen (1.5 ml/min) and argon (0.9 l/min) before entering the ICP. The following isotopes were measured: ⁷Li, ²³Na, ²⁴Mg, ³¹P, ⁵⁵Mn, ⁶⁶Zn, ⁸⁸Sr, ¹³⁷Ba, ²⁰⁸Pb and ²³⁸U, with integration times varying between 30 and 200 ms depending on the element and the session. Typical minimum detection limits (in ppmw or µg/g) were Li = 0.04, Na = 0.3, Mg = 0.2, P = 4.5, Mn = 0.7, Zn = 0.2, Sr = 0.02, Ba = 0.12, Pb = 0.02 and U = 0.01. The mean Ca abundance measured by electron microprobe for each coral species was used as an internal standard and NIST SRM 610 glass was used as an external standard (Gagnon *et al.* 2008). The glasses NIST SRM 612 and USGS BCR-2G (Gao *et al.* 2002) were analysed to check the accuracy and precision of the analyses. A typical signal

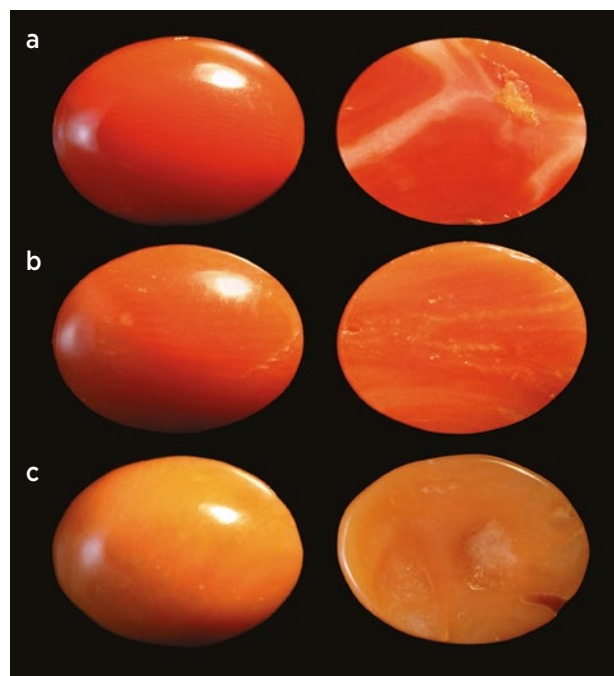


Figure 3: Three coral cabochons of known origin were analysed for this study, and each is shown here from the top and bottom: (a) *C. japonicum* (0.24 g; 9.4 × 7.0 × 2.7 mm), (b) *C. rubrum* (0.21 g; 9.0 × 7.0 × 2.4 mm) and (c) *C. rubrum* Sciacca coral (0.24 g; 8.7 × 6.7 × 3.0 mm). Samples courtesy of Antonino de Simone SRL; composite photo by D. Vielzeuf.

acquisition consisted of collecting a background signal for 30 s followed by the laser firing for 70 s. Trace-element reductions were done with Glitter software (Van Achterbergh *et al.* 2001).

Because analyses were obtained during different sessions, care was taken (1) to analyse the same sample of *C. rubrum* (from Medes Island, Spain) at the beginning of each session to check for analytical consistency, and (2) to use similar instrumental configurations that ensure the reproducibility of the analyses from one session to another. During the analytical process, the signal stability was monitored to identify potential anomalies (e.g. holes or foreign material in the coral). The samples (other than cabochons) were cut perpendicular to the main axis of the coral branch, with or without removal of the dried organic tissues, and mounted in epoxy and polished. The cabochons were analysed without any preparation. Five laser ablation spots were made on the flat base of each cabochon, in zones with the deepest colour. (The specific location of the analyses on the cabochons was probably of little importance, as we found previously that Ba and Pb concentrations are not significantly different in medullar and annular zones; Vielzeuf *et al.* [2018].) The analyses of the three cabochons (plus standards) were carried

out by one of the authors (J-LD), and the 'blind' results were then transmitted to author DV for identification.

Statistical processing of the data, in particular using principal component analysis (PCA), was performed with R! software using the FactoMineR package (Lê *et al.* 2008). PCA is a relevant statistical tool to determine whether populations can be distinguished, with a good degree of confidence, within a given set of data. Two-dimensional scatterplots and circles of elemental correlations demonstrate visually the organisation and clustering of the data and any correlation, inverse correlation or absence of correlation among variables (here, the concentrations of elements).

RESULTS AND DISCUSSION

Discriminating Elements

Figure 4 shows a two-dimensional scatterplot of the PCA results for 542 LA-ICP-MS analyses from 20 samples of *C. rubrum* and 281 analyses from 11 samples of *C. japonicum*. Among the analysed elements, concentrations of seven of them (Li, Na, Mg, Sr, Ba, Pb and U) were reduced to two new variables (principal components PC1 and PC2) that were computed to preserve the maximum amount of information and investigate

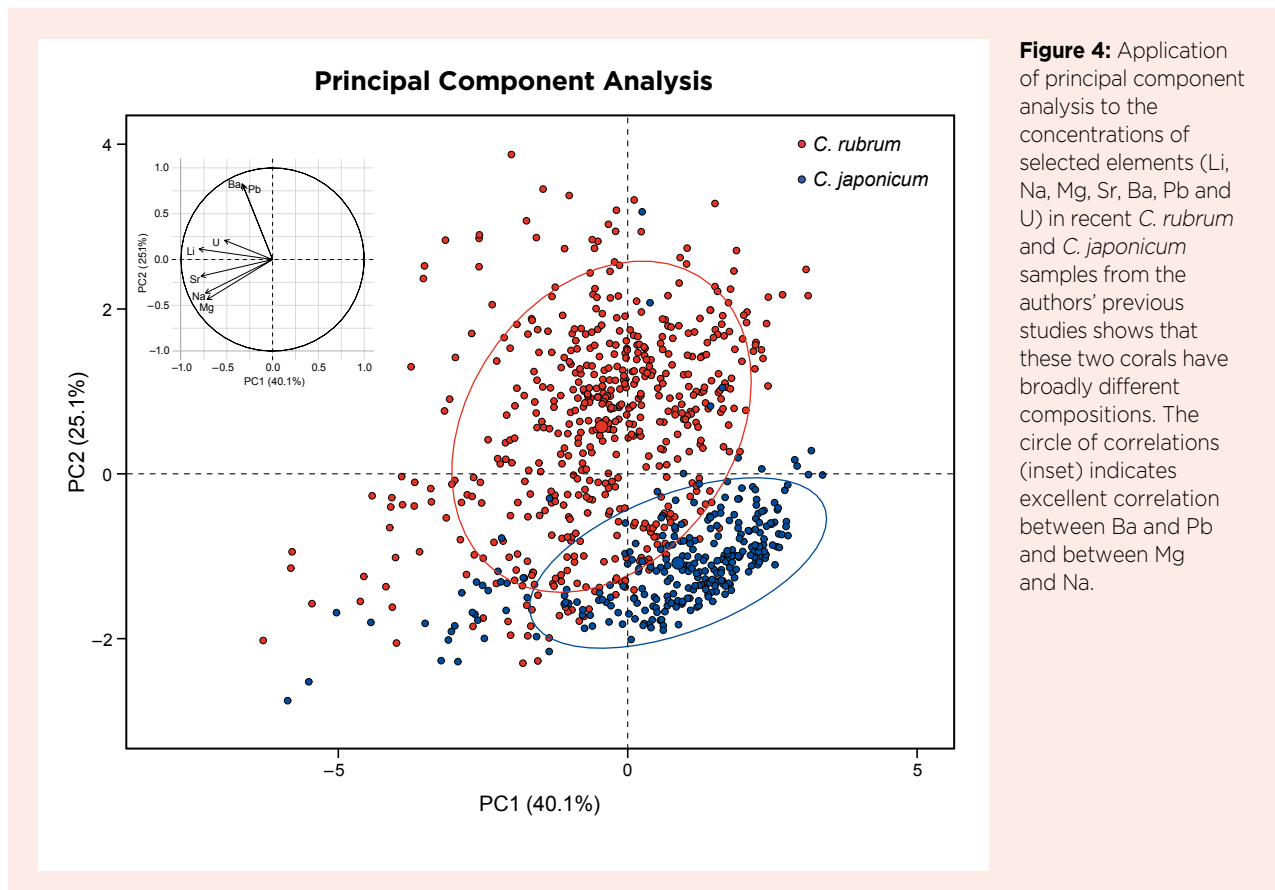


Figure 4: Application of principal component analysis to the concentrations of selected elements (Li, Na, Mg, Sr, Ba, Pb and U) in recent *C. rubrum* and *C. japonicum* samples from the authors' previous studies shows that these two corals have broadly different compositions. The circle of correlations (inset) indicates excellent correlation between Ba and Pb and between Mg and Na.

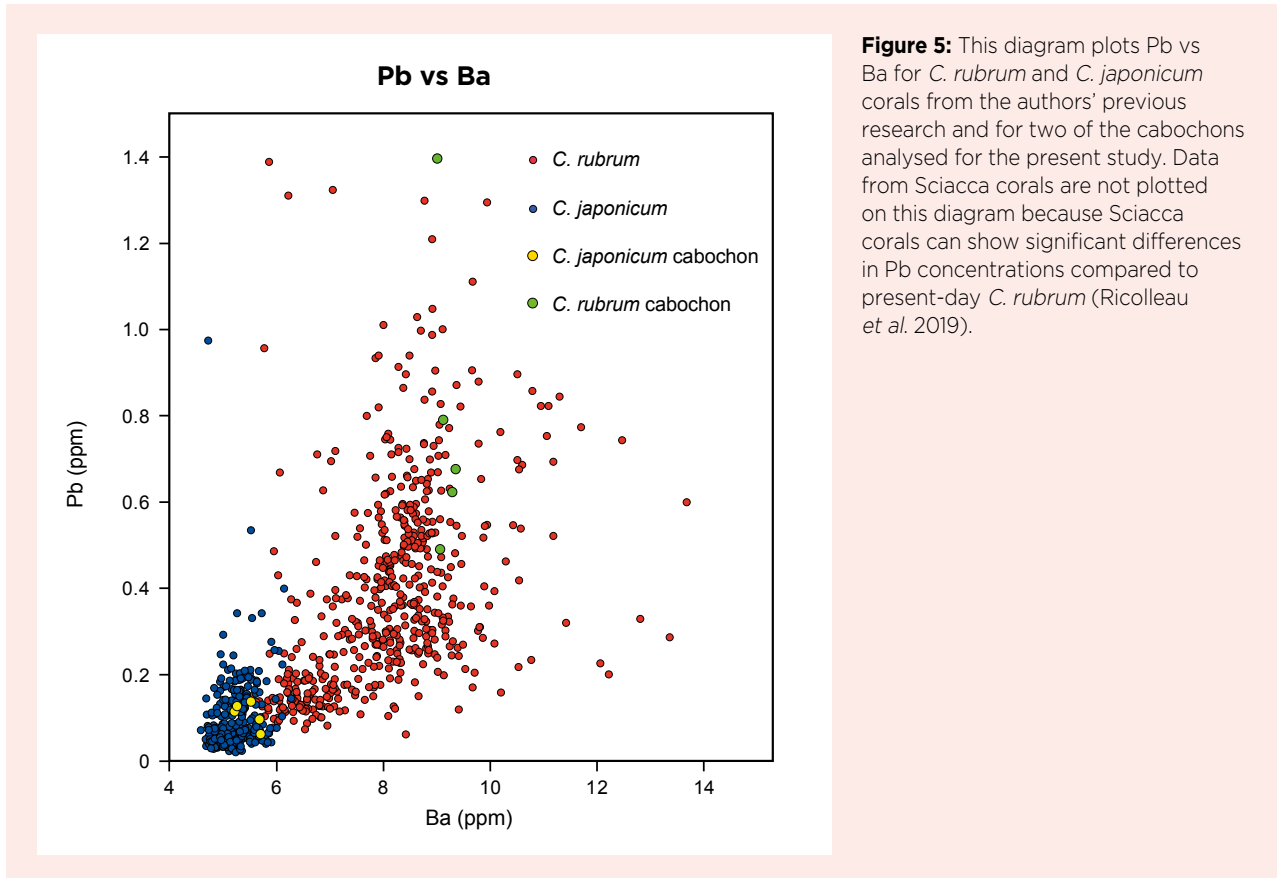


Figure 5: This diagram plots Pb vs Ba for *C. rubrum* and *C. japonicum* corals from the authors' previous research and for two of the cabochons analysed for the present study. Data from Sciacca corals are not plotted on this diagram because Sciacca corals can show significant differences in Pb concentrations compared to present-day *C. rubrum* (Ricolleau *et al.* 2019).

whether the populations were different or not. (The elements P and Zn were not used in the statistical processing as their effect was minor and they mainly added noise to the results. The utility of Mn will be discussed separately below.) Figure 4 shows an obvious clustering of the two groups with limited overlap of the *C. rubrum* and *C. japonicum* domains, meaning that the two populations have statistically different compositions overall. The percentage values shown on the x- and y-axes indicate how much of the variance in the original dataset is explained by each principal component axis. In the present case, PC1 and PC2 account for or 'explain' 40.1% and 25.1% of the overall variability of the data, respectively. Therefore, the explanation rate of the total variance by the two components exceeds 65%.

The circle of correlation in Figure 4 (inset) is a tool to explain the significance of the two principal components. A coincidence of vector direction for two elements indicates a perfect correlation between them. Opposite directions (180°) mean the elements are inversely correlated, while vector directions at 90° point to an absence of correlation between the two elements. Also, the vector length is an indication of the importance of the element in the PCA. In Figure 4, the circle of correlation indicates that Mg and Na, and to a lesser extent Sr,

Li and U, are positively correlated with one another (and inversely correlated with Ca and S, not shown here but demonstrated by Vielzeuf *et al.* [2018]). Furthermore, the vector direction for these elements indicates that they are responsible for the variation along the PC1 axis. This variability—in other words, variations in Mg and Na (and, somewhat, in Sr, Li and U)—can be attributed to differences in growth rate both between annular and medullar zones and within growth rings in *Corallium* skeletons (see Vielzeuf *et al.* [2018] for an extended discussion). The circle of correlation in Figure 4 also shows a strong positive correlation between Ba and Pb in the PC2 vector direction, and no correlation between these two elements and the previous group of elements (Mg and Na). Thus, Ba and Pb are responsible for the variations along the PC2 axis and favour the separation between the *C. rubrum* and *C. japonicum* populations in Figure 4.

This observation led us to plot the data into a binary Pb vs Ba diagram (Figure 5), which shows that the domains of *C. rubrum* and *C. japonicum* overlap only slightly, with Ba and Pb concentration boundaries at 6 and 0.2 ppm, respectively. Indeed, 96% of the *C. rubrum* analyses have Ba contents >6 ppm and 98% of the *C. japonicum* analyses have Ba ≤6 ppm. In addition, 77% of

the *C. rubrum* analyses have Pb contents ≥ 0.2 ppm and 94% of the *C. japonicum* analyses have Pb < 0.2 ppm. These critical values could change slightly as more data become available. These observations agree with the potential of Ba as a strong indicator of the geographic origin of precious corals, as previously proposed by Hasegawa *et al.* (2012) and Vielzeuf *et al.* (2018).

The differences in Ba and Pb concentrations in *Corallium* species from the Pacific Ocean and the Mediterranean Sea can be attributed to the fact that the Mediterranean Sea is a relatively small and closed sea in which concentrations of these elements are higher than in the Pacific Ocean (Lea & Boyle 1991; Ricolleau *et al.* 2019). We carried out a similar statistical analysis on different species of precious corals from the Mediterranean Sea (*C. rubrum*) and Pacific Ocean (*C. japonicum*, *P. elatius* and *P. konojoi*; see diagram in *The Journal's* online data repository). The results show that the Ba and Pb contents of the different Pacific species are too close to distinguish them from each other. Because some pink-to-red corals from the Pacific Ocean are included in CITES Appendix III (i.e. those listed in Table I, as well as *P. secundum*)—while *C. rubrum* is not—it is most important to know whether coral species fished from the Pacific Ocean have a different chemical signature than *C. rubrum* from the Mediterranean Sea.

We did not observe any relationship between colour and Ba or Pb contents in the precious corals we studied, so the chemical fingerprinting method that we propose can be applied to samples encompassing a wide range of colour, from white to pink to deep red.

To summarise, in all these precious corals, we attribute PC1 variations to differences in the growth rates in the skeletons, and we assign PC2 variations to differences in element concentrations between the Mediterranean Sea and Pacific Ocean. The circles of correlations indicate that the most important elements associated with PC1 are Mg and Na, while those associated with PC2 are Ba and Pb.

We therefore carried out additional PCA statistical processing on the same database taking into consideration only the four elements Mg, Na, Ba and Pb. Figure 6 shows that the *C. rubrum* and *C. japonicum* ellipses containing 75% of the data do not overlap and that the explanation rate by the two components rises to 77% (rather than 65%).

The elements Sr, Li and U occupy an intermediate position in the circle of correlation of Figure 4, which could indicate that their variations in the coral skeletons are due not only to growth rate factors, as proposed by Vielzeuf *et al.* (2018), but also to slight differences in

composition, with those from the Mediterranean Sea being slightly richer in these elements than those from the much larger Pacific Ocean. Further work is needed to verify this correlation.

Sciacca Coral

Based on unpublished data mentioned in Rajola (2012) and on further analyses of Sciacca red corals, Ricolleau *et al.* (2019) noted that these long-dead *C. rubrum* corals have slightly lower concentrations of Na, slightly higher concentrations of U and Cu, and much higher concentrations of Mn and Fe than present-day (or recent) samples. We have previously proposed that reducing conditions might have existed in the organic-rich sediments surrounding the dead corals, such that the oxidation states of Mn and Fe changed, allowing these elements to enter the calcitic skeletons (Ricolleau *et al.* 2019). The above-mentioned elements, and especially Mn, could be indicators of diagenetic transformations in the red coral and a distinctive feature of Sciacca versus present-day (or recent) Mediterranean *C. rubrum*. The mean Mn contents in non-Sciacca *C. rubrum* and *C. japonicum* are both close to 1 ppm (Vielzeuf *et al.* 2018). Based on presently available data, we consider that Mn contents greater than 10 ppm indicate diagenetic transformations that affected long-dead Sciacca precious corals.

To the authors' knowledge, chemical data for long-dead precious corals from the Pacific Ocean are not yet available. It would be interesting to check if the chemical features observed in the Sciacca *C. rubrum* samples also apply to long-dead precious corals from the Pacific Ocean.

Results of Blind Testing on the Cabochons

The LA-ICP-MS technique proved to be minimally destructive, as the craters from the analyses were hardly visible on the back surfaces of the cabochons, even under magnification.

Chemical data for the three cabochons are listed in Table II. On the basis of the criteria of Ba > 6 ppm and Pb > 0.2 ppm for distinguishing *C. rubrum* corals, analyses 8, 11, 14, 21 and 24 were identified as *C. japonicum*, and all other analyses came from the two *C. rubrum* cabochons (i.e. Sciacca and present-day or recent coral). The Mn contents in analyses 10, 13, 16, 23 and 26 were approximately 20 times higher than in analyses 9, 12, 15, 22 and 25, which allows the separation of the Sciacca cabochon from the present-day or recent *C. rubrum* sample. In addition, the Na and U contents in the Sciacca corals are, respectively, lower and higher than in the present-day corals (see Table II), as expected from the trends noted by Ricolleau *et al.* (2019). Using

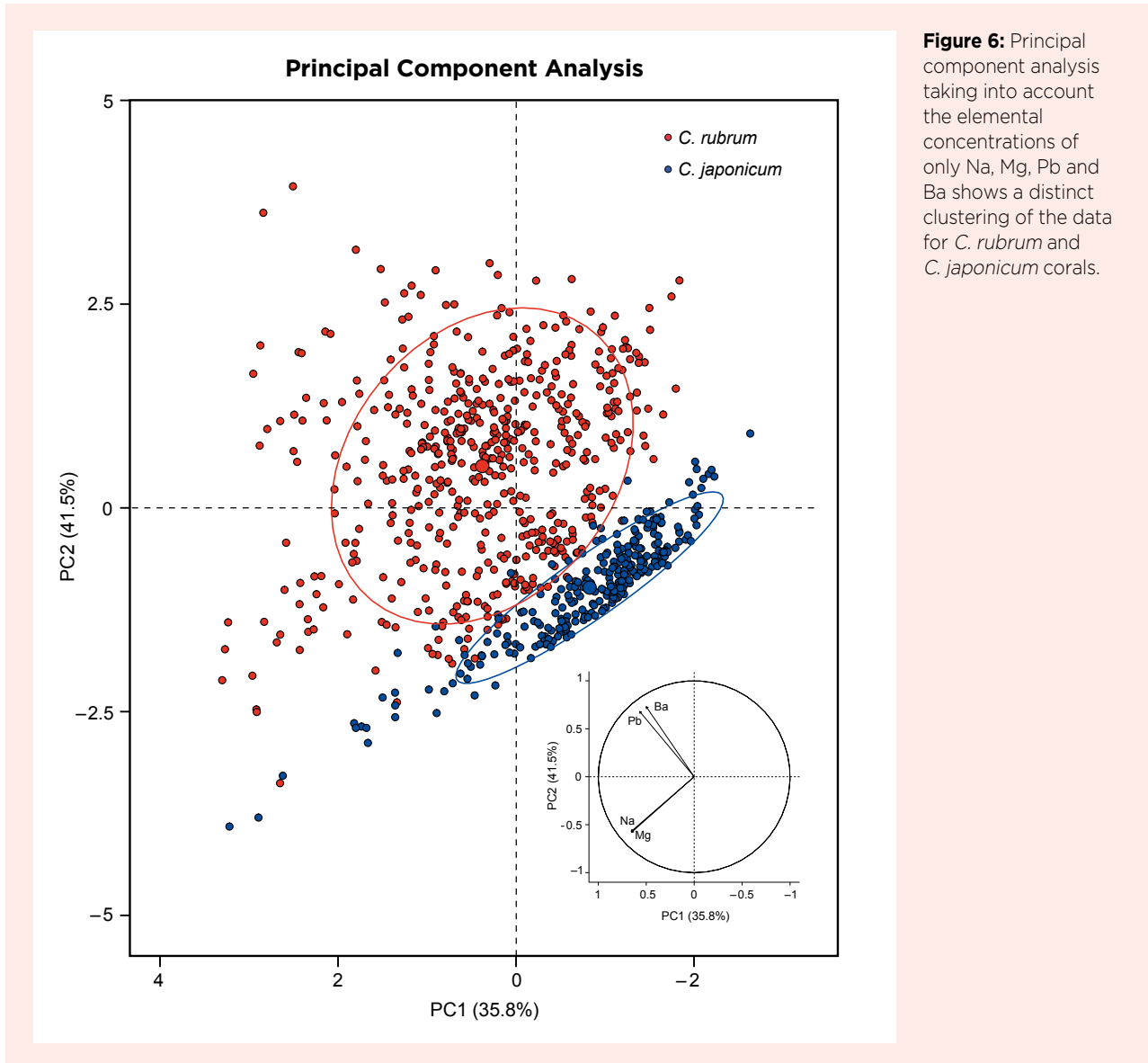


Figure 6: Principal component analysis taking into account the elemental concentrations of only Na, Mg, Pb and Ba shows a distinct clustering of the data for *C. rubrum* and *C. japonicum* corals.

these criteria, all three cabochons were correctly identified. The data for the *C. japonicum* cabochon and the present-day or recent *C. rubrum* sample are plotted in Figure 5. Data for the Sciacca cabochon are not included in this figure because Sciacca coral can show significant differences in Pb concentrations compared to present-day corals (see below and Ricolleau *et al.* 2019).

Suggestions for a Protocol

To determine the provenance of polished corals of unknown origin using LA-ICP-MS chemical analysis, two protocols can be followed: (1) analyse the samples and compare them to data from the present study by plotting the unknowns in the Pb vs Ba diagram, or (2) analyse known samples of *C. rubrum* and *C. japonicum* and use them as standards to compare with samples of unknown origin. The second protocol allows more

accurate determinations, as it avoids comparison of data obtained with different instruments and analytical configurations. As discussed above, the use of a limited number of elements (i.e. Mg, Na, Ba and Pb) could prove more efficient in discriminating populations of precious corals than using all elements commonly measured by LA-ICP-MS. We suggest analysing at least five spots on each sample to assess for any anomalous compositions and to reach a robust conclusion. We expect the concentrations of Ba and Pb in a given sample to be insensitive to the specific location of the analytical spot or variations of colour.

Limitations and Comparison with Other Methods

From a logistical standpoint, a standard LA-ICP-MS sample chamber can accommodate samples up to 17 × 13 × 2.2 cm.

Table II: LA-ICP-MS analyses (in ppm) of three coral cabochons: *C. japonicum*, *C. rubrum* and Sciacca (long-dead *C. rubrum*).*

Analysis no.	Li	Na	Mg	P	K	Mn	Sr	Ba	Pb	U	Identification
8	2.5	3726	30023	194	111	0.9	2653	5.2	0.11	0.08	<i>C. japonicum</i>
11	2.6	3822	29929	204	118	<0.6	2644	5.3	0.13	0.06	<i>C. japonicum</i>
14	2.3	3442	28642	234	122	<0.7	2530	5.7	0.10	0.05	<i>C. japonicum</i>
21	2.6	3656	30171	223	113	1.0	2660	5.7	0.06	<0.03	<i>C. japonicum</i>
24	2.5	3552	29117	197	113	0.8	2533	5.5	0.14	<0.03	<i>C. japonicum</i>
9	3.0	3694	26477	118	127	<0.6	2766	9.1	0.49	0.08	<i>C. rubrum</i>
12	3.1	3645	27567	202	124	0.9	2754	9.1	0.79	0.06	<i>C. rubrum</i>
15	3.5	4109	28166	169	137	1.1	2779	9.3	0.62	0.13	<i>C. rubrum</i>
22	4.7	4853	29776	177	157	0.7	2950	9.4	0.68	0.10	<i>C. rubrum</i>
25	2.4	3187	25692	202	130	1.2	2648	9.0	1.40	0.07	<i>C. rubrum</i>
10	2.1	3069	24792	170	141	22	2683	10.1	0.69	0.22	<i>C. rubrum</i> (Sciacca)
13	2.5	3517	25461	189	145	22	2710	9.1	0.70	0.19	<i>C. rubrum</i> (Sciacca)
16	2.6	3371	26215	166	135	17	2677	9.2	0.72	0.15	<i>C. rubrum</i> (Sciacca)
23	2.4	3231	26351	168	131	17	2690	8.7	0.68	0.18	<i>C. rubrum</i> (Sciacca)
26	2.3	3215	26657	168	135	20	2746	8.4	0.77	0.15	<i>C. rubrum</i> (Sciacca)

* The shaded data show the trends of higher Ba and Pb in *C. rubrum* than in *C. japonicum* corals. In addition, Sciacca corals are enriched in Mn and contain slightly more U and less Na (on average) than present-day or recent *C. rubrum* skeletons.

This may be problematic for larger-sized coral carvings, and also for some *objets d’art* containing coral, as well as some necklaces (e.g. those with coral set in non-articulated metalwork), although special sample chambers are available that can accommodate objects greater than 20 cm in diameter and 12 cm in height.

As with any other discriminating method, applying chemical criteria has some limitations. Although Ba contents are constant within a given coral colony (i.e. no differences between medullar and annular zones) and are stable over time (Vielzeuf *et al.* 2018; Ricolleau *et al.* 2019), one study has shown that Ba concentration in Japanese precious corals increases at ocean depths below about 300 m (Yoshimura *et al.* 2015). Thus, deep-water red Japanese corals might attain Ba contents similar to those of near-surface Mediterranean corals. Further studies are needed to determine if, under extreme circumstances, Ba contents in Mediterranean and Pacific corals overlap. Concerning Pb, Ricolleau *et al.* (2019) showed that *Corallium* skeletons are proxies of the Pb content in

seawater and may show enrichment correlating to peak lead pollution during 1970–1990. Thus, it should be kept in mind that Pb concentrations in precious corals can vary with time and space. Nevertheless, despite these caveats, our studies demonstrate that the discriminating factors we determined are statistically robust.

Characteristics of the organic matrix in the axial skeleton of precious corals are species-specific and also could be used as an identification tool. However, this has been investigated in only a single study that included a limited number of species (Debreuil *et al.* 2011), and so far this method has not been shown to be a standardised or easy-to-use tool (Ledoux *et al.* 2016; Lendvay *et al.* 2020).

Recently, some studies have explored the identification of precious coral species using DNA-based techniques. DNA sequencing methods are promising, but they are easier to implement on soft tissues than on coral skeletons (del Gaudio *et al.* 2004; McFadden *et al.* 2006; Uda *et al.* 2011, 2013; Ledoux *et al.* 2013). Moreover, DNA extraction

from soft tissues is not feasible when working with processed pieces of precious coral. Cartier *et al.* (2018) proposed DNA analysis as a tool in gemmology to distinguish coral species, but noted that DNA fingerprinting required significant amounts of sample material and was difficult to apply on items that cannot be destructively tested. More recently, Lendvay *et al.* (2020) tested different DNA extraction methods to produce high-purity DNA in sufficient quantities from minimal amounts of skeletal material. These authors amplified and sequenced the recovered DNA, and taxonomically identified coral samples through mitochondrial barcoding markers. With this method, *C. rubrum* could be unambiguously distinguished from *C. japonicum* when sufficient skeletal sample material was used. The method was 100% accurate when 100 mg (equivalent to 0.5 ct) of coral was used, but the success rate declined to 64% with a sample size of only 2.3 mg (about 0.01 ct).

CONCLUSIONS

The development of advanced analytical methods is needed to aid in the identification of biogenic gem materials and to separate CITES-listed coral species from those not listed by CITES, in order to address fraud and illegal trading (Cartier *et al.* 2018). The chemical fingerprinting method proposed in this article proved successful for separating *C. rubrum* (e.g. Figure 7) from *C. japonicum* precious corals. More generally, the method allows separation of polished coral specimens from the Pacific and Mediterranean regions. Indeed, an important conclusion of this work is that the primary factor controlling the concentrations of Ba and Pb in the skeletons of precious corals is not the species itself but the composition of the seawater in which it grew. Barium and Pb are of critical importance in marine environments, and therefore this chemical fingerprinting method has implications for scientific disciplines as disparate as gemmology, archaeology, economics, marine ecology,



Figure 7: The Mediterranean coral in this bracelet consists of a naturally closed central branch and 3-mm-diameter beads. Photo courtesy of Antonino de Simone SRL.

and climate and environmental sciences. Regarding the gemmological implications, it must be remembered that identifying a sample as *C. japonicum* does not automatically mean that it is protected by CITES. If such a sample was fished before the species was included in CITES, then it can be traded. Furthermore, samples identified as *C. rubrum* can be freely traded since they are not protected by CITES.

Compared to other advanced analytical techniques, and especially to DNA fingerprinting, the statistically tested chemical fingerprinting method presented here (1) is relatively easy to implement; (2) is minimally destructive, as extremely small amounts of material ($\sim 2 \times 10^{-4}$ mg or $\sim 4 \times 10^{-5}$ ct) are required per analysis; (3) does not require any special preparation of samples; (4) is based on LA-ICP-MS equipment found in several well-equipped gemmological laboratories; and (5) is efficient and relatively affordable, as tens of samples can be analysed in a single day. As such, the method proposed in this article can contribute to the enforcement of international CITES regulations and national laws, and thus to the preservation of the always exquisite *Corallium* species.

REFERENCES

- Bavestrello, G., Bo, M., Calcagnile, L., Canessa, M., D'Elia, M., Quarta, G., Spagnoli, F. & Cattaneo-Vietti, R. 2021. The sub-fossil red coral of Sciacca (Sicily Channel, Mediterranean Sea): Colony size and age estimates. *Facies*, **67**(2), <https://doi.org/10.1007/s10347-020-00620-x>.
- Bussoletti, E., Cottingham, D., Bruckner, A., Roberts, G. & Sandulli, R. (eds) 2010. *Proceedings of the International Workshop on Red Coral Science, Management, and Trade: Lessons from the Mediterranean*. NOAA Technical Memorandum CRCP-13, National Oceanic and Atmospheric Administration, Silver Spring, Maryland, USA, 233 pp.
- Cartier, L.E., Krzemnicki, M.S., Lendvay, B. & Meyer, J.B. 2018. DNA fingerprinting of pearls, corals and ivory: A brief review of applications in gemmology. *Journal of Gemmology*, **36**(2), 152–160, <https://doi.org/10.15506/JoG.2018.36.2.152>.

- Cattaneo-Vietti, R., Bo, M., Cannas, R., Cau, A., Follesa, C., Meliadoro, E., Russo, G.F., Sandulli, R. *et al.* 2016. An overexploited Italian treasure: Past and present distribution and exploitation of the precious red coral *Corallium rubrum* (L., 1758) (Cnidaria: Anthozoa). *Italian Journal of Zoology*, **83**(4), 443–455, <https://doi.org/10.1080/11250003.2016.1255788>.
- CIBJO 2020. *The Coral Book*. CIBJO Coral Commission, version 2020-4, www.cibjo.org/wp-content/uploads/2020/04/20-12-22-Official-Coral-Blue-Book.pdf.
- Cooper, E.W.T., Torntore, S.J., Leung, A.S.M., Shadbolt, T. & Dawe, C. 2011. *Guide to the Identification of Precious and Semi-Precious Corals in Commercial Trade*. TRAFFIC North America and WWF Canada, Vancouver, British Columbia, Canada, 218 pp.
- Debreuil, J., Tambutté, S., Zoccola, D., Segonds, N., Techer, N., Marschal, C., Allemand, D., Kosuge, S. *et al.* 2011. Specific organic matrix characteristics in skeletons of *Corallium* species. *Marine Biology*, **158**(12), 2765–2774, <https://doi.org/10.1007/s00227-011-1775-7>.
- del Gaudio, D., Fortunato, G., Borriello, M., Gili, J.M., Buono, P., Calcagno, G., Salvatore, F. & Sacchetti, L. 2004. Genetic typing of *Corallium rubrum*. *Marine Biotechnology*, **6**(6), 511–515, <https://doi.org/10.1007/s10126-004-3001-9>.
- Fürst, S., Müller, K., Gianni, L., Paris, C., Bellot-Gurlet, L., Pare, C. & Reiche, I. 2016. Raman investigations to identify *Corallium rubrum* in Iron Age jewelry and ornaments. *Minerals*, **6**(2), article 56 (23 pp.), <https://doi.org/10.3390/min6020056>.
- Gagnon, J.E., Fryer, B.J., Samson, I.M. & Williams-Jones, A.E. 2008. Quantitative analysis of silicate certified reference materials by LA-ICPMS with and without an internal standard. *Journal of Analytical Atomic Spectrometry*, **23**(11), 1529–1537, <https://doi.org/10.1039/b801807n>.
- Gao, S., Liu, X., Yuan, H., Hattendorf, B., Günther, D., Chen, L. & Hu, S. 2002. Determination of forty two major and trace elements in USGS and NIST SRM glasses by laser ablation-inductively coupled plasma-mass spectrometry. *Geostandards and Geoanalytical Research*, **26**(2), 181–196, <https://doi.org/10.1111/j.1751-908X.2002.tb00886.x>.
- Hasegawa, H., Rahman, M.A., Luan, N.T., Maki, T. & Iwasaki, N. 2012. Trace elements in *Corallium* spp. as indicators for origin and habitat. *Journal of Experimental Marine Biology and Ecology*, **414–415**, 1–5, <https://doi.org/10.1016/j.jembe.2012.01.005>.
- Hickson, S.J. 1924. *An Introduction to the Study of Recent Corals*. The University Press, Manchester, xiv + 257 pp.
- Iwasaki, N. 2010. *A Biohistory of Precious Corals—Scientific, Cultural and Historical Perspectives*. Tokai University Press, Hadano-shi, Kanagawa, Japan, 286 pp.
- Kishinouye, K. 1903. Preliminary note on the Coralliidae of Japan. *Zoologischer Anzeiger*, **26**(705), 623–626.
- Lê, S., Josse, J. & Husson, F. 2008. FactoMineR: An R package for multivariate analysis. *Journal of Statistical Software*, **25**(1), 1–18, <https://doi.org/10.18637/jss.v025.i01>.
- Lea, D.W. & Boyle, E.A. 1991. Barium in planktonic foraminifera. *Geochimica et Cosmochimica Acta*, **55**(11), 3321–3331, [https://doi.org/10.1016/0016-7037\(91\)90491-m](https://doi.org/10.1016/0016-7037(91)90491-m).
- Ledoux, J.-B., Aurelle, D., Féral, J.-P. & Garrabou, J. 2013. Molecular forensics in the precious Mediterranean red coral, *Corallium rubrum*: Testing DNA extraction and microsatellite genotyping using dried colonies. *Conservation Genetics Resources*, **5**(2), 327–330, <https://doi.org/10.1007/s12686-012-9795-2>.
- Ledoux, J.-B., Antunes, A., Haguenaer, A., Pratlong, M., Costantini, F., Abbiati, M. & Aurelle, D. 2016. Molecular forensics into the sea: How molecular markers can help to struggle against poaching and illegal trade in precious corals? In: Goffredo, S. & Dubinsky, Z. (eds) *The Cnidaria, Past, Present and Future*. Springer, Cham, Switzerland, 729–745, https://doi.org/10.1007/978-3-319-31305-4_45.
- Lendvay, B., Cartier, L.E., Gysi, M., Meyer, J.B., Krzemnicki, M.S., Kratzer, A. & Morf, N.V. 2020. DNA fingerprinting: An effective tool for taxonomic identification of precious corals in jewelry. *Scientific Reports*, **10**(1), article 8287 (12 pp.), <https://doi.org/10.1038/s41598-020-64582-4>.
- Linnaeus, C. 1758. *Systema Naturae per Regna Tria Naturae, Secundum Classes, Ordines, Genera, Species, cum Characteribus, Differentiis, Synonymis, Locis*, Vol. 1, 10th revised edn. Laurentius Salvius, Holmiae [Stockholm, Sweden], 824 pp., <https://biodiversitylibrary.org/page/726886>.
- McFadden, C.S., France, S.C., Sánchez, J.A. & Alderslade, P. 2006. A molecular phylogenetic analysis of the Octocorallia (Cnidaria: Anthozoa) based on mitochondrial protein-coding sequences. *Molecular Phylogenetics and Evolution*, **41**(3), 513–527, <https://doi.org/10.1016/j.ympev.2006.06.010>.
- Mesue, J. 1544. *Ioannis Mesuae Damasceni, De Re Medica, Libri Tres, Iacobo Sylvio Medico Interprete*. Christianum Wechelum, Paris, France, 350 pp. (see p. 341).
- Nonaka, M., Nakamura, M. & Muzik, K. 2014. Sexual reproduction in precious corals (Coralliidae) collected in the Ryukyu Archipelago. *Pacific Science*, **69**(1), 1–58.
- Okumura, T., Kumon, F. & Tokuyama, H. 2021. Radiocarbon dating of precious corals off the southwest coast of Kochi Prefecture, southwest Japan. *Radiocarbon*, **63**(1), 195–212, <https://doi.org/10.1017/rdc.2020.114>.

- Precious Coral Protection and Development Association (ed) 2012. *Proceedings of International Precious Coral Forum 2012: IPCF 2012 in Kochi*. Precious Coral Protection and Development Association, Kochi, Japan, 137 pp.
- Rajola, G. 2012. *The Sciacca Mystery: A History of Coral of Times Gone*. Edizioni Scientifiche e Artistiche, Torre del Greco, Italy, 258 pp.
- Ricolleau, A., Floquet, N., Devidal, J.-L., Bodnar, R.J., Perrin, J., Garrabou, J., Harmelin, J.-G., Costantini, F. et al. 2019. Lead (Pb) profiles in red coral skeletons as high resolution records of pollution in the Mediterranean Sea. *Chemical Geology*, **525**, 112–124, <https://doi.org/10.1016/j.chemgeo.2019.07.005>.
- Ridley, S.O. 1882. On the arrangement of the *Coralliidae*, with descriptions of new or rare species. *Proceedings of the Zoological Society of London*, **60**, 221–234.
- Santangelo, G., Bramanti, L., Priori, C. & Iannelli, M. 2012. The Mediterranean red coral: Conservation and management of a high valuable resource. In: *Proceedings of International Precious Coral Forum 2012: IPCF 2012 in Kochi*. Precious Coral Protection and Development Association, Kochi, Japan, 12–26.
- Tsounis, G., Rossi, S., Grigg, R., Santangelo, G., Bramanti, L. & Gili, J.-M. 2010. The exploitation and conservation of precious corals. In: Gibson, R.N., Atkinson, R.J.A., Gordon, J.D.M. & Barnes, H. (eds) *Oceanography and Marine Biology: An Annual Review*. CRC Press, Boca Raton, Florida, USA, **48**, 161–212.
- Uda, K., Komeda, Y., Koyama, H., Koga, K., Fujita, T., Iwasaki, N. & Suzuki, T. 2011. Complete mitochondrial genomes of two Japanese precious corals, *Paracorallium japonicum* and *Corallium konojoi* (Cnidaria, Octocorallia, Coralliidae): Notable differences in gene arrangement. *Gene*, **476**(1–2), 27–37, <https://doi.org/10.1016/j.gene.2011.01.019>.
- Uda, K., Komeda, Y., Fujita, T., Iwasaki, N., Bavestrello, G., Giovine, M., Cattaneo-Vietti, R. & Suzuki, T. 2013. Complete mitochondrial genomes of the Japanese pink coral (*Corallium elatius*) and the Mediterranean red coral (*Corallium rubrum*): A reevaluation of the phylogeny of the family Coralliidae based on molecular data. *Comparative Biochemistry and Physiology Part D: Genomics and Proteomics*, **8**(3), 209–219, <https://doi.org/10.1016/j.cbd.2013.05.003>.
- Van Achterbergh, E., Ryan, C.G., Jackson, S.E. & Griffin, W.L. 2001. Appendix III: Data reduction software for LA-ICP-MS. In: Sylvester, P.J. (ed) *Laser-Ablation-ICPMS in the Earth Sciences: Principles and Applications*. Mineralogical Association of Canada Short Course Series Vol. 29, Ottawa, Ontario, Canada, 239–243.
- Vielzeuf, D., Gagnon, A.C., Ricolleau, A., Devidal, J.-L., Balme-Heuze, C., Yahiaoui, N., Fonquernie, C., Perrin, J. et al. 2018. Growth kinetics and distribution of trace elements in precious corals. *Frontiers in Earth Science*, **6**, article 167 (18 pp.), <https://doi.org/10.3389/feart.2018.00167>.
- Yoshimura, T., Suzuki, A. & Iwasaki, N. 2015. Ba, B, and U element partitioning in magnesian calcite skeletons of *Octocorallia* corals. *Biogeosciences Discussions*, **12**(1), 413–444, <https://doi.org/10.5194/bgd-12-413-2015>.
- Zibrowius, H., Monteiro Marques, V. & Grasshoff, M. 1984. La répartition du *Corallium rubrum* dans l'Atlantique (Cnidaria : Anthozoa : Gorgonaria). *Téthys*, **11**(2), 163–170.

The Authors

Dr Daniel Vielzeuf¹, Bruna Giordano^{1, 2}, Dr Jean-Luc Devidal³, Dr Angèle Ricolleau¹, Dr Jonathan Perrin⁴, Catherine Balme-Heuze⁵ and Dr Nicole Floquet¹

¹ Aix Marseille Université, CNRS, Centre Interdisciplinaire de NanoScience de Marseille, UMR 7325, 13288 Marseille, France
E-mail: vielzeuf@cinam.univ-mrs.fr

² CNRS-Sorbonne Université, Laboratoire d'Ecogéochimie des Environnements Benthiques, LECOB, Observatoire Océanologique de Banyuls sur Mer, Banyuls-sur-Mer, France

³ Laboratoire Magmas et Volcans, Université Clermont Auvergne – CNRS – IRD, OPGC, 6 Avenue Blaise Pascal, campus universitaire des Cézeaux, 63178 Aubière, France

⁴ Synchrotron SOLEIL, L'Orme des Merisiers, Saint-Aubin, BP48, 91192 Gif-sur-Yvette, France

⁵ Corallium, 1 Pl. Sadi Carnot, La Ciotat, France

Acknowledgements

This work was supported by the Centre National de la Recherche Scientifique (CNRS), the Institut National des Sciences de l'Univers (INSU) and the Agence Nationale pour la Recherche (ANR) through ANR MOBi 2018-2021. This study benefitted from the generosity of numerous contributors who supplied samples. We thank P. Raffin, J. G. Harmelin, J. Garrabou, N. Yahiaoui, F. Costantini and C. Marschal for providing *C. rubrum* samples from various places in the Mediterranean region. G. Rajola (Torre del Greco, Italy) supplied some Sciacca samples, while Antonino de Simone SRL (Torre del Greco) provided the cabochons. Samples of *C. japonicum*, *C. elatius* or *C. konojoi* were kindly provided by S. Tambutté of the Centre Scientifique de Monaco (CSM) and G. Tanaka of the Precious Coral Protection and Development Association of Japan. We also thank K. Saiki of Osaka University for establishing our fruitful exchange with G. Tanaka. Comments from three anonymous reviewers were also helpful. This is contribution ANR MOBi no. 3.

Iridescent Ammonite Fossil Shell Material from Norilsk, Krasnoyarsk Krai, Russia

Viktor A. Radko, Sergey A. Ananyev, Dmitry A. Petrochenkov and Svetlana S. Bondina

ABSTRACT: In 2017, small quantities of ammonites showing a colourful iridescent nacreous surface began to appear on the Russian market. The deposit is located near Norilsk in the former Taymyr (Dolgan-Nenets) Autonomous Okrug, Krasnoyarsk Krai, north-western Siberia. The ammonites (*Placentoceras* sp. nov.) are encased in calcareous sandstone concretions associated with Late Cretaceous (Turonian) sedimentary deposits, and were glacially transported from an unknown location. The nacreous surface consists of 93 wt. % aragonite with minor apatite, vaterite, calcite and siderite; traces of pyrite and quartz are also present. Iridescence of the fossilised nacreous surface is associated with preserved platy aragonite layers of the ammonite shell. The aragonite microcrystals are 1.5–2.5 µm wide and 0.4–0.6 µm thick, and their structure and size determine the iridescence colour. The colourful appearance of the material is enhanced by treatment (impregnation with epoxy resin), and the resulting product can be used to make a wide range of decorative products and jewellery items.

The Journal of Gemmology, 37(6), 2021, pp. 608–617, <https://doi.org/10.15506/JoG.2021.37.6.608>
© 2021 Gem-A (The Gemmological Association of Great Britain)

Collector-quality ammonites are widely available on the global market. They are used as fossil specimens, ornamental and decorative pieces, and jewellery material (e.g. doublets and triplets). The main sources of such ammonites are Madagascar (Walaszczyk *et al.* 2014; Zakharov *et al.* 2016), Morocco (Bockwinkel *et al.* 2013) and Canada, which produces fine-quality iridescent material called *Ammolite* that was introduced to the gem market in the late 1960s (Wight 1981; Mychaluk *et al.* 2001; Mychaluk 2009; Petrochenkov *et al.* 2018). There are several sources of collector- and jewellery-quality ammonites in Russia, which come from Jurassic and Cretaceous deposits in the Ulyanovsk, Ryazan, Saratov and Yaroslavl regions, as well as in the republics of Dagestan and Adygeya (Bystrov *et al.* 2018; Petrochenkov & Bykhovskiy 2018; Petrochenkov 2019; Petrochenkov & Baraboshkin 2019).

In 2002, ammonite fragments showing beautiful

iridescent nacreous surfaces (e.g. Figure 1) were found 130–150 km north-east of Norilsk in the former Taymyr (Dolgan-Nenets) Autonomous Okrug (which was merged into Krasnoyarsk Krai in 2007) in north-western Siberia (Radko 2013; Figure 2). Geographically, the site is located at the junction of the north-western part of the Kharayelakh Range and the western end of the North Siberian Lowland. The area is underlain by sedimentary rocks of the Yenisei-Khatanga Basin (Figure 2a) and is almost completely covered with glacial moraine sediments (Strunin *et al.* 1994). In the lower reaches of the Ikon, Kumga and Tal'mi Rivers (eastern tributaries of the Pyasina River), alluvial and moraine sediments contain fragments of Mesozoic rocks consisting of rounded concretions of dark brown sandstone that sometimes contain fossilised pelecypods, ostracods and belemnites, as well as rare large ammonites (*Placentoceras* sp. nov.; Petrochenkov *et al.* 2019; Radko 2019).

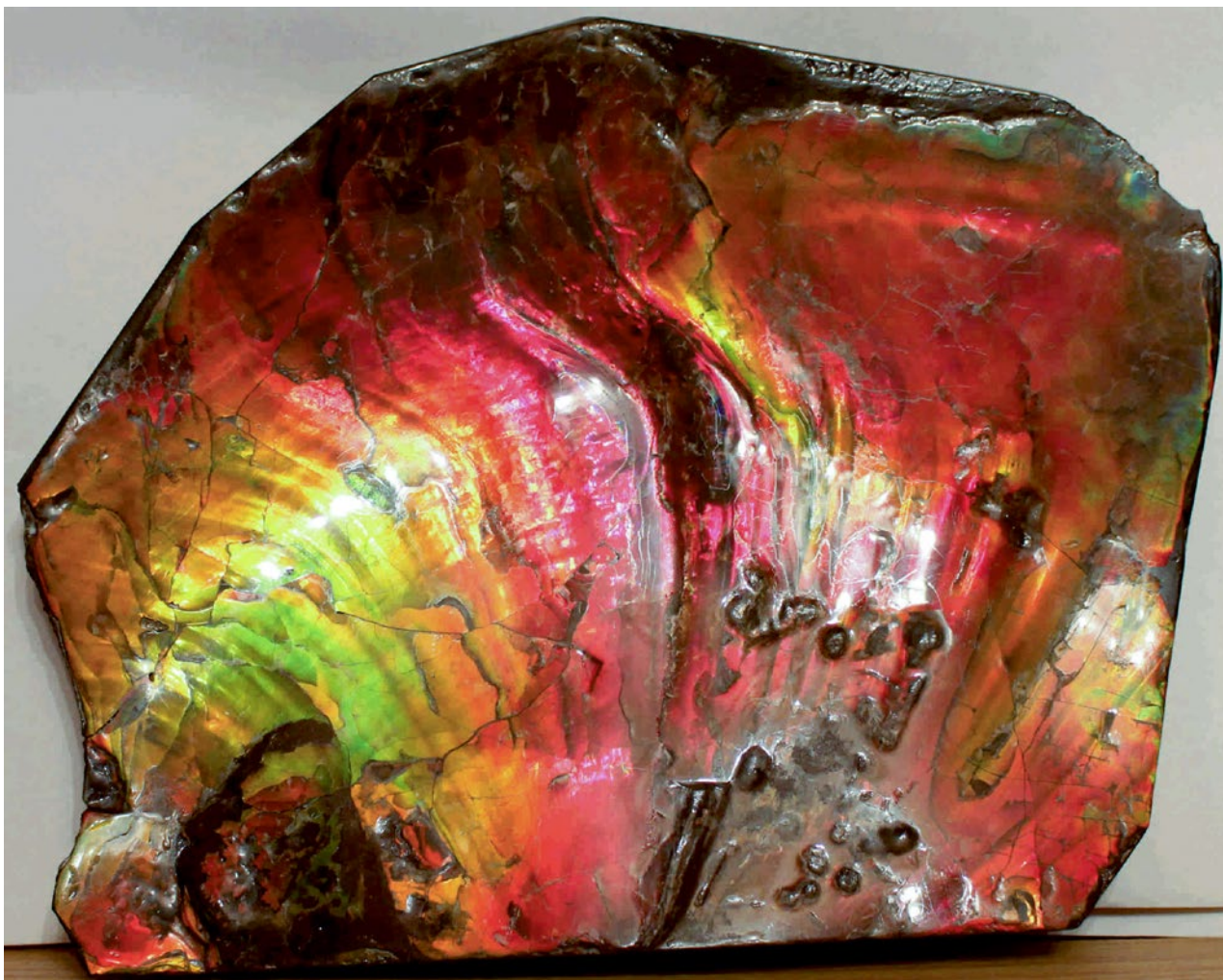


Figure 1: This specimen of ammonite fossil shell material from north-east of Norilsk, Russia, displays bright iridescence. The pattern created by the colour bands resembles tongues of fire. The piece measures 32 × 25 cm, and has been reassembled and impregnated with epoxy resin. Photo by V. A. Radko.

GEOLOGICAL BACKGROUND

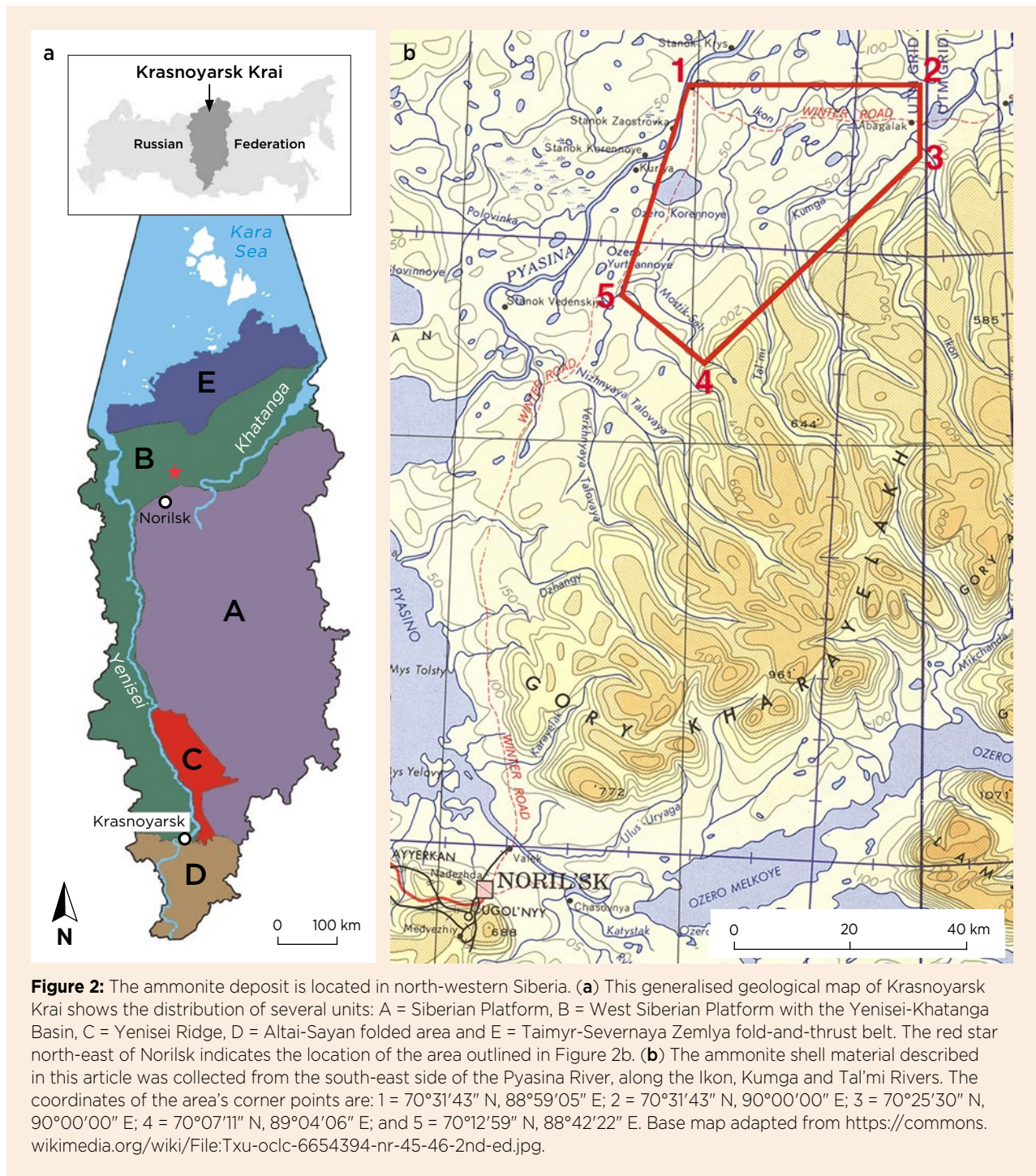
The ammonite-bearing area is difficult to access (i.e. requiring off-road transport or helicopter) and is poorly studied in terms of geology. The first geological description of the locality dates to 1945 and was reported by Saks and Ronkina (1957). The earliest fossil faunal determinations from the Late Cretaceous sediments of the Ikon and Tal'mi Rivers were given by V. A. Markovsky in 1962 (as reported in Strunin *et al.* 1994). He noted that faunal accumulations, including large *Placenticerias* sp. nov.¹ ammonites, were observed in concretions up to 1.2 m across. This genus is known from Turonian-age (90–94 million years) sediments in the Ust-Yeniseisky District (Strunin *et al.* 1994), part of the former Taymyr (Dolgan-Nenets) Autonomous Okrug. According to V. Z. Malkin's description (as reported in Strunin *et al.* 1994), concretions from this area also contain other fossils of

Santonian–Turonian age (about 84–94 million years) in addition to the *Placenticerias* sp. nov. ammonites.

Markovsky reported that these deposits crop out in erosional windows of the overlying strata. In an additional geological study (GDP-200; cf. Strunin *et al.* 1994), V. V. Komarov identified only glacial moraine deposits in the area. According to information gathered during the drilling of wells as part of a geological survey at 1: 50 000 scale, S. A. Vilinsky found that Cretaceous sediments of the Ikon River valley occur at least 200 m below the surface (cf. Strunin *et al.* 1994).

In the summer of 2002, author VAR initially identified the presence of collector- or ornamental-quality fossilised shell material in the area while collecting agates and

¹ The designation 'sp. nov.' means *species nova* and refers to a new species.



ornamental jasperoids in the basins of the Ikon, Kumga and Tal'mi Rivers (Radko 2013; Figures 2b and 3). At that time, nacreous surfaces on the ammonites were noted, with the thought that they might be of interest to collectors and as ornamental material.

Further prospecting showed that the paleontological remains are hosted by rounded (sometimes flattened) concretions composed of carbonate-bearing quartz-feldspar sandstone. The concretions commonly occur as

broken fragments due to fracturing that took place during glacial transport. They are relatively common along the slopes and riverbeds of the lower reaches of the Ikon, Kumga and Tal'mi Rivers, where they are distributed sporadically within a stratum of brownish yellow and greenish grey sand. The condition of the concretions suggests they were transported a relatively short distance.

Most (93%) of the concretions do not contain any



Figure 3: (a) One of the ammonite prospecting areas north-east of Norilsk is seen here in summertime. (b) Author VAR extracts a large *Placentoceras* sp. nov. ammonite from a sandstone concretion. Photos by V. A. Radko.

fossilised remains. Approximately 4% of them host large shells of pelecypods (bivalved molluscs), sometimes up to 25 cm in diameter. In 3% of the concretions, usually of spherical shape and up to 80 cm in diameter, are bioherms composed of quartz-feldspar sandstone containing up to 30% of detritus consisting of pelecypod shells, ostracods (crustaceans) and ammonites that are typically up to 10 cm in diameter. Small belemnites, up to 7 cm long, are observed very rarely. The bioherms typically form the inner rounded part of such concretions, composing one-third of their total diameter. Large ammonites are found in approximately every 30th concretion (e.g. Figure 4). Well-preserved whole shells of large ammonites have not been found, since they were evidently broken to some extent before burial. However, pieces of such shells can sometimes be reconstructed into more-or-less complete specimens. As a rule,

the lower side of the fossils is better preserved, while the upper part is much more deformed or compacted, which gives the shells a basin-like shape. In some cases, double-sided triangular indentations are present on the sides of the shells, as well as scoring on their surfaces 1–2 mm deep, up to 7 mm wide and 10–15 cm long. We consider these to be bite marks from predators such as ichthyosaurs or other marine reptiles.

Between 2017 and 2020, 28 concretions were discovered that contained ammonites ranging from 20 to 63 cm in maximum dimension. Among them, 12 shells were well preserved and the others broke into pieces while being extracted from the concretions. Approximately half of the ammonites showed distinct iridescence in green and red colours. The total weight of collected specimens exceeds 3,300 kg, and so far about 1,000 cabochons have been cut and polished in sizes ranging from 1 to 5 cm.



Figure 4: The ammonite fossil in Figure 3b is shown here after being removed further from the sandstone concretion. It measures 80 cm in maximum dimension. Photo by V. A. Radko.

MATERIALS AND METHODS

For this study, 58 cabochons and numerous rough samples were selected for analysis at the Mineralogy and Gemology Department of the Russian State Geological Prospecting University, Moscow. Author VAR enhanced all of the cabochons and some of the rough shell material by impregnation with a colourless epoxy resin under vacuum. This treatment fills the pores, binds together the nacreous plates of the shell material and significantly improves the iridescent appearance after polishing (e.g. Figure 5). The basal portion of the cabochons included some of the sandstone underlying the nacreous layer, which adds significant strength to the material. The dome of some of the cabochons consisted simply of the polished iridescent surface, but the majority of them were affixed to a quartz (rock crystal) cap, creating doublets.

Specimens were examined with a gemmological microscope, as well as with a petrographic microscope after being cut into thin sections. Refractive indices were measured on five polished samples using a Russian-built Klio refractometer. Specific gravity was determined hydrostatically on five cabochons (without quartz caps) using a Sartorius G150D scale. Vickers hardness testing was performed on several samples using a Russian PMT-3 microhardness indenter with 50 g load and 15 s exposure. UV fluorescence was tested on five samples using a System Eickhorst Multispec UV lamp with 4-watt short-wave (254 nm) and long-wave (365 nm) bulbs.

The mineral composition of one rough sample was determined by powder X-ray diffraction using a PANalytical X'Pert Pro diffractometer. The microstructure of one rough sample was studied using a Tesla BS 301 scanning electron microscope (SEM). In addition, the

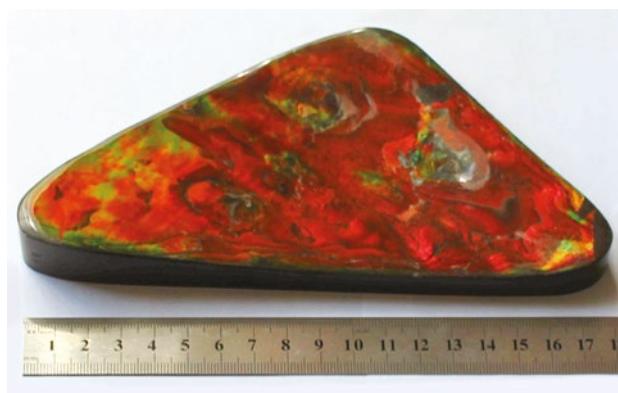


Figure 5: This epoxy-impregnated ammonite doublet (with a quartz cap) displays red and green iridescence. The nacreous surface is underlain by sandstone matrix. The ruler seen here and in other photos in this article is in centimetres. Photo by V. A. Radko.

chemical composition of the sample was analysed in the SEM using energy-dispersive spectroscopy. The trace elements Sr and Ba were also analysed in one polished sample using the energy-dispersive spectrometer of a JEOL JXA-8100 electron microprobe. The oxygen content was calculated on the basis of stoichiometry, and the loss on ignition (a measure of the content of volatiles such as water and CO₂) of one rough sample was measured by thermogravimetric analysis.

RESULTS

Nacreous Surface of the Fossil Shell Material

The ammonites may display dark (black) or light (white) iridescent nacreous surfaces. The white surfaces comprise about 90% of the iridescent material. The light colour of the material is due to the substitution of microporous aragonite by secondary calcite, accompanying the transformation of the ammonites into limestone that is typical of paleontological remains. This ‘chalking’ of the shells might have occurred as far back as the Paleocene. The black variety comprises no more than 10% of the ammonite shell material, and in half of those the aragonite with primary micropores was replaced by iron hydroxides, which also diminishes the iridescence. Shells with a black iridescent surface often have broad white margins, which are a weathering product. The lustre of both the white and black iridescent surfaces is vitreous.

The nacreous surface is found on the outer wall of the ammonite and is 1–2 mm thick (rarely exceeding 3 mm). The internal wall and shell partitions are less than 1 mm in thickness. Crushed shells have been found in which the internal wall and partitions coalesced. In such compressed fragments the thickness of the nacreous surface can increase up to 5 mm, and the individual aragonite layers are separated by sandstone or, less often, by calcite.

The nacreous surfaces of the ammonites were dense and, in some fragments, stratified into thin plates. In the samples examined, they were not transparent but were somewhat translucent in thin layers (up to 1 mm thick).

Gemmological Properties

Spot RI values ranged from 1.52 to 1.67 and the birefringence was 0.13–0.14. No relationship was noted between RI (or birefringence) and the iridescence colour. Specific gravity ranged from 2.84 to 2.86, which is slightly lower than that of aragonite (2.94) and might result from the presence of pores and microfractures. The microhardness of the nacreous surface in the direction perpendicular to

the layering was 366 kg/mm², and increased to 387 kg/mm² parallel to the layering. The microhardness of the inner walls and partitions of the ammonite parallel to the layering varied from 260 to 367 kg/mm², with higher values corresponding to greater preservation of aragonite layers (i.e. less conversion to calcite). No UV luminescence of the nacreous layers or partitions was observed.

The nacreous walls and shell partitions take a good polish, resulting in a high lustre.

Appearance of the Iridescence

Various appearances of the coloured iridescence were observed in the fossilised nacreous surfaces (Figure 6). The most common iridescent colours were red, yellow and brown when samples were viewed perpendicular to their surface. Violet colour was observed only in specimens with a thin white iridescent nacreous surface. In rare samples, the iridescence appeared opalescent. Such material displays many small, multicoloured areas



Figure 6: The ammonite cabochons shown here are up to 3 × 2 cm in size. All samples have been resin impregnated and most of them consist of doublets. **(a)** The ammonite shell material most commonly displays red, yellow and brown iridescence. At a glance, such samples usually appear black or brown, but when observed in some directions the iridescent colours are seen. **(b)** Viewed perpendicular to their surface, the ammonite cabochons commonly display red iridescence. The colour appearance of such material usually shifts to green when observed at an oblique angle, but yellow and, even less often, blue iridescence may be seen. **(c)** Some of the ammonite cabochons show polychrome iridescence in bright red, golden yellow, green and blue-green when viewed at various angles. This material shows practically no 'dead zones' when polished into cabochons. **(d)** Rarely, the ammonite cabochons may display a pearly iridescent effect under natural or artificial daylight. Photos by V. A. Radko.

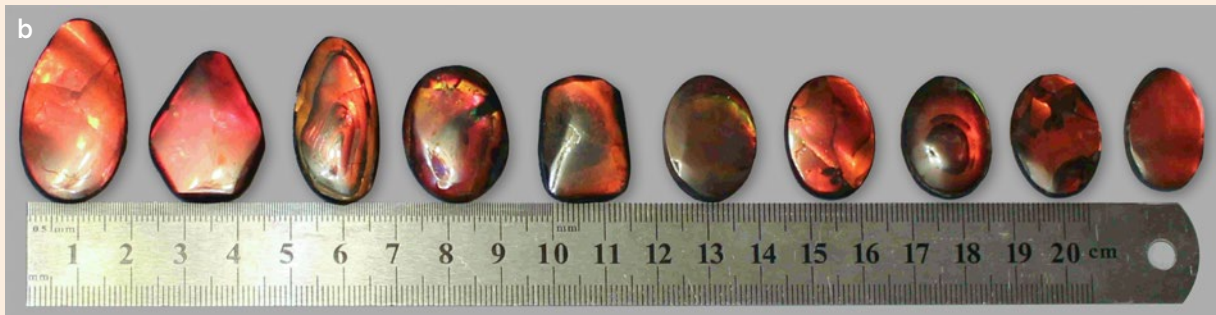




Figure 7: This 10 × 9 cm reconstructed and epoxy-impregnated specimen of ammonite shell material with a white iridescent surface was carved by craftsman S. S. Kochemasov (Norilsk) to display an image of a horse. Pale green iridescence is visible around the horse's neck, and areas showing bright 'pearly' iridescence are locally seen. Photo by V. A. Radko.

that change to different colours when viewed at an angle. This contrasts with the typical iridescent appearance of most specimens, in which a single colour shifts simultaneously throughout the specimen (or in large areas of the sample) as the viewing angle changes.

Also rarely seen was a pearly effect, in which a bright iridescent strip moved across the surface depending on the angle of view (Figure 6d). This appearance was most typically seen in white-type treated material (e.g. Figure 7).

Patchiness of the iridescence colour was observed in all the specimens. This patchiness is due to the internal heterogeneity of the nacreous layers. In addition, some specimens had significant transverse and longitudinal fracturing, along which areas of the nacreous surface had shifted. These areas showed spotty or patchy iridescence after a sample was shaped and polished.

In rare cases, patterns can be seen in the iridescent nacreous surface that can create the appearance of various shapes or scenes, such as a 'bouquet of flowers', 'green mountains with a pink sky' or 'tongues of flame' (again, see Figure 1).

Mineral and Chemical Composition

X-ray diffraction analysis of the nacreous surface of a powdered sample containing marl inclusions revealed that it was composed of 93 wt.% aragonite, 2.5 wt.% apatite, 2 wt.% vaterite, 1.5 wt.% calcite and 1 wt.% siderite, with traces of pyrite and quartz. This composition indicates a high amount of preservation of the original aragonite in the nacreous surface. The aragonite was partially replaced by other minerals, including vaterite, which is an unstable hexagonal form of CaCO_3 that is transitional between aragonite and calcite (Kostov 1971). The presence of quartz and pyrite—as well as some calcite, apatite and siderite—is probably associated with the host sandstone.

The chemical data were consistent with the mineral composition of the nacreous surface. The overall composition (in wt.%) was as follows: $\text{Na}_2\text{O} = 0.42$, $\text{MgO} = 0.06$, $\text{Al}_2\text{O}_3 = 0.07$, $\text{SiO}_2 = 0.19$, $\text{P}_2\text{O}_5 = 1.07$, $\text{S} = 0.76$, $\text{K}_2\text{O} = 0.01$, $\text{CaO} = 52.97$, $\text{TiO}_2 = 0.01$, $\text{MnO} = 0.01$, $\text{Fe}_2\text{O}_3 = 0.34$, $\text{Sr} = 0.51$, $\text{Ba} = 0.01$ and loss on ignition = 42.81.

Microstructural Features

Optical-petrographic and SEM studies provided details of the structural features and mineral composition of the ammonite shells. The walls and partitions of the ammonites were found to be well preserved, with sharp and distinct contacts with the surrounding sandstone (Figure 8a). Microfractures and pores (1–50 μm) were present in the aragonite layers. The pores were concentrated near the edges of the walls and partitions, and were accompanied

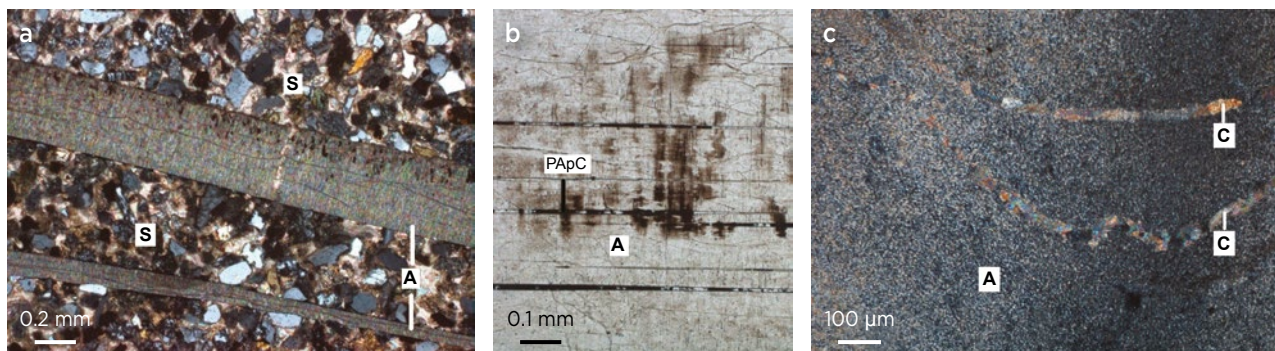


Figure 8: (a) This thin section seen with crossed polarisers shows the ammonite shell walls (A) cemented by sandstone (S). (b) In plane-polarised light, another thin section shows an ammonite shell wall (A) with microfractures oriented parallel and perpendicular to the layers that are filled with pyrite, apatite and calcite (PApC). (c) Another thin section seen with crossed polarisers reveals calcite microveinlets (C) in the ammonite shell wall (A). Reprinted from Petrochenkov *et al.* (2019).



Figure 9: The microstructure of the aragonite layers in the fossilised nacreous surface is shown here with scanning electron microscopy. (a) A step-like fracture surface is caused by the layered structure of the nacre. (b, c) Higher magnification shows the nacre is composed of layers of prismatic aragonite. The arrows point to some individual aragonite crystals. Reprinted from Petrochenkov *et al.* (2019).

by microfractures. Larger fractures were oriented along the aragonite layers. Microfractures crossing layers in individual fragments frequently formed a grid-like pattern that was clearly visible at high magnification. Within the fractures, calcite microveinlets and micrometre-size pyrite and apatite inclusions were present (Figure 8b, c). The microveinlets ranged up to 0.03 mm wide and contained prismatic calcite crystals up to 0.1 mm long.

The nacreous surface disintegrated into plates along the contacts of the layers, which caused further destruction of the aragonite. However, the exterior aragonite layers of the ammonite shell were well preserved. SEM examination of a fragment of nacreous surface (1.8 mm thick) showing red and orange iridescence provided details of the structure of the fossilised nacreous surface. It contained no fractures or mineral impurities, and the sample clearly showed a step-like fracture surface (Figure 9a) that reflected the layered texture of the nacreous surface. The step thickness was 0.1–0.6 mm. Two platy layers of prismatic aragonite crystals were present, and each one consisted of aggregates of individual crystals measuring 1.5–2.5 µm long and 0.4–0.6 µm thick (Figure 9b, c). The elongated prismatic crystals were oriented perpendicular to the layering and arranged as vertical columns in one direction and parallel layers in the other. The layers were composed of tightly intergrown aggregates measuring 10–15 µm long and 1–1.5 µm thick. Contacts between the platy layers were distinct and even, and the width of the layers was dependent on the thickness of the aragonite crystals.

DISCUSSION

Our observations showed that the iridescence and colour of the nacreous surface are determined by the size and structure of the platy layers of prismatic aragonite crystals. As the thickness of the crystals decreases, the colour of iridescence changes from red towards violet,

which corresponds to a decrease in the wavelength of light. There is no iridescence seen when the thickness of the crystals exceeds 0.9 µm. Disturbances in the aragonite layers lead to light scattering, causing the iridescence to become less distinct or disappear completely.

In general, iridescence is rarely observed in this ammonite shell material as it occurs naturally (see Figure 4). This explains why indigenous peoples from the area did not use it for ornamental purposes. However, the iridescence is significantly enhanced after treatment of the nacreous surface, because filling the micropores in the nacre with epoxy resin modifies the behaviour of the light passing through the translucent layers and reflecting from the inner surfaces of the nacre. Various iridescence colours are seen (i.e. red, yellow, green, blue and, in one specimen, purple), which we infer depend on the spacing of the aragonite layers and any gaps between them in the nacre. It is also likely that variations in the size and shape of the micropores in the different layers of the nacre could influence the iridescent colours. We infer that the gaps between aragonite layers and the micropores in the original shell were filled with organic material (conchiolin), which was subsequently broken down during the fossilisation process. Therefore, by filling these cavities with colourless epoxy resin, the optical properties of the nacre (i.e. translucence and iridescence) are enhanced.

Comparing this Russian material with Ammolite from Alberta, Canada (cf. Mychaluk *et al.* 2001) shows some similarities as well as differences. The Russian ammonites are hosted by concretions composed of quartz-feldspar sandstone, which in turn are located in a stratum of coarse glacial sand. The Canadian ammonites are found *in situ* within unglaciated shale, lying loose or encased within sideritic concretions. As for colour effects, Canadian Ammolite is more brightly coloured and more often shows bright blue iridescence when viewed from a perpendicular direction. In the Russian material, blue colour is visible in cabochons only from

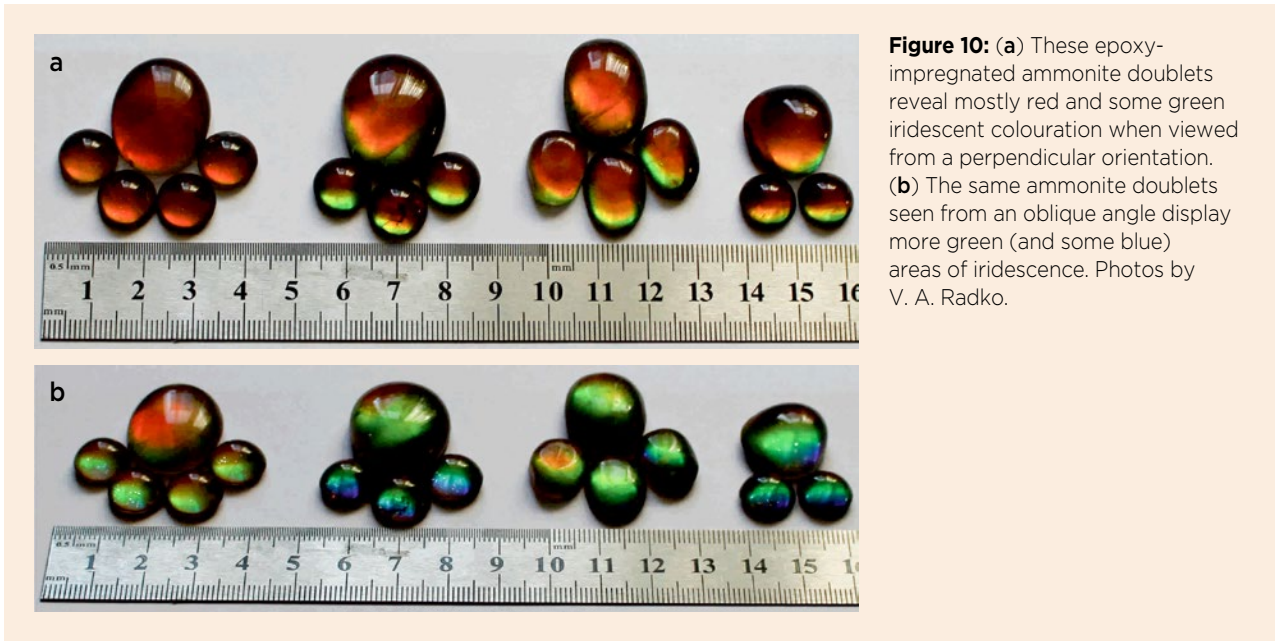


Figure 10: (a) These epoxy-impregnated ammonite doublets reveal mostly red and some green iridescent colouration when viewed from a perpendicular orientation. (b) The same ammonite doublets seen from an oblique angle display more green (and some blue) areas of iridescence. Photos by V. A. Radko.

an oblique direction, as can be seen in Figure 10.

Compared to all other presently known occurrences of collector- and ornamental-quality ammonites in Russia, those from the Norilsk area are superior in terms of their iridescence and size. Some reconstructed ammonites from this locality are quite impressive and could decorate the showroom of any museum (Figure 11). Such specimens are now included in the collections of geological museums in Krasnoyarsk and Norilsk.

CONCLUSION

Small quantities of ammonite fossil shell material showing an iridescent nacreous surface have been collected from

the Norilsk area in northern Krasnoyarsk Krai (north-western Siberia, Russia). After treatment by impregnation with colourless epoxy resin, the material displays attractive iridescence and is suitable for producing a wide range of jewellery and other decorative items, as well as collectible specimens. The authors propose that this ammonite be given the commercial name of *Pearlano-risk* (перланориск, an abbreviated version of перламутр норильский ископаемый, meaning ‘Pearl of Norilsk’). However, no trademark has been registered.

This deposit has good potential for commercial development, although the remoteness of the locality and difficulty of extracting the material from the concretions will limit its production in the future.

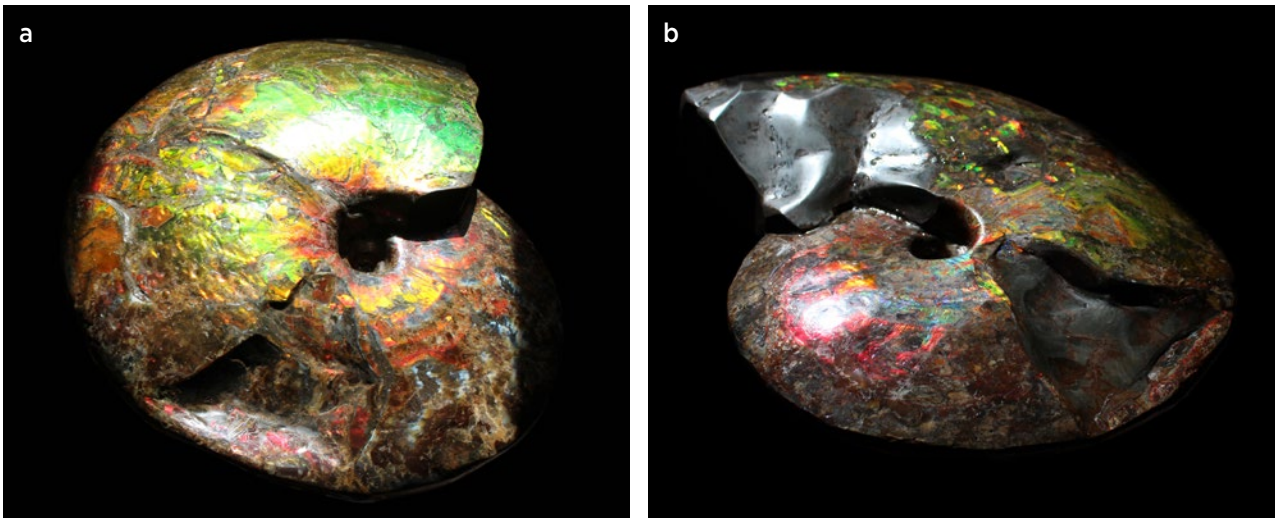


Figure 11: The ‘Emperor of Taymyr’ ammonite (62 × 46 × 15 cm) is shown here from the (a) front and (b) back sides. It has undergone restoration and epoxy impregnation, followed by polishing, and provides an exceptional example of an almost complete specimen. Photos by V. A. Radko.

REFERENCES

- Bockwinkel, J., Becker, R.T. & Ebbighausen, V. 2013. Late Givetian ammonoids from Hassi Nebech (Tafilalt Basin, Anti-Atlas, southern Morocco). *Fossil Record*, **16**(1), 5–65, <https://doi.org/10.1002/mmng.201300001>.
- Bystrov, I.G., Petrochenkov, D.A. & Baraboshkin, E.Y. 2018. Lower Cretaceous jewellery-ornamental ammonites of the Republic of Dagestan. *Dagestan State Pedagogical University Journal: Natural and Exact Sciences*, **12**(1), 32–41, <https://doi.org/10.31161/1995-0675-2018-12-1-32-41> (in Russian with English abstract).
- Kostov, I. 1971. *Mineralogy: Basic Works of Foreign Scientists on Geology, Geophysics, and Geochemistry*. MIR, Moscow, Russia, 584 pp. (in Russian).
- Mychaluk, K.A. 2009. Update on Ammolite production from southern Alberta, Canada. *Gems & Gemology*, **45**(3), 192–196, <https://doi.org/10.5741/gems.45.3.192>.
- Mychaluk, K.A., Levinson, A.A. & Hall, R.L. 2001. Ammolite: Iridescent fossilized ammonite from southern Alberta, Canada. *Gems & Gemology*, **37**(1), 4–25, <https://doi.org/10.5741/gems.37.1.4>.
- Petrochenkov, D.A. 2019. Mineral composition and gemological characteristics of the interior and jewellery ammonites of the Yaroslavl region. *Vestnik of the Institute of Geology of the Komi Science Center of the Ural Branch of the Russian Academy of Sciences*, No. 2, 22–28, <https://doi.org/10.19110/2221-1381-2019-2-22-28> (in Russian with English abstract).
- Petrochenkov, D.A. & Bykhovskiy, L.Z. 2018. Jewellery/ornamental ammonite: Problems of valuation and production prospects. *Mineral Resources of Russia. Economics and Management*, No. 4, 15–22 (in Russian).
- Petrochenkov, D.A. & Baraboshkin, E.Y. 2019. Collection, interior and jewellery ammonites from of [sic] the Lower Aptian deposits, Ulyanovsk region. *National Geology*, No. 1, 79–88, <https://doi.org/10.24411/0869-7175-2019-10009> (in Russian with English abstract).
- Petrochenkov, D.A., Kulikov, V.V., Litvinenko, A.K. & Onikiyenko, L.D. 2018. Gem-quality ammonites of Canada: Features of mining and processing. *Mining Journal*, No. 11, 65–70, <https://doi.org/10.17580/gzh.2018.11.12> (in Russian with English abstract).
- Petrochenkov, D.A., Radko, V.A. & Baraboshkin, E.Y. 2019. Upper Cretaceous collection and ornamental ammonites from the north of Krasnoyarsk region. *National Geology*, No. 5, 76–84, <https://doi.org/10.24411/0869-7175-2019-10041> (in Russian with English abstract).
- Radko, V.A. 2013. *Agates, Carnelians, and Jasperoids of Norilsk*. Published by the author, St Petersburg, Russia, 128 pp. (in Russian).
- Radko, V.A. 2019. Pearl of Norilsk, fossilized. *Nauchny Vestnik Arktiki*, No. 6, 23–26 (in Russian with English abstract on p. 141).
- Saks, V.N. & Ronkina, Z.Z. 1957. The Jurassic and Cretaceous sediments of the Ust'-Yenisei Trough. *Proceedings of NIIGA (Nauch.-Issled. Inst. Geol. Arkt.)* [Scientific Research Institute of Arctic Geology], Gostoptekhizdat, Moscow, Russia, 232 pp. (in Russian).
- Strunin, B.M., Dyzhikov, O.A., Barmina, O.A. & Komarov, V.V. 1994. *Geological Map of the Noril'sk Ore District, Scale 1:200000. Explanatory Note*. Geoinformmark, Moscow, Russia, 118 pp. (in Russian).
- Walaszczyk, I., Kennedy, W.J., Dembiczy, K., Gale, A.S., Praszquier, T., Rasoamiamanana, A.H. & Randrianaly, H. 2014. Ammonite and inoceramid biostratigraphy and biogeography of the Cenomanian through basal Middle Campanian (Upper Cretaceous) of the Morondava Basin, western Madagascar. *Journal of African Earth Sciences*, **89**, 79–132, <https://doi.org/10.1016/j.jafrearsci.2013.10.007>.
- Wight, W. 1981. 'Korite'—Fossil ammonite shell from Alberta, Canada. *Journal of Gemmology*, **17**(6), 406–415, <https://doi.org/10.15506/jog.1981.17.6.406>.
- Zakharov, Y.D., Tanabe, K., Shigeta, Y., Safronov, P.P., Smyshlyaeva, O.P. & Dril, S.I. 2016. Early Albian marine environments in Madagascar: An integrated approach based on oxygen, carbon and strontium isotopic data. *Cretaceous Research*, **58**, 29–41, <https://doi.org/10.1016/j.cretres.2015.08.014>.

The Authors

Dr Viktor A. Radko

Nord-Prospector LLC,
Naberezhnaya Urvantseva 33, Norilsk,
Krasnoyarsk Krai, Russia 663300

**Dr Sergey A. Ananyev and
Dr Svetlana S. Bondina**

Mining, Geology and Geotechnology Institute,
Siberian Federal University, Svobodny 79,
Krasnoyarsk, Russia 660041
Email: sananiev@mail.ru

Dr Dmitry A. Petrochenkov

Russian State Geological Prospecting University,
Miklukho-Maklaya 23, Moscow, Russia 117997



Figure 1: This rough 'indicolite' tourmaline specimen (9.3 mm high) from near Elahera, Sri Lanka, shows strong dichroism. The specimen was photographed twice, with unpolarised transmitted light, after rotation by 90°, showing its appearance roughly along the *c*-axis (left) and with the *c*-axis oriented roughly horizontal to the plane of view (right).
Photos by C. Chanmuang N.

Blue Dravite ('Indicolite') from the Elahera Gem Field, Sri Lanka

Lutz Nasdala, Manfred Wildner, Gerald Giester, Chutimun Chanmuang N., Maria Rosa Scicchitano and Christoph Hauzenberger

ABSTRACT: A strongly dichroic (vivid blue to near-colourless) tourmaline specimen from the Elahera gem field, central Sri Lanka, was identified as dravite. The sample shows strong Fe²⁺-related optical absorption (E_{Lc}) in the red range and comparably weak red emission due to Cr³⁺. The discovery of virtually Cu-free blue dravite (with a Li content of only about 3 ppm) shows that blue colour in gem tourmaline is not restricted to Cu- and/or Fe-bearing elbaite and other lithium tourmalines. Also, this study reconfirms the usefulness of Raman spectroscopy for non-destructive mineral identification. The sensitivity of Raman shifts of O–H stretching bands to their nearest-neighbour cations allowed us to exclude the presence of significant amounts of Li ions, even before obtaining results of light-element analysis.

The Journal of Gemmology, 37(6), 2021, pp. 618–630, <https://doi.org/10.15506/JoG.2021.37.6.618>
© 2021 Gem-A (The Gemmological Association of Great Britain)

Among the almost complete spectrum of colours of gem tourmaline (Pezzotta & Laurs 2011), some of the blue hues are perhaps the most sought after and highly valued. This is especially true of ‘neon’-blue Paraiba-type tourmaline, which is coloured by Cu^{2+} (Fritsch *et al.* 1990; Laurs *et al.* 2008; Merkel & Breeding 2009). The blue colour of tourmaline commonly referred to as ‘indicolite’ in the trade is mainly caused by Fe^{2+} (Faye *et al.* 1968; Merkel & Breeding 2009). Such colouration is seen mostly in Fe-bearing lithium tourmalines, including elbaite, fluor-elbaite and fluor-liddicoatite (Pezzotta & Laurs 2011 and references therein). By contrast, blue colour does not seem to be common in lithium-free tourmalines such as dravite and uvite (Novák 1998; Selway *et al.* 1998; Garda *et al.* 2002; Pieczka 2007; Nicastro & Sun 2016).

Even though gem ‘indicolite’ from Sri Lanka has been mentioned occasionally in the literature (e.g. Herath 1984; Ariyaratna 1993), we know of no published mineralogical description of this material thus far. In the present article we characterise in detail a strongly dichroic blue tourmaline (Figure 1) originating from the southern part of the Elahera gem field, where gravels of the Kalu Ganga

are currently mined from numerous pits and extraction sites on both sides of the Elahera-Pallegama road. The stone described in this paper was acquired from a local miner during a field trip to Sri Lanka in February 2020.

LOCATION AND MINING

Kalu Ganga (or *Kalu Gaṅga*, Sinhalese for ‘Black River’) is in the Matale District, Central Province, Sri Lanka (Figure 2). It should not be confused with its much more well-known namesake in the Ratnapura area of south-western Sri Lanka (Western and Sabaragamuwa provinces). The Kalu Ganga of the Central Province originates in the Knuckles Mountain Range, north-east of the town of Kandy. About 5 km east of the village of Elahera, this creek flows into the Amban Ganga, a tributary of the Mahaweli Ganga. Eluvial (also referred to as *residual*) gem deposits are located along the lower stretch of the Kalu Ganga as well as further north, east of Bakamuna, in the Amban Ganga valley. They have been exploited by small- to large-scale mining activities along a south-north distance of roughly 25–30 km (again, see Figure 2). These gem mines have a long history, dating

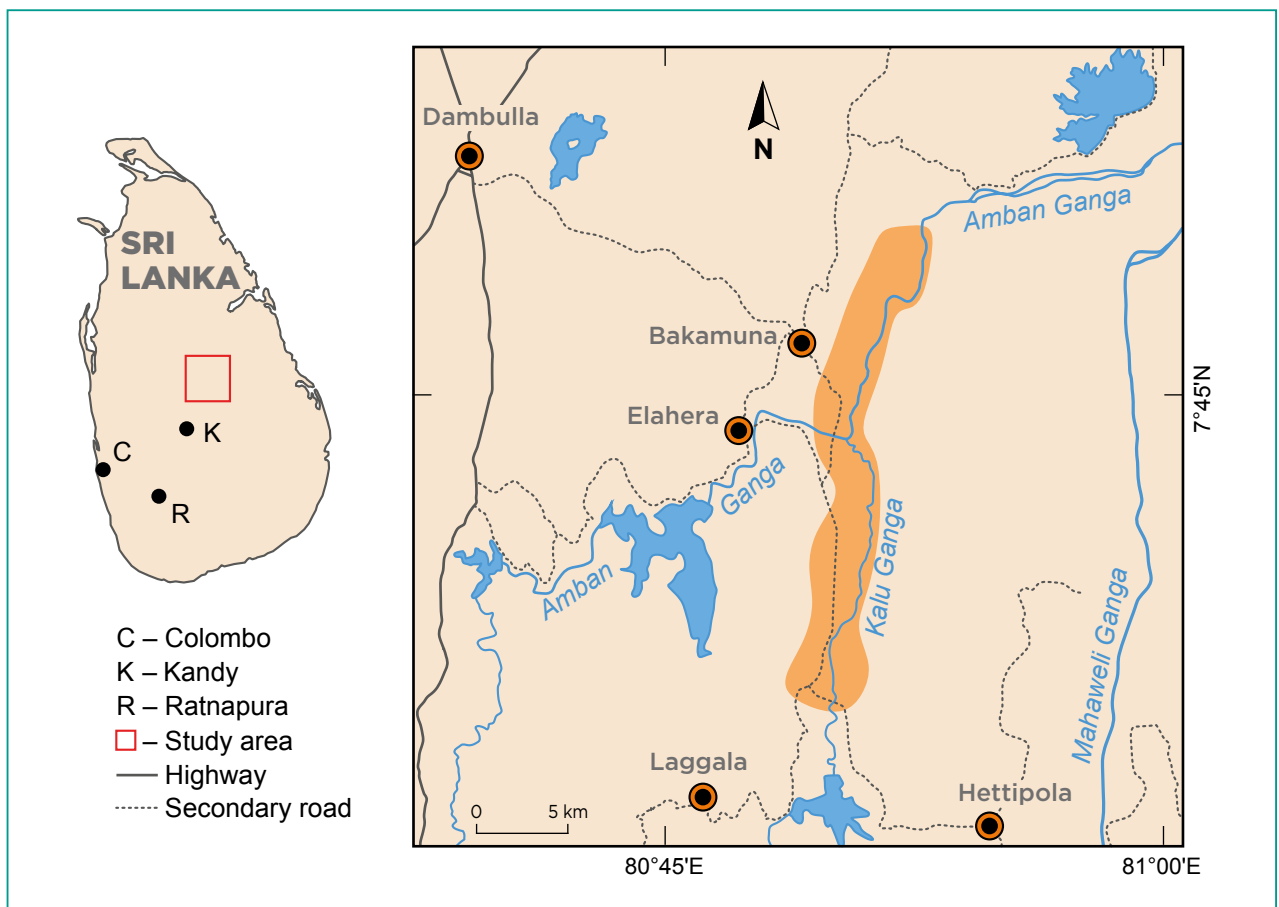


Figure 2: The location of the gem-bearing sediments east of Elahera, central Sri Lanka, is shaded in orange on this map.



Figure 3: Both small- and large-scale gem mining takes place in the Elahera gem field. (a) Workers extract gem-bearing gravels from about 2 m below the surface in a small pit, using pick, spade and shovel. (b) Gravel panning is done using reed baskets (*watti*). Larger amounts of machine-excavated sediments are washed and sorted using sluices, trommel scrubbers and vibrating bins, either on site (c) or after being transported by truck to washing plants (d). Photos by L. Nasdala (a and b, taken February 2013) and Ralf Grunert (c and d, taken February 2020).

back to the 12th century, with recent activities lasting more than six decades. (For a more detailed history, see Gunawardene and Rupasinghe [1986].) The Elahera gem field has produced a variety of valuable and rare gems, notably fine blue sapphire and blue star sapphire, as well as spinel, rhodolite, kornerupine and others. Brown to greenish brown and dark green tourmaline is also known to be occasionally found here (Gunawardene & Rupasinghe 1986; Henn & Schramm 1986).

At many locations in the Elahera area, gems are not concentrated in particular sediment layers but occur more-or-less uniformly distributed in gravel, sand and clay. Gem-bearing sediments—that is, predominantly lateritic material with a thickness corresponding to that of the ancient riverbed—are generally located between 0.5 and 10 m below the surface (Dissanayake & Rupasinghe 1995; Dissanayake & Chandrajith 2003; Zoysa 2014), and most mining in the area is open cast (Figure 3). Small-scale mining is done in ‘backyard pits’ a few

metres across. By contrast with the loose sediments in the Ratnapura gem field, the sedimentary overburden in the Elahera area tends to be fairly stable. As a result, the common Sri Lankan practice of holding up pit walls with wooden planks and fern leaves is rarely needed.

MATERIALS AND METHODS

The sample examined for this study was a transparent eluvial fragment weighing 0.523 g ($9.3 \times 6.4 \times 6.2$ mm). To the best of our knowledge, this is the first, and as of this writing, only specimen of its kind. Therefore we did not perform any special sample preparation for analysis (such as production of oriented, plane-parallel slabs), in order to preserve the specimen for cutting as a gemstone.

Mass density was determined by weighing the rough sample in air and in distilled water (to which a drop of liquid detergent was added to reduce surface tension).

The procedure was repeated five times. Subsequently, after the gemstone was cut, RI measurements were taken four times from the table facet using a Krüss ER601-LED refractometer with 589 nm light.

For further analysis, a small portion of the rough sample (at the lower edge in Figure 1) about 1.8 mm thick was cut off using a 0.17 mm diamond-coated steel wire and fragmented into smaller chips. A small fragment (<100 µm long) was subjected to single-crystal X-ray diffraction analysis. Data were collected at ambient conditions with a Bruker Kappa Apex II diffractometer equipped with an Incoatec Microfocus Source IµS X-ray source (30 W, multilayer mirror, Mo[Kα] radiation) and a charge-coupled device (CCD) area detector. For details, see Ertl *et al.* (2010).

For chemical analysis, several fragments were embedded in araldite epoxy, along with small pieces of the NIST SRM 610 glass standard (Jochum *et al.* 2011), two reference tourmalines (dravite 108796 and schorl 112566; Dyar *et al.* 2001; Wiedenbeck *et al.* 2021) and Suprasil 3002 silica glass (Wetzel *et al.* 2015). The resulting one-inch sample mount was ground and polished for analysis. For electron probe micro-analysis (EPMA), the mount was coated with carbon. For secondary ion mass spectrometry (SIMS), the mount was subsequently cleaned with ethanol and coated with about 35 nm Au for conductivity.

Major-element analysis was done using a JEOL JXA-8530FPlus HyperProbe EPMA system operated in wavelength-dispersive mode, at 15 kV accelerating voltage and 10 nA beam current, with an electron-beam diameter of about 1 µm at the sample surface. The following calibrant materials were used (with respective X-ray lines analysed shown in parentheses): phlogopite (F[Kα]), albite (Na[Kα]), diopside NMNH 117733 (Mg[Kα] and Ca[Kα]), garnet (Al[Kα], Si[Kα] and Fe[Kα]), tugtupite (Cl[Kα]), microcline NMNH 143966 (K[Kα]), ilmenite NMNH 96189 (Ti[Kα]), chromite (Cr[Kα]) and rhodonite (Mn[Kα]). The three reference materials with NMNH numbers are Smithsonian 'microbeam standards' (Jarosewich *et al.* 1980; Jarosewich 2002) and all others are in-house calibrant materials. Peak and background counting times were set to 20 s and 10 s, respectively, in all cases. The X-PHI matrix correction routine (Merlet 1994) was used for data reduction.

Trace-element analysis was performed by laser ablation inductively coupled plasma mass spectrometry (LA-ICP-MS) using an Agilent 7500cx quadrupole ICP-MS system coupled to an ESI NWR193 laser-ablation system with a spot size of 75 µm. The USGS reference glass BCR-2G (Rocholl 1998) was measured for quality

control and data were reproduced within 10% error. Data for all elements were reduced using the NIST SRM 612 standard (Jochum *et al.* 2011) and Si was used as the internal calibrant. For data reduction, GLITTER 4.0 software (Griffin *et al.* 2008) was utilised. For more analytical details, see Kruzsliz *et al.* (2020).

Concentrations of H, Li and B were analysed with a Cameca IMS 1280-HR SIMS system. A primary ¹⁶O⁻ beam of about 14 nA was focused to an approximately 30 µm diameter spot with a total impact energy of 23 keV. Data were collected in mono-collection mode using a single electron multiplier. The mass resolution was set at $M/\Delta M \approx 3800$. The following masses were collected sequentially over 12 cycles: ⁷Li⁺ (2 s per cycle), ¹¹B⁺ (2 s), ³⁰Si⁺ (1 s) and ²⁹Si¹H (10 s). Repeated measurements of H, Li and B mass fractions in Suprasil 3002 glass and reference tourmalines 108796 and 112566 ensured that there was no significant signal drift. Dravite reference 108796 was used for quality control, and 1σ repeatabilities (n = 6) were better than ±6%, ±9% and ±1% for H, Li and B, respectively. For more analytical details, see Wiedenbeck *et al.* (2021).

An optical absorption spectrum in the 'blue direction' (beam parallel to the *c*-axis; unpolarised light with E⊥*c*) of the rough sample was obtained at room temperature in the spectral range 27 000–5400 cm⁻¹ using a Bruker IFS 66v/S Fourier-transform infrared (FTIR) spectrometer equipped with a quartz beam splitter. The following combinations of light sources and detectors were used: Xe lamp and GaP detector for >20 000 cm⁻¹ (spectral resolution 40 cm⁻¹; 1,024 averaged scans), W lamp and Si detector for 20 000–10 000 cm⁻¹ (spectral resolution 20 cm⁻¹; 1024 averaged scans), and W lamp and Ge detector for <10 000 cm⁻¹ (spectral resolution 20 cm⁻¹; 512 averaged scans). The final spectrum consisted of a combination of the three sub-spectra, which were aligned to match in absorbance. We were unable to obtain a spectrum with E||*c*, presumably because the sample was unprepared and too thick, so the signal intensity and signal-to-noise ratio were too poor. Therefore, an unpolarised absorption spectrum in the 'colourless direction' (27 000–10 500 cm⁻¹) was obtained by means of a GL Gem Spectrometer. Absorption intensities for the two orientations were adjusted using an additional spectrum in the 'blue direction' obtained with the latter system.

Laser-induced photoluminescence (PL) and Raman spectra were obtained in the 'colourless' orientation of the rough stone (with E||*c*) by means of a Horiba LabRAM HR Evolution spectrometer. This dispersive system was equipped with an Olympus BX-series optical

microscope, Rayleigh-rejection filter, a diffraction grating with 1,800 grooves per millimetre in the optical pathway, and a Peltier-cooled, Si-based CCD detector. Spectra were obtained using a 473 nm diode-pumped solid-state laser (7 mW at the sample). An Olympus 50× objective (numerical aperture 0.55) was used to focus the laser light onto the sample surface and to collect the emitted and Raman-scattered light to be analysed. Spectral calibration was done using the spectrometer's zero-order signal, the Rayleigh line and the emissions of a Kr lamp, resulting in a wavenumber accuracy better than 0.5 cm⁻¹. The spectral resolution was between about 1.2 cm⁻¹ (blue region) and 0.7 cm⁻¹ (NIR range). Since high-volume resolution was not needed in our case, analyses were done with the spectrometer operated in non-confocal mode. More details of spectroscopic analyses performed in our laboratory are reported elsewhere (Zeug *et al.* 2018).

RESULTS AND DISCUSSION

Basic Properties and X-ray Diffraction Analysis

The sample exhibited strong dichroism from vivid blue to virtually colourless (again, see Figure 1). The SG (herein reported as mass density) was determined as 3.06 ± 0.01 g/cm³. The RIs measured from the table facet of the cut stone were 1.630 ± 0.004. The SG and RI values are fairly typical for gem tourmaline. Note, however, that RI was measured in a single orientation almost along the crystallographic *c*-axis since only the table facet was large enough to obtain RI measurements with our refractometer.

Single-crystal X-ray diffraction analysis confirmed the mineral as tourmaline, with dimensions of the trigonal unit cell (rhombohedral space group *R3m*) of *a* = 15.906(3) Å, *c* = 7.180(1) Å and *V* = 1573.1(1) Å³. These unit-cell parameters alone do not provide the means for a more precise mineral assignment (as the cell dimensions of tourmaline-super group minerals widely overlap), but the stone's identity as a lithium tourmaline (e.g. elbaite, fluor-liddicoatite, etc.) seemed to be excluded, as the *c* dimension of this type of tourmaline is significantly smaller (see, e.g., Henry *et al.* 2011).

Chemical Composition

Results of chemical analyses are presented in Table I. The corresponding mineral formula is (Na_{0.62}Ca_{0.35}□_{0.03}) (Mg_{2.48}Al_{0.37}□_{0.08}Fe_{0.07})Al₆(BO₃)₃(Si_{5.86}Al_{0.11}B_{0.03}O₁₈)(OH)₃[(OH)_{0.42}O_{0.38}F_{0.20}]. This normalised formula was estimated based on 31 (O, OH, F) per formula unit (Henry

Table I: Mean chemical composition of the blue dravite.^a

EPMA and SIMS results ^b			
Oxide	Concentration (wt.%)	Element	Content (apfu)
SiO ₂	36.09 ± 0.11	Si	5.856
B ₂ O ₃	10.81 ± 0.10	B	3.028
Al ₂ O ₃	33.89 ± 0.28	Al	6.481
FeO	0.54 ± 0.04	Fe ²⁺	0.073
MgO	10.23 ± 0.12	Mg	2.475
CaO	1.99 ± 0.03	Ca	0.346
Na ₂ O	1.99 ± 0.05	Na	0.625
K ₂ O	0.02 ± 0.01	K	0.004
H ₂ O	3.16 ± 0.22	OH	3.424
F	0.39 ± 0.05	F	0.200
-O=F	0.16	O	0.376
Total	99.02 ± 0.29	Sum cations	18.890
LA-ICP-MS and SIMS results ^c			
Element	Isotope measured	Concentration (ppm)	
Li	7	3.41 ± 1.79	
Be	9	0.39 ± 0.08	
Ti	49	56.1 ± 23.2	
V	51	12.9 ± 1.0	
Cr	53	16.4 ± 2.7	
Mn	55	12.6 ± 0.51	
Fe	56	4290 ± 110	
Co	59	0.75 ± 0.06	
Ni	60	0.72 ± 0.16	
Zn	66	4.25 ± 0.49	
Ga	71	22.2 ± 0.4	
Sr	88	327 ± 16	
Zr	90	0.72 ± 0.09	
Sn	118	4.48 ± 0.50	
Ba	137	2.84 ± 0.95	
La	139	1.55 ± 0.12	
Ce	140	1.55 ± 0.10	
Pr	141	0.10 ± 0.01	
Nd	146	0.28 ± 0.05	
Eu	151	0.47 ± 0.04	
Pb	208	5.68 ± 0.06	

^a All errors are given at the 2σ level.

^b H and B were determined by SIMS (n = 14) and all other constituents by EPMA (n = 10). Total Fe is given as FeO. Ti, Cr, Mn and Cl were also analysed, but mean concentrations were below EPMA detection limits. Atoms per formula unit (apfu) were calculated on the basis of 31 (O, OH, F).

^c Li was determined by SIMS (n = 14) and all other elements by LA-ICP-MS (n = 6). Cu was also analysed, but its concentration was below the LA-ICP-MS detection limit of <1 ppm.

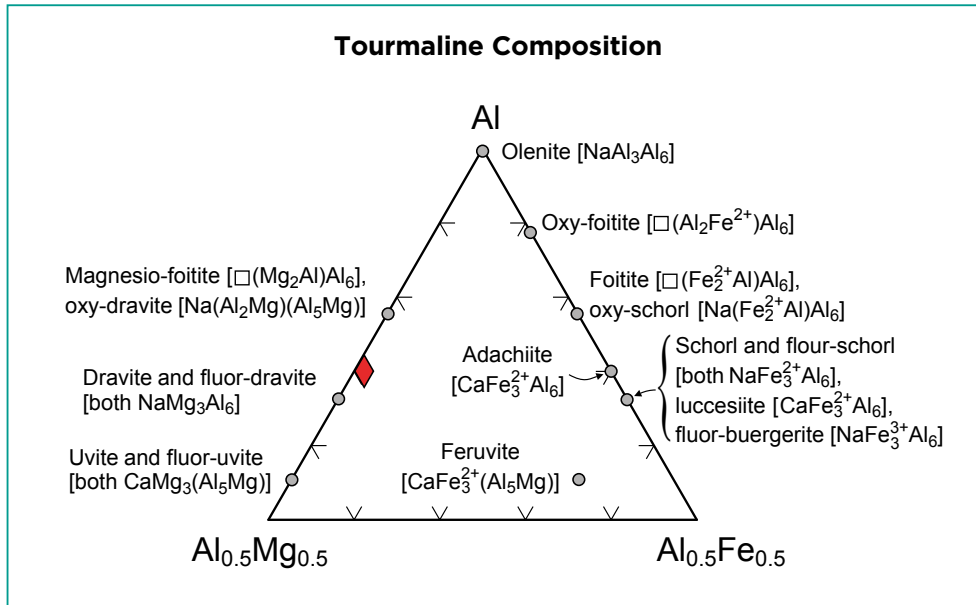


Figure 4: A triangular diagram with total Al-Mg-Fe (apfu) shows the chemical composition of the blue Elahera dravite (red diamond symbol). Ideal chemical compositions of Li-free, Al-Mg-Fe tourmaline end members (cf. Bosi 2018) are shown by grey circles. Only the XY_3Z_6 cations in the formulae are given.

& Dutrow 1996; Clark 2007), assuming complete occupation of the $^{[4]}T$ and $^{[6]}Z$ sites (see Appendix for information on the site occupancy of tourmaline). Also, by assuming $^{[6]}Z$ to be occupied completely by Al^{3+} , we disregarded the possibility of Al-Mg disorder (that is, partial incorporation of Mg^{2+} at the $^{[6]}Z$ site and compensated by increased Al^{3+} at the $^{[6]}Y$ site; Hawthorne *et al.* 1993). The V site was assumed to be occupied completely by $(OH)^-$ ions (although the possible presence of a fraction of O^{2-} at the V site cannot be excluded). Detailed structural analysis addressing these aspects was beyond the scope of the present study.

The above formula characterises this tourmaline as dravite, and excludes elbaite or another lithium tourmaline (note the Li content of only about 3 ppm; Table I). The sample has remarkably low Fe content (Figure 4). It is a dravite close to the nomenclature boundary for oxy-dravite, that is, an Na-Mg-Al tourmaline with the W site dominated by OH (0.42 atoms per formula unit [apfu]) over O (0.38 apfu) and F (0.20 apfu). It is worthy of note that a brown dravite from Elahera characterised by Henn and Schramm (1986) had a similar chemical composition to the blue stone described herein, except for higher Ti (0.59 wt. % TiO_2) and slightly more Fe (0.78 wt. % FeO) and Mn (0.04 wt. % MnO).

Optical Absorption Spectroscopy

Unpolarised optical absorption spectra are presented in Figure 5. The absorption in the 'blue direction' (beam parallel to the c -axis, with E \perp c) is dominated by a broad band in the NIR region centred at about 8900 cm^{-1} (1120 nm) and a composite feature in the red-to-NIR region with maximum intensity at about $13\,600\text{ cm}^{-1}$ (735 nm).

A Gaussian two-band deconvolution of the composite red-NIR absorption feature yielded components at about $13\,050$ and $14\,500\text{ cm}^{-1}$ (765 and 690 nm). The fairly sharp signal at 6980 cm^{-1} (1433 nm), atop the low-energy wing of the 1120 nm band, is due to a vibrational (O-H combination) mode. The unpolarised absorption spectrum in the 'colourless direction' shows a single, low-intensity band at about $12\,700\text{ cm}^{-1}$ (785 nm). In the higher-energy range, up to the onset of the absorption edge at roughly $26\,000\text{ cm}^{-1}$ (385 nm), only weak and rather poorly-defined absorption features are found at around $20\,200\text{ cm}^{-1}$ (495 nm; E \perp c) and $23\,300\text{ cm}^{-1}$ (430 nm; both orientations).

The sample's strong dichroism from vivid blue to virtually colourless is mainly due to the strong E \perp c polarisation of the 690 nm band. This and the other two main absorption bands at 765 and 1120 nm are generally accepted (e.g. Wilkins *et al.* 1969; Smith 1978a, b; Mattson & Rossman 1987; Taran *et al.* 1993) to arise from the split, spin-allowed $^5T_2 \rightarrow ^5E\text{ }d-d$ transition of Fe^{2+} at the larger $^{[6]}Y$ site (presumably with some minor contribution of Fe^{2+} at the smaller $^{[6]}Z$ site; see Appendix). These Fe^{2+} absorptions are strongly intensified by exchange-coupled $Fe^{2+}-Fe^{3+}$ pairs (in Y-Y and Y-Z sites; Mattson & Rossman 1987). The lack of a significant absorption band near $11\,000\text{ cm}^{-1}$ (909 nm) concurs well with the virtual absence of Cu (see footnote to Table I) in our sample. By contrast, blue Paraiba-type tourmaline, with colouration caused by Cu^{2+} (commonly containing about 0.15–2 wt. % CuO and exceptionally up to 3.59 wt. % CuO, as reported by Vereshchagin *et al.* [2013]) shows strong absorption in the red range, as well as a prominent band in the NIR region (Fritsch *et*

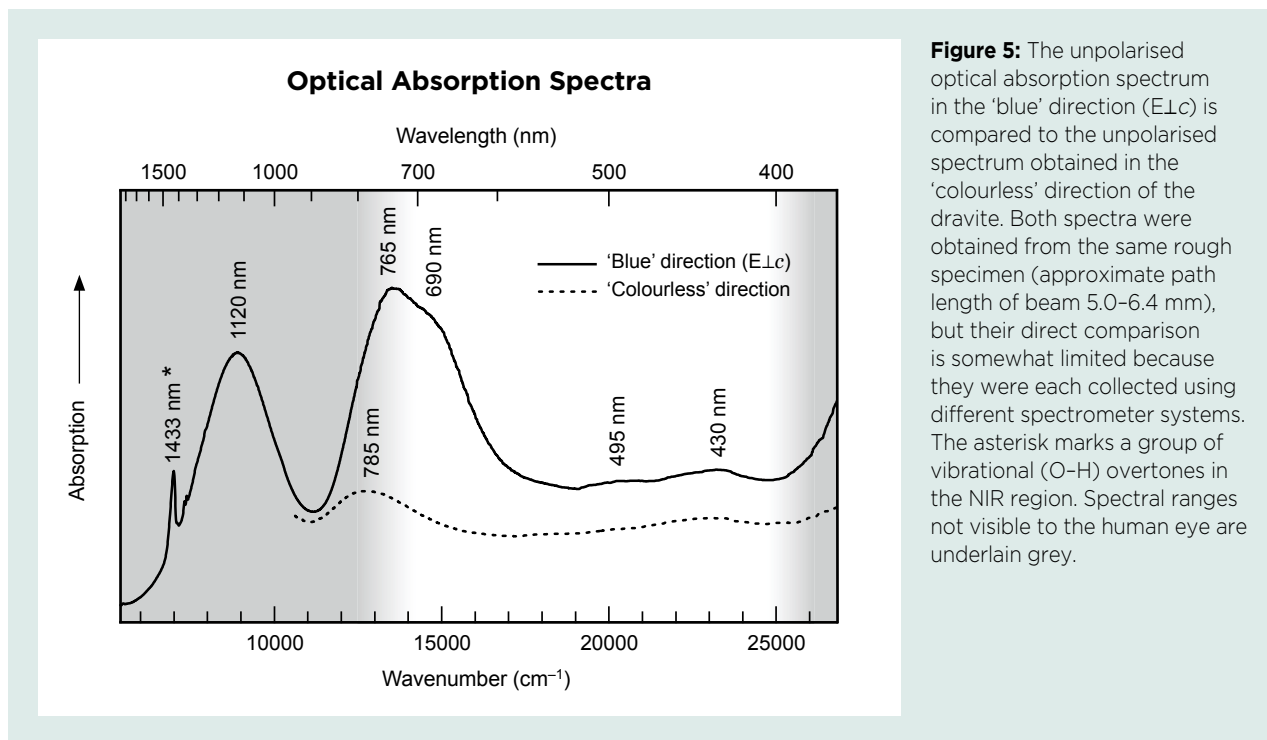


Figure 5: The unpolarised optical absorption spectrum in the ‘blue’ direction ($E_{\perp c}$) is compared to the unpolarised spectrum obtained in the ‘colourless’ direction of the dravite. Both spectra were obtained from the same rough specimen (approximate path length of beam 5.0–6.4 mm), but their direct comparison is somewhat limited because they were each collected using different spectrometer systems. The asterisk marks a group of vibrational (O–H) overtones in the NIR region. Spectral ranges not visible to the human eye are underlain grey.

al. 1990; Rossman *et al.* 1991; Laurs *et al.* 2008; Merkel & Breeding 2009).

The ‘blue spectrum’ of the dravite (Figure 5) is similar to spectra of Fe^{2+} -coloured greenish blue lithium tourmalines (Merkel & Breeding 2009). The blue colour is due to a combination of strong Fe^{2+} -related absorption in the red range and insignificant absorption in the blue-green portion of the visible spectrum. The latter provides strong indication of a low Fe^{3+}/Fe^{2+} ratio in our sample, whereas Fe^{3+} -rich dravite has several strong absorption bands above $18\,000\text{ cm}^{-1}$ (below 556 nm), resulting in brown to red colour (Mattson & Rossman 1984; Taran *et al.* 2015). Also, the absence of major absorption features at $\geq 556\text{ nm}$ in the present sample is consistent with insignificant amounts of other colouring cations, such as Mn, Cr, V and Ti (da Fonseca-Zang *et al.* 2008; Ahn *et al.* 2013). For instance, V-coloured green dravite and uvite (Schmetzer *et al.* 2007; Merkel & Breeding 2009; Schwarzinger *et al.* 2019) were reported to contain at least 0.12–0.25 wt.% (1200–2500 ppm) V, whereas the V concentration in our dravite is about two orders of magnitude lower (see Table I).

Photoluminescence Spectroscopy

The stone was apparently inert to long- and short-wave UV radiation, and correspondingly only relatively weak luminescence was recorded in its emission spectra. The unpolarised laser-induced PL spectrum is presented in Figure 6. It is dominated by a broad band in the

$11\,900\text{--}14\,500\text{ cm}^{-1}$ ($840\text{--}690\text{ nm}$) range and a narrow, slightly asymmetric band at $14\,660\text{ cm}^{-1}$ (682.2 nm). Both features, in the red to NIR range, relate to Cr^{3+} . The narrow band is assigned to the spin-forbidden ${}^2E \rightarrow {}^4A_2$ electronic transition, and the broad emission to the thermally populated, spin-allowed ${}^4T_2 \rightarrow {}^4A_2$ transition (O’Bannon *et al.* 2018 and references therein). A possible contribution to the narrow-band emission at 682.2 nm by V^{2+} , which has a d^3 electronic structure equivalent to that of Cr^{3+} (O’Bannon *et al.* 2018), is likely minor, given the relatively narrow half-height width (about 6 nm or 130 cm^{-1}) of this feature. Note, however, that V^{2+} in tourmaline is characterised by much stronger R-line splitting than is Cr^{3+} (O’Bannon *et al.* 2018). A possible contribution of Fe^{3+} to the broad-band red-to-NIR emission (Gaft *et al.* 2015) can be excluded in this case because the optical absorption spectra do not indicate the presence of significant amounts of ferric iron. Above $16\,000\text{ cm}^{-1}$ (below 625 nm) there was a complete absence of laser-induced emission.

Raman Spectroscopy

The Raman spectrum (obtained in the ‘colourless’ orientation, with $E_{\parallel c}$) is presented in Figure 7. The pattern in the range below 1200 cm^{-1} (Figure 7a) corresponds to that of dravite (Gasharova *et al.* 1997; Watenphul *et al.* 2016), ideally $NaMg_3Al_6Si_6O_{18}(BO_3)_3(OH)_3OH$. However, there is wide similarity and overlap in this range among the reference spectra available for dravite and other

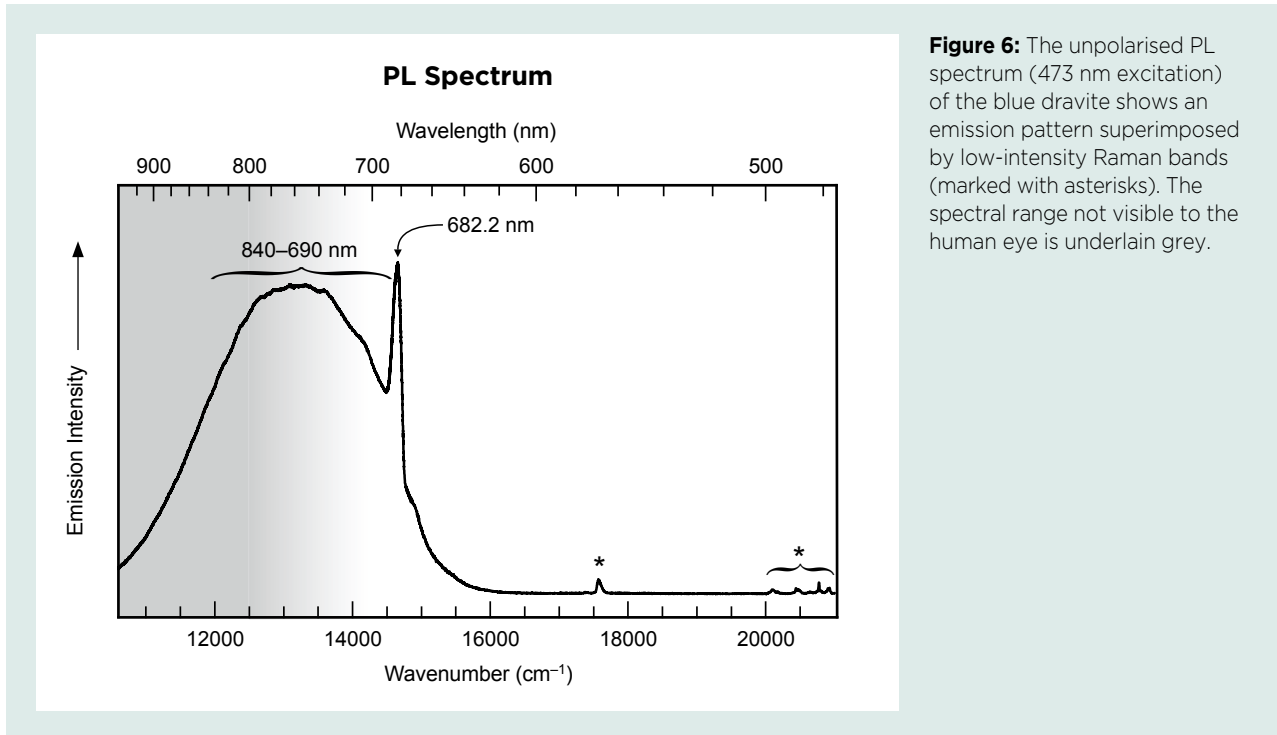


Figure 6: The unpolarised PL spectrum (473 nm excitation) of the blue dravite shows an emission pattern superimposed by low-intensity Raman bands (marked with asterisks). The spectral range not visible to the human eye is underlain grey.

members of the tourmaline group (e.g. elbaite, foitite and uvite) in various databases.

Raman bands in the 3400–3800 cm^{-1} range, assigned to O–H stretching, are particularly sensitive to chemical composition, so they offer a much more reliable means for mineral identification. An explanation of the assignment nomenclature for O–H stretching bands is provided in the Appendix. The dominant O–H band in the spectrum of our sample, at 3571 cm^{-1} (Figure 7b), is assigned to V-site OH groups with $3^{\text{Y}}\text{Mg}^{\text{Z}}\text{Al}^{\text{Z}}\text{Al}$ configuration, and its low-energy shoulder (near 3530 cm^{-1}) is assigned predominantly to OH groups with $2^{\text{Y}}\text{Mg}^{\text{Z}}\text{Al}^{\text{Z}}\text{Al}-^{\text{Y}}\text{Al}^{\text{Z}}\text{Al}^{\text{Z}}\text{Al}$ configuration. The two bands at 3741 and 3770 cm^{-1} correspond to W-site OH groups with $^{\text{Y}}\text{Mg}^{\text{Y}}\text{Mg}^{\text{Y}}\text{Al}-^{\text{X}}\text{Na}$ and $^{\text{Y}}\text{Mg}^{\text{Y}}\text{Mg}^{\text{Y}}\text{Mg}-^{\text{X}}(\text{Na} + \text{Ca})$ configurations, respectively. The low-intensity 3630 cm^{-1} band points to W-site OH groups adjacent to an X-site vacancy (all assignments according to Watenphul *et al.* 2016).

However, even O–H-range Raman spectra cannot distinguish chemically similar tourmaline species, especially when the composition of the unknown is close to a nomenclature boundary. Thus, the Elahera sample cannot be assigned unequivocally to either dravite or uvite, and even less to either dravite or oxy-dravite, on the basis of its Raman spectra. However, based on reliable reference spectra (Fantini *et al.* 2013; Berryman *et al.* 2016; Watenphul *et al.* 2016), the Raman spectrum we obtained for the O–H stretching range (Figure 7b) does allow us to exclude lithium

tourmalines, even without the results of light-element analysis. This provides an additional example of the usefulness of Raman spectroscopy for quick and efficient gem characterisation.

Dravite Nomenclature

It seems appropriate to point to an existing nomenclature issue, as the term *dravite* is referred to inconsistently in the gem trade. *Dravite* is still used fairly often by miners and gem dealers as a variety name that describes brown to yellow tourmaline—analogueous to how *indicolite* is used for blue, *achroite* for colourless, *verdelite* for green and *rubellite* for pink-to-red tourmaline. The colour-related use of *dravite* is incorrect because this name refers to a clearly defined mineral of the tourmaline supergroup, namely, the $\text{NaMg}_3\text{Al}_6\text{Si}_6\text{O}_{18}(\text{BO}_3)_3(\text{OH})_3\text{OH}$ end member; fluor-dravite and oxy-dravite are also recognised minerals (Bosi 2018). The name *dravite* was given by the Austrian mineralogist Gustav Tschermak (1836–1927), who applied it to brown Mg-rich tourmaline from the Drave (or Drau) river valley in Carinthia, Austria (Tschermak 1884), near the village of Dobrova pri Dravogradu in present-day Slovenia.

Gem-quality dravite is mostly brown, yellow or green (Schmetzer *et al.* 2007; Schwarzinger *et al.* 2019; Sun *et al.* 2019 and references therein). Gem-quality dravite can also, less commonly, be red (Mattson & Rossman 1984; Taran *et al.* 2015 and references therein), whereas blue hues (Dunn 1978) seem to be extremely rare.

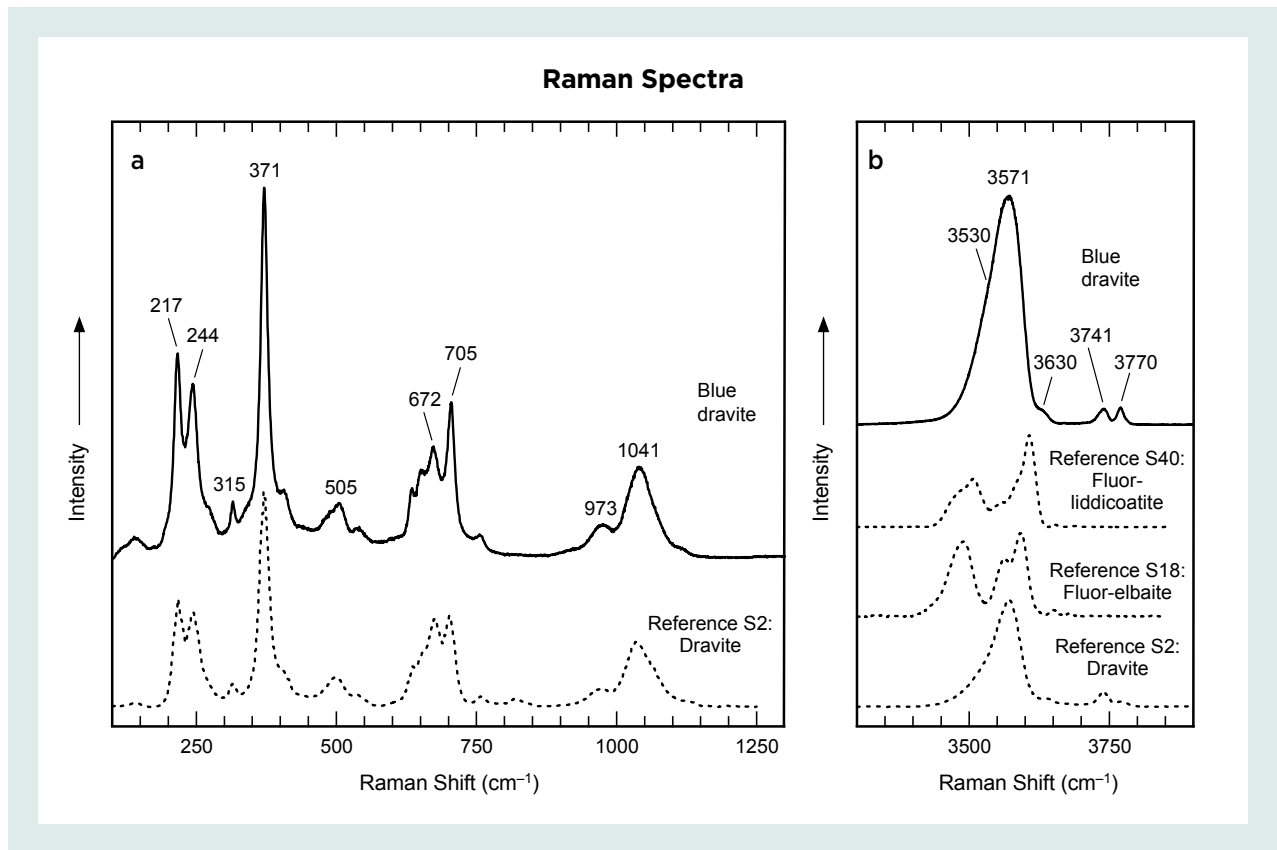


Figure 7: Raman spectra (473 nm excitation; E||c) for the blue dravite in the (a) low-energy and (b) O-H stretching ranges are compared to a reference spectrum for dravite (Li-free), and the latter range also shows reference spectra for fluor-elbaite (1.01 apfu Li) and fluor-liddicoatite (1.85 apfu Li). The reference spectra (obtained in cc geometry) are from Watenphul *et al.* (2016). The spectra are offset vertically for clarity. Note the clearly different fingerprint pattern of the O-H stretching bands of dravite compared to those of the Li-bearing tourmalines.

CONCLUSION

In this article, blue dravite of gem quality is characterised for the first time. The blue colour (with E||c) of the Elahera ‘indicolite’ is predominantly due to Fe²⁺, which causes absorption in the red range of the visible spectrum that is amplified significantly by very low amounts of exchange-coupled Fe²⁺-Fe³⁺ pairs in Y-Y

and Y-Z sites. The strength of this absorption intensification, and the fact that neighbouring Y and Z cations lie in planes perpendicular to the c-axis (see Figure A-1 in the Appendix), explain the very strong directional dependence of the Fe²⁺-related absorption and, with that, the strong vivid blue to near-colourless dichroism (Figure 8).

Figure 8: This 0.90 ct round brilliant, photographed in two different positions under daylight illumination (no polariser used), was cut from the rough in Figure 1. It was faceted in an orientation with the c-axis not exactly perpendicular to the table facet, because otherwise the stone would have appeared too dark. Photos by M. Wildner.



Red absorption by Fe²⁺ is a common phenomenon in lithium-free tourmaline. However, it leads to blue colour in the present case only because concentrations of cations that absorb in the blue-green region (such as Fe³⁺, Ti⁴⁺, Mn³⁺ and V³⁺) are unusually low. Note that a brown dravite from Elahera characterised by Henn and Schramm (1986) had a similar composition to the present blue stone except for higher Ti. The brown colour of that stone was attributed to Fe²⁺-Ti⁴⁺ inter-valence charge transfer. The lack of Ti in the present

blue sample allowed the blue Fe²⁺ colouration to be developed, and it appears that the reason why blue is such a rare colour in dravite is because this tourmaline species almost always contains appreciable Ti (and possibly some iron as Fe³⁺).

Should more blue dravite be found in the Elahera field, it will be worthwhile to prepare slabs for polarised absorption measurements, and to subject some powdered material to Mössbauer analysis for determination of the Fe²⁺/Fe³⁺ ratio.

REFERENCES

- Ahn, Y., Seo, J. & Park, J. 2013. Electronic and vibrational spectra of tourmaline – The impact of electron beam irradiation and heat treatment. *Vibrational Spectroscopy*, **65**, 165–175, <https://doi.org/10.1016/j.vibspec.2013.01.002>.
- Ariyaratna, D.H. 1993. *Gems of Sri Lanka*, 5th edn. Self-published, London, 109 pp.
- Barton Jr., R. 1969. Refinement of the crystal structure of buergerite and the absolute orientation of tourmalines. *Acta Crystallographica Section B: Structural Science, Crystal Engineering and Materials*, **25**(8), 1524–1533, <https://doi.org/10.1107/s0567740869004286>.
- Berryman, E.J., Wunder, B., Ertl, A., Koch-Müller, M., Rhede, D., Scheidl, K., Giester, G. & Heinrich, W. 2016. Influence of the X-site composition on tourmaline's crystal structure: Investigation of synthetic K-dravite, dravite, oxy-uvite, and magnesio-foitite using SREF and Raman spectroscopy. *Physics and Chemistry of Minerals*, **43**(2), 83–102, <https://doi.org/10.1007/s00269-015-0776-3>.
- Bosi, F. 2018. Tourmaline crystal chemistry. *American Mineralogist*, **103**(2), 298–306, <https://doi.org/10.2138/am-2018-6289>.
- Clark, C.M. 2007. Tourmaline: Structural formula calculations. *Canadian Mineralogist*, **45**(2), 229–237, <https://doi.org/10.2113/gscanmin.45.2.229>.
- da Fonseca-Zang, W.A., Zang, J.W. & Hofmeister, W. 2008. The Ti-influence on the tourmaline color. *Journal of the Brazilian Chemical Society*, **19**(6), 1186–1192, <https://doi.org/10.1590/s0103-50532008000600020>.
- Dissanayake, C.B. & Rupasinghe, M.S. 1995. Classification of gem deposits of Sri Lanka. *Geologie en Mijnbouw*, **75**, 79–88.
- Dissanayake, C.B. & Chandrajith, R. 2003. *Gem-bearing Stream Sediments of Sri Lanka: Geology and Geochemistry*. Gem and Jewellery Research and Training Institute and National Gem and Jewellery Authority, Colombo, Sri Lanka, 121 pp.
- Donnay, G. & Barton Jr., R. 1972. Refinement of the crystal structure of elbaite and the mechanism of tourmaline solid solution. *Tschermaks Mineralogische und Petrographische Mitteilungen*, **18**(4), 273–286, <https://doi.org/10.1007/bf01082837>.
- Dunn, P. 1978. Gemmological Notes: Blue-green gem dravite from East Africa. *Journal of Gemmology*, **16**(2), 92.
- Dyar, M.D., Wiedenbeck, M., Robertson, D., Cross, L.R., Delaney, J.S., Ferguson, K., Francis, C.A., Grew, E.S. et al. 2001. Reference minerals for the microanalysis of light elements. *Geostandards and Geoanalytical Research*, **25**(2–3), 441–463, <https://doi.org/10.1111/j.1751-908X.2001.tb00616.x>.
- Ertl, A., Marschall, H.R., Giester, G., Henry, D.J., Schertl, H.P., Ntaflos, T., Luvizotto, G.L., Nasdala, L. et al. 2010. Metamorphic ultrahigh-pressure tourmaline: Structure, chemistry, and correlations to P-T conditions. *American Mineralogist*, **95**(1), 1–10, <https://doi.org/10.2138/am.2010.3283>.
- Fantini, C., Tavares, M.C., Krambrock, K., Moreira, R.L. & Righi, A. 2013. Raman and infrared study of hydroxyl sites in natural uvite, fluor-uvite, magnesio-foitite, dravite and elbaite tourmalines. *Physics and Chemistry of Minerals*, **41**(4), 247–254, <https://doi.org/10.1007/s00269-013-0642-0>.
- Faye, G.H., Manning, P.G. & Nickel, E.H. 1968. The polarized optical absorption spectra of tourmaline, cordierite, chloritoid and vivianite: Ferrous-ferric electronic interaction as a source of pleochroism. *American Mineralogist*, **53**(7–8), 1174–1201.
- Fritsch, E., Shigley, J.E., Rossman, G.R., Mercer, M.E., Muhlmeister, S.M. & Moon, M. 1990. Gem-quality cuprian-elbaite tourmalines from São José da Batalha, Paraíba, Brazil. *Gems & Gemology*, **26**(3), 189–205, <https://doi.org/10.5741/gems.26.3.189>.
- Gaft, M., Reisfeld, R. & Panczer, G. 2015. Luminescent minerals. In: *Modern Luminescence Spectroscopy of Minerals and Materials*, 2nd edn. Springer, Cham, Switzerland, 45–219, https://doi.org/10.1007/978-3-319-24765-6_4.

- Garda, G.M., Beljavskis, P., Juliani, C. & Silva, D. 2002. The occurrence of intermediate schorl-dravite and alkali-deficient, Cr-(V)bearing tourmalines in the volcanic-sedimentary sequence of the Serra do Itaberaba Group–SP. *Anais da Academia Brasileira de Ciências*, **74**(3), 543–544, <https://doi.org/10.1590/s0001-37652002000300023>.
- Gasharova, B., Mihailova, B. & Konstantinov, L. 1997. Raman spectra of various types of tourmaline. *European Journal of Mineralogy*, **9**(5), 935–940, <https://doi.org/10.1127/ejm/9/5/0935>.
- Gatta, G.D., Bosi, F., McIntyre, G.J. & Skogby, H. 2014. First accurate location of two proton sites in tourmaline: A single-crystal neutron diffraction study of oxy-dravite. *Mineralogical Magazine*, **78**(3), 681–692, <https://doi.org/10.1180/minmag.2014.078.3.15>.
- Griffin, W.L., Powell, W., Pearson, N.J. & O'Reilly, S.Y. 2008. GLITTER: Data reduction software for laser ablation ICP-MS. In: Sylvester, P. (ed) *Laser Ablation ICP-MS in the Earth Sciences: Current Practices and Outstanding Issues*. Mineralogical Association of Canada, Québec, Canada, 308–311.
- Gunawardene, M. & Rupasinghe, M.S. 1986. The Elahera gem field in central Sri Lanka. *Gems & Gemology*, **22**(2), 80–95, <https://doi.org/10.5741/gems.22.2.80>.
- Hawthorne, F.C., MacDonald, D.J. & Burns, P.C. 1993. Reassignment of cation site occupancies in tourmaline: Al-Mg disorder in the crystal structure of dravite. *American Mineralogist*, **78**(3–4), 265–270.
- Henn, U. & Schramm, M. 1986. Some observations on brown tourmalines from Elahera, Sri Lanka. *Journal of Gemmology*, **20**(3), 154–156, <https://doi.org/10.15506/jog.1986.20.3.154>.
- Henry, D.J. & Dutrow, B.L. 1996. Metamorphic tourmaline and its petrologic applications. In: Grew, E.S. & Anovitz, L.M. (eds) *Boron: Mineralogy, Petrology and Geochemistry*. Reviews in Mineralogy, Mineralogical Society of America, Washington DC, USA, Vol. 33, 503–558, <https://doi.org/10.1515/9781501509223-012>.
- Henry, D.J., Novak, M., Hawthorne, F.C., Ertl, A., Dutrow, B.L., Uher, P. & Pezzotta, F. 2011. Nomenclature of the tourmaline-supergroup minerals. *American Mineralogist*, **96**(5–6), 895–913, <https://doi.org/10.2138/am.2011.3636>.
- Herath, J.W. 1984. Geology and occurrence of gems in Sri Lanka. *Journal of the National Science Foundation of Sri Lanka*, **12**(2), 257–271, <https://doi.org/10.4038/jnsfsr.v12i2.8364>.
- Jarosewich, E. 2002. Smithsonian microbeam standards. *Journal of Research of the National Institute of Standards and Technology*, **107**(6), 681–685, <https://doi.org/10.6028/jres.107.054>.
- Jarosewich, E., Nelen, J.A. & Norberg, J.A. 1980. Reference samples for electron microprobe analysis. *Geostandards and Geoanalytical Research*, **4**(1), 43–47, <https://doi.org/10.1111/j.1751-908X.1980.tb00273.x>.
- Jochum, K.P., Weis, U., Stoll, B., Kuzmin, D., Yang, Q., Raczek, I., Jacob, D.E., Stracke, A. *et al.* 2011. Determination of reference values for NIST SRM 610–617 glasses following ISO guidelines. *Geostandards and Geoanalytical Research*, **35**(4), 397–429, <https://doi.org/10.1111/j.1751-908X.2011.00120.x>.
- Kruzsliz, Á.B., Nasdala, L., Wildner, M., Škoda, R., Redhammer, G.J., Hauzenberger, C. & Wanthanachaisaeng, B. 2020. Black spinel—A gem material from Bo Phloi, Thailand. *Journal of Gemmology*, **37**(1), 66–79, <https://doi.org/10.15506/JoG.2020.37.1.66>.
- Laurs, B.M., Zwaan, J.C., Breeding, C.M., Simmons, W.B., Beaton, D., Rijdsdijk, K.F., Befi, R. & Falster, A.U. 2008. Copper-bearing (Paraíba-type) tourmaline from Mozambique. *Gems & Gemology*, **44**(1), 4–30, <https://doi.org/10.5741/gems.44.1.4>.
- Mattson, S.M. & Rossman, G.R. 1984. Ferric iron in tourmaline. *Physics and Chemistry of Minerals*, **11**(5), 225–234, <https://doi.org/10.1007/bf00308137>.
- Mattson, S.M. & Rossman, G.R. 1987. Fe²⁺–Fe³⁺ interactions in tourmaline. *Physics and Chemistry of Minerals*, **14**(2), 163–171, <https://doi.org/10.1007/bf00308220>.
- Merkel, P.B. & Breeding, C.M. 2009. Spectral differentiation between copper and iron colorants in gem tourmalines. *Gems & Gemology*, **45**(2), 112–119, <https://doi.org/10.5741/gems.45.2.112>.
- Merlet, C. 1994. An accurate computer correction program for quantitative electron probe microanalysis. *Mikrochimica Acta*, **114–115**(1), 363–376, <https://doi.org/10.1007/bf01244563>.
- Nasdala, L. & Schmidt, C. 2020. Applications of Raman spectroscopy in mineralogy and geochemistry. *Elements*, **16**(2), 99–104, <https://doi.org/10.2138/gselements.16.2.99>.
- Nicastro, I. & Sun, Z. 2016. Gem News International: Blue dravite-uvite tourmaline from Koksha Valley, Afghanistan. *Gems & Gemology*, **52**(4), 428–429.
- Novák, M. 1998. Blue dravite as an indicator of fluid composition during subsolidus replacement processes in Li-poor granitic pegmatites in the Moldanubicum, Czech Republic. *Journal of the Czech Geological Society*, **43**(1–2), 24–30.
- O'Bannon, E., Beavers, C.M., Kunz, M. & Williams, Q. 2018. High-pressure study of dravite tourmaline: Insights into the accommodating nature of the tourmaline structure. *American Mineralogist*, **103**(10), 1622–1633, <https://doi.org/10.2138/am-2018-6486>.
- Pezzotta, F. & Laurs, B.M. 2011. Tourmaline: The kaleidoscopic gemstone. *Elements*, **7**(5), 333–338, <https://doi.org/10.2113/gselements.7.5.333>.
- Pieczka, A. 2007. Blue dravite from the Szklary pegmatite (Lower Silesia, Poland). *Mineralogia*, **38**(2), 209–218, <https://doi.org/10.2478/v10002-007-0027-4>.

- Rocholl, A. 1998. Major and trace element composition and homogeneity of microbeam reference material: Basalt glass USGS BCR-2G. *Geostandards and Geoanalytical Research*, **22**(1), 33–45, <https://doi.org/10.1111/j.1751-908X.1998.tb00543.x>.
- Rossmann, G.R., Fritsch, E. & Shigley, J.E. 1991. Origin of color in cuprian elbaite from São José da Batalha, Paraíba, Brazil. *American Mineralogist*, **76**(9–10), 1479–1484.
- Schmetzer, K., Bernhardt, H.-J., Dunaigre, C. & Krzemnicki, M. 2007. Vanadium-bearing gem-quality tourmalines from Madagascar. *Journal of Gemmology*, **30**(7), 413–433, <https://doi.org/10.15506/JoG.2007.30.7.413>.
- Schwarzinger, C., Wildner, M., Ulatowski, S. & Sawyer, M. 2019. Vanadium-bearing tourmaline from the Commander mine, Nadojuki, Tanzania. *Journal of Gemmology*, **36**(6), 534–543, <https://doi.org/10.15506/JoG.2019.36.6.534>.
- Selway, J.B., Černý, P. & Hawthorne, F.C. 1998. Feruvite from lepidolite pegmatites at Red Cross Lake, Manitoba. *Canadian Mineralogist*, **36**(2), 433–439.
- Smith, G. 1978a. Evidence for absorption by exchange-coupled Fe²⁺–Fe³⁺ pairs in the near infra-red spectra of minerals. *Physics and Chemistry of Minerals*, **3**(4), 375–383, <https://doi.org/10.1007/bf00311848>.
- Smith, G. 1978b. A reassessment of the role of iron in the 5,000–30,000 cm⁻¹ region of the electronic absorption spectra of tourmaline. *Physics and Chemistry of Minerals*, **3**(4), 343–373, <https://doi.org/10.1007/bf00311847>.
- Sun, Z., Palke, A.C., Breeding, C.M. & Dutrow, B. 2019. A new method for determining gem tourmaline species by LA-ICP-MS. *Gems & Gemology*, **55**(1), 2–17, <https://doi.org/10.5741/gems.55.1.2>.
- Taran, M.N., Lebedev, A.S. & Platonov, A.N. 1993. Optical absorption spectroscopy of synthetic tourmalines. *Physics and Chemistry of Minerals*, **20**(3), 209–220, <https://doi.org/10.1007/bf00200123>.
- Taran, M.N., Dyar, M.D., Naumenko, I.V. & Vyshnevsky, O.A. 2015. Spectroscopy of red dravite from northern Tanzania. *Physics and Chemistry of Minerals*, **42**(7), 559–568, <https://doi.org/10.1007/s00269-015-0743-z>.
- Tschermak, G. 1884. *Lehrbuch der Mineralogie*. Alfred Hölder, Vienna, Austria, 589 pp.
- Vereshchagin, O.S., Rozhdestvenskaya, I.V., Frank-Kamenetskaya, O.V., Zolotarev, A.A. & Mashkovtsev, R.I. 2013. Crystal chemistry of Cu-bearing tourmalines. *American Mineralogist*, **98**(8–9), 1610–1616, <https://doi.org/10.2138/am.2013.4408>.
- Watenphul, A., Burgdorf, M., Schlüter, J., Horn, I., Malcherek, T. & Mihailova, B. 2016. Exploring the potential of Raman spectroscopy for crystallochemical analyses of complex hydrous silicates: II. Tourmalines. *American Mineralogist*, **101**(4), 970–985, <https://doi.org/10.2138/am-2016-5530>.
- Wetzel, D.T., Hauri, E.H., Saal, A.E. & Rutherford, M.J. 2015. Carbon content and degassing history of the lunar volcanic glasses. *Nature Geoscience*, **8**(10), 755–758, <https://doi.org/10.1038/ngeo2511>.
- Wiedenbeck, M., Trumbull, R.B., Rosner, M., Boyce, A., Fournelle, J.H., Franchi, I.A., Halama, R., Harris, C. *et al.* 2021. Tourmaline reference materials for the *in situ* analysis of oxygen and lithium isotope ratio compositions. *Geostandards and Geoanalytical Research*, **45**(1), 97–119, <https://doi.org/10.1111/ggr.12362>.
- Wilkins, R.W.T., Farrell, E.F. & Naiman, C.S. 1969. The crystal field spectra and dichroism of tourmaline. *Journal of Physics and Chemistry of Solids*, **30**(1), 43–56, [https://doi.org/10.1016/0022-3697\(69\)90337-0](https://doi.org/10.1016/0022-3697(69)90337-0).
- Zeug, M., Nasdala, L., Wanthanachaisaeng, B., Balmer, W.A., Corfu, F. & Wildner, M. 2018. Blue zircon from Ratanakiri, Cambodia. *Journal of Gemmology*, **36**(2), 112–132, <https://doi.org/10.15506/JoG.2018.36.2.112>.
- Zoysa, G. 2014. The geology and gem deposits of Sri Lanka. *InColor*, No. 27, 38–41.

The Authors

Prof. Dr Lutz Nasdala, Prof. Dr Manfred Wildner, Prof. Dr Gerald Giester and Dr Chutimun Chanmuang N.

Institut für Mineralogie und Kristallographie, Universität Wien, Althanstr. 14, 1090 Vienna, Austria
E-mail: lutz.nasdala@univie.ac.at

Dr Maria Rosa Scicchitano

GFZ German Research Centre for Geosciences, Telegrafenberg, 14473 Potsdam, Germany

Prof. Dr Christoph Hauzenberger

Institut für Erdwissenschaften, Naturwissenschaftliche Fakultät, Universität Graz, Universitätsplatz 2/II, 8010 Graz, Austria

Acknowledgements

The specimen was obtained during a field trip organised by Prof. Dr G. W. A. Rohan Fernando. Local guidance in the Elahera area by M. A. Kumara Gurusinghe and K. A. Geeth Sameera is gratefully acknowledged. Sample preparation for analysis was done by Andreas Wagner, and the gemstone was faceted by Christian Riedel (Waldviertler Lapidarie, Messern, Austria). Thanks are due to Frederic Couffignal and Dr Manuela Zeug for experimental assistance, to Dr Andreas Ertl and E. Gamini Zoysa for fruitful discussions, and to Ralf Grunert for providing field photographs. Constructive reviews by three anonymous experts are also greatly appreciated. Author LN acknowledges travel support from the Faculty of Geosciences, Geography and Astronomy, University of Vienna.

APPENDIX: TOURMALINE IDENTIFICATION FROM O-H RAMAN BANDS

Tourmaline-supergroup minerals have the general chemical formula ${}^{[9]}X{}^{[6]}Y_3{}^{[6]}Z_6({}^{[4]}T_6O_{18})({}^{[3]}BO_3)_3V_3W$ (Henry *et al.* 2011; for cations, their coordination to oxygen is given as prefix superscript numbers in brackets). The most common constituents at each of these sites are:

- X = Na⁺, Ca²⁺, □ (vacancy), K⁺
 Y = Fe²⁺, Mg²⁺, Mn²⁺, Al³⁺, Li⁺, Fe³⁺, Cr³⁺, Cu²⁺
 Z = Al³⁺, Mg²⁺, Fe²⁺, Fe³⁺, Cr³⁺
 T = Si⁴⁺, Al³⁺, B³⁺
 V = (OH)⁻, O²⁻
 W = (OH)⁻, F⁻, O²⁻

A detailed discussion of the tourmaline structure is beyond the scope of the present study; the reader is referred to the pioneering descriptions of Barton (1969) and Donnay and Barton (1972). Important for the interpretation of Raman spectra is that hydroxyl groups occupy two different structural sites: V and W (Gatta *et al.* 2014; see Figure A-1). This is crucial insofar as

vibrations of OH groups are sensitive to their nearest neighbouring cations. Consequently, each of the three OH groups at a V site is affected by the occupation of its neighbouring (one) Y and (two) Z sites. However, the three H atoms at V sites participate in a single vibration and, therefore, the neighbouring cations of all three of them need to be considered in band assignments (referred to as YZZ-YZZ-YZZ configuration; Watenphul *et al.* 2016).

Analogously, OH groups at the W site are affected by the occupation of their three neighbouring Y sites. Here the occupation of the nearest X site affects the O–H vibration via H⋯X interaction (W-type OH-stretching bands are therefore described by their YYY-X configuration; Watenphul *et al.* 2016).

In the dravite Raman spectrum, we detected V-site O–H vibrations in the range below about 3600 cm⁻¹, whereas at higher Raman shifts there were W-site O–H vibrations. Consequently, and in particular depending on the cation-site occupation, tourmalines have decidedly diverse Raman spectra in the O–H stretching range. Given reliable reference spectra (Fantini *et al.* 2013; Berryman *et al.* 2016; Watenphul *et al.* 2016), mineral assignment of gem-quality tourmaline can be straightforward in some cases (Nasdala & Schmidt 2020).

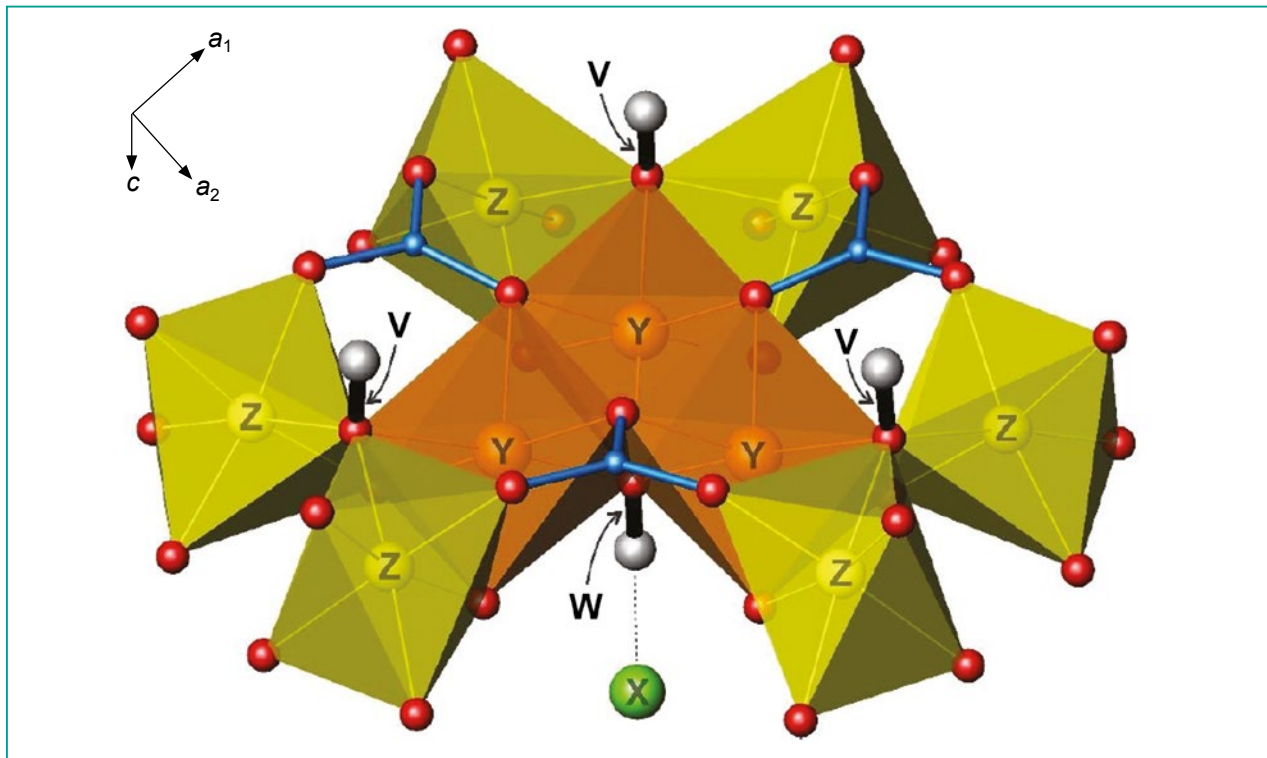


Figure A-1: The crystal structure of dravite shows triangular BO₃ groups (blue), oxygen ions (red spheres), and X (green), Y (orange) and Z (yellow) spheres corresponding to the respective cations in the general formula. For clarity, SiO₄ tetrahedra are not shown. Note that OH groups (positions of hydrogen ions shown as grey spheres) can occupy two distinct sites (V and W). Drawing by G. Giester, using the ATOMS v. 6.5 program (Shape Software, Kingsport, Tennessee, USA) and atomic coordinates of Gatta *et al.* (2014).



Gem-A
INSTRUMENTS



**OVER 100
PRODUCTS
AVAILABLE**

Buy Gem-A Instruments online!



View the full collection at:
shop.gem-a.com

GEM-A MEMBERS!

Login to the Gem-A Instruments website and gain instant access to discounted rates.

Username is the email address that you have provided to Gem-A Membership.

Password is your membership number.

You must login before adding products to your basket.

We recommend changing your password in the account settings.



An Investigation of Grinding Hardness of Some Ornamental Stones

Henry A. Hänni, Richard Brunk and Leander Franz

ABSTRACT: As an extension to the typical ‘scratch hardness’ (e.g. Mohs scale) of minerals, at the end of the 19th century Austrian mineralogist August Rosiwal postulated a ‘grinding hardness’ scale. He published values expressing different amounts of resistance to abrasion of ornamental and building stones in comparison to quartz. For the present paper, 25 different ornamental stone materials were ground under normalised conditions to measure their grinding hardness (GH) relative to single-crystal quartz (GH 100). Not surprisingly, the values varied greatly, from GH 174 for fibrous chalcedony to GH 11 for rhodochrosite. A remarkable result was the GH 103 value obtained for nephrite, which consists of monomineralic aggregates of clinoamphibole with a distinctly lower Mohs hardness than quartz. These investigations show that a fibrous, intensely interlocked texture provides increased resistance against grinding, which is consistent with previous investigations.

The Journal of Gemmology, 37(6), 2021, pp. 632–643, <https://doi.org/10.15506/JoG.2021.37.6.632>

© 2021 Gem-A (The Gemmological Association of Great Britain)

Towards the end of the 19th century, mineralogy was a well-cultivated discipline at universities in Europe and elsewhere, where the properties of minerals were characterised, discussed and published. Special attention was given to the hardness of minerals and its method of determination. Various researchers investigated the resistance to abrasion of minerals, rocks and similar materials (e.g. Figure 1) using their own (proprietary) methods. Experiments to determine scratch hardness, grinding hardness or resistance to deformation resulted in various hardness scales, such as those of Brinell, Mohs, Rockwell and Vickers. Today, the one that is best known among gemmologists is the Mohs scale (Friedrich Mohs, 1733–1839), which expresses relative hardness according to 10 reference minerals that range from talc (Mohs 1) to diamond (Mohs 10). The practical use of hardness pencils has contributed to this scale’s broad acceptance, although the differences between hardness levels are not proportional. In addition, some minerals possess different hardness values according to crystallographic direction or the crystal face on which the scratch is performed. The best-known example is kyanite; also known as disthene (in Greek δις σθένος), its name

expresses the existence of two hardness values (Mohs 4½ and 7). Hermann Tertsch reported that this feature was first observed by R. Franz in 1850 (Tertsch 1949).

In rocks containing complex mineral associations, scratch hardness is not applicable because the various components commonly have different hardness values. Also, the polycrystalline character and texture could have an influence on scratch resistance. It is useful to know the relative resistance against abrasion of rocks used for ornamental purposes, as well as for industrial and construction applications. At the end of the 19th century, A. K. Rosiwal (Vienna, Austria) conducted experiments to establish a scale of relative grinding hardness values (Rosiwal 1895, 1896). At that time, silicon carbide (SiC) had just been invented in the USA and was not readily available, so Rosiwal used corundum powder (0.2 mm or 200 µm sieve size) as the abrasive agent. His mineral and rock samples consisted of 2 × 2 cm blocks. He used a grinding time of 8 minutes on a metal lap, but unfortunately the pressure exerted on the samples was not reported in his papers. He tested several minerals in various crystallographic orientations and, from the resulting loss of weight, he created a list of



Figure 1: The samples used in this study were selected from a variety of ornamental materials. The pieces shown here range from 2 to 6 cm in maximum dimension. Photo © H. A. Hänni.

relative grinding hardness values. For corundum he fixed a value of 1,000, and for quartz he measured a value of 117 (Rosiwal 1896; both of these numbers are averages). In a later publication he set the relative grinding hardness of quartz (single crystal, abrasion perpendicular to the *c*-axis) to 100 (Rosiwal 1916). Similar investigations of grinding hardness using a fully automated abrasive disc were performed by Tertsch (1934).

In this article, we re-examine the methodology of determining grinding hardness and report data in comparison to quartz for some ornamental stones that are commonly used in the gem and jewellery industry. Accordingly, we

hope to provide helpful information on the resistance of various ornamental stones to processing and wear.

Grinding hardness is one aspect of the mechanical resistance of gem materials; another consideration is brittleness, which is not addressed in this article. Diamond is the hardest gem material, but it is somewhat friable and susceptible to chipping, as seen from wear marks on ring stones (Figure 2a). Corundum, with a Mohs hardness of 9, can also get badly worn on the edges when exposed to daily wear over time (Figure 2b). Comprehensive treatments of gemstone durability have been published elsewhere by Martin (1987) and Hänni (2009a, b).

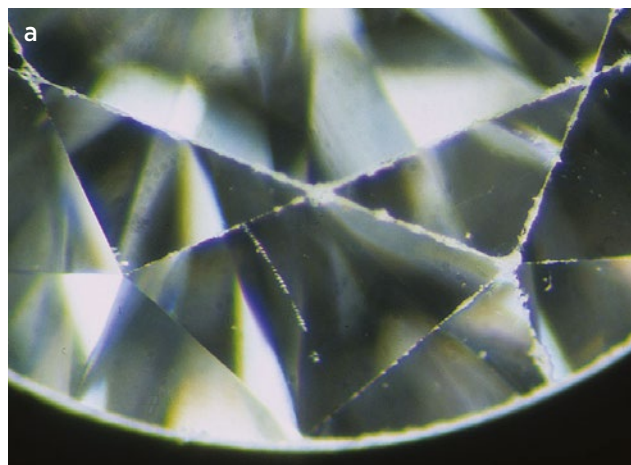


Figure 2: Even 'hard' gem materials can show evidence of abrasion, scratching, chipping, etc. These images illustrate wear marks on (a) a diamond (about 1 ct) and (b) a sapphire (about 3.5 ct). Photos © H. A. Hänni.

MATERIALS AND METHODS

Samples

For the present study, 25 different gem and ornamental materials were selected from the inventory of Groh & Ripp in Idar-Oberstein, Germany, and are listed here in alphabetical order:

1. Aventurine quartz, green—foliated quartzite with fuchsite mica
2. Aventurine quartz, orangey red—foliated (mylonitic) quartzite with hematite
3. Chalcedony, light grey—cryptocrystalline quartz
4. Chrysoprase—green chalcedony
5. Dumortierite—quartzite containing dumortierite
6. Granite—igneous rock used in the building industry
7. Green quartz—non-foliated (granoblastic) quartzite with fuchsite mica
8. Heliotrope (bloodstone)—green chalcedony with red spots
9. Jadeite—spotted white and green
10. Jasper, red—cryptocrystalline granular quartz
11. Lapis lazuli—complex blue rock
12. Magnesite—white to creamy polycrystalline (with quartz)
13. Malachite—fibrous aggregate
14. Nephrite—dense fibrous texture
15. Obsidian, ‘mahogany’—volcanic glass
16. ‘Opal’, pink (‘Andes opal’)—palygorskite with chalcedony and common opal
17. Quartz, smoky—large single crystal
18. Quartz, rose—massive
19. Rhodochrosite—massive, randomly oriented
20. Rhodonite—polycrystalline, often with black manganese oxide
21. Sannan-Skarn—complex metamorphic rock (see Hänni *et al.* 2016)
22. Sodalite—polycrystalline rock
23. Sugilite—complex metamorphic rock
24. Tiger’s-eye—quartz containing channels filled with iron oxides
25. Verdite—complex metamorphic rock with fuchsite and corundum

The samples were precisely cut by Groh & Ripp into 20 × 20 mm blocks (with a precision of 1/10 mm) of variable thickness (mostly cubes; e.g. Figure 3), and then polished thoroughly.



Figure 3: Six 20 × 20 mm blocks of each material were prepared for the abrasion tests, as shown by these sample groups, which consist of (from top left to bottom right): red jasper, rhodonite, sodalite, heliotrope, chrysoprase, dumortierite, orangey red aventurine quartz, obsidian, lapis lazuli, rose quartz, smoky quartz and green aventurine quartz. Photo © H. A. Hänni.

Petrographic Investigations

For each sample type, polished thin sections were produced for detailed petrographic examination. This enabled us to determine the content of the mineral phases and their modal amounts, as well as the structure and texture (i.e. fabric and grain size) of the samples. These properties have a significant influence on the mechanical resistance to grinding.

Petrographic investigations were performed with a Leica DMRD polarising microscope with transmitted and reflected light. In addition, confocal Raman micro-spectroscopy was used to characterise all of the minerals in the samples non-destructively. The investigations were performed with a Bruker Senterra Raman dispersive microscope spectrometer equipped with two lasers. For silicates, the green YAG laser (532 nm) was used with a power of 20 mW and 10–50 s counting time. Opaque phases were investigated with the red diode laser (785 nm), employing a power of 10 mW and 100 s counting time. For both lasers, we used an objective lens with 50× magnification and an aperture of 25 µm. Mineral identification was performed using the RRUFF database (Downs 2006) and our own Raman mineral database at Basel University (Switzerland).

The rocks were named according to the scientific nomenclature established by the International Union of Geological Sciences, following Le Bas and Streckeisen (1991) and Schmid *et al.* (2007). The modal amounts (i.e. mineral abundances) were determined from the thin sections. In coarse-grained samples, point counting was applied; for very fine-grained specimens, an estimation was done using comparison images. For samples with intense microcrystalline intergrowths, such as jasper or tiger's-eye, the specific gravity (SG) was considered in order to determine the modal composition. The SG values of the samples were obtained by hydrostatic weighing.

Grinding Procedure

A Logitech 1LA511 automated lapping and polishing machine located at the Earth Science Institute of Basel University was used to grind the samples (Figure 4). Six blocks of each sample material were weighed and then affixed to a glass disc. Each sample group was placed in a metal ring and held against the cast-iron lap wheel using a 4 kg lead weight. (The flatness of the lap was maintained with an electronically controlled diamond-charged dressing tool.) The lap had radial grooves and was fed with an abrasive slurry (25 drops per minute) consisting of 700 g SiC mixed with 3000 ml of water. The 400-grit SiC powder corresponded to a particle size of 22 µm.



Figure 4: A Logitech automated lapping and polishing machine was used to grind the samples for 30 minutes for this study. At the top, a rotating barrel contains the abrasive slurry. On the steel lap are two oscillating sample discs, weighted down with 4 kg of lead. At the back of the lap, a diamond-charged dressing tool keeps the lap wheel flat. Resting on the front-left side of the machine is a glass disc affixed with six magnesite samples. Photo © H. A. Hänni.

We chose a grinding duration of 30 minutes. The lap wheel turned at 50 rotations per minute, and two rings (each containing a set of six sample blocks) moved in an oscillating fashion over the lap. The six blocks of each material (with a total surface area of 24 cm² subjected to grinding) were used to minimise measurement error. Fresh SiC slurry was used for each run, and during the experiment the grinding materials were immediately flushed away into the drain. After each run, the machine was diligently cleaned to avoid any contamination between materials.

After grinding, the blocks were detached from the glass disc and the loss of weight was measured. The amount of weight loss for each group of six samples was used to calculate the relative grinding hardness. Weights were measured with a Mettler carat balance with a precision of 0.001 ct.

Calculation of Relative Grinding Hardness

The weight loss (W) in grams of the samples was divided by the SG in order to obtain the loss of volume. Following Rosiwal (1916), this number was scaled to

100 for quartz, and all measured values of weight loss are relative to this quartz value. The grinding hardness values were therefore calculated as a percentage of the quartz value: $[100 \times (W/SG)_{\text{quartz standard}}] / [(W/SG)_{\text{sample}}]$. This yielded a grinding hardness value for each type of sample material, relative to quartz.

RESULTS

Table I presents the most important petrographic and mineralogical features of the investigated samples, which are listed in alphabetical order. Most of the materials are polyminerally and can be classified as magmatic or metamorphic rocks. A few samples, such

as chalcedony and quartz, are monomineralic or single crystals. A detailed petrographic description and photomicrographs of all the materials are available in *The Journal's* online data depository.

A wide range of rock fabrics was observed, including randomly oriented textures (e.g. chalcedony, chrysoprase and granite), deformation or flow textures (e.g. aventurine quartz, lapis lazuli and obsidian), and complex compositional layering (e.g. dumortierite, jasper and verdite). Our petrographic investigations also revealed some anomalous or unexpected minerals in the ornamental stones, such as significant amounts of quartz and blue tourmaline in the dumortierite, spessartine in the rhodonite, and andradite in the jasper.

Table I: Petrographic features of the investigated samples, in alphabetical order.

No.	Sample material (origin)	Petrographic name	Rock or mineral fabric	Modal phase composition* (vol.%)	SG measured	SG calculated
1	Aventurine quartz, green (India)	Fuchsite quartzite	Foliated	Qz (>93), Fu (7), Acc (<<1)	2.67	2.66
2	Aventurine quartz, orangey red (Australia)	Muscovite-bearing mylonitic quartzite	Foliated	Qz (>99), Acc (<1)	2.65	2.65
3	Chalcedony, light grey (Turkey)	Chalcedony	Randomly oriented (decussate)	Chc (100)	2.63	2.62
4	Chrysoprase (Australia)	Chrysoprase	Randomly oriented	Chc and Qz (>98), Shs (2), Acc (<<1)	2.63	2.62
5	Dumortierite (Mozambique)	Tourmaline-dumortierite quartzite	Compositionally layered	Qz (60), Dum (30), Tur (9), Acc (1)	3.07	2.91
6	Granite (Germany)	Monzogranite	Randomly oriented	Pl (35), Qz (32), Or (25), Bt (7), Acc (1)	2.80	2.69
7	Green quartz (Zimbabwe)	Fuchsite quartzite	Randomly oriented (granoblastic)	Qz (95), Fu (<5), Acc (<<1)	2.66	2.66
8	Heliotrope (India)	Green chalcedony	Randomly oriented	Chc (98), Hem (2)	2.63	2.67
9	Jadeite (Myanmar)	Fluoro-richterite Cr-omphacite jadeitite	Inhomogeneous, partly foliated	Jd (>40), Cr-Omp (35), F-Rct (25), Acc (<1)	3.35	3.26
10	Jasper, red (South Africa)	Andradite- and hematite-bearing quartzite	Compositionally layered	Qz (99), Acc (1)	2.68	2.68
11	Lapis lazuli (Afghanistan)	Phlogopite-diopside-lazurite schist	Compositionally layered, partly foliated	Lzr (42), Di (35), Plh (20), Acc (3)	3.01	2.84
12	Magnesite (USA)	Quartz-magnesite marble	Randomly oriented with veins	Mgs (>96), Qz (4), Acc (<<1)	2.89	2.99
13	Malachite (Congo)	Malachite	Monomineralic layering	Mlc (>>99), Acc (<<1)	3.87	3.80
14	Nephrite (Russia)	Uvarovite- and magnesiochromite-bearing actinolite	Fibrous, randomly oriented	Act (99), Acc (1)	3.00	3.04

The strongly inhomogeneous nature of some samples (e.g. dumortierite) created challenges for determining their modal phase amounts. We therefore compared their measured SG values (as determined by hydrostatic weighing) with SG values that were calculated from the average densities of their constituent phases (from www.webmineral.com) and their estimated modal amounts. For most samples, we found a fair agreement between the measured and calculated SGs (see, e.g., the values for 'green quartz' in Table I). Larger deviations were recorded mainly for compositionally layered samples such as dumortierite, verdite or lapis lazuli. In such strongly inhomogeneous samples, the process of point counting a single thin section was often not representative of the

whole rock. Furthermore, fractures and other hollow spaces in the samples might account for differences between the measured and calculated SG values.

Table II summarises the measured values of the samples, and representative samples are shown in Figure 5, in order of decreasing grinding hardness. To test the reproducibility of these investigations, the smoky quartz and light grey chalcedony were subjected to a second round of grinding, which yielded differences of 4–6%. Due to the inhomogeneity of the polycrystalline samples, an even larger deviation for those rocks can be expected.

The highest grinding hardness values (GH 167–174) were recorded for chalcedony-bearing samples, followed by 'pink opal' (GH 105), nephrite (GH 103) and the

Table I: (continued)

No.	Sample material (origin)	Petrographic name	Rock or mineral fabric	Modal phase composition* (vol.%)	SG measured	SG calculated
15	Obsidian, 'mahogany' (Mexico)	Obsidian	Streaky interwoven (flow structured)	Obs (98), Acc (2)	2.36	2.40
16	'Opal', pink or 'Andes' (Peru)	Quartz- and opal-bearing chalcedony palygorskite	Inhomogeneous, randomly oriented	Plg (83), Chc (15), Acc (2)	2.16	2.18
17	Quartz, smoky (Brazil)	Smoky quartz	Single crystal	Qz (>100), Acc (<0.1)	2.65	2.65
18	Quartz, rose (South Africa)	Rose quartz	Massive	Qz (>100)	2.65	2.65
19	Rhodochrosite (Argentina)	Rhodochrosite	Massive, randomly oriented	Rds (>99), Acc (<1)	3.36	3.69
20	Rhodonite (Madagascar)	Spessartine rhodonite	Inhomogeneous, randomly oriented	Rdn (80), Sps (16), Acc (4)	3.65	3.66
21	Sannan-Skarn (Pakistan)	Calcite-aegirine-winchite skarn	Inhomogeneous, deformed texture	Wnc (75), Aeg (21), Cal (3), Acc (1)	2.98	3.10
22	Sodalite (Namibia)	Carbonate-paragonite-natrolite sodalite	Randomly oriented with veins	Sdl (73), Ntr (20), Pg (3), Crb (3), Acc (1)	2.32	2.31
23	Sugilite (South Africa)	Aegirine-phlogopite-pectolite-quartz sugilite	Inhomogeneous, randomly oriented	Sug (>40), Qz (35), Pct (15), Phl (7), Aeg (3), Acc (<<1)	2.77	2.75
24	Tiger's-eye (South Africa)	Goethite-bearing quartzite	Fibrous	Qz (>99), Acc (<1)	2.67	2.65
25	Verdite (South Africa)	Diaspore-corundum-margarite-fuchsite schist	Compositionally layered, partly foliated	Fu (65), Mrg (24), Crn and Dia (10), Acc (1)	2.71	2.98

* Mineral abbreviations after Whitney and Evans (2009): Acc = accessory minerals, Act = actinolite, Aeg = aegirine, Bt = biotite, Cal = calcite, Cr-Omp = chrome omphacite, Crb = carbonate, Crn = corundum, Chc = chalcedony, Dia = diaspore, Di = diopside, Dum = dumortierite, F-Rct = fluoro-richterite, Fu = fuchsite, Hem = hematite, Jd = jadeite, Lzr = lazurite, Mgs = magnesite, Mlc = malachite, Mrg = margarite, Ntr = natrolite, Obs = obsidian, Or = orthoclase, Pct = pectolite, Pg = paragonite, Phl = phlogopite, Pl = plagioclase, Plg = palygorskite, Qz = quartz, Rds = rhodochrosite, Rdn = rhodonite, Sdl = sodalite, Shs = sheet silicates, Sps = spessartine, Sug = sugilite, Tur = tourmaline and Wnc = winchite. A detailed petrographic description of the samples is given in the data depository.

Table II: Measured and calculated values for 25 selected ornamental stones in order of decreasing grinding hardness. Average Mohs hardness is based on the modal phase amounts listed in Table I.

Sample material	SG measured	Loss in weight (g)	Loss of volume (cm ³)	Grinding hardness	Average Mohs hardness
Chalcedony, light grey	2.63	1.18	0.45	174	7.0
Chrysoprase	2.63	1.19	0.45	172	6.9
Heliotrope	2.63	1.23	0.47	167	7.0
'Opal', pink or 'Andes'	2.16	1.60	0.74	105	3.0
Nephrite	3.00	2.27	0.76	103	5.5
Quartz, smoky	2.65	2.06	0.78	100	7.0
Dumortierite	3.07	2.43	0.79	99	7.5
Quartz, rose	2.65	2.12	0.80	98	7.0
Jadeite	3.35	3.25	0.97	80	6.0
Rhodonite	3.65	3.92	1.07	73	6.1
Green quartz	2.66	2.82	1.06	73	6.8
Tiger's-eye	2.67	2.97	1.11	70	7.0
Aventurine quartz, green	2.67	3.13	1.17	66	6.7
Sugilite	2.77	3.32	1.20	65	6.0
Aventurine quartz, orangey red	2.65	3.55	1.34	58	7.0
Jasper, red	2.68	3.87	1.44	54	7.0
Granite	2.80	5.09	1.82	43	6.2
Obsidian, 'mahogany'	2.36	4.75	2.01	39	5.5
Lapis lazuli	3.01	7.35	2.44	32	5.0
Sodalite	2.32	8.75	3.77	21	5.7
Verdite	2.71	10.31	3.81	20	3.4
Magnesite	2.89	13.39	4.64	17	4.1
Malachite	3.87	17.58	4.54	17	3.8
Sannan-Skarn	2.98	20.10	6.74	12	5.5
Rhodochrosite	3.36	23.91	7.12	11	3.0



Figure 5: The 25 selected ornamental stones (each 20 × 20 mm), including the quartz reference, are labelled here with their relative grinding hardness values. Photo © H. A. Hänni.

single-crystal and massive quartz samples (GH 98–100). Polycrystalline and polymineralic silicate rocks such as dumortierite, sugilite, aventurine and jasper had high-to-intermediate grinding hardness (GH 54–99), while felsic magmatic rocks such as obsidian and granite had somewhat smaller values (GH 39–43). At the lower end of the scale were complex siliceous rocks such as verdite, sodalite and lapis lazuli (GH 20–32), and the lowest grinding hardness was recorded for carbonate-rich rocks such as magnesite, malachite and rhodochrosite, as well as Sannan-Skarn (GH 11–17).

Based on the modal phase amount of each sample (cf. Table I) and the Mohs hardness of each phase (from

www.webmineral.com), the average Mohs hardness for each material was calculated (Table II, last column). At first look, the samples with the highest grinding hardness values also showed a relatively high average Mohs hardness, while those with a low grinding hardness mostly had a low average Mohs hardness. However, there are some remarkable exceptions. Dumortierite had the highest average Mohs hardness (7.5) but possessed a grinding hardness of ‘only’ 99, whereas nephrite, with a moderate Mohs hardness of 5.5, had a grinding hardness of 103. Furthermore, the ‘pink opal’, with a low average Mohs hardness of 3.0 (due to the presence of abundant palygorskite), had a grinding hardness of 105.

DISCUSSION

The detailed petrographic analysis of thin sections of the samples was of great value. In addition to characterising their mineralogical composition, information was also obtained on their modal phase amounts and texture. Some surprising discoveries were made, such as the presence of andradite in the jasper and considerable amounts of quartz and blue tourmaline in the dumortierite. Moreover, one must always be aware that some ornamental stones are very inhomogeneous, with irregular monomineralic sections and compositional layering, and this is mirrored by differences between their measured SG and the SG value calculated on the basis of the modal phase composition (Table I). In the case of the verdite, these calculations point to hollow spaces due to fracturing in the sample.

Of the samples tested, those that were most resistant to grinding were chalcedony, chrysoprase and heliotrope (GH 167–174). These are mainly or completely comprised of chalcedony, which consists of twisted fibres of microcrystalline α -quartz (Flörke *et al.* 1991). The decussate (or intertwined) microstructure gives chalcedony an outstanding grinding hardness, as previously observed by Rosiwal (1916) for flint (or chert, GH 150). Although tiger's-eye also consists of α -quartz fibres, its low grinding hardness of 70 is distinctly below that of single-crystal or massive quartz. This is probably due to the lack of an interlocked fabric and to the different shape of the tiger's-eye fibres, which measure up to 10×0.3 mm and are intergrown with relatively soft goethite. Single-crystal quartz (with GH 100, by definition) is somewhat more resistant than polycrystalline quartzite (GH 58–73) in which softer impurity minerals lower the overall hardness. This is consistent with the observations of Rosiwal (1916) for impure quartzites from Czechia (also known currently as the Czech Republic) and France (GH 76–92). The relatively low grinding hardness of jasper (GH 54), which contains only granular quartz with traces of impurities, is remarkable. A coating effect of minute amounts of hematite on the quartz grain boundaries might facilitate the abrasion of jasper. Also unexpected is the anomalously high grinding hardness (GH 105) of our 'pink opal' sample, which exceeds that of single-crystal quartz despite the presence of a large amount of palygorskite, which has a Mohs hardness of only $2\frac{1}{2}$. This can only be explained by the shielding effect of the chalcedony, which surrounded the areas containing palygorskite (see petrographic description and photomicrographs in the data depository).

Also of note is the result obtained for nephrite, the

felty variety of polycrystalline tremolite-actinolite (clino-amphibole). Although amphibole monocrystals possess a Mohs hardness of 5–6, the nephrite had a grinding hardness of 103, exceeding that of single-crystal quartz. This is probably due to the high 'fracture surface energy' of nephrite described by Bradt *et al.* (1973; see also Newnham 1981), which reflects the work required to propagate a stable crack over a specific volume of a sample (see also Nakayama 1965). According to experiments performed by Bradt *et al.* (1973), the fracture surface energy of polycrystalline nephrite is 226 000 ergs/cm², which is distinctly higher than that of jadeite (122 000 ergs/cm²) and quartzite (4350 ergs/cm²; Wiederhorn 1969a). Remarkably, single-crystal quartz has a fracture surface energy of only 1030 ergs/cm² (Brace & Walsh 1962), which clearly shows the influence of the rock fabric on the fracture surface energy. According to Bradt *et al.* (1973), the fibrous nature of nephrite, with its different fibre sizes and intergrown texture at random orientation, distinctly increases the fracture surface energy in comparison with the more blocky texture of polycrystalline jadeite. Unfortunately, no measurements have been published for the fracture surface energy of chalcedony, which had the highest grinding hardness measured in the present study.

CONCLUSIONS

We have demonstrated that polycrystalline materials (e.g. chalcedony) can have a distinctly higher grinding hardness than monocrystalline specimens (e.g. smoky quartz) composed of the same mineral. A similar behaviour was previously observed by Rosiwal (1916), who found a grinding hardness of 150 for chert compared to 100 for single-crystal quartz abraded parallel to (0001). This is probably due to the interlocked, decussate texture of chalcedony, which would be expected to effectively resist abrasion (cf. Rosiwal 1916; Bradt *et al.* 1973). These findings are consistent with the elevated fracture surface energy of some polycrystalline materials (again, see Bradt *et al.* 1973), as demonstrated by the relatively high grinding hardness of nephrite. Unfortunately, only a few investigations of the fracture surface energy of natural single crystals and polycrystalline materials have been published (e.g. Brace & Walsh 1962; Bryant *et al.* 1963; Wiederhorn 1969a, b; Bradt *et al.* 1973). It seems, however, that grinding hardness can be attributed to a blend of Mohs hardness and fracture surface energy.

Polycrystalline rocks composed of different mineral components appear to be more susceptible to grinding. Dumortierite, which had the highest average Mohs

hardness (7.5) among the materials we tested, had a grinding hardness of 'only' 99, which could be due to its inhomogeneous compositional layering and highly variable grain size. Our investigations showed that even a tough and resilient rock such as granite can have only a moderate grinding hardness (GH 43), which is consistent with observations of Rosiwal (1916) on different types of granite (GH 42–52). Conspicuous are the very low grinding hardness values (GH 12–32) obtained for lapis lazuli, sodalite, Sannan-Skarn and verdite. These rocks contained distinct fracturing and compositional layering of soft and hard components. Although the plucking of harder grains during grinding could accelerate the abrasion of such materials, such effects can largely be excluded here since our sample blocks displayed perfectly polished surfaces after the grinding experiments. The lowest grinding hardness values were recorded for the carbonate rocks magnesite, malachite and rhodochrosite (GH 11–17), consistent with their low Mohs hardnesses and the numerous cleavage planes of carbonates.

This study calls attention to grinding hardness as an important property of minerals and rocks (i.e. ornamental stones; Figures 6 and 7). Furthermore, we established a standard procedure to quantify the grinding hardness of such materials. Nevertheless, this investigation should be seen as a basic research study, and further studies are planned such as testing the grinding hardness of the same sample in different orientations (e.g. parallel or perpendicular to foliation, compositional banding or inhomogeneous layering).

Finally, a personal note from author HAH: As a young man I started my professional career as a workshop assistant in the Mineralogical Institute of Basel University. Among other skills, I learned to produce petrographic thin sections. This involved cutting rock plates (2 × 3 cm), gluing them onto glass slides, and sawing and grinding them with SiC down to 0.03 mm thickness (by hand at the final stage). Coincidentally, embarking on the present study at the end of my career has brought me back full circle to my initial work making thin sections.



Figure 6: Ornamental stones have a wide variety of compositions and textures, which influence their grinding hardness and affect the cutting and polishing process. Shown here are cabochons consisting of: 1 = tiger's-eye, 2 = heliotrope, 3 = carnelian, 4 = obsidian, 5 = rhodochrosite, 6 = anyolite (light green zoisite and dark green pargasite), 7 = dumortierite quartzite, 8 = lapis lazuli, 9 = graphic granite, 10 = lazulite, 11 = sodalite, 12 = pietersite, 13 = sugillite, 14 = labradorite/spectrolite, 15 = Sannan-Skarn, 16 = dalmatian stone (white plagioclase and quartz with black arfvedsonite), 17 = chalcedony, 18 = common opal, 19 = chrysoprase, 20 = nephrite, 21 = clinocllore, 22 = variscite, 23 = malachite and 24 = verdite. Each stone box measures 25 × 25 mm. Photo © H. A. Hänni.



Figure 7: When different gem materials are combined in a single piece of jewellery, variations in grinding hardness can affect the uniformity of their finish. This pectoral and necklace was found in the Egyptian tomb of Princess Sithathoryunet and dates to ca. 1887–1878 BCE. The pectoral (4.5 × 8.2 cm) consists of gold, carnelian, lapis lazuli, turquoise and garnet. Courtesy of the Metropolitan Museum of Art (accession no. 16.1.3a, b), New York, New York, USA.

REFERENCES

- Brace, W.F. & Walsh, J.B. 1962. Some direct measurements of the surface energy of quartz and orthoclase. *American Mineralogist*, **47**(9–10), 1111–1122.
- Bradt, R.C., Newnham, R.E. & Biggers, J.V. 1973. The toughness of jade. *American Mineralogist*, **58**(7–8), 727–732.
- Bryant, P.J., Taylor, L.H. & Gutshall, P.L. 1963. Cleavage studies of lamellar solids in various gas environments. In: Bancroft, G.H. (ed) *Transactions of the Tenth National Vacuum Symposium of the American Vacuum Society*. Macmillan Co., New York, New York, USA, **15**, 21–26, [https://doi.org/10.1016/0042-207x\(65\)91499-5](https://doi.org/10.1016/0042-207x(65)91499-5).
- Downs, R.T. 2006. The RRUFF Project: An integrated study of the chemistry, crystallography, Raman and infrared spectroscopy of minerals. *19th General Meeting of the International Mineralogical Association*, Kobe, Japan, 23–28 July, abstract O03-13, 117.
- Flörke, O.W., Graetsch, H., Martin, B., Röller, K. & Wirth, R. 1991. Nomenclature of micro- and non-crystalline silica minerals, based on structure and microstructure. *Neues Jahrbuch für Mineralogie, Abhandlungen*, **163**(1), 19–42.
- Hänni, H.A. 2009a. Beschädigungen an geschliffenen Edelsteinen. *Gemmologie: Zeitschrift der Deutschen Gemmologischen Gesellschaft*, **58**(3–4), 127–130.
- Hänni, H.A. 2009b. Durability, damage and distress. *Gems&Jewellery*, **18**(2), 3–8.
- Hänni, H.A., Franz, L. & Wei, Z. 2016. A new ornamental gemstone from Pakistan: Sannan-Skarn. *Proceedings: The 5th GIT International Gem and Jewelry Conference*, Pattaya, Thailand, 14–15 November, 55–61.
- Le Bas, M.J. & Streckeisen, A.L. 1991. The IUGS systematics of igneous rocks. *Journal of the Geological Society*, **148**(5), 825–833, <https://doi.org/10.1144/gsjgs.148.5.0825>.
- Martin, D.D. 1987. Gemstone durability: Design to display. *Gems & Gemology*, **23**(2), 63–77, <https://doi.org/10.5741/gems.23.2.63>.
- Nakayama, J. 1965. Direct measurement of fracture energies of brittle heterogeneous materials. *Journal of the American Ceramic Society*, **48**(11), 583–587, <https://doi.org/10.1111/j.1151-2916.1965.tb14677.x>.
- Newnham, R.E. 1981. Jade. In: Frye, K. (ed) *Mineralogy. Encyclopedia of Earth Science*. Springer, Boston, Massachusetts, USA, 209–210, https://doi.org/10.1007/0-387-30720-6_63.
- Rosival, A. 1895. Über die Härte der Mineralien mit besonderer Berücksichtigung der Edelsteine. *Monatsblätter des Wissenschaftlichen Club*, **17**(2), 17–21.

- Rosiwal, A. 1916. Neuere Ergebnisse der Härtebestimmung von Mineralien und Gesteinen – Ein absolutes Mass für die Härte der Körper. *Verhandlungen der k.k. geologischen Reichsanstalt*, No. 28, 117–147 (see p. 142).
- Schmid, R., Fettes, D., Harte, B., Davis, E., & Desmons, J. 2007. 2.1 How to name a metamorphic rock. In: Fettes, D. & Desmons, J. (eds) *Metamorphic Rocks: A Classification and Glossary of Terms*. Cambridge University Press, Cambridge, 3–15.
- Tertsch, H. 1934. Über Schleifhärtenanisotropie. *Zeitschrift für Kristallographie – Crystalline Materials*, **89**(1–6), 541–552, <https://doi.org/10.1524/zkri.1934.89.1.541>.
- Tertsch, H. 1949. *Die Festigkeitserscheinungen der Kristalle*. Springer-Verlag, Vienna, Austria, viii + 312 pp., <https://doi.org/10.1007/978-3-7091-7733-4>.
- Whitney, D.L. & Evans, B.W. 2009. Abbreviations for names of rock-forming minerals. *American Mineralogist*, **95**(1), 185–187, <https://doi.org/10.2138/am.2010.3371>.
- Wiederhorn, S.M. 1969a. Fracture of ceramics. In: Wachtman, J.B (ed) *Mechanical and Thermal Properties of Ceramics*. National Bureau of Standards, Washington DC, USA, 217–241.
- Wiederhorn, S.M. 1969b. Fracture of sapphire. *Journal of the American Ceramic Society*, **52**(9), 485–491, <https://doi.org/10.1111/j.1151-2916.1969.tb09199.x>.

The Authors

Prof. Dr Henry A. Hänni FGA
GemExpert GmbH, Postfach 921,
CH-4001 Basel, Switzerland
Email: info@gemexpert.ch

Richard Brunk
Groh & Ripp, Idar-Oberstein, Germany

Prof. Dr Leander Franz
Departement Umweltwissenschaften,
Universität Basel, Bernoullistrasse 30,
CH-4056 Basel, Switzerland

Acknowledgements

We owe our thanks to Dr Vera Hammer (Museum of Natural History Vienna, Austria) for valuable assistance with referencing older literature. We appreciate the donation of the testing material and the preparation of the sample blocks by Willi Ripp of Groh & Ripp. Without his engaged cooperation, this study could not have been performed. We thank Pascal Tschudin of the Earth Sciences department of Basel University for producing the thin sections and for lapping the samples with the Logitech device. Thanks also go to Dr H. H. Klein (Basel) for his critical and constructive review of the manuscript.

Gem-A
THE GEMMOLOGICAL ASSOCIATION
OF GREAT BRITAIN

Membership Survey 2021

What we heard...

Thank you to all those who took part in our recent membership survey.

To renew your membership at gem-a.com/membership

OVERALL SATISFACTION: 73% ARE SATISFIED WITH THE GEM-A MEMBERSHIP PACKAGE

JOURNAL READERSHIP: 95% ENJOY THE JOURNAL OF GEMMOLOGY MAGAZINE

JOURNAL QUALITY: 98% RATE THE QUALITY OF THE JOURNAL AS GOOD OR BETTER

RECOMMEND TO OTHERS: 70% WOULD RECOMMEND MEMBERSHIP TO A FRIEND

f t in i e w

Gem-A Notices

COVID-19 NOTICE FROM GEM-A CEO ALAN HART



This has been a time like no other in our lives. While the COVID-19 pandemic continues to produce uncertainty in our communities, we have renewed hope as life slowly returns to a new normal. For the UK, the year 2021 started with another lockdown,

but it has been lifted and at Gem-A we are thrilled to have our students back on site. With the easing of lockdown measures, we are implementing our return-to-work strategy and have seen an increase in the number of staff coming back into the offices at Ely Place. Over the past 12 months, huge efforts were made to adapt and modify our operations and maintain the standard and delivery of our Education and Membership offerings.

Like many other businesses, Gem-A is on track for a gradual recovery, and as the Association comes out of the pandemic we have many exciting initiatives in the pipeline including development of a new short introductory gemmology course that will be offered fully online.

I'm not alone in being grateful for the support of our Gem-A Members during this difficult time. I continue to receive numerous emails from Members and our valued partners from around the world wishing Gem-A well. Here I would like to extend my appreciation once again to Gem-A staff who have worked tirelessly in an uncertain environment to continue providing our world-class services to our students and Members. My own efforts are now fully focused on what the global recovery from COVID-19 will look like and how Gem-A can best play its role. The Association will continue to do its part to support the gem and jewellery trade while building on its rich history and legacy of being a global leader in providing gemmological education.

GIFTS TO THE ASSOCIATION

Gem-A is most grateful to the following for their generous donations that will support continued research and teaching:

Meg Berry, Megagem, Fallbrook, California, USA, for three pieces of rough grandidierite from Madagascar.

Boris Brianceau, France, for an 8 ct citrine from Madagascar.

GEM-A GRADUATION AND PRESENTATION OF AWARDS

This year, we look forward to holding a combined 2020/2021 Gem-A Graduation and Presentation of Awards at London's historic Church House on 8 November 2021. Further details will be published in due course.



GLOBAL MEMBERSHIP SURVEY

Thank you to Gem-A Members who submitted their responses to the global Membership survey. Over 70% stated that they were satisfied with Gem-A's Membership offering and a majority were likely to recommend Gem-A to a friend or colleague. We are pleased that

over 90% of our Membership periodically access and read *The Journal of Gemmology*, and that over 80% rate the quality of this publication as excellent or very good. We have listened to our Members' feedback and we will be announcing some exciting new initiatives for our Membership in due course.

A WEBINAR WITH THE EDITOR

Go behind the scenes at *The Journal of Gemmology* by tuning in to our ongoing webinar series with Editor-in-Chief Brendan Laurs FGA, on 7 July 2021 at 17:00 GMT. Join us as we hear Brendan discuss the current issue of *The Journal* with Gem-A's CEO Alan Hart FGA DGA, explaining how the issue was developed and focusing in greater detail on some of the fascinating feature articles and Gem Notes. To register your place,

head to: <https://linktr.ee/gemaofgb>. Did you miss our last session of Gem-A Live with Brendan? Head to Gem-A's YouTube Channel and watch it now: www.youtube.com/c/GemAOfficialChannel.



OBITUARIES

Marc Jobin FGA

1957–2021

When I first went to Madagascar in 1994, Marc Jobin was already known in the country for his research on gems and minerals and for his trade and export business. He was a highly respected character, and also a bit feared by local traders and miners for his attitude of not being easily fooled.

He initially moved around the country on his motorbike, facing long and dangerous journeys from the capital city of Antananarivo to various mining areas such as Ambaton-drazaka (aquamarine, chrysoberyl, rose quartz and amethyst), Andilamena (ruby and sapphire), Ankazobe (aquamarine and topaz) and Tsiroanomandidy (topaz, inclusion quartz and optical quartz), or in the opposite



Marc Jobin (right) and the mine foreman at the Anjahamiary tourmaline deposit in November 2000. Photo by F. Pezzotta.

direction to Antsirabe and Betafo (tourmaline, morganite and other varieties of beryl, kunzite, spessartine and rose quartz), Mandoto (aquamarine and amethyst), Ambositra (aquamarine and tourmaline), Ambatofinandrahana and Amborompotsy (quartz varieties). He became famous in the Antsirabe–Betafo region for trekking on his motorbike (at times pushing it through unrideable areas) to the remote Vohitrakanga tourmaline field, which required a difficult journey over 70 km of mountain trails heading west-south-west from Antsirabe. At the time, he was perhaps the only foreigner to have visited there since the end of the French colonial period.

After acquiring his Land Rover he made longer journeys, to the northern part of the island in search of minerals such as titanite (sphene), green and blue apatite, amethyst and optical quartz, or to the south for yellow orthoclase, emerald, iolite and many other stones. Often Marc was among the very first to source and market new gems and minerals when they were discovered in Madagascar. In parallel with more valuable stones, he also collected and exported large quantities of jasper, labradorite, petrified wood, etc., which he presented in his large sales area at the gem and mineral shows in Tucson, Arizona, USA.

Marc also pursued rare and collectible mineral specimens, even if they weren't his main interest. He collaborated with me in the search for pezzottaite immediately after its discovery, and had the merit of recovering a large block which I studied and reduced into several specimens consisting of the rare mineral chiavennite in association with pezzottaite, hambergite,

milarite, etc. This was by far the richest specimen of chiavennite ever found.

However, Marc's main activity was working the Anjahamiary tourmaline deposit, located in the far south of Madagascar. The mine was known for producing polychrome crystals and magnificent gem-quality pencils of blue tourmaline. Marc obtained a mining permit in the second half of the 1990s and invested considerable financial resources doing large excavations but unfortunately, to my knowledge, he was never able to find sufficient quantities of gems to make this project economically satisfactory.

Tragically, Marc passed away in February 2021 after

becoming ill during a visit to the Anjahamiary mine. When his car, driven by his driver, returned to Antananarivo carrying his body, in every city along the way (Ihosy, Ambalavao, Fianarantsoa, Ambositra and Antsirabe) a procession was formed with the many people of the Malagasy world of stones who wanted to honour him.

Editor's Note: Marc obtained his FGA in 1979 and generously donated various gem materials to Gem-A's educational and research collections from 1993 to 2017.

Dr Federico Pezzotta

Museo Civico di Storia Naturale di Milano
Milan, Italy



Judith at Atlantic College (Wales) in 2011. Photo by M. Mendelssohn.

Dr H. Judith Milledge

1927–2021

Older members of the mineralogical and crystallographic communities will remember Dr H. Judith Milledge (née Grenville-Wells), who died in London on 23 January 2021 at age 94.

Judith was an examiner for the Gemmological Association of Great Britain from 1973 to 1982.

Judith's parents moved from England in 1923, and she was born in 1927 in Kokstad, South Africa. After earning BSc and MSc degrees from Rhodes University (Grahamstown, South Africa), Judith went to work in the new De Beers Diamond Research Laboratory in Johannesburg, but she soon realised that she needed a PhD degree in crystallography. Initially she approached Dr R. W. James,

Chair of Physics at the University of Cape Town, but he was too unwell to take her as a student, so he referred her to Prof. Kathleen Lonsdale FRS at University College London (UCL), who had a particular interest in diamond crystallography. In 1949, Judith moved to London to begin her PhD on diamond studies there. After completing her dissertation, Judith moved to a post-doctoral position with Dr Sidney Abrahams at the Massachusetts Institute of Technology (Cambridge, Massachusetts, USA). She then returned to UCL and re-joined Prof. Lonsdale's research group in the Department of Chemistry, eventually achieving the position of Reader in Crystallography at the University of London, by which time the university also awarded her a Doctor of Sciences degree. Prof. Lonsdale was one of the most important influences on Judith's life, and they became close collaborators. After Prof. Lonsdale's retirement, Judith transferred her Readership to the Geology Department—a good decision, both for Judith and for the Geology Department, as it laid the foundation for the excellence in mineral physics at UCL that continues to this day. Judith continued to work until well after the normal age of retirement; she was still active scientifically until her late 80s and co-authored her last paper at age 87.

Judith published more than 100 scientific articles on an extremely wide range of topics in crystallography and mineralogy, concentrating on crystal disorder, phase transitions and solid-state reactions. Her interest in crystallographic techniques extended from an apparatus for calculating Fourier transforms (in the pre-computer age) to ingenious devices for collecting data from single crystals. Judith also was a pioneer of crystallographic

computing, working on a Pegasus computer with assistance from Derek Milledge of the Ferranti London Computer Centre, whom she married in 1958.

During her time in the Geology Department at UCL, Judith continued to collaborate with colleagues in other departments (principally Engineering), but her major research emphasis returned to the study of diamond, which was her dominant interest throughout her career. Judith was aware of the inhomogeneity of a diamond's growth phases, and in collaboration with me at UCL and colleagues in other universities, she co-authored some highly regarded papers on diamond formation, isotopic variations, micro- and macro-inclusions, and defects within a single stone. She revealed variations in nitrogen concentration using infrared microscopy mapping. As one example, she used this technique on a faceted Sumitomo synthetic diamond to determine that it was type Ib (see *The Journal*, Vol. 20, No. 7–8, 1987, p. 407).

An obvious necessity for diamond research is that the researcher should have access to diamonds for which the source is accurately recorded, although such provenance information is often exceedingly difficult, or impossible,

to obtain. It is probably in this area that Judith's work will have its most long-lasting legacy because she very diligently, over many years, accumulated and characterised a large collection of well-provenanced samples. After Judith retired, she arranged for her collection to be divided between South Africa and the UK, thus providing an invaluable resource for mineralogists for many years to come.

In March 1999, Judith gave a lecture at the Gem Tutorial Centre titled 'Some current problems in diamond research'. This title is a succinct description of Judith's life and work. In a very meaningful memorial to Judith, a 0.9 ct gem-quality synthetic diamond is currently being produced by Algordanza (Switzerland) from her cremation ashes. Such gems are of varying shades of blue, depending on the concentration of boron present. This seems fitting, as during her career Judith collected some extremely rare type IIb boron-containing blue diamonds from the Premier mine in South Africa.

Dr Monica Mendelssohn
London

Gem-A: over **110** years of experience in gemmology education

Our FGA and DGA Members are located around the world –
join them by studying with Gem-A

**STUDY
IN ONE
OF THREE
WAYS**

At Gem-A HQ
London



Worldwide at one
of our ATC's



Online with
practical lab classes
in your area



Find out more by contacting: education@gem-a.com

Creating gemmologists since 1908



Learning Opportunities

Note: Event dates and formats are subject to change depending on the COVID-19 situation.

CONFERENCES AND SEMINARS

Association for the Study of Jewelry and Related Arts Conference

26–27 June 2021

Online

www.jewelryconference.com

Mediterranean Gemmological & Jewellery Conference

9–11 July 2021 Postponed to Spring–Summer 2022

Thessaloniki, Greece

<https://gemconference.com>

NAJA 56th Ace® It Mid-Year Conference

14–17 August 2021

Location TBA

www.najaappraisers.com/html/conferences.html

9th International Conference Mineralogy and Museums

24–26 August 2021

Sofia, Bulgaria

www.bgminsoc.bg

Note: Gem minerals and archaeogemmology are among the topics that will be covered.

JCK Las Vegas

27–30 August 2021

Las Vegas, Nevada, USA

<https://lasvegas.jckonline.com>

Note: Includes a seminar programme

3rd European Mineralogical Conference (emc2020)

29 August–2 September 2021

Online

<https://emc2020.ptmin.eu>

Sessions of interest: The Geology of Gem Deposits: A Session in Honour of Gaston Giuliani; Materials Sciences and Archaeometry for Cultural Heritage

31st International Conference on Diamond and Carbon Materials

6–9 September 2021

Online

www.elsevier.com/events/conferences/international-conference-on-diamond-and-carbon-materials

3rd International Conference on Tourmaline (TUR2021)

9–11 September 2021

Elba Island, Italy (and online)

www.tur2021.com

JVA Registered Valuer Conference 2021

10–12 September 2021

Loughborough

<https://thejva.org/jewellery-watch-valuer-conference>

NAJ Summit

11–13 September 2021

Northampton, East Midlands

www.naj.co.uk/summit

American Gem Society Conclave

12–14 September 2021

Dallas, Texas, USA

www.americangemsociety.org/conclave-2021

Denver Gem & Mineral Show

16–19 September 2021

Denver, Colorado, USA

www.denvermineralshow.com

Note: Includes a seminar programme

HardRock Summit 2021

16–19 September 2021
 Denver, Colorado, USA
<https://hardrocksummit.com>
Note: Includes a seminar programme

13th Annual Portland Jewelry Symposium

September 2021 (exact dates TBA)
 Portland, Oregon, USA
<https://portlandjewelrysymposium.com>

Geological Society of America Annual Meeting (GSA Connects 2021)

10–13 October 2021
 Portland, Oregon, USA (hybrid online)
<https://community.geosociety.org/gsa2021/home>
Session of interest: Gemological Research in the 21st Century—Gem Minerals and Localities

Canadian Gemmological Association (CGA) Conference

22–24 October 2021
 Vancouver, British Columbia, Canada
<https://canadiangemmological.com>

The Munich Show

22–24 October 2021
 Munich, Germany
<https://munichshow.de/?lang=en>
Note: Includes a seminar programme

GAC-MAC London 2021 Joint Annual Meeting

3–5 November 2021
 London, Ontario, Canada
<https://gacmac2021.ca>
Session of interest: Diamonds in Cratons, Diamond-bearing Rocks and Mantle Xenoliths

2021 International Gems & Jewelry Academic Conference

Mid-November 2021 (exact dates TBA)
 Beijing, China
 Email: ngtcyjb@ngtc.com.cn

7th International Gem & Jewelry Conference (GIT 2021)

1–2 December 2021
 Chanthaburi, Thailand
 Email: gitconference@git.or.th

23rd Federation for European Education in Gemmology (FEEG) Symposium

29–30 January 2022
 Paris, France
www.feeg-education.com/symposium

NAJA 57th Ace® It Winter Conference

30–31 January 2022
 Tucson, Arizona, USA
www.najaappraisers.com/html/conferences.html

AGTA Gemfair Tucson

1–6 February 2022
 Tucson, Arizona, USA
<https://agta.org/agta-gem-fair-tucson>
Note: Includes a seminar programme

Tucson Gem and Mineral Show

10–13 February 2022
 Tucson, Arizona, USA
www.tgms.org/show
Note: Includes a seminar programme

Inhorgenta Munich

11–14 February 2022
 Munich, Germany
www.inhorgenta.com/en
Note: Includes a seminar programme

Hasselt Diamond Workshop 2020: SBDD XXV

9–11 March 2022
 Hasselt, Belgium
www.uhasselt.be/SBDD

MJSA Expo

Spring 2022 (exact dates TBA)
 New York, New York, USA
https://mjsa.org/eventsprograms/mjsa_expo
Note: Includes a seminar programme

34th Annual Santa Fe Symposium

22–26 May 2022
 Albuquerque, New Mexico, USA
www.santafesymposium.org

International Colored Gemstone Association (ICA) Congress

September 2022 (exact dates TBA)
 Shenzhen, China
www.gemstone.org/ica-congresses

OTHER EDUCATIONAL OPPORTUNITIES

Gem-A Workshops and Courses

Gem-A, London

<https://gem-a.com/education>**Gemstone Safari to Tanzania**

12–29 January 2022

www.free-form.ch/tanzania/gemstonesafari.html**Lectures with Gem-A's Midlands Branch**

Fellows Auctioneers, Augusta House, Birmingham

Email Louise Ludlam-Snook at

gemamidlands@gmail.com

- Rachel Church—The Brooch: A Jewel for Everyone
25 June 2021 (online)

Lectures with The Society of Jewellery Historians

Society of Antiquaries of London, Burlington House

www.societyofjewelleryhistorians.ac.uk/

current_lectures

- Charlotte Gere—Colour in Victorian Jewellery
28 September 2021

- Akis Goumas—Learning and Experimenting with Ancient Jewellery of the Aegean Region
26 October 2021 (online only)
- Ute Decker—Sculptural Minimalism & Fairtrade Gold – Philosophy, Provenance and Process
23 November 2021
- Tim Schroder—Jewels at the Court of Henry VIII
25 January 2022
- TBA
22 February 2022
- Natasha Awais-Dean—Jewels Captured in Perpetuity: The Jewellery Book of Anne of Bavaria
22 March 2022
- Gonçalo de Vasconcelos e Sousa—An Aspect of Portuguese Jewellery
24 May 2022
- Karl Schmetzer—The Late 14th-Century Royal Crown of Blanche of Lancaster
28 June 2022



Gem-A

THE GEMMOLOGICAL ASSOCIATION
OF GREAT BRITAIN

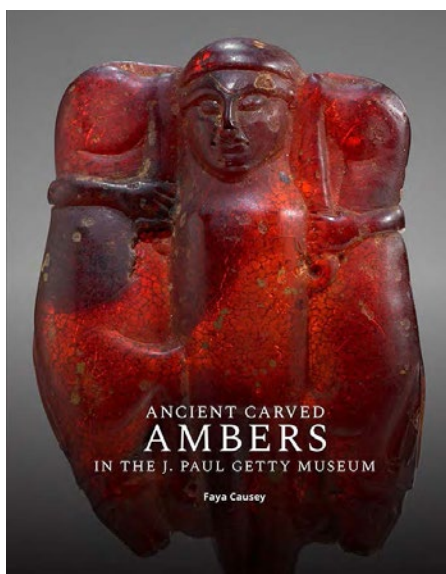
Study gemmology online!

- Online class groups
- Virtual learning
- Interactive quizzes
- Start your journey to FGA Membership with online learning by leading provider, Gem-A



Contact education@gem-a.com for more information

New Media



Ancient Carved Ambers in the J. Paul Getty Museum

By Faya Causey, with a technical essay by Jeff Maish, Herant Khanjian and Michael R. Schilling, 2020. J. Paul Getty Museum, Los Angeles, California, USA, 307 pages, illus., ISBN 978-1606066348. USD75.00 softcover or free download at www.getty.edu/publications/virtuallibrary/9781606060513.html.

Approximately a decade ago, the J. Paul Getty Museum in Los Angeles published online its extensive holdings of ancient carved amber—56 Etruscan and Italic objects. The introduction to this online catalogue formed the basis for Faya Causey's book *Amber and the Ancient World* (J. Paul Getty Museum, 2011 or 2012¹). In 2019, this online catalogue was moved to a new site (<https://ambers.netlify.app>), where it can be freely viewed or downloaded, with superb, high-resolution photographs that are fully zoomable. A reference edition of the catalogue, titled *Ancient Carved Ambers in the J. Paul Getty Museum*, was published online in PDF format in 2019 and as a softcover book in 2020; the latter is reviewed here.

Author Faya Causey was formerly head of academic programs at the National Gallery of Art, Washington DC, USA, and is an expert on early amber, as is amply shown

by this book. The introductory chapter to the catalogue—essentially the text of her previous book—shows the extent of her knowledge; the 18 sections cover such topics as the nature of amber, ancient names for amber, optical characteristics, sources, trade, forgeries and how it was worked. Unlike some museum catalogues, this is clearly not just a book of glossy photographs.

The 56 ancient objects (and one fake) that are described in this catalogue all come from Italy and are dated from the 6th to late 5th century BC. They are mainly arranged thematically, and are predominantly human or animal figures, or parts thereof. Most were pendants, although a few might have formed parts of larger objects. One such is a lion's head (Cat 34) that appears to have been a spout of some sort; another is a ram's head (Cat 53). The catalogue descriptions are lengthy, typically multiple pages, with references. As can be seen from the photographs of the objects, their condition varies hugely. Some look almost pristine, while others are poorly preserved. My only real criticism of the book is that the catalogue entries only provide a single image of each object; in some cases a second view would have been useful to help visualise the whole object. This is, however, remedied by the online version of the catalogue, where a variety of views and close-ups are provided. (Note that the website address for the downloadable PDF of the book is different from the full online catalogue, as shown by the links above.)

This reviewer is mindful that *The Journal's* core gemmological audience is more interested in the material properties of amber than the art and history aspects. A detailed technical section is one of the strengths of the book, a witness to the resources available to the J. Paul Getty Museum and the importance of using modern science to help shed light on the past. This final chapter, titled 'Technical Essay: Analysis of Selected Ambers from the Collections of the J. Paul Getty Museum', is the work of Jeff Maish, Herant Khanjian and Michael R. Schilling, who are all with the Getty and are, respectively, a conservator, a scientist specialising in organic materials and a senior scientist in charge of organic materials. As this line-up might suggest, this technical essay covers both conservation and analysis, and the importance of the latter with regard to the former.

¹ The book under review indicates that Causey's *Amber in the Ancient World* was published in 2012, as was the online catalogue, but this reviewer's copy of *Amber in the Ancient World* is clearly dated 2011, and it refers to the online catalogue.

The deterioration of amber is a huge challenge to conservators, as well as being heart-rending aesthetically. The passing of a millennium or two can turn a once-beautiful amber carving into what looks like a block of compacted brown sugar that can crumble at a touch. (This reviewer can speak from experience.) Various organic stabilisers have been used over the years to halt further deterioration and restore some semblance of shine and translucency. But, as pointed out in the essay, all such treatments should be meticulously recorded because they could interfere with future analytical studies. One of the goals of the scientific studies carried out at the Getty was to gauge such impact.

The main purpose of the scientific studies, however, was to determine whether all the ancient ambers were of Baltic origin, as is usually assumed. The primary technique used was FTIR spectroscopy. The spectrum of Baltic amber shows characteristic absorption bands and is well known to gemmologists. The Getty researchers also used THM-pyrolysis gas-chromatography mass-spectrometry (THM-Py-GC/MS). This minimally destructive technique has been employed previously to characterise early ambers—and help expose forgeries²—but is far less familiar to gemmologists. Perhaps with this in mind, the authors of this chapter include nine tables of their THM-Py-GC/MS results, including marker compounds.

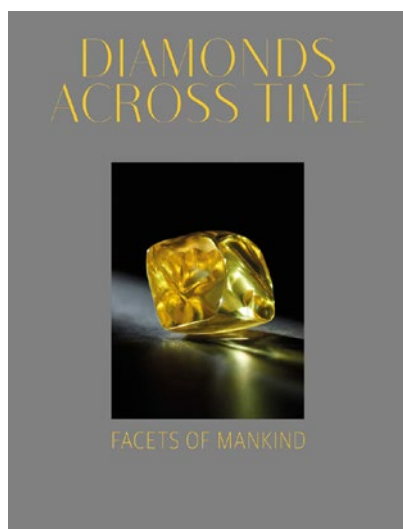
As anticipated, all the ancient objects proved to consist of Baltic amber. A comparative analysis of surface and core samples showed that the surfaces of the ancient objects become slightly depleted in succinate but extensively reduced in sesquiterpenes and diterpenes due to leaching in burial. As the authors conclude, their study has demonstrated that the analytical techniques they used can provide information about the sources, burial conditions and past treatment history of early amber.

In summary, this book is a welcome addition to the study of early gem materials. Both the archaeological and scientific aspects are dealt with in a masterly manner, with the latter in particular a useful addition to a gem lab's library. That it is freely accessible online for download makes it irresistible, but many, I imagine, will also want the 'real book' on their library shelves.

Dr Jack M. Ogden FGA

London

² Shedrinsky, A.M., Grimaldi, D.A., Boon, J.J. & Baer, N.S. 1993. Application of pyrolysis-gas chromatography and pyrolysis-gas chromatography/mass spectrometry to the unmasking of amber forgeries. *Journal of Analytical and Applied Pyrolysis*, **25**, 77–95, [https://doi.org/10.1016/0165-2370\(93\)80034-W](https://doi.org/10.1016/0165-2370(93)80034-W).



Diamonds Across Time

Ed. by Usha R. Balakrishnan, 2020.

World Diamond Museum, London,

[https://facetsofmankind.org/product/](https://facetsofmankind.org/product/diamonds-across-time)

[diamonds-across-time](https://facetsofmankind.org/product/diamonds-across-time), 432 pages, illus.,

ISBN 978-18380485402. GBP95.00 hardcover.

In the introduction to *Diamonds Across Time*, editor and co-author Usha R. Balakrishnan (chief curator of the World Diamond Museum) defines the book's scope. On the one hand, there is diamond itself: a stone with extraordinary characteristics that has fascinated women and men alike. On the other hand, diamonds are linked to so many fields—history, social life, trade, art, individual fate—all of which are intertwined. In an ever-changing world, diamonds are eternal. This volume features diamonds in the context of the times in which they were discovered or first noted, and examines the political, social and cultural stages on which their histories are etched. The book contains 10 chapters, each by a different author, covering discoveries, historic jewels, diamond colours and trading. Underpinning them all are the human stories that weave together our fascination with diamonds.

Usha R. Balakrishnan wrote the first chapter, 'The Nizam Diamond: Bala Koh-i-Noor, in the Sacred Trust of the Nizam of Hyderabad'. This large pear-shaped diamond became famous during the 19th century as the most precious jewel in the treasury of the Nizams of

Hyderabad. Since then, virtually no one had seen it for more than a century, and the little information available was dispersed in letters, reports, official correspondence, newspaper articles and travel accounts. The diamond mysteriously disappeared from the treasury of the Nizams sometime around 1900. In 2019, it reappeared during the TEFAF art fair in Maastricht, the Netherlands—a magnificent D-flawless, pear-shaped brilliant of 120.80 ct, which formed the pendant of an Indian-style emerald bead necklace.

Next, François Farges covers ‘Diamonds of the French Crown Jewels: Between East and West’. Diamonds were scarce throughout the Middle Ages, but they have been documented in the royal treasuries of France since around 1300. As early as 1380, diamond mills were established in Paris and diamantaires were registered. Farges describes the chronology of evolving diamond trade relations, especially with India, the role of important personalities such as Tavernier and the development of diamond cutting. He goes on to cover the growth and changes of the French crown jewels—from François I, Mazarin and Louis XIV to the theft of the crown jewels from the Garde-Meubles in 1798 and their sale in 1887. He gives special attention to the important historic diamonds that were or are still part of this treasure, such as the Sancy, the Mazarin diamonds, the Tavernier Blue and the Regent.

Derek J. Content relates ‘A Concise History of Diamonds from Borneo’. While considerable evidence exists that the Romans had trade relations (including gems and diamonds) with Borneo, the first written record in Europe is found in a letter by Jorge de Albuquerque in 1515. Nevertheless, since at least the 15th century, the alluvial deposits of southern Borneo provided most of the diamonds in Southeast Asia. Indian and, later, Chinese influence was followed first by the Portuguese and then by the Dutch, and the diamond trade shifted accordingly. Today, Borneo plays a minor role as a diamond producer. Content closes his chapter with a description of some large and historic diamonds, including the Star of Sarawak, the Banjarmasin and the Matan.

Hugo Miguel Crespo discusses the role of ‘Indian Diamonds and the Portuguese During the Rise of the Mughal Empire’. Not long after Vasco da Gama’s first voyage (1497–1499), the Portuguese invaded Goa (1510) and set up a maritime connection with Lisbon. Quickly, Goa developed into an important centre for the trade and distribution of gemstones during the 16th century, linking Portugal with the Asian gem trade networks. Previously, the Indian rulers strictly controlled the diamond business and kept all important stones for themselves. Only after

the arrival of the Portuguese could larger diamonds reach Europe. Through this trade channel, enormous wealth poured into Portugal, and soon important jewels and diamonds, such as the Florentine, were added to the treasuries of the Portuguese monarchs.

Jack Ogden compares the history of ‘Two Large Diamonds from India’—the Pigot and the Nassak—and compiles what is known of their histories. At the times of their arrival in Britain, they were each represented as the largest diamond in the country. The Pigot, first mentioned in 1764, has an interesting history of failed attempts to sell it; even Napoleon didn’t want the gem. Finally, in 1823, it was acquired by Mohammed Ali, Pasha of Egypt. Its current whereabouts are unknown. The Nassak, which arrived in Britain in 1821, also turned out to be difficult to sell. In 1837, Robert Grosvenor, 1st Marquis of Westminster, finally acquired it for a very low sum. In 1927, the Nassak was sold again and, in 1940, Harry Winston had it recut to a beautiful—but absolutely ordinary—emerald cut.

Stefano Papi summarises ‘The Romanov Diamonds: History of Splendour’. The history of the Russian crown jewels basically started with Catherine the Great, who commissioned her Swiss court jeweller Jérémie Pauzié to create the Russian regalia for her own coronation. Catherine and her successors built an incredible collection of gemstones, pearls and jewels, including the Orlov and the Shah diamonds, as well as a spectacular necklace of 36 large diamonds totalling 475 carats. During the turmoil of the Russian Revolution and the following years, many jewels were stolen, lost or ‘disappeared’. In 1927, a part of the treasury was sold at Christie’s, London. What remains in Russia today is still breathtaking and is exhibited in the Kremlin Armoury in Moscow.

In ‘The Londonderry Jewels, 1819–1959’, Diana Scarisbrick covers the period from the fall of Napoleon to the middle of the 20th century, when the Marquesses of Londonderry were among the most respected, wealthy and influential noblemen in Great Britain. During this era, they built one of the most splendid jewellery collections ever. These jewels were worn during many official events, from coronations to balls, and accentuated the family’s leading role. By the middle of the 20th century, the Londonderry family had lost much of their influence, and the famous jewels ‘are now lent to the Victoria and Albert Museum so that the public may appreciate them and dream of the vanished world they epitomise’ (p. 306).

In ‘Dress to Impress in Southeast Asia’, René Brus describes the adornment of the royals and nobles before

the foundation of modern Indonesia, after which they lost most of their power. Large parts of their regalia and jewels in gold and diamonds were transferred to the National Museum of Indonesia in Jakarta. During the 1980s, Brus had the rare opportunity to be granted a meeting with Prince Surjobrong of the Yogyakarta dynasty, and he was shown many objects of the gold- and diamond-studded Yogyakarta regalia. The objects were considered holy, so he was not allowed to touch them. The story is reminiscent of Tavernier's visit to the court of the Great Moghul, but Brus had one advantage: he could take photos (e.g. those on pp. 328–332).

Ruth Peltason presents portraits of 'Powerful Women, Important Diamonds' and their leading role in society since the beginning of the 20th century. The women featured have 'power, prestige, privilege and provenance....These women are spotlighted because they are, above all, an indelible part of our culture' (p. 341). Among them are women of widely varied backgrounds: from Queen Alexandra to Wallis Simpson and Jacqueline Kennedy Onassis; from movie stars such as Marlene Dietrich, Grace Kelly and Elizabeth Taylor to socialites and philanthropists like Marjorie Merriweather Post, Evalyn Walsh McLean, Ganna Walska and Barbara Hutton. All were remarkable not only for their activities, but also for their shared passion for jewellery. Their magnificent collections contained important and historical diamonds, including the Hope, Pasha, Elizabeth Taylor/Krupp and Walska Briolette.

John M. King concludes the chapters with 'One in Ten Thousand: The Unique World of Coloured Diamonds'. He answers numerous questions, such as: Why (with the exception of Tavernier's time) was hardly anyone

interested in coloured diamonds until some 30 years ago? What are the causes of their colours? Which special problems do cutters have to bear in mind? What is the significance of important exhibitions on diamonds and events such as Oscar nights, auctions and media coverage, as well as the use of coloured diamonds in jewellery or as investments?

The volume concludes with endnotes (including references), photo credits and short portraits of the authors.

The chapters in this volume are quite diverse, linked mainly by the book's common topic. 'It took a team of dedicated scholars, researchers, editors, photographers, and designers more than three years to put this project together' (p. 9), and the result is not only informative, but also very entertaining to read.

Even if you happen to be a 'lazy reader', you should find the breathtaking illustrations simply stunning. The volume contains more than 300 photos, some 120 of which occupy a full page, plus a dozen two-page spreads. These include high-resolution images of gems and jewels—some from rarely seen collections—as well as historic documents and drawings, and photos of places and people. Generally, they are of excellent quality, although the colours are sometimes a bit 'too good to be true' (see, e.g., the Oppenheimer Blue on p. 408). Especially fascinating are the realistic computer-generated images of historical diamonds.

All in all, this is a marvellous book, and although it is a weighty tome (3 kg and measuring 32.5 × 24.5 cm), you will love every ounce (or gram) of it.

Dr Rolf Tatje

Duisburg, Germany

Other Book Titles

COLOURED STONES

Emerald Modern Gemmology

By Dietmar Schwarz and Martial Curti, 2020.
Bellerophon Gemlab Ltd, Bangkok, Thailand, 481 pages, no ISBN. USD99.00 hardcover.

Seventeenth Annual Sinkankas Symposium: Agate and Chalcedony

Ed. by Lisbet Thoresen and Stuart Overlin, 2021.
Pala International, Fallbrook, California, USA,

124 pages, ISBN 978-0991532056. USD35.00 softcover or free PDF download from <https://sinkankas.dpidirect.com>.

CULTURAL HERITAGE

Celestial Beings and Bird-Men—Human Flight in Chinese Jade

By Angus Forsyth, 2020. Philip Wilson Publishers, London, 336 pages, ISBN 978-1781300718. GBP40.00 hardcover.

DIAMOND

Argyle: The Impossible Story of Australian Diamonds

Stuart Kells, 2021. Melbourne University Publishing, Carlton, Victoria, Australia, 320 pages, ISBN 978-0522877250 or ASIN B08XZMKN2Z. AUD34.99 softcover or AUD12.01 Kindle edn.

JEWELLERY HISTORY

The Smithsonian National Gem Collection— Unearthed: Surprising Stories Behind the Jewels

By Jeffrey Edward Post, 2021. Abrams, New York, New York, USA, 192 pages, ISBN 978-1419745805 or e-ISBN 978-1683359401. USD29.99 softcover or USD23.32 eBook.

JEWELLERY AND OBJETS D'ART

The Art of Breguet

By George Daniels, 2021. Philip Wilson Publishers, London, 408 pages, ISBN 978-1781301074. GBP95.00 hardcover.

Christie's: The Jewellery Archives Revealed

By Vincent Meylan, 2021. ACC Art Books, New York, New York, USA, 360 pages, ISBN 978-1788841375. USD95.00 hardcover.

Masterpieces in Miniature: Treasures from the Rosalinde and Arthur Gilbert Collection

By Alice Minter, with contributions by Jacques Schuhmacher and Joanna Whalley, 2021. V&A Publishing, London, 112 pages, ISBN 978-9078487197. GBP12.00 softcover.

Munnu: Vision & Passion

By Usha R. Balakrishnan, 2021. The World Diamond Museum, London, 248 pages, ISBN 978-1838048419. GBP80.00 hardcover.

New Bracelets: 400+ Contemporary Jewellery Designs

Ed. by Nicolás Estrada, 2021. Promopress, Barcelona, Spain, 250 pages, ISBN 978-8417412500. EUR29.95 hardcover.

Stones of the Grand Bazaar:

Mevâris Jewellery from Istanbul

By Fatma Altınbas, 2021. Rizzoli, New York,

New York, USA, 224 pages, ISBN 978-8891830135. USD90.00 hardcover.

MISCELLANEOUS

A Cabinet of Curiosities: The Myth, Magic and Measure of Meteorites

By Martin Beech, 2021. World Scientific Publishing Co., Singapore, 572 pages, ISBN 978-9811224911 or e-ISBN 978-9811224935, <https://doi.org/10.1142/11954>. USD128.00 hardcover or USD102.00 eBook.

The Smale Collection II

Ed. by Gloria Staebler, Dave Bunk and Brittany MacRostie, 2021. Lithographie, Arvada, Colorado, USA, 176 pages, ISBN 978-1734131024. USD60.00 hardcover.

ORGANIC/BIOGENIC GEMS

Pearls – A Practical Guide

By Wendy Graham, 2021. The Crowood Press, Marlborough, Wiltshire, 96 pages, ISBN 978-1785008122 or e-ISBN 978-1785008139. GBP12.99 softcover or GBP9.99 eBook.

Tortoiseshell

By Maggie Campbell Pedersen, 2021. The Crowood Press, Marlborough, Wiltshire, 192 pages, ISBN 978-0719831447. GBP25.00 hardcover.

SOCIAL STUDIES

Blood and Diamonds: Germany's Imperial Ambitions in Africa

By Steven Press, 2021. Harvard University Press, Cambridge, Massachusetts, USA, 352 pages, ISBN 978-0674916494. USD35.00 hardcover.

SYNTHETICS AND SIMULANTS

Encyclopedia of Glass Science, Technology, History, and Culture

Ed. by Pascal Richet, 2021. John Wiley & Sons Inc., Hoboken, New Jersey, USA (for the American Ceramic Society), 1,495 pages, ISBN 978-1118799420 or e-ISBN 978-1118799499, <https://doi.org/10.1002/9781118801017>. USD550.00 hardcover or USD440.00 eBook.

Literature of Interest

COLOURED STONES

Application of statistical analyses for lapis lazuli stone provenance determination by XRL and XRF.

M. Saleh, L. Bonizzoni, J. Orsilli, S. Samela, M. Gargano, S. Gallo and A. Galli, *Microchemical Journal*, **154**, 2020, article 104655 (9 pp.), <https://doi.org/10.1016/j.microc.2020.104655>.

Chemometric modeling of trace element data for origin determination of demantoid garnets.

S.G. Bindereif, F. Rüll, S. Schwarzingler and C. Schwarzingler, *Minerals*, **10**(12), 2020, article 1046 (15 pp.), <https://doi.org/10.3390/min10121046>.*

Color origins of two types of natural lavender jadeite jades. W. Han, Y. Liu, J. Zhang and T. Lu, *Acta Mineralogica Sinica*, **40**(5), 2020, 549–555 (in Chinese with English abstract).

Comparative study on characteristics of peridot from three different origins. Q. Li, Q. Xu, J. Wei, Y. Liu and Q. Ruan, *Superhard Material Engineering*, **32**(5), 2020, 54–58 (in Chinese with English abstract).

Determination of spectroscopic features and gemstone potential of garnet crystals from the Çamköy region (Aydın - SW Turkey) using XRPD, XRF, confocal Raman spectroscopy, EPMA and gemological test methods. T. Koralay and U. Ören, *Periodico di Mineralogia*, **89**(2), 2020, 105–123, <https://tinyurl.com/r3ykf27j>.*

Fire agate from Deer Creek deposit (Arizona, USA) – New insights into structure and mineralogy.

L. Natkaniec-Nowak, M. Dumańska-Słowik, A. Gawel, A. Łatkiewicz, J. Kowalczyk-Szpyt, A. Wolska, S. Milovská *et al.*, *Mineralogical Magazine*, **84**(2), 2020, 343–354, <https://doi.org/10.1180/mgm.2020.8>.

Gemmological characteristics of green low type zircon. N. Chen, *Superhard Material Engineering*, **32**(3), 2020, 51–55 (in Chinese with English abstract).

Gemmological identification characteristics of single crystal or aggregate jadeite and feicui. L. Li,

Y. Xiong and N. Liu, *Superhard Material Engineering*, **32**(4), 2020, 52–56 (in Chinese with English abstract).

Gemmological characteristics and origin of the Zhanguohong agate from Beipiao, Liaoning Province, China: A combined microscopic, X-ray diffraction, and Raman spectroscopic study.

X. Zhang, L. Ji and X. He, *Minerals*, **10**(5), 2020, article 401 (20 pp.), <https://doi.org/10.3390/min10050401>.*

Identification characteristic and formation of Libyan desert glass. Y. Fu, M. Sun, X. Li, T. Zheng, L. Chen and H. Wei, *Journal of Gems & Gemmology*, **22**(4), 2020, 34–42 (in Chinese with English abstract).

Identification of opaque sulfide inclusions in rubies from Mogok, Myanmar and Montepuez, Mozambique. W. Vertriest and A. Palke, *Minerals*, **10**(6), 2020, article 492 (17 pp.), <https://doi.org/10.3390/min10060492>.*

Une inclusion qui a du chien dans un quartz à hydrocarbures liquéfiés de Madagascar [An inclusion with some character in a quartz with liquefied hydrocarbons from Madagascar].

I. Lerouyer and E. Fritsch, *Revue de Gemmologie A.F.G.*, No. 211, 2021, 4–5 (in French).

Investigation of turquoise gemstone using micro-PIXE imaging technique. T. Nikbakht, *Nuclear Instruments and Methods in Physics Research Section B: Beam Interactions with Materials and Atoms*, **484**, 2020, 5–11, <https://doi.org/10.1016/j.nimb.2020.10.004>.

Jewellery use of a transparent green orthoclase from Luc Yen in Vietnam. R. Hanus and J. Štubňa, *Gemlogický spravodajca/Gemmological Newsletter*, **2**(10), 2020, 5–11, www.gu.fpv.ukf.sk/images/GS/2020_2_hanus.pdf.*

La luminescence orange des corindons, une origine pas classique pour les gemmologues [The orange luminescence of corundum, an unconventional origin for gemologists]. M. Vigier, E. Fritsch and O. Segura, *Revue de Gemmologie A.F.G.*, No. 211, 2021, 12–19 (in French with English abstract).

Mineralogical comparison between omphacite-bearing jadeite from Guatemala and that from Myanmar. H. Xue, T. Chen and Z. Li, *Acta Petrologica et Mineralogica*, **39**(4), 2020, 481–494 (in Chinese with English abstract).

Multi-element analysis of minerals using laser ablation inductively coupled plasma time of flight mass spectrometry and geochemical data visualization using t-distributed stochastic neighbor embedding: Case study on emeralds. H.A.O. Wang and M.S. Krzemnicki, *Journal of Analytical Atomic Spectrometry*, **36**(3), 2021, 518–527, <https://doi.org/10.1039/d0ja00484g>.*

The nature of the Mn(III) color centers in elbaite tourmalines. D.A. Kurtz, G.R. Rossman and B.M. Hunter, *Inorganic Chemistry*, 2020, article 0c00722 (9 pp.), <https://doi.org/10.1021/acs.inorgchem.0c00722>.

Optical properties of hackmanite and sodalite. S.K. Lee and R. Luo, *Wooshin Gem Lab Magazine*, **7**, 2020, 13–16.

Origin identification of white nephrite based on terahertz time-domain spectroscopy. T. Yang, X. Wang, B. Huang, Z. Zang, J. Wang and S. Yan, *Acta Petrologica et Mineralogica*, **39**(3), 2020, 314–322 (in Chinese with English abstract).

Our friends the inclusions. The detective at the party of inclusions. Ninth episode. L. Costantini and C. Russo, *Rivista Italiana di Gemmologia/Italian Gemological Review*, No. 11, 2020–21, 7–12.

Physico-chemical characterization of Iranian turquoises: A tentative [sic] to trace middle-eastern turquoise-bearing artifacts. N. Mousavipak, PhD thesis, University of Lyon, France, 2020, 128 pp., <https://tel.archives-ouvertes.fr/tel-02487545/document>.*

Raman spectroscopic investigation of zircon in gem-quality sapphire: Application in origin determination. W. Xu and M.S. Krzemnicki, *Journal of Raman Spectroscopy*, **52**(5), 2021, 1011–1021, <https://doi.org/10.1002/jrs.6092>.

Some complementary data about the spectroscopic properties of manganese ions in spodumene crystals. M. Czaja, R. Lisiecki, M. Kądziołka-Gaweł

and A. Winiarski, *Minerals*, **10**(6), 2020, article 554 (17 pp.), <https://doi.org/10.3390/min10060554>.*

Speaking the same language – [grading of] coloured gemstones (Part One). *Gemmology Today*, March 2021, 42–55, <https://tinyurl.com/ytzsrj38>.*

Spectrographic identification of two similar quartz gemstones and its enlightenment. L. Yu and H. Zhang, *Superhard Material Engineering*, **32**(4), 2020, 62–65 (in Chinese with English abstract).

Study on chemical composition and provenience differentiation of turquoises excavated from two sites in Xinjing. Y. Xian, X. Li, X. Zhou, J. Ma, Y. Li and R. Wen, *Spectroscopy and Spectral Analysis*, **40**(3), 2020, 967–970 (in Chinese with English abstract).

Study on gemological characteristics of iridescent feldspars. P. Ning, C. Meng, H. Pan and T. Zhang, *Superhard Material Engineering*, **32**(3), 2020, 41–45 (in Chinese with English abstract).

Sub-microstructures of nephrite from five sources based on multispectral imaging and effect enhancement. C. Wang, W. Luo, M. Yu and D. Chen, *Asian Journal of Advanced Research and Reports*, **12**(3), 2020, 13–24, <https://doi.org/10.9734/ajarr/2020/v12i330288>.*

Theoretical infrared spectra of OH defects in corundum ($\alpha\text{-Al}_2\text{O}_3$). E. Balan, *European Journal of Mineralogy*, **32**(5), 2020, 457–467, <https://doi.org/10.5194/ejm-32-457-2020>.*

An X-ray absorption near-edge structure (XANES) study on the oxidation state of chromophores in natural kunzite samples from Nuristan, Afghanistan. H.U. Rehman, G. Martens, Y.L. Tsai, C. Chankhantha, P. Kidkhunthod and A.H. Shen, *Minerals*, **10**(5), 2020, article 463 (11 pp.), <https://doi.org/10.3390/min10050463>.*

X-ray induced luminescence, optical, compositional and structural investigations of natural and imitation rubies: Identification technique. Y. Tariwong, N. Chanthima, R. Rajaramakrishna, H.J. Kim and J. Kaewkhao, *Radiation Physics and Chemistry*, **177**, 2020, article 109089 (7 pp.), <https://doi.org/10.1016/j.radphyschem.2020.109089>.

CULTURAL HERITAGE

The ancient jade mine discovered in Dunhuang Hanxia of northern Gansu Province: A potential important source of jade material in early stage of China. Z. Qiu, Y. Zhang, J. Yang, H. Wang, G. Chen and Y. Li, *Journal of Gems & Gemmology*, **22**(5), 2020, 1–12 (in Chinese with English abstract).

Complex raw materials and supply system: Mineralogical and geochemical study for the jade artefacts of Longshan culture (2400~2000BC) from Sujiacun site in coastal Shandong, China. B. Zhang, X. Wu, Y. Sun, M. Ritchey, A. Fan, Y. Zhang, G. Yu and Y. Song, *Archaeometry*, 2020, article 12634 (18 pp.), <https://doi.org/10.1111/arcm.12634>.

Raman microspectroscopy of garnets from S-fibulae from the archaeological site Lajh (Slovenia). S. Kos, M. Dolenc, J. Lux and S. Dolenc, *Minerals*, **10**(4), 2020, article 325 (21 pp.), <https://doi.org/10.3390/min10040325>.*

Trace elements content and cause of color in ancient treated carnelian and its natural counterpart from SE Asia. S. Saminpanya, C. Saiyasombat, N. Chanlek, N. Thammajak, E. Sirisurawong, R. Viriyasunsakun, P. Kingkanlaya and P. Rakponramuang, *Archaeological and Anthropological Sciences*, **12**, 2020, article 3 (11 pp.), <https://doi.org/10.1007/s12520-019-00953-x>.*

DIAMONDS

Analysis of formation reason of arrows and hearts effect of diamond by using simulation software. X. Wan, X. Yuan, S. Zhai, Q. Wu and Z. Xu, *Journal of Gems & Gemmology*, **22**(5), 2020, 57–64 (in Chinese with English abstract).

Application of photoluminescence spectroscopy in identifying small diamonds. Y. Wang, N. Chen, J. Guo and Z. Xu, *Superhard Material Engineering*, **32**(6), 2020, 57–63 (in Chinese with English abstract).

Diamonds from the Deep: What have diamond ages taught us? K.V. Smit and S.B. Shirey, *Gems & Gemology*, **56**(4), 2020, 534–541, www.gia.edu/gg-issue-search?ggissueid=1495323758428&articlesubtype=diamondsfromthedeep.*

Enduring legacy of the Argyle pinks. B. Sto. Domingo, *JNA*, No. 423, 2020, 14–21, https://jewellerynet.com/uploads/ebook//jna/2020/Issue423_Sep2020/v4/14.*

Flawless precision [Opsidia subsurface marking technology]. A. Rimmer, *Gems&Jewellery*, **30**(1), 2021, 28–30.

From boom to bust, and back again: The Tortiya diamond fields of Côte d'Ivoire, 1947–2018. S. Van Bockstael, *Canadian Journal of Development Studies*, **41**(3), 2020, 450–466, <https://doi.org/10.1080/02255189.2020.1799339>.*

The future of pink diamonds. J. Cherry, *Gems&Jewellery*, **30**(1), 2021, 32–35.

Gemmological characteristic of yellow diamond with 480 nm absorption peak of UV-visible spectrum. Y. Luo and J. Chen, *Journal of Gems & Gemmology*, **22**(5), 2020, 39–43 (in Chinese with English abstract).

Gemmological characteristics and identification of blue diamonds. Y. Wang, *Superhard Material Engineering*, **32**(4), 2020, 47–51 (in Chinese with English abstract).

Identification of natural type IIa colourless diamond with 270 nm absorption peak of UV-visible spectrum. J. Chen and Y. Luo, *Journal of Gems & Gemmology*, **22**(5), 2020, 44–48 (in Chinese with English abstract).

Infrared spectral characterization of diamonds and its significance on identification. H. Zhou, X. Jin, W. Huang and L. Wand, *Superhard Material Engineering*, **32**(5), 2020, 18–25 (in Chinese with English abstract).

Morphology and genesis of ballas and ballas-like diamonds. A. Pavlushin, D. Zedgenizov, E. Vasil'ev and K. Kuper, *Crystals*, **11**(1), 2020, article 17 (23 pp.), <https://doi.org/10.3390/cryst11010017>.*

The mysterious chameleon diamond. L. Langeslag, *Gemmology Today*, March 2021, 88–90, <https://tinyurl.com/zt4weyvjv>.*

Preservation conditions of CLIPPIR diamonds in the earth's mantle in a heterogeneous metal-sulphide-silicate medium (experimental modeling). A.I. Chepurov, V.M. Sonin, E.I. Zhimulev and A.A.

Chepurov, *Journal of Mineralogical and Petrological Sciences*, **115**(3), 2020, 236–246, <https://doi.org/10.2465/jmps.190818>.*

Quantification of hydrogen in natural diamond by secondary ion mass spectrometry (SIMS).

F.V. Kaminsky, S.N. Shilobreeva, B.Y. Ber and D.Y. Kazantsev, *Doklady Earth Sciences*, **494**(1), 2020, 699–703, <https://doi.org/10.1134/s1028334x20090093>.

Spectroscopic evidence of the origin of brown and pink diamonds family from Internatsionalnaya kimberlite pipe (Siberian craton).

O.P. Yuryeva, M.I. Rakhmanova, D.A. Zedgenizov and V.V. Kalinina, *Physics and Chemistry of Minerals*, **47**, 2020, article 20 (19 pp.), <https://doi.org/10.1007/s00269-020-01088-5>.

Will Angola became [sic] no. 1 diamond producer in the world?

P. Minieri, *Rivista Italiana di Gemmologia/Italian Gemological Review*, No. 11, 2020–21, 26–31.

FAIR TRADE

Jewellery sector: A rising sustainability leader.

B. Sto. Domingo, *JNA*, No. 426, 2021, 20–27, https://jewellerynet.com/uploads/ebook//jna/2021/issue426_Mar2021/v3/20.*

GEM LOCALITIES

Demantoid from the Telyansky Klyuch deposit

(Middle Urals) – Is the place of the first discovery in the Urals. S.Y. Kropantsev, *News of the Ural State Mining University*, **1**(57), 2020, 37–46, <https://doi.org/10.21440/2307-2091-2020-1-37-46>.*

The diaspore mines near Pinarcik in the Ilbir Mountains, Mğla [sic] Province, Turkey.

W.E. Wilson and T.P. Moore, *Mineralogical Record*, **51**(4), 2020, 541–554.

Emerald from the Habachtal: New observations.

R. Thomas, P. Davidson and A. Rericha, *Mineralogy and Petrology*, **114**(3), 2020, 161–173, <https://doi.org/10.1007/s00710-020-00700-4>.

Formation, origin and geographic typing of corundum (ruby and pink sapphire) from the Fiskeneset

complex, Greenland. N. Keulen, T.B. Thomsen, J.C. Schumacher, M.D. Poulsen, P. Kalvig, T. Vennemann and R. Salimi, *Lithos*, **366–367**, 2020, article 105536 (24 pp.), <https://doi.org/10.1016/j.lithos.2020.105536>.

Gemstones-bearing sediments in the Mbiame floodplain, northwestern Cameroon.

M.E.M.M. Etutu, C.E. Suh, A. Vishiti, E.M. Shemang, C.M. Agyingi and J.C. Mendes, *Journal of Sedimentary Environments*, **5**(4), 2020, 537–557, <https://doi.org/10.1007/s43217-020-00033-4>.*

The genesis of color zonation of emerald from Dayakou, Yunnan Province: Implication for multi-stage mineralization.

X. Yu, Y. Zheng, T. Zhang, H. Guo, Z. Long, J. Wan and C. Zhang, *Earth Science Frontiers*, **27**(5), 2020, 116–125 (in Chinese with English abstract).

Mapping the extent and methods of small-scale emerald mining in the Panjshir Valley,

Afghanistan. J.D. DeWitt, P.G. Chirico, K.E. O’Pry and S.E. Bergstresser, *Geocarto International*, 2020, article 1716394 (22 pp.), <https://doi.org/10.1080/10106049.2020.1716394>.*

Metamorphosed carbonate platforms and controls on the genesis of sapphire, gem spinel, and lapis lazuli: Insight from the Lake Harbour Group,

Nunavut, Canada and implications for gem exploration. P.M. Belley and L.A. Groat, *Ore Geology Reviews*, **116**, 2020, article 103259 (10 pp.), <https://doi.org/10.1016/j.oregeorev.2019.103259>.

Mineral chemistry and geochronology of the

Rajasthan emerald deposits, NW India. P. Alexandre, *Canadian Mineralogist*, **58**(3), 2020, 335–346, <https://doi.org/10.3749/canmin.1900055>.

Mineral inclusions in sapphire from basaltic terranes in southern Vietnam: Indicator of

formation model. D.T.A. Vu, A. Salam, A. Fanka, E. Belousova and C. Sutthirat, *Gems & Gemology*, **56**(4), 2020, 498–515, <https://doi.org/10.5741/gems.56.4.498>.*

Mineralogy, geochemistry, and petrogenesis of green nephrite from Dahua, Guangxi, southern

China. F. Bai, J. Du, J. Li and B. Jiang, *Ore Geology Reviews*, **118**, 2020, article 103362 (13 pp.), <https://doi.org/10.1016/j.oregeorev.2020.103362>.

Multistages of original sapphire formation related to basaltic magmatism in the Bo Phloi basaltic gem field, Kanchanaburi, western Thailand: Evidence from trace elements and ages of zircons.

C. Sutthirat, V. Pisutha-Arnond, P. Khamloet and T. Assawincharoenkij, *Journal of Asian Earth Sciences*, **187**, 2020, article 104068 (13 pp.), <https://doi.org/10.1016/j.jseas.2019.104068>.

A new emerald occurrence from Kruta Balka, western Peri-Azovian region, Ukraine: Implications for understanding the crystal chemistry of emerald.

G. Franz, O. Vyshnevskiy, M. Taran, V. Khomenko, M. Wiedenbeck, F. Schiperski and J. Nissen, *American Mineralogist*, **105**(2), 2020, 162–181, <https://doi.org/10.2138/am-2020-7010>.

Petrogenesis of the Snezhnoe ruby deposit, central Pamir.

A.K. Litvinenko, E.S. Sorokina, T. Häger, Y.A. Kostitsyn, R.E. Botcharnikov, A.V. Somsikova, T. Ludwig *et al.*, *Minerals*, **10**(5), 2020, article 478 (22 pp.), <https://doi.org/10.3390/min10050478>.*

Ruby mineralization in Murzinka–Adui metamorphic complex, Central Urals. A.Y. Kisin, V.V. Murzin, A.V. Tomilina, V.N. Smirnov and M.E. Pritchkin, *Geology of Ore Deposits*, **62**(4), 2020, 332–350, <https://doi.org/10.1134/s1075701520040042>.

Timing of syenite-charnockite magmatism and ruby and sapphire metamorphism in the Mogok Valley region, Myanmar. M.P. Searle, J.M. Garber, B.R. Hacker, K. Htun, N.J. Gardiner, D.J. Waters and L.J. Robb, *Tectonics*, **39**(3), 2020, article e2019TC005998 (21 pp.), <https://doi.org/10.1029/2019tc005998>.

INSTRUMENTATION AND TECHNOLOGY

Accurate trace element reporting in corundum: Development of secondary ion mass spectrometry relative sensitivity factors. J.L. Stone-Sundberg, Y. Guan, Z. Sun and T. Ardon, *Geostandards and Geoanalytical Research*, **45**(1), 2020, article 12360 (15 pp.), <https://doi.org/10.1111/ggr.12360>.

Application of synchrotron radiation X-ray fluorescence spectroscopy in gem test: Take agate from Alashan as example. L. Zhang, B. Lin and Z. Qian, *Journal of Gems & Gemmology*, **22**(5), 2020, 23–30 (in Chinese with English abstract).

Combining Fourier transform infrared and Raman spectroscopies with Gaussian deconvolution: An improved approach for the characterization of emeralds.

C. Branca, A. Arcovito, E. Cosio, M. Interdonato, G. Sabatino, U. Wanderlingh and G. D'Angelo, *Journal of Raman Spectroscopy*, **51**(4), 2020, 693–701, <https://doi.org/10.1002/jrs.5810>.

Effects of repetition rate on the identification of elements in gemstone using the LIBS method.

A. Bagaskara, Q.M.B. Soesanto, H. Sugito and A. Khumaeni, *Journal of Physics: Conference Series*, **1524**, 2020, article 012025 (7 pp.), <https://doi.org/10.1088/1742-6596/1524/1/012025>.*

External reflectance FTIR dataset (4000–400 cm⁻¹) for the identification of relevant mineralogical phases forming cultural heritage materials.

F. Izzo, C. Germinario, C. Grifa, A. Langella and M. Mercurio, *Infrared Physics & Technology*, **106**, 2020, article 103266 (9 pp.), <https://doi.org/10.1016/j.infrared.2020.103266>.

Technological game changers for the jewellery trade. O. Quinquini, *JNA*, No. 422, 2020, 48–53, www.jewellerynet.com/en/jnanews/features/23915.*

JEWELLERY HISTORY

An archaeometric investigation of glass beads decorating the reliquary of Saint Simètre from Lierneux, Belgium. Y. Bruni, F. Hatert, P. George and D. Strivay, *Journal of Archaeological Science: Reports*, **32**, 2020, article 102451 (6 pp.), <https://doi.org/10.1016/j.jasrep.2020.102451>.*

The power of marvellous objects: Charles IV of Luxembourg, Charles V of Valois and their gemstones. I. Ciulisová, *Journal of the History of Collections*, publ. online 27 August 2020, article fhaa023 (13 pp.), <https://doi.org/10.1093/jhc/fhaa023>.*

LAPIDARY TECHNIQUES

Baroque-era rose cuts of colored stones: Highlights from the second half of the seventeenth century. K. Schmetzer, *Gems & Gemmology*, **56**(4), 2020, 458–482, <https://doi.org/10.5741/gems.56.4.458>.*

Improving the design of artwork and jewelry made of chalcedony. A. Zheltenkov, V. Zhukov,

L. Zhukova, K. Ponomareva and A. Mottaeva, *E3S Web of Conferences*, **164**, 2020, article 14006 (10 pp.), <https://doi.org/10.1051/e3sconf/202016414006>.*

MISCELLANEOUS

The American Museum of Natural History.

G. Harlow, *Gems&Jewellery*, **30**(1), 2021, 18–20.

Episodes of fast crystal growth in pegmatites.

P.R. Phelps, C.-T.A. Lee and D.M. Morton, *Nature Communications*, **11**(1), 2020, article 4986 (10 pp.), <https://doi.org/10.1038/s41467-020-18806-w>.*

Fluorescence in gems. M. Mauthner, *Rocks & Minerals*, **96**(1), 2021, 38–43, <https://doi.org/10.1080/00357529.2021.1827909>.

Machine learning algorithms for diamond price prediction. W. Alsuraihi, E. Al-hazmi, K. Bawazeer and H. Alghamdi, *Proceedings of the 2020 2nd International Conference on Image, Video and Signal Processing*, 2020, 150–154, <https://doi.org/10.1145/3388818.3393715>.

Temperatures and duration of crystallization within gem-bearing cavities of granitic pegmatites.

D. London, L.E. Hunt and C.L. Duval, *Lithos*, **360–361**, 2020, article 105417 (15 pp.), <https://doi.org/10.1016/j.lithos.2020.105417>.

Tout ce que vous avez toujours voulu savoir sur les Juifs et les diamants (sans jamais oser le demander...). Fantasmes et réalités sur les Juifs et le monde du diamant [Everything you always wanted to know about Jews and diamonds (without ever daring to ask...)]. *Fantasies and realities about the Jews and the diamond world*. G. Panczer and S. Cohen-Scali, *Revue de Gemmologie A.F.G.*, No. 211, 2021, 6–11 (in French).

Weight watchers [price points for gemstones and other valuable substances]. G. Dominy, *Gemmology Today*, March 2021, 22–31, <https://tinyurl.com/3x8v95>.*

NEWS PRESS

All that glitters: Flood of fake ancient jewellery dupes buyers. D. Alberge, *The Guardian*, 16 May 2021, www.theguardian.com/lifeandstyle/2021/

www.theguardian.com/lifeandstyle/2021/may/16/all-that-glitters-flood-of-fake-ancient-jewellery-dupes-buyers.*

The hoard of centuries old jewels found buried under one of London's busiest streets

[Cheapside Hoard]. D. Wiggins, MyLondon, 16 May 2021, www.mylondon.news/news/nostalgia/hoard-centuries-old-jewels-found-20570671.*

Jewellery industry makes slow progress on responsible supply chains.

C. Palmer, *Financial Times*, 9 April 2021, www.ft.com/content/7983b80f-f430-40eb-b6b1-8ece720aaab4.*

Myanmar sanctions take the shine off Burmese rubies.

R. Taylor, *Financial Times*, 9 April 2021, www.ft.com/content/05ce073b-9fb6-4804-a7df-72d2f31826dd.*

Playing the 'green lottery': Life inside Colombia's emerald mines.

J.P. Ramirez, *New York Times*, 4 January 2021, www.nytimes.com/2021/01/04/travel/colombia-emerald-mines.html.*

Rediscovering Saudi heritage: Pearl kings of Farasan Islands.

T. Al-Thaqafi, *Arab News*, 2 January 2021, www.arabnews.com/node/1786421/saudi-arabia.*

In Zimbabwe, women dig for aquamarine.

G. Brownell, *New York Times*, 23 May 2021, www.nytimes.com/2021/05/23/fashion/jewelry-women-aquamarine-miners-zimbabwe.html.*

ORGANIC/BIOGENIC GEMS

The amber collection in Grünes Gewölbe

Dresden. J. Kappel, *Bursztynisko (The Amber Magazine)*, No. 44, 2020, 46–53, https://issuu.com/internationalamberassociation/docs/b44_issuu_teaser (in English and Polish).*

Behind the ivory trade shutdown in China.

I.M. Permata and E. Wahyuni, *Journal of International Wildlife Law & Policy*, **23**(3), 2020, 151–165, <https://doi.org/10.1080/13880292.2020.1825055>.

Characterization of Burmese amber with three-dimensional fluorescence. Y. Bai, X. Zheng and Z. Yin, *Spectroscopy and Spectral Analysis*, **40**(5), 2020, 1473–1477 (in Chinese with English abstract).

Disguising elephant ivory as other materials in the online trade. S. Venturini and D.L. Roberts, *Tropical Conservation Science*, **13**(1–8), 2020, <https://doi.org/10.1177/1940082920974604>.

Fluorescence characteristics of blue amber from the Dominican Republic. Z. Zhang, X. Jiang, Y. Wang, F. Kong and A.H. Shen, *Gems & Gemology*, **56**(4), 2020, 484–496, <https://doi.org/10.5741/gems.56.4.484>.*

Fossil resins – Constraints from portable and laboratory near-infrared Raman spectrometers. B. Naglik, M. Mroczkowska-Szerszeń, M. Dumańska-Słowik, L. Natkaniec-Nowak, P. Drzewicz, P. Stach and G. Żukowska, *Minerals*, **10**(2), 2020, article 104 (17 pp.), <https://doi.org/10.3390/min10020104>.*

A glimpse into the past – Valviloculus pleristaminis [flower inclusion in Burmese amber]. G. Poinar Jr., *Gemmology Today*, March 2021, 80–82, <https://tinyurl.com/2ew779mx>.*

Nondestructive identification of a jet bead from the Changle cemetery in Ningxia, China. N. Sun, R. Wang, B. Han, H. Rao, M. Yang and Y. Yang, *Microchemical Journal*, **157**, 2020, article 104907 (7 pp.), <https://doi.org/10.1016/j.microc.2020.104907>.

The spectrum characteristic research of color change effect and “light tarry effect” amber from Burma. C. Shuai, Z. Yin, Q. Xue, S. Wan and X. Wu, *Spectroscopy and Spectral Analysis*, **40**(4), 2020, 1174–1178 (in Chinese with English abstract).

Unravelling the mystery of “Madagascar copal”: Age, origin and preservation of a recent resin. X. Delclòs, E. Peñalver, V. Ranaivosoa and M.M. Solórzano-Kraemer, *PLoS ONE*, **15**(5), 2020, article e0232623 (32 pp.), <https://doi.org/10.1371/journal.pone.0232623>.*

PEARLS

Bead nucleated freshwater pearls from China. E. Jeong, *Wooshin Gem Lab Magazine*, **7**, 2020, 8–12.

Comparative study on gemmological characteristic of ordinary *Tridacna* and petrified *Tridacna*. Y. Chen, J. Li and L. Wang, *Journal of Gems & Gemmology*, **22**(4), 2020, 23–33 (in Chinese with English abstract).

Inside black pearls. Y. Dauphin, O. Belhadj, L. Bellot-Gurlet, M. Cotte, C. Lo, K. Medjoubi, A. Somogyi *et al.*, *Materials Characterization*, **163**, 2020, article 110276 (13 pp.), <https://doi.org/10.1016/j.matchar.2020.110276>.

New pearl tech. B. Sto. Domingo, *JNA*, No. 424, 2020, 36–41, https://jewellerynet.com/uploads/ebook//jna/2020/Issue424_Nov2020/v1/36.*

Pearl oyster farming and pearl production. S. Athithan, *Coastal Aquacultures and Mariculture*. CRC Press, London, 2020, 156–162, <https://doi.org/10.1201/9781003142416-28>.

Raman scattering: Fingerprint for identification of nature and color origin of pearls. S.A. Athavale and M.S. Hambarde, *International Research Journal of Engineering and Technology*, **7**(4), 2020, 2065–2078, <https://irjet.net/archives/V7/i4/IRJET-V7I4395.pdf>.*

SIMULANTS

Elemental tracing of original with plastic pearl by atomic emission spectra. M.S. Roslan, M.M.A. Rahman, R. Rosley, A.H. Ali and S.Z. Haider, *Multidisciplinary Applied Research and Innovation*, **2**(1), 2021, 396–400, <https://doi.org/10.30880/mari.2021.02.01.041>.*

Gemmological characteristic of a malachite imitation. H. Zhu, X. Ma, T. Li, R. Du, X. Ding and S. Chen, *Superhard Material Engineering*, **32**(4), 2020, 57–61 (in Chinese with English abstract).

Gemmological characteristics and identification of a luminous pearl imitation. Z. Zhao and L. Yu, *Superhard Material Engineering*, **32**(3), 2020, 56–59 (in Chinese with English abstract).

SYNTHETICS

Defect and stress reduction in high-pressure and high-temperature synthetic diamonds using gradient cooling technology. N. Chen, G. Zhang, R. Li, G. Xu, F. Wang, H. Ma and X. Jia, *Crystal Growth & Design*, **20**(5), 2020, 3358–3364, <https://doi.org/10.1021/acs.cgd.0c00148>.

Effect of cooling circulating water on gem grade diamond synthesized by hexahedral press. N. Wu, K. Liu, K. Zhang, Y. Tian, J. Zhang and T. Wang,

Superhard Material Engineering, **32**(4), 2020, 14–17 (in Chinese with English abstract).

From the analyst's notebook. Biron synthetic emerald and its identification. C. Cumo, *Rivista Italiana di Gemmologia/Italian Gemological Review*, No. 11, 2020–21, 55–63.

Gemmological characteristic of “recrystallized” (synthetic) corundum in market. J. Fu, F. Lyu, T. Shao, S. Li and A.H. Shen, *Journal of Gems & Gemmology*, **22**(6), 2020, 9–19 (in Chinese with English abstract).

An innovation in obtaining the aggregation N of the synthesized diamond under HPHT conditions. Y. Li, J. Liao, Y. Wang, Y. She, Z. Xiao and J. An, *Optical Materials*, **101**, 2020, article 109735 (5 pp.), <https://doi.org/10.1016/j.optmat.2020.109735>.

Morphology of quartz crystals: Natural and synthetic. M. Kawasaki, *Journal of the Gemmological Society of Japan*, **34**(1–4), 2020, 3–12, https://doi.org/10.14915/gsjapan.34.1-4_3 (in Japanese with English abstract).

Nitrogen-doped CVD diamond: Nitrogen concentration, color and internal stress. A.M. Zaitsev, N.M. Kazuchits, V.N. Kazuchits, K.S. Moe, M.S. Rusetsky, O.V. Korolik, K. Kitajima *et al.*, *Diamond and Related Materials*, **105**, 2020, article 107794 (13 pp.), <https://doi.org/10.1016/j.diamond.2020.107794>.

Photoluminescence studies of the 640nm center in electron irradiated Ila [CVD synthetic] diamond. Y. Zhang, K. Wang, S. Chang, Y. Tian and J. Li, *Spectroscopy Letters*, 2020, article 1796713 (7 pp.), <https://doi.org/10.1080/00387010.2020.1796713>.

Quand tout s'oppose à la croissance de la « moissanite » cubique (β -SiC) [When everything is against the growth of cubic “moissanite” (β -SiC)]. D. Chaussende, *Revue de Gemmologie A.F.G.*, No. 211, 2021, 20–24 (in French).

The role of isolated nitrogen in phosphorescence of high-temperature-high-pressure synthetic type IIb diamonds. T. Shao, F. Lyu, X. Guo, J. Zhang, H. Zhang, X. Hu and A.H. Shen, *Carbon*, **167**, 2020, 888–895, <https://doi.org/10.1016/j.carbon.2020.05.061>.

Single crystal diamond growth by MPCVD at subatmospheric pressures. A.P. Bolshakov, V.G. Ralchenko, G. Shu, B. Dai, V.Y. Yurov, E.V. Bushuev, A.A. Khomich, A.S. Altakhov *et al.*, *Materials Today Communications*, **25**, 2020, article 101635 (10 pp.), <https://doi.org/10.1016/j.mtcomm.2020.101635>.

Spectroscopic feature and identification application of the impurity and inclusion in type Ila HPHT synthetic diamond. Y. Ma, Z. Qiu, Y. Zhuang, S. Lai, T. Lu and X. Deng, *Journal of Gems & Gemmology*, **22**(6), 2020, 1–8 (in Chinese with English abstract).

Study on crystal morphology of large single crystal diamond synthesized at high temperature and high pressure. X. Wan, X. Liu, S. Zhai and L. Zheng, *Superhard Material Engineering*, **32**(4), 2020, 8–13 (in Chinese with English abstract).

TREATMENTS

Application of coating technology on gemstone optimization. H. Mu, J. Lin, T. Zhang, C. Xin and Y. Li, *Superhard Material Engineering*, **32**(5), 2020, 59–65 (in Chinese with English abstract).

Behandelte Edelsteine – Nomenklatur und Handel [Treated gemstones – Nomenclature and trade]. U. Henn, T. Lind, T. Stephan, C.C. Milisenda and S. Müller, *Gemmologie: Zeitschrift der Deutsche Gemmologischen*, **69**(3/4), 2020, 3–6 (in German).

Cause of color modification in tanzanite after heat treatment. T. Pluthametwisute, B. Wanthanachaisaeng, C. Saiyasombat and C. Sutthirat, *Molecules*, **25**(16), 2020, article 3743 (15 pp.), <https://doi.org/10.3390/molecules25163743>.*

The color center of beryllium-treated yellow sapphires. N. Monarumit, T. Lhuaamporn, S. Sakkaravej, P. Wathanakul and W. Wongkokua, *Journal of Physics Communications*, **4**(10), 2020, article 105018 (8 pp.), <https://doi.org/10.1088/2399-6528/abc7ea>.*

The coloration mechanism of Be, Fe ion-implanted natural sapphire. W. Lu, S. He, J. Cao, Q. Zhang and P. Ma, *Journal of Kunming University of Science and Technology (Natural Science)*, **45**(5), 2020, 21–25 (in Chinese with English abstract).

Diamond treatments and pricing. R.B. Drucker, *GemGuide*, **40**(2), 2021, 4–10.

**Edelsteine und ihre künstlichen Eigenschafts-
veränderungen [Gemstones and their artificial
changes in properties].** U. Henn, T. Lind, T. Stephan,
C.C. Milisenda and S. Müller, *Gemmologie: Zeitschrift
der Deutsche Gemmologischen*, **69**(3/4), 2020, 17–81
(in German).

**Effect of HPHT treatment on spectroscopic features
of natural type Ib-IaA diamonds containing Y
centers.** I.N. Kupriyanov, Y.N. Palyanov, A.A. Kalinin
and V.S. Shatsky, *Crystals*, **10**(5), 2020, article 378
(12 pp.), <https://doi.org/10.3390/cryst10050378>.*

**Gemological identification characteristics of natural
and dyed red chalcedony and its rapid testing process
in laboratory.** Q. Luo, S. Dai, D. Chen, Y. Hu, W. Qu,
S. Xu and J. Liao, *Journal of Mineralogy and Petrology*,
40(3), 2020, 6–19 (in Chinese with English abstract).

**High pressure and high temperature annealing of
Ni-containing, nitrogen-rich synthetic diamonds
and the formation of NE8 centers.** L. Chen, W. Shen,
C. Fang, Y. Zhang, P. Mu, G. Zhou, Q. Wang *et al.*,
Crystal Growth & Design, **20**(5), 2020, 3257–3263,
<https://doi.org/10.1021/acs.cgd.0c00080>.

**Low-temperature heat treatment of pink sapphires
from Ilakaka, Madagascar.** S. Saeseaw, C. Khowpong
and W. Vertriest, *Gems & Gemology*, **56**(4), 2020,
448–457, <https://doi.org/10.5741/gems.56.4.448>.*

**Methoden der künstlichen Eigenschaftsverände-
rungen bei Edelsteinen [Methods of artificial
property changes in gemstones].** U. Henn, T. Lind,
T. Stephan, C.C. Milisenda and S. Müller, *Gemmologie:
Zeitschrift der Deutsche Gemmologischen*, **69**(3/4),
2020, 7–12 (in German).

**Methodik – Grundlegende und weiterführende
Methoden zum Nachweis künstlicher Eigenschafts-
veränderungen bei Edelsteinen [Methodology –
Basic and advanced methods for the detection
of artificial property changes in gemstones].**
U. Henn, T. Lind, T. Stephan, C.C. Milisenda and
S. Müller, *Gemmologie: Zeitschrift der Deutsche
Gemmologischen*, **69**(3/4), 2020, 13–16 (in German).

**Modeling of color improvement of ruby corundum
gemstone via oxygen ion implantation treatment.**

W. Buaprasert, B. Kaewkham-ai and K. Uthaichana,
*17th International Conference on Electrical Engineering/
Electronics, Computer, Telecommunications and
Information Technology (ECTI-CON)*, 2020, 447–451,
<https://doi.org/10.1109/ecti-con49241.2020.9158295>.

**Rapid detection of color-treated pearls and
separation of pearl types using fluorescence
analysis.** T.H. Tsai, C. Zhou, C.F. Hahlweg and
J.R. Mulley, *Novel Optical Systems, Methods, and
Applications XXIII*, 2020, article 1148307 (11 pp.),
<https://doi.org/10.1117/12.2566590>.

COMPILATIONS

G&G Micro-World. Blue apatite in pyrope-spessartine
• CVD synthetic diamond ‘landscape’ • UV fluorescence
of emerald filler • Inclusions in rubies from the John
Saul mine, Kenya • Lazurite in ruby from Mogok,
Myanmar • ‘Snowflakes’ in ruby from Mong Hsu,
Myanmar • Metal sulphide crystal in sapphire
• Elongated rutile in blue sapphire • Zircon in jadeite
• Garnets in aquamarine from Pakistan. *Gems &
Gemology*, **56**(4), 2020, 526–533, [www.gia.edu/
gg-issue-search?ggissueid=1495323758428&
articlesubtype=microworld](http://www.gia.edu/gg-issue-search?ggissueid=1495323758428&articlesubtype=microworld).*

Gem News International. Emerald from southern
California, USA • Inclusions in emerald from Davdar,
China • Dendritic inclusions in nephrite from
Dahua, China • Resin imitation of ivory • Laser-
engraved imitation of phantom quartz • Rh-plated
iron meteorites • Oiled tanzanite • Report on the
World Pearl Congress. *Gems & Gemology*, **56**(4), 2020,
542–554, [www.gia.edu/gg-issue-search?ggissueid=
1495323758428&articlesubtype=gni](http://www.gia.edu/gg-issue-search?ggissueid=1495323758428&articlesubtype=gni).*

Lab Notes. Blue ‘graining’ in green-yellow diamond
• Irradiated blue diamond • 1.16 ct type IIa diamond
from Arkansas, USA • Artificial glass imitating Paraíba
tourmaline • Chromite inclusions in green common
opal • Intense purplish pink sapphire from Montana,
USA • 7.07 ct CVD synthetic diamond • Unusual
absorption in blue flux-grown synthetic sapphire.
Gems & Gemology, **56**(4), 2020, 516–525, [www.gia.
edu/gg-issue-search?ggissueid=1495323758428&
articlesubtype=labnotes](http://www.gia.edu/gg-issue-search?ggissueid=1495323758428&articlesubtype=labnotes).*

*Article freely available for downloading or reading online, as of press time

Over 110 years of experience in gemmology education

**Our FGA and DGA Members are located around the world
– join them by studying with Gem-A in one of three ways**

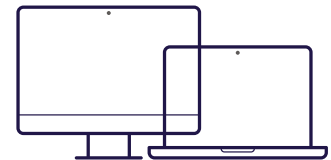
AT GEM-A HQ
London



WORLDWIDE
at one of our ATC's



ONLINE
with in-person
practical lab classes



Find out more by contacting: education@gem-a.com

Buy Gem-A Instruments online



**OVER 100
PRODUCTS
AVAILABLE**

View the full collection and offers at: shop.gem-a.com



Gem-A

THE GEMMOLOGICAL ASSOCIATION
OF GREAT BRITAIN



Gem-A, 21 Ely Place, London, EC1N 6TD, UK
+44 (0)20 7404 3334 www.gem-a.com.
Registered charity no. 1109555

CREATING GEMMOLOGISTS SINCE 1908

